博士論文

Doctoral Dissertation

Research on Micro Electrochemical Machining Using Electrostatic Induction Feeding Method

(静電誘導給電法を用いた微細電解加工の研究)

Supervisor Professor Masanori KUNIEDA

Dept. of Precision Engineering, School of Engineering

The University of Tokyo

Wei Han

韓　偉

Research on Micro Electrochemical Machining Using Electrostatic Induction Feeding Method

Wei Han

This paper describes micro electrochemical machining (ECM) using the electrostatic induction feeding method.

In conventional ECM, the dissolution rate was determined by the current density in electrolyte with the application of DC voltage, thus machining accuracy was limited to spatial resolution of about 0.1 mm. In recent years, the machining accuracy was improved by the application of ultrashort voltage pulse of only nanosecond duration, achieving machining accuracy of nanometer to micrometer range. This technique utilizes the electrode double layer formed on the surface of electrodes. The current density is low in the large gap width, hence, it takes a longer time to form the electric double layer compared to the smaller gap width. By turning off the voltage pulse before the double layer in the large gap is fully developed, the electrochemical reaction can be localized at a small gap width by using ultrashort pulse duration current, because the electrochemical dissolution only occurs at the place where the electrical double layers are fully charged during the short pulse duration. On the other hand, with the newly developed electrostatic induction feeding method, pulse current of several tens of ns in pulse duration can be easily obtained without the use of an expensive ultrashort pulse generator. In addition, this method enables non-contact electric feeding by replacing the feeding capacitance C_1 with a gap between the feeding electrode and rotating spindle, allowing high speed rotation of the tool electrode.

First, the principle of electrostatic induction feeding ECM was discussed in Chapter 2. Then in order to avoid short circuit in the small working gap of several micrometers, a servo feeding control system based on monitoring the peak of gap voltage was developed. Compared with the old method, which monitors the average of gap voltage, controllability of the working gap width with a higher response was obtained because of the higher S/N ratio. This is because the average of the gap voltage is only 200 mV due to the low duty factor with the pulse duration of several tens ns, while the detected peak of the gap voltage is about 2 V, leading to a much higher S/N ratio. In Chapter 3, using the developed servo feed control systems, the machining characteristics with different reference voltages were investigated. The results showed that higher MRR and smoother surface can be obtained with lower reference voltages, due to the higher current density in the working gap, resulting in higher current efficiency. However, the MRR decreased when the reference

voltage was too low, as a result of the interruption of machining by the frequent retreat of the tool electrode due to short circuit. On the other hand, the MRR increased with increasing feeding capacitance C_1, because electric charge per each pulse increases in proportion to C_1. The inlet side gap width was independent of C_1, due to the higher MRR and shorter machining time with larger C_1. Based on the preliminary study, through-holes of 50 μm in diameter were machined on a stainless steel (SUS304) plate with a thickness of 50 μm to investigate the straightness of the holes. The diameter of the hole at the inlet and outlet sides was 58.5 μm and 55.5 μm, respectively. The straightness and the side gap width obtained were equivalent to those of micro EDM, indicating that the machining accuracy of the present ECM method can compete with that of micro EDM.

In Chapter 4, micro-rods were machined by electrochemical machining using the electrostatic induction feeding method. Based on the previous research results in Chapter 3, the peak voltage method was used to control the feeding of workpiece during micro-rods machining, and the experimental results were described. A tungsten plate and stainless steel (SUS304) rod were used as tool electrode and workpiece, respectively. The workpiece can be fed either in axial or radial direction to fabricate a micro-rod. When the workpiece was fed in the axial direction normal to the top surface of the tool electrode, the diameter of micro-rod was determined by the depth of cut in the radial direction, and length of micro-rod was determined by the feed distance in axial direction. The influences of voltage amplitude, thickness and surface area of tool electrode on the machining characteristics were investigated from the aspects of machinable length limitation, straightness of micro-rod and surface finish to improve the machining accuracy. The results of machining experiment and current density simulation showed that the influence of stray current on the machining accuracy was obviously decreased by decreasing the thickness of tool electrode, thereby micro-rods with higher aspect ratio and better surface finish were fabricated. However, the influence of the top surface area of tool electrode on machining accuracy was small due to the significantly small change in the average current density on the shoulder surface of workpiece, resulting in small change in material removal rate (MRR), with different top surface areas of tool electrodes. In addition, when the workpiece was fed in radial direction, the limit of the maximum length of the micro-rod was shorter due to the stray current flowing through the end of the micro-rod during all the machining time. The simulation results of the material removal process were qualitatively in agreement with the experimental results. However, the influence of the pitting corrosion was insignificant with the radial feeding method compared with the axial feeding method, because the current flowing through the side surface of micro-rod was

used for material dissolution. The probability of pitting corrosion was decreased using a higher current density.

In Chapter 5, to improve the machining accuracy of micro-rod, the influence of the annealing process of the workpiece and different electrolytes on the machining characteristics were investigated. The machinable length limitation was decreased with the annealed workpiece due to the influence of corrosion. It is considered that the annealing process damaged the workpiece, because the annealing process was not completed in a protective gas atmosphere. Then the machining characteristics with the different electrolytes of NaCl and $NaNO_3$ aqueous solution were investigated with feeding the workpiece in axial direction method. It was found that the influence of pitting corrosion was eliminated with the electrolyte of $NaNO_3$ aqueous solution. This is because the chloride ion is a tiny and aggressive ion compared with the nitrate ion, and easily penetrates the passive oxide layer on the surface of metal resulting in the higher occurrence probability of pitting corrosion. In addition, the taper angle and gap width were also decreased with the electrolyte of $NaNO_3$ aqueous solution, compared with that of the electrolyte of NaCl aqueous solution. This is because the gap width decreased under the same feed speed due to the lower current efficiency of $NaNO_3$ aqueous solution, resulting in less material dissolution in the gap. With the $NaNO_3$ aqueous solution, micro-rod with the high aspect ratio of 20 was easily machined. Compared with EDM, the electrochemical reaction was difficult to be localized in a small working gap with the ECM method resulting in the low machining accuracy. Therefore, the EDM has an obvious advantage in the miniaturization of size compared with the electrostatic induction feeding ECM. However, there is no residual stress and cracks generated in ECM and the surface roughness is better. Hence, there is a possibility that the machining accuracy and miniaturization limit of ECM will be able to exceed the machining ability of EDM in the future.

In Chapter 6, the influences of different materials, including the tungsten, high-speed steel (SKH51) and tungsten carbide, on the machining characteristics were investigated with the electrostatic induction feeding ECM. When the tungsten is used as workpiece material, bipolar current is needed for machining, because of the influence of the tungsten oxide layer generated on the surface of workpiece which is not conductive. The tungsten oxide layer can be dissolved with the bipolar current when the polarity of tungsten electrode is negative, because sodium hydroxide is generated on the tungsten electrode surface. The tool wear, which was generated with the use of the bipolar current, was investigated. The tool wear ratio increased with increasing the feeding capacitance when

the feed speed was the same. The tool wear ratio decreased with electrolyte of 6 wt% in concentration compared with 2 wt%, because the pulse duration of current decreased with the higher concentration of electrolyte resulting in a better machining accuracy. Compared with the electrolyte of NaCl aqueous solution, the tool wear ratio was decreased with the electrolyte of $NaNO_3$ aqueous solution. There are many research reports about tungsten rods machining using the alkaline electrolyte such as NaOH and KOH, which are harmful to the environment and human. Compared with them, the neutral electrolyte NaCl and $NaNO_3$ aqueous solutions were used to fabricate tungsten micro-rods in this research, which decreased the harmful influence of the electrolyte on the environment.

Compared with the ECM, the EDM has an obvious advantage in the machining tungsten and tungsten carbide. Since the process is based on thermal erosion of metallic materials, EDM can be used for any difficult-to-machine materials regardless of electrochemical properties. However, because EDM is a thermal process, the machined surface is characterized by recast layers, including cracks and residual tensile stresses, which result in overall degeneration of the component's mechanical capabilities. In contrast, ECM relies on the mechanism of anodic electrochemical dissolution to remove material, with the advantage that the machined surface has no recast layers and is free of residual stress and micro cracks. The main problem in ECM is to create conditions for the electrochemical dissolution localization, because during machining the area of dissolution is larger than the area of the electrode tool (machining delocalization).

In Chapter 7, a hybrid machining of micro-ECM and micro-EDM in the same setup and same electrolyte was proposed by utilizing the passive oxide layer formed on the surface of tungsten electrode. The conversion of EDM and ECM modes can be realized using the passive oxide layer formed on the surface of the tungsten electrode. To switch to the EDM mode, a diode is placed in parallel with the working gap so that the pulse voltage can be applied to the gap when the polarity of the tungsten tool electrode is positive. Thereby, the oxide layer is left on the tool surface, generating arc discharges in the gap. To switch to the ECM mode, the diode is removed to obtain the bipolar pulse current in the gap. Thus, the oxide layer cannot be formed on the tool surface, realizing the electrolytic dissolution of the workpiece.

As a conclusion, the machining accuracy and limit of miniaturization of the electrostatic induction feeding ECM are becoming equivalent to micro EDM. Considering the advantages of ECM: no residual stress, no cracks, and better surface

roughness, micromachining processes which are now performed by micro EDM can be replaced by the present ECM method. However, there are some disadvantages, such as the low material removal rate (especially in micro ECM) compared with the EDM method, and difficulty to machine metallic materials, such as W, WC, Pt, and Au, which can be easily machined using the EDM method. Hence, the hybrid machining of micro-ECM and micro-EDM in the same setup and same electrolyte was proposed. The machining process was converted to EDM mode with the oxide layer formed on the surface of tungsten electrode, and ECM mode without the oxide layer. The generation of the oxide layer was controlled by a diode placed in parallel with the working gap with the bipolar current. With the hybrid system, difficult-to-machine materials can be machined using the EDM mode. Rough machining can also be performed using the EDM mode, while the ECM mode is used for the requirement of a high surface finish.

In the future, machining of various kinds of materials, drilling holes with high aspect ratio and ECM milling of 3D shapes with simple shaped electrode should be investigated furthermore with the electrostatic induction feeding ECM.

Content

Chapter 1 Introduction

1.1 Background of electrochemical machining[1, 2, 3)]

In traditional machining, metal material is removed by utilizing hard material to cut the workpieces of relatively softer materials[2)]. However, the design requirement is increasing for the practical applications, as well as the needs for higher processing efficiency, are posing these traditional metal machining technologies restrictions. The motivation for the development of electrochemical machining (ECM) was mainly for the growing use of extremely hard alloys, which is difficult to be machined satisfactorily by conventional methods. The metal removal process of ECM is a controlled anodic dissolution which was known in the previous century, but it was not used as a machining technology until 1960s. In recent years, ECM has been effectively used for high-precision machining of parts achieving a machining accuracy of micrometers regardless of workpiece hardness, because of its advantages like no tool wear, no residual stress or cracks generated on the machined surface, smooth surface finish, and high material removal rate, and so on.

The ECM principle was first discovered in the nineteenth century by Michael Faraday (1791-1867). The laws of electrolysis were established in 1833, which are the foundation of both the well-known electrodeposition and dissolution methods. In 1929, the Russian researcher W. Gusseff first used electrolytic process to machine metal anodically. The development of the aircraft and aerospace industries made ECM one of the major technologies to machine many kinds of hard alloys, leading to significant advances in ECM technologies during 1950s and 1960s[1, 3)]. In 1959, Anocut Engineering Company of Chicago established the anodic metal machining techniques and used them in commercial applications. After one year, Steel Improvement and Forge Company also used this technique in a commercial application, based on research by the Battelle Memorial Institute. In the 1960s and the 1970s, the ECM technique showed an obvious advantage in the machining of large components made of advanced and difficult-to-cut metals, such as the gas turbine blades. Although ECM was initially developed to machine these difficult-to-machine materials, almost any metals, except for noble metals like gold and platinum, can easily be machined. Thus ECM has been widely used in many ways from the 1980s, for example, by automotive, offshore petroleum, and medical engineering industries, as well as by aerospace firms, which are its principal users still now.

1.2 Principle of electrochemical machining[4, 5)]

1.2.1 Electrolysis

Electrolysis is a chemical process, in which an electric current is passed between two electrodes dipped into a liquid solution[1, 4, 5, 6)], which is the basic principle of ECM. The electrolyte can be different aqueous solutions, such as acidic, alkaline and neutral aqueous solutions. With the electrolyte, the current flows through the circuit, including the electrodes and power supply and makes the ECM technique possible to be used for material remove. The electrodes in electrochemical machining are connected with the positive and negative polarity of the power supply and immersed in the electrolytes. The whole system of electrodes and electrolyte combined is known as an electrolytic cell.

The ions in the electrolyte move toward the surfaces of the electrodes due to the potential difference from the power supply. The cations move toward the cathode because of the positive charge, while the anions move toward the anode with the negative charge. On the surface of electrodes, the electrons move to and away the electrodes, by which process the materials are removed from the electrode or deposited on the surface of electrode. These techniques can be used for material processing, such as ECM technique based on a material removal process from a metallic electrode, and the electroplating is another application by utilizing the metal deposition on the surface of the cathode.

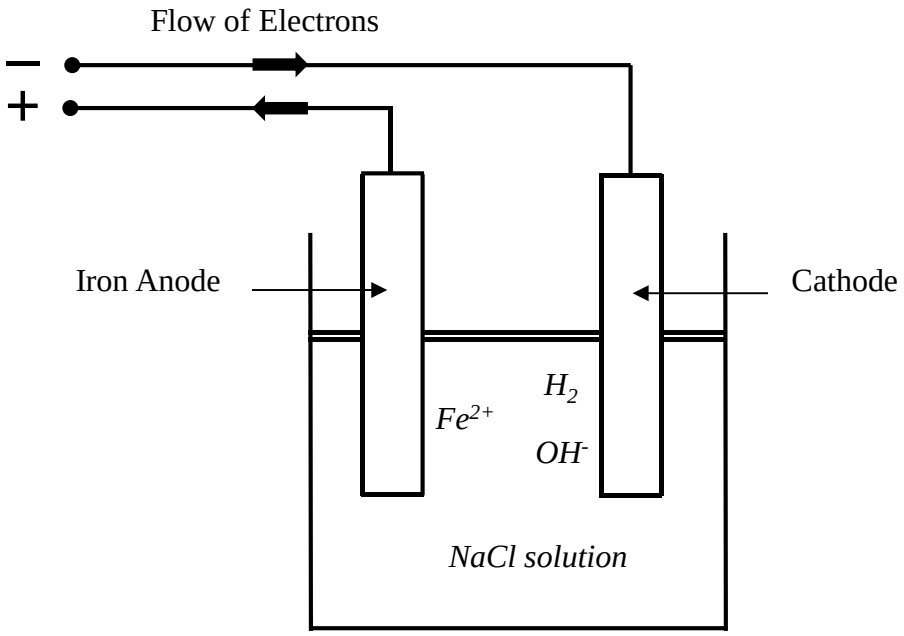

Fig. 1.1 Electrolysis of iron

A schematic of the electrolysis of iron in a sodium chloride (NaCl) solution is shown in Fig. 1.1. The prominent chemical reactions which occur in the electrolytic cell are described as following[6].

The dissolution of iron into the metal ion occurs on the anodic reactions. Oxygen is generated by the dissolution of water.

$$\mathrm{Fe} \rightarrow Fe^{2+} + 2e^{-}$$

$$H_2O \rightarrow 2H^{+} + 2e^{-} + \frac{1}{2}O_2 \uparrow$$

The hydrogen gas and hydroxyl ions are primarily generated by the cathodic reactions.

$$NaCl \rightarrow Na^{+} + Cl^{-}$$

$$H_2O \rightarrow H^{+} + OH^{-}$$

$$2H^{+} + 2e^{-} \rightarrow H_2 \uparrow$$

Ferrous hydroxide is formed due to the reaction of the metal ions with hydroxyl ions after the overall reaction. The reaction between the ferrous hydroxide and water produces ferric hydroxide.

$$Fe + 2H_2O \rightarrow Fe(OH)_2 + 2H^{+} + 2e^{-}$$

$$4Fe(OH)_2 + 2H_2O + O_2 \rightarrow 4Fe(OH)_3$$

After the overall electrolysis process, the iron is dissolved from the anode and the hydrogen is generated on the surface of cathode with some electrochemical products such as ferrous hydroxide.

1.2.2 Electrochemical machining

Electrochemical machining (ECM) is a controlled anodic dissolution process, in which an anode and a cathode are immersed in an electrolytic cell to form an electrolysis process[1, 4, 6, 7]. Electrochemical machining is based on the principle outlined in Fig. 1.2, with the workpiece and tool electrode used as the anode and cathode, respectively. In the ECM process, a gap voltage is applied across them by the power supply. The electrolyte flows through the working gap between electrodes to remove the electrochemical products and to decrease unwanted effects, such as the influence of bubble, which easily causes the generation of discharge in the working gap, and temperature rise of electrolyte due to the Joule heating. When an electric current flows through the working gap, the anode workpiece dissolves in a small working gap, so that the shape of the machined workpiece is approximately a negative mirror image of that of the tool electrode. Machining performance in ECM is determined by the anodic dissolution of the workpiece material in a given electrolyte[1, 3, 4, 6, 8].

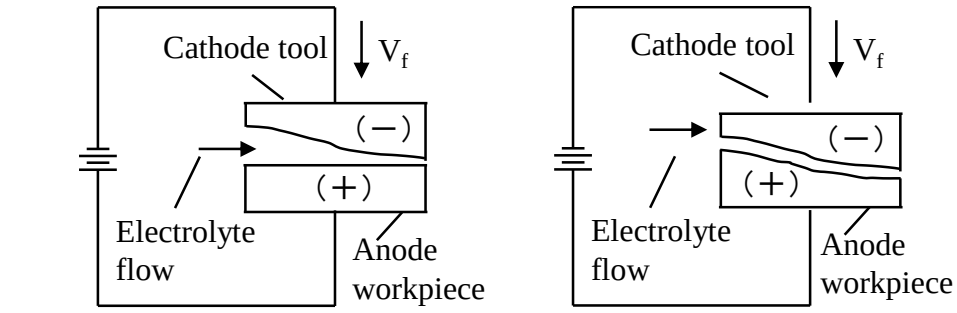

(a) ECM process

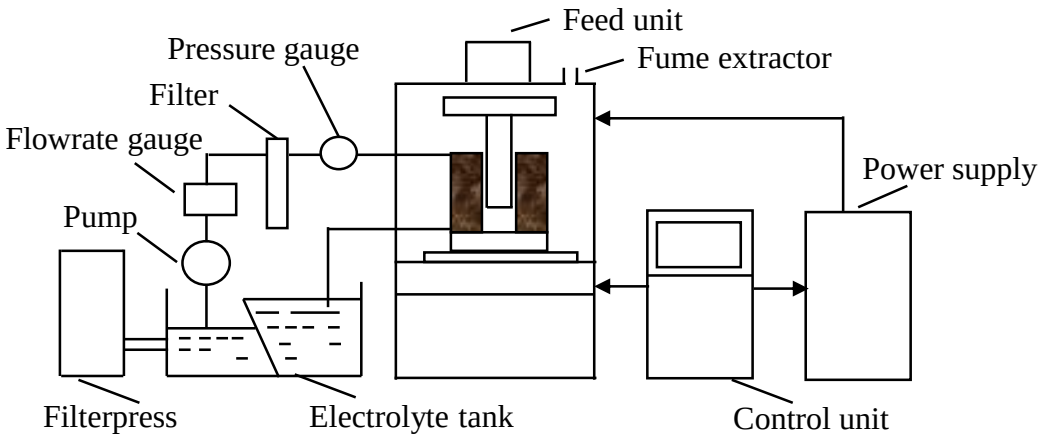

(b) ECM equipment

Fig. 1.2 ECM process and equipment

Fig. 1.2 illustrates the equipments for the ECM process. AC or DC voltage (usually about 10 to 25 volts) is supplied by the power supply and applied between the working gap formed by a pre-shaped cathode tool and an anode workpiece. The electrolyte (e.g. $NaNO_3$ aqueous solution) flows at a high speed through the gap to flush away the bubbles and electrochemical products and decrease the gap temperature caused by the Joule heating.

1.2.3 Electrode potential [4, 9, 10, 11)]

In ECM process, the dissolution of the metal workpiece needs the current flowing through the working gap, and the current is generated by an external potential difference. With a larger current flowing through the working gap, the difference in potential between the equilibrium value and the working value is higher. Polarization can be defined as the change of the electrode potential from the equilibrium value to the machining value due to the passage of the current in the circuit. The extent of polarization is described by the over potential.

Over potential, $\eta = E - E_{eq}$

Fig. 1.3 illustrates the influence of different over potentials on the total potential drop in the ECM process. The value of current density is determined by a certain over potential as shown in Fig. 1.3. This over potential can be considered as a sum of terms associated with the different reaction steps: the mass transfer, charge transfer associated with a preceding reaction, etc.[6, 9, 10)]

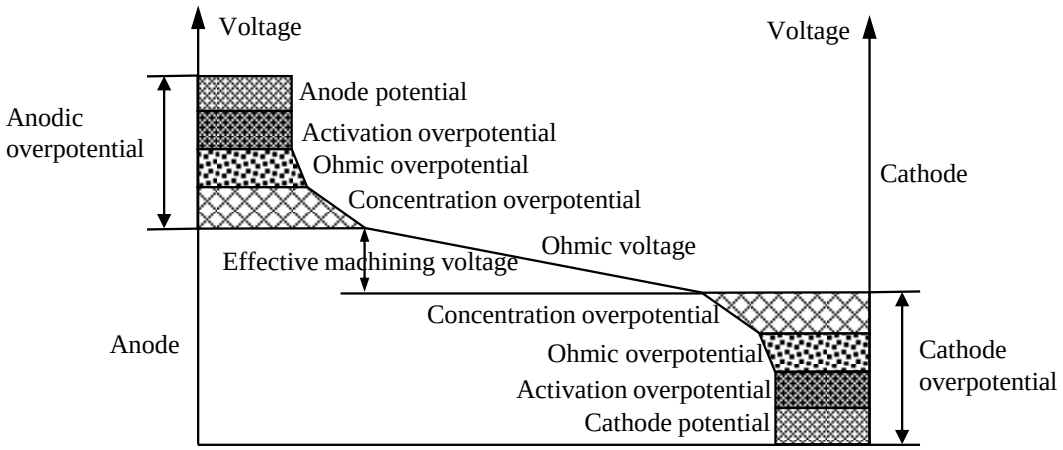

Fig. 1.3 Total potential drop in ECM cell[6, 9, 10)]

The electrochemical changes occurring at an electrode are in equilibrium without current flowing condition. The electrode potential between the interface of the electrode and the electrolyte acts as an obstacle to increase the rate of reaction. In order to activate the ions discharged at the required rate to promote current flowing, additional energy must be applied by the power supply in the electrochemical cell. With a high activation energy of the charge transfer reaction, an over potential is needed to drive the reaction in the desirable direction to obtain an appreciable rate. It is called activation over potential (η_{ac}).

The movement of ions in the electrochemical cell is determined by migration, convection, and diffusion. Movement of ions under the influence of potential difference is called migration. In convection, ions move because of the physical movement of the electrolyte solution. In addition, movement of ions due to the difference in gradient of ion concentration in the solution is diffusion. Ions migrate toward the electrode surface and form a layer of concentrated ions which generates a concentration barrier. The charge of the ions can only be released at the electrode surface when the ions pass through this concentration barrier. On the other hand, newly formed ions have to pass through this barrier into the bulk electrolyte. The extra potential, which is required for the movement of ion through this concentration layer, is known as concentration over potential.

Oxide layer is often formed on the surface of metal, which offers resistance to the current flowing through the surface. Resistance over potential is generally regarded as the

potential drop across this thin layer on the electrode surface. The migration of ions are also restricted by the film of metal hydroxides deposited on the cathode (tool) surface during ECM, which process makes the current path more restrictive. Oxide film at the anode (workpiece) surface will also offer resistance and sometimes prevent ions from reaching the anode surface creating passivation which makes the machining process difficult in the ECM. The magnitude of resistance depends principally on the current flowing in the cell and on the nature and electrolyte conductivity and material.

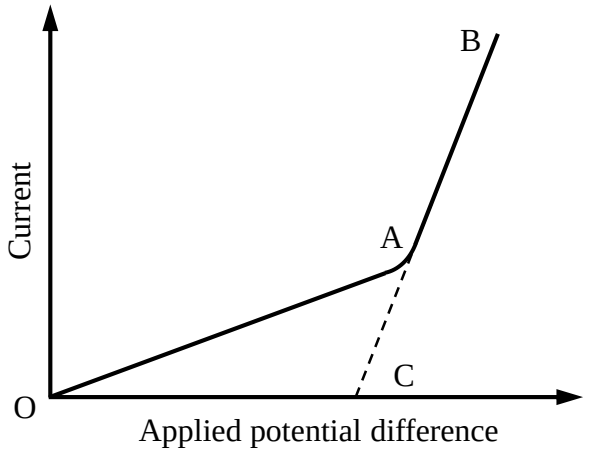

Fig. 1.4 Decomposition potential

In ECM, the material removal rate at the workpiece and hydrogen evolution at the tool electrode can be increased with the higher potential difference. Fig. 1.4 shows the curve of applied potential difference against current. At initial time, values of potential difference is low along OA. When the values of the potential difference reach the region A, the current rises sharply as shown in the figure. With the potential difference further increasing, the current increases appreciably along AB. Point A on the curve represents the onset of anodic dissolution of the process. The curve AB is extrapolated back to the zero value current and meets the axis of the applied potential difference at point C. The potential at point C is known as decomposition potential[6].

1.3 Gap phenomena of ECM

1.3.1 Anodic dissolution

The materials are dissolved in the electrochemical reaction due to an electric charge transport Q following Faraday's law.

The material dissolution amount follows Faraday's two laws of electrolysis:

① The amount of material dissolved or deposited is proportional to the electricity.

$$m \propto Q$$

Where *m*=mass of material dissolved or deposited

Q=amount of charge passed

② The amount of material dissolved or deposited by the same quantity of electricity is proportional to their chemical equivalent weights.

As one gram of workpiece is dissolved, the electric quantity needed is *F* coulomb and *F* is the Faraday's constant. The electric charge quantity for the dissolution of one gram of workpiece can be expressed as:

$$C = \frac{nF}{M}$$

where,

n=Valency

F=Faraday's constant

M=Atomic weight

When *m* gram of workpiece dissolved with the current *I*A and time *t*s, the following equation can be obtained.

$$It = \frac{mnF}{M} = Cm$$

Hence,

$$m = \frac{MIt}{nF} = \frac{It}{C} \tag{1.1}$$

1.3.2 Material removal rate

The machining performance is influenced by various predominant process parameters, such as current density, gap width, electrolyte flushing, concentration of electrolyte and type of electrolyte, and also the anode reactions[12, 13]. Material removal rate (MRR) is an important characteristic to evaluate efficiency of ECM process. In ECM, material removal takes place due to atomic dissolution from the workpiece. The material removal rate is defined as the volume of material removed per unit time, as shown in the foregoing sections, since the electrochemical dissolution is governed by Faraday's laws, then it can be expressed as

$$\text{MRR} = \frac{m}{t\rho} = \frac{IM}{F\rho n} \tag{1.2}$$

where *I*=current

ρ= material density

Alloys are widely used as engineering materials compared with a single element, consisting of different elements with a given proportions.

There are "*N*" elements in an alloy and the atomic weights are given as M_1, M_2, M_3, ……, M_n with valency during electrochemical dissolution as n_1, n_2, n_3, ……, n_n. In addition, the

weight percentages of different elements are $\alpha_1, \alpha_2, \ldots\ldots, \alpha_n$ (in decimal fraction). Now for passing a current of *I* for a time *t*, the dissolved material for any element "*I*" can be expressed as

$$m_i = \Gamma_a \rho \alpha_i$$

Where Γ_a is the total volume of alloy dissolved. A certain amount of charges Q_i are needed to dissolve each element present in the alloys.

$$m_i = \frac{Q_i M_i}{F n_i}$$

Therefore,

$$Q_i = \frac{F m_i n_i}{M_i} = \frac{F \Gamma_a \rho \alpha_i n_i}{M_i}$$

The total charge passed can be expressed as,

$$Q_T = It = \sum Q_i$$

Hence,

$$Q_T = It = F \Gamma_a \rho \sum \frac{\alpha_i n_i}{M_i}$$

Now

$$\text{MRR} = \frac{\Gamma_a}{t} = \frac{1}{F\rho} . \frac{I}{\sum \frac{\alpha_i n_i}{M_i}} \qquad (1.3)$$

1.3.3 Gap width[1, 4, 14)]

The gap width has a significant influence on the material removal rate in the micro-machining[8, 13, 15)]. There is a requirement to improve the material removal rate and machining accuracy to achieve the full potential of ECM[4, 6, 9, 16)]. ECM can be undertaken without any feed of the tool electrode to the workpiece or with a feed of the tool so that a steady machining gap is maintained. The dynamics without feeding of the tool is considered first. Fig. 1.5 schematically shows the machining without feeding of the tool and an instantaneous gap between the tool and workpiece of "*h*".

Now over a small time period "*dt*" a current of *I* is passed through the electrolyte and that leads to an electrochemical dissolution of the material of amount "*dh*" over an area of *s* with the gap voltage of *V*.

Hence,

$$I = \frac{V}{R} = \frac{V}{\frac{rh}{s}} = \frac{Vs}{rh}$$

Where *r* is the resistivity of the electrolyte.

According to equation (1.2)

$$\frac{dh}{dt} = \frac{1}{F}\frac{M_x}{\rho n_x}\frac{V}{rh} \tag{1.4}$$

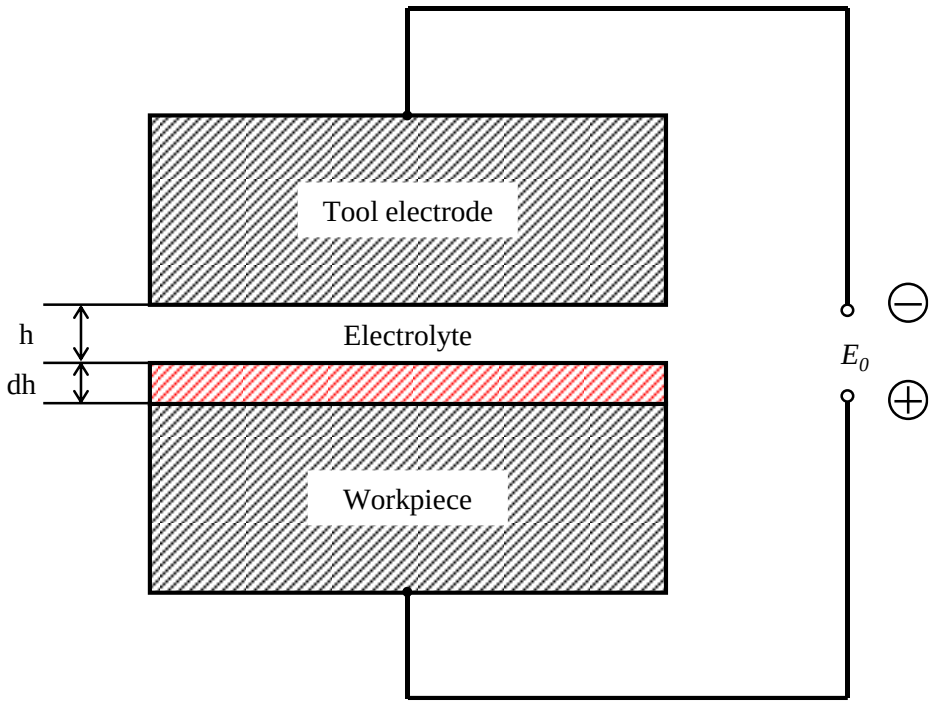

Fig. 1.5 Schematic representation of the ECM process with no feed

For a given potential difference and alloy

$$\frac{dh}{dt} = \frac{M_x V}{F\rho n_x r}\frac{1}{h} = \frac{c}{h} \tag{1.5}$$

where c is a constant

$$\mathrm{c} = \frac{M_x V}{F\rho n_x r} = \frac{V}{F\rho r \sum \frac{\alpha_i n_i}{M_i}}$$

Hence,

$$\frac{dh}{dt} = \frac{c}{h}$$
$$hdh = cdt$$

At t=0, h=h_0 and t=t_1, h=h_1, then

$$\int_{h_0}^{h_1} hdh = c\int_0^t dt$$

Hence,

$$h_1^2 - h_2^2 = 2ct \tag{1.6}$$

It is found that the gap width with zero feed speed grows gradually following a parabolic curve as shown in Fig. 1.6.

Thus the electrochemical dissolution rate would gradually decrease with increase in the gap width because the gap resistance across the electrolyte would increase.

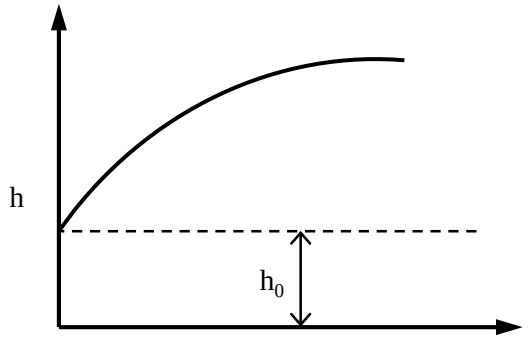

Fig. 1.6 Change of gap width under zero feed speed condition

Now consider the general ECM process, in which a feed speed f is given to the tool electrode.

Hence $$\frac{dh}{dt} = \frac{c}{h} - f$$

Under the steady state condition, the gap width is constant i.e. the feed distance of the tool is compensated by dissolution of the workpiece material. Thus with respect to the tool, the workpiece is not moving

Hence, $$\frac{dh}{dt} = 0 = \frac{c}{h} - f$$

$$f = \frac{c}{h}$$

Or, $$h^* = steady\ state\ gap = \frac{c}{f}$$

Now under practical ECM conditions, it is not possible to set exactly the value of h^* as the initial gap. Thus it is required to investigate the influence of the initial gap width on the process to reach the steady state.

Now $$\frac{dh}{dt} = \frac{c}{h} - f$$

Define h' as

$$h' = \frac{h}{h^*} = \frac{hf}{c}$$

Then $$t' = \frac{ft}{h^*} = \frac{f^2 t}{c}$$

$$\frac{dh'}{dt'} = \frac{f/_c}{f^2/_c}\frac{dh}{dt} = \frac{1}{f}\frac{dh}{dt}$$

Since $$\frac{dh}{dt} = \frac{c}{h} - f$$

$$f\frac{dh'}{dt'} = \frac{c}{h'h*} - f = \frac{cf}{h'c} - f$$

$$f\frac{dh'}{dt'} = f\left(\frac{1-h'}{h'}\right)$$

$$\frac{dh'}{dt'} = \frac{1-h'}{h'}$$

Hence $$\mathrm{d}t' = \frac{h'}{1-h'}dh'$$

Now integrating between t'=0 to t'=t' when h' changes from h_0' to h_1'

$$\int_0^{t'} dt' = \int_{h_0'}^{h_1'} \frac{h'}{1-h'}dh'$$

$$t' = \int_{h_0'}^{h_1'} -\frac{d(1-h')}{(1-h')} + \int_{h_0'}^{h_1'} d(1-h')$$

$$t' = h_0' - h_1' + ln\frac{h_0' - 1}{h_1' - 1}$$

Now for different value of h_0', h_1' seems to approach 1 as shown in Fig. 1.7.
Thus irrespective of initial gap

$$h' = \frac{h}{h*} = 1 = \frac{fh}{c}$$

$$f = \frac{c}{h} = \frac{M_x V}{F\rho v n_x r}\frac{1}{h}$$

Hence $$f = \frac{M_x}{F\rho n_x}\frac{V}{rh} = \frac{M_x}{F\rho n_x}\frac{I}{s} = MRR\ in\ mm/s$$

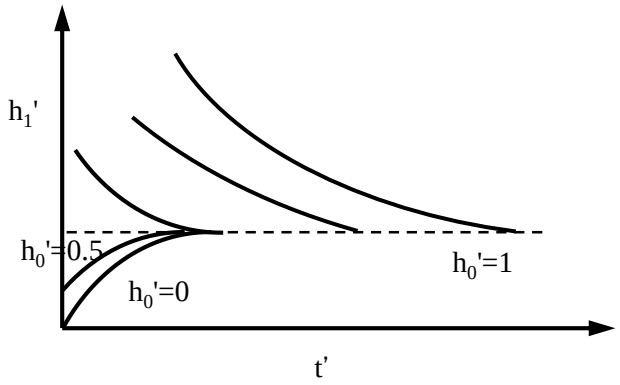

Fig. 1.7 Variation in steady state gap width with time for different initial gap

Thus it seems from the above equation that ECM is a self regulating process because MRR is equal to feed rate. With the same current density *I*/*s*, the feed speed is kept constant regardless of the machining surface area *s*. In electrical discharge machining (EDM) however, discharge occurs only at a signal discharge location per each pulse. Hence, volumetric removal rate is constant, thereby the feed speed is inversely proportional to the machining surface area. As a result, the volumetric removal rate of ECM is significantly high, compared with EDM when the machining area is large. In micro machining however, the advantage of the high removal rate of ECM is lost, because the machining area is small.

1.3.4 Electrode polarization[1, 4, 6)]

Without current flowing through the circuit, the electrochemical reactions in an electrochemical cell are in equilibrium. A potential difference between electrode-electrolyte interfaces exists as “electrode potential”. The electrode potential between the electrode and electrolyte acts as a barrier to a higher rate of reaction, which is the electrochemical force of the cell. External energy must be supplied for the ions to be discharged at the required rate, therefore current flow is promoted. The “polarization” is used to describe the departure of electrode potential from the equilibrium value with the flowing of current. Current potential curves, particularly those obtained under steady-state conditions, are called as “polarization curves”. Fig. 1.8 shows two extremes of polarization curves: ideal polarizable and ideal nonpolarizable. An ideal polarized electrode shows a very large change in potential with the passage of an infinitesimal current. However, an ideal nonpolarizable electrode does not show obvious change with passage of current, with the electrode potential fixed. Nonpolarizable electrode are generally used as reference electrode in low-current electrochemical reactions.

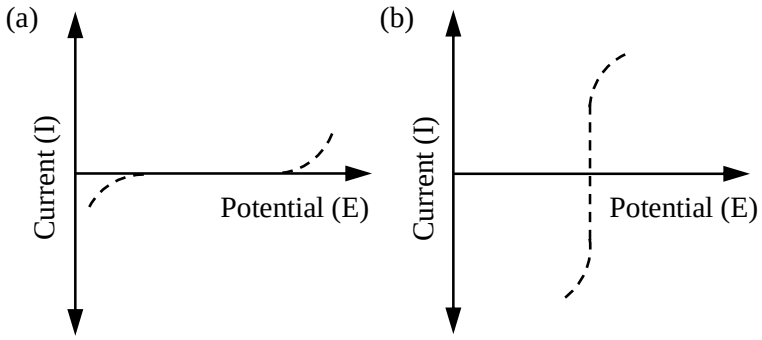

Fig. 1.8 Current-potential curves for ideal (a) polarizable and (b) nonpolarizable electrodes

Anode potential and current density are significantly important during ECM and affect the process in which the material is dissolved from the workpiece, which in turn determines the surface finish. Polarization curves are often used to investigate the influence of potential and current density on electrochemical dissolution process. Fig. 1.9 shows different polarization curves and their characteristic behavior on the progress of electrochemical dissolution. Curve 1 represents occurrence of etching where metal dissolves more preferentially from the areas which have lower electrode-chemical potentials. Thus, the discontinuous dissolution rate across the grain boundaries results in the generation of an uneven surface. Curve 2 represents passivation phenomenon in which the passive oxide film is generated in region (i). The current density becomes lower resulting in lower electrochemical dissolution rate. However, when the potential increases further, transpassive phenomenon occurs due to breakdown of the passive film. Hence, material dissolution becomes uniform resulting in good surface finish.

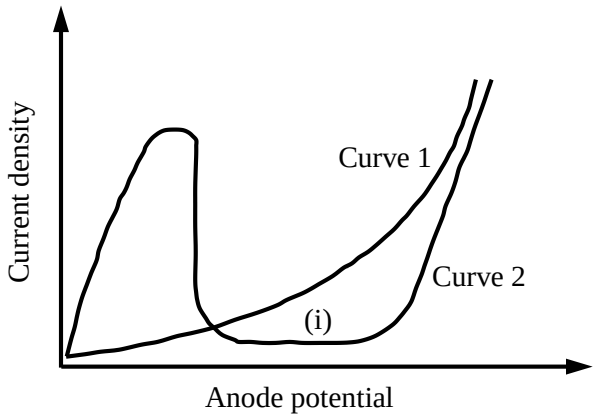

Fig. 1.9 Anode potential-current density polarization curves

1.4 Important factors of ECM

1.4.1 Gap control and status monitoring

Any unstable status in the working gap will lead to undesired machining results, such as rough surface finish. In addition, micro-discharges occurring in the working gap causes uncontrolled material removal and results in improper shape and low accuracy. The probability of the discharge in the working gap is increased by the accumulation of electrochemical dissolution products, bubbles generated by electrochemical reaction such as hydrogen and oxygen gases, bubbles due to electrolyte boiling, and anodic metal hydroxide in the gap. The discharge easily occurs when the electrolyte is not refreshed sufficiently in the working gap. The ignition of discharge can usually be avoided by monitoring and controlling of the process parameters[16].

A proper control of the gap results in smaller gap resulting in better shape and machining accuracy. The gap width can be controlled by monitoring the transient current flowing through the electrochemical cell. Another way is to monitor the potential difference between the tool and workpiece during machining. The potential drop is used for controlling the feed of the tool electrode[17] as shown in Fig. 1.10. During the machining, the potential between the workpiece and tool electrode is monitored, and used for controlling the feed of the tool electrode. Depending on the average potentials of tool and workpiece, Kock et al.[18] achieved the machining precisions below 100nm by the application of 500ps voltage pulses.

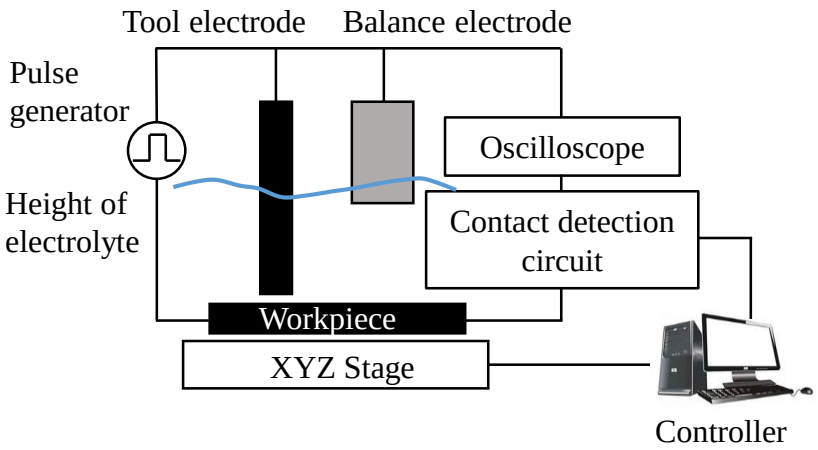

Fig. 1.10 System for micro ECM[17]

In the ECM process, it is very important to flush away machining products, bubbles and decrease the temperature rise due to Joule heating by controlling the speed and the direction of the electrolyte flow. However, it is difficult to obtain a uniform electrolyte

flow between the two electrodes because of the narrow working gap, especially with the ultra-short pulse voltage. The working gap is easily unstable by the vibration of the generated bubbles. The pulse voltage amplitude and pulse on-time should be kept as low as possible[17)] to suppress the formation of bubbles and reduce the machining gap width.

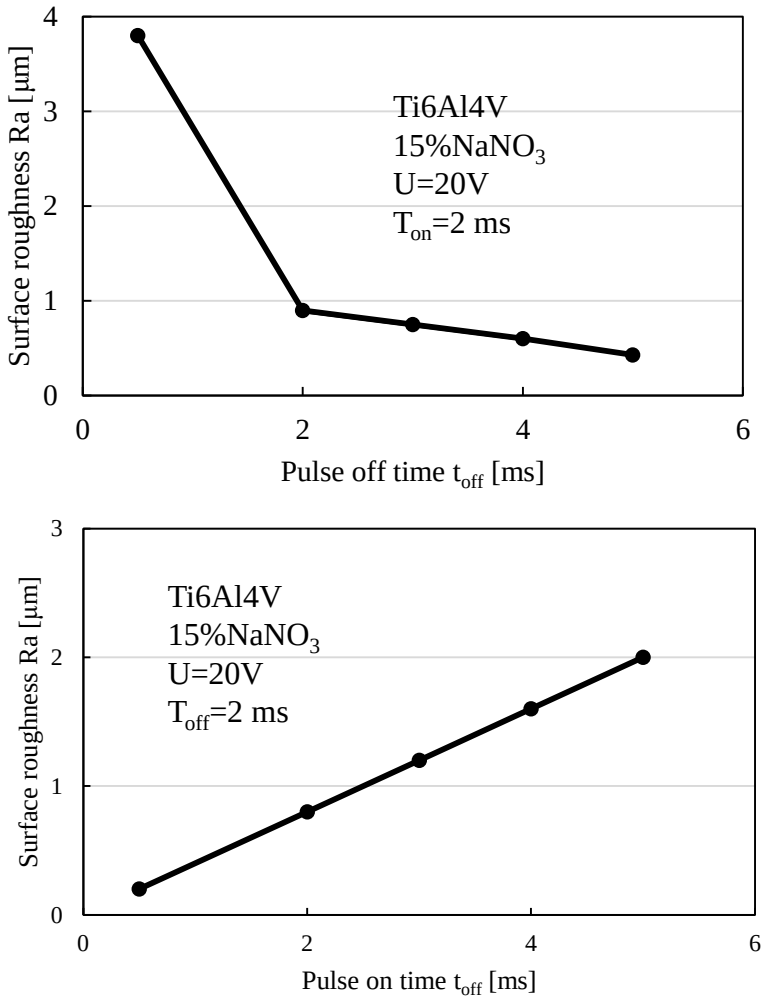

Fig. 1.11 Effects of pulse parameters on surface quality of Ti6A14V[23)]

1.4.2 Pulse ECM

At first, DC current was used in ECM. However, instead of the continuous D.C. current, the pulse ECM uses the short pulse current, achieving a much higher machining accuracy. Experimental results show that the electrolyte is periodically replaced in the working gap with the pulse ECM, resulting in a higher instant current density during the pulse on time which leads to a good surface finish. In addition, the machining accuracy is obviously increased with a smaller working gap[19, 20, 21)], because the working gap width is significantly decreased by using the short pulse voltage. With the pulse ECM, it is

possible to produce complex shapes, such as dies, precision electronic components and turbine blades, with an machining accuracy of 0.02～0.10 mm[22].

The application of short voltage pulses enables the machining process to be stable at small working gaps. The machining accuracy increases with decreasing the gap width. The length and duty factor of pulse voltage have been found to significantly affect the surface quality. Experimental results show that short pulse on time and relatively long pulse off time give an improved surface with less pitting for pulse ECM of TiAl4V alloy, a material commonly used in turbine blade manufacturing, as shown in Fig. 1.11[23].

1.4.3 Electrolyte

The electrolyte is one of the main components of the electrochemical cell. It supplies a path for current to flow from the workpiece to the tool electrode by completing the electric circuit. It will flush away the bubbles and products of electrochemical reaction from the working gap, and decrease the temperature rise due to Joule heating. These can increase the conductivity of electrolyte and avoid deterioration of the machining accuracy.

There are broadly two kinds of electrolytes: passive electrolyte and non-passive electrolyte[6, 24, 25, 26, 27]. The passive electrolytes, which contain oxidizing anions such as sodium nitrate, generally give better machining precision[25, 26, 27, 28]. In addition, non-passive electrolytes contain aggressive anions such as sodium chloride. For example, compared with the sodium chloride aqueous solution, sodium nitrate aqueous solution is more advantageous due to its lower current efficiency resulting in a smaller working gap width, which increases the machining accuracy[4, 24]. Sodium chloride is a widely used non-passivating electrolyte and the current efficiency is almost constant at 100% during machining[1, 4, 6, 29] and hence has a higher material removal rate. In addition, the acidic electrolyte like HNO_3 and alkaline electrolyte like NaOH are also used in ECM. However, the acidic and alkaline electrolyte are harmful to human health and environment, and also more easily corrode the machining equipment than the neutral electrolyte.

It is a difficult task to maintain the flow of electrolyte to flush the machining products away from the extremely small gap without affecting the machining stability[4, 6, 9, 24], especially in micro ECM, because of the significantly small gap between the tool and the electrode. Hence, in order to obtain a high machining accuracy in ECM process, electrolytes need to satisfy the following requirements so that they can be used effectively.

① The anions permit the dissolution of the workpiece without forming a film on the workpiece surface and the cations do not deposit on the tool resulting in the deterioration of the machining accuracy.

② In order to flow easily in the narrow gap between the tool and the workpiece, the electrolyte needs to have a low viscosity. To reduce the energy consumption and to

avoid the boiling of the electrolyte due to Joule heating, the electrical conductivity of the electrolyte should be sufficiently high.

③ The electrolyte should be such that it is safe to use, nontoxic, and does not erode the machine.

④ The electrolyte should be cheap and readily available and should not exhibit large variations in its properties during the machining progresses.

1.4.4 Tool electrode

Attention was paid to tool design when the ECM was introduced into the manufacturing industries. A practical tool design is not easy because it should not only provide the cathode dimensions but also a suitable electrolyte path providing an effective electrolyte flushing in the working gap. The tool shape should not be a perfect negative mirror image of the workpiece to be produced because of the uneven distribution of the gap width depending on the tool geometry, electrolyte flow, and non-uniform distribution of temperature and volume fraction of bubbles[30, 31, 32]. Hence, prediction of the tool shape is a formidable inverse boundary problem involving not only Laplace equations[33, 34], but also the equations related to heat conduction, fluid dynamics, and electrochemisty[24, 35]. A lack of adequate understanding of the process makes the designing ECM tools to be a difficult task, and the multiphysics phenomena and mathematical complexities allow calculation of only a first approximation of the final tool shape[28].

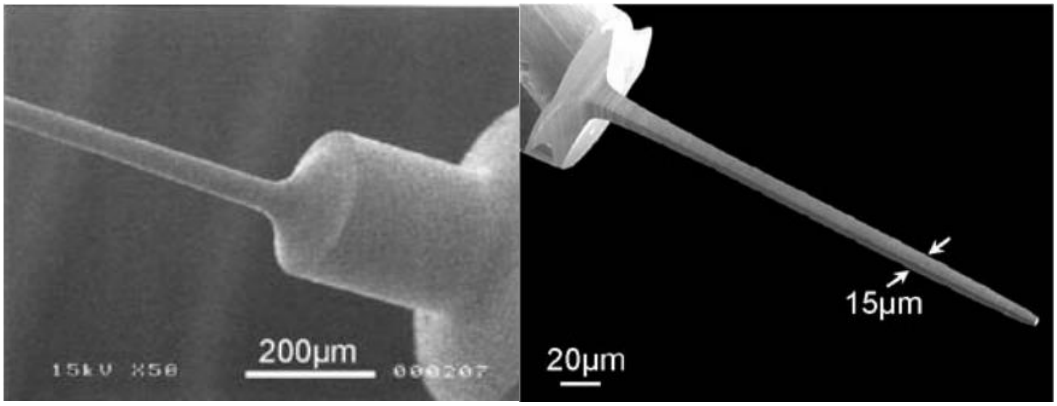

Fig. 1.12 High aspect ratio micro tools[42]

Recent studies have conducted the numerical calculations for more accurate tool electrode design instead of simple geometrical approximations[36, 37, 38]. Thanks to the development of powerful computer and multiphysics simulation software, the simulation accuracy is being improved to obtain the tool electrode shapes precisely. Furthermore, the tool electrode does not wear in ECM, while the tool wear makes the simulation more difficult in EDM.

Tool electrodes in ECM are made of any electrical conductive materials which are cost effective and easy to be machined, like brass, steel, copper, and so on. Micro tools are mainly fabricated using processes such as electrochemical etching and micro EDM[39, 40, 41]. Fig. 1.12 shows micro tools in the range of 15-20 μm in diameter, which were produced on a special precision grinding machine[42]. Use of multiple electrodes and disk-type electrodes increases accuracy as well as productivity. Fig. 1.13 shows dual micro columns which were machined with dual disk-type electrodes[17].

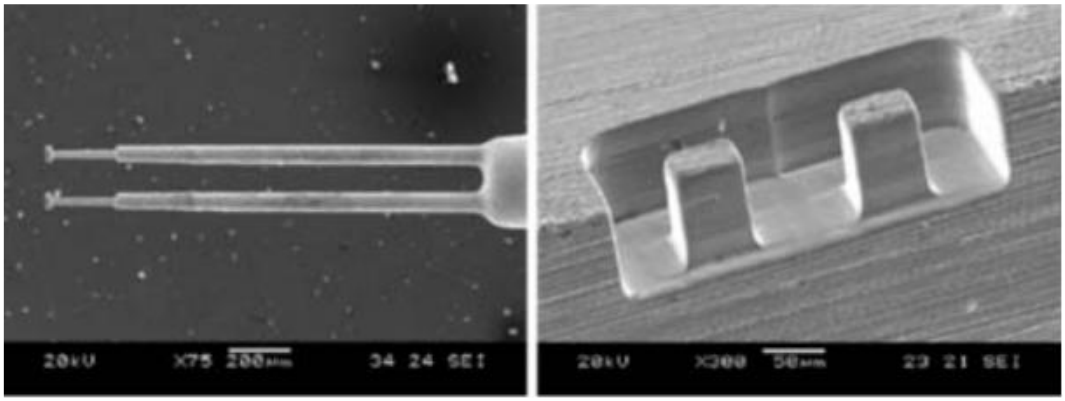

Fig. 1.13 Dual columns machined with dual disk-type electrodes[17]

1.5 Characteristics and applications of ECM

In nonconventional machining, most of the machining processes are thermal processes, such as Electrical discharge machining (EDM), Laser beam machining (LBM), Electron bean machining (EBM) etc. Hence, thermal distortion is possibly caused on the machined surface[43, 44] in these machining processes. In the thermal-free process of ECM, the material is removed by anodic dissolution that does not generate any residual stress. Since ECM removes the material in a level of an atomic unit, the surface finish of the machined surface is significantly good and not influenced by residual stress or heat-affected zone under the surface. Since the anode metal dissolves electrochemically. The hardness, toughness, and thermal resistance do not influence the MRR. It is also not relevant for the machining of a product whether it is processed before or after the hardening step. In addition, the 3D micro features can be processed in a single step by designing a shaped tool electrode or adopting micro tool movement strategies. Using the ECM technique, a microproduct is more easily generated with a high degree of freedom of design. The modern process can obtain high dimensional accuracy and high surface quality.

Hence, ECM is a very promising machining technology due to its advantages, which include high MRR, good surface finish, no tool wear, and it can also machine chemically

resistant materials like titanium, copper alloys and stainless steel, which are widely used in biomedical, electronic and MEMS applications[45, 46, 47].

Fig. 1.14 shows some applications of ECM. ECM is used for (a) die sinking, (b) profiling and contouring, (c) drilling and (d) trepanning and micro-machining.

On the other hand, the ECM process has the following disadvantages:

- ECM was previously known as a process that harms the environment, because the by-products may be harmful to the human beings and environment.
- Each product and material requires new research. So, higher production numbers are essential for the cost effectiveness of the process.
- Machining accuracy is lower than EDM because the gap width is comparatively large.
- There are some materials which are difficult to be machined by ECM, even if the materials are electrically conductive.
- Material removal rate is low when the machining area is small as described below.

In EDM, the discharge occurs only at a single discharge location per each pulse, hence, volumetric removal rate is constant. On the contrary, in ECM, removal occurs at the same time over the working surface. Since the potential difference between the tool electrode and workpiece is keep constant, the current density is almost the same, thereby the tool feed speed is constant, independent of the working surface area. As a result, the volumetric removal rate of ECM is significantly high, compared with EDM when the machining area is large. In micro ECM, however, the advantage of the high removal rate is lost, because the machining area is small.

In recent years, the environment-friendly manufacturing is advocated. Waste-free processes are expected by industry, through minimizing the waste generation and treating the waste to be converted into an environment-friendly material before disposal. However, acidic and alkaline solutions are often used as electrolyte during ECM process, which are harmful to the human beings as well as to the environment. Even in the case of neutral electrolytes, used electrolyte may be harmful to the environment and finally to the human beings because it sometimes contains toxic ions such as hexavalent chromium.

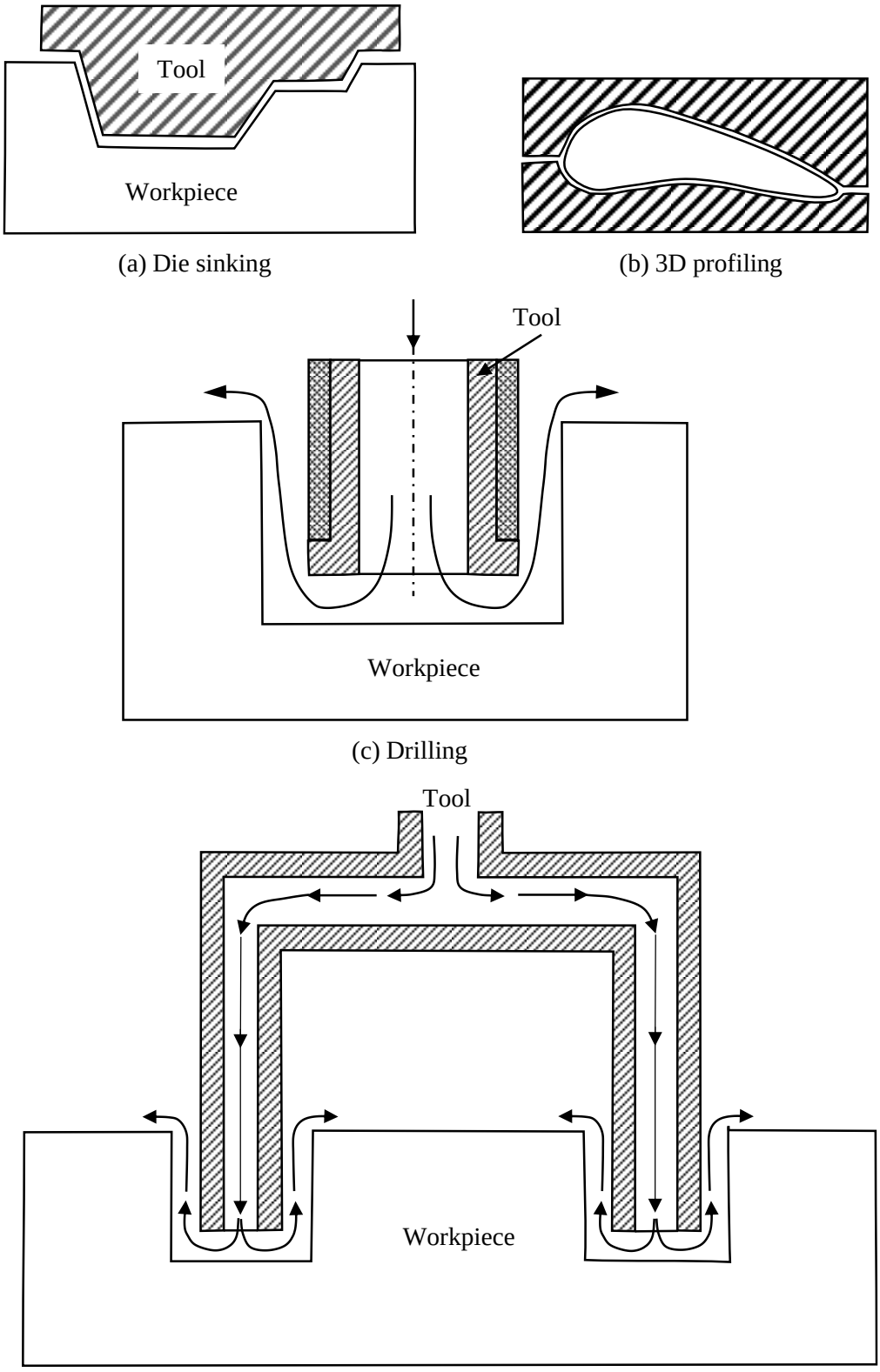

Fig. 1.14 Different applications of ECM

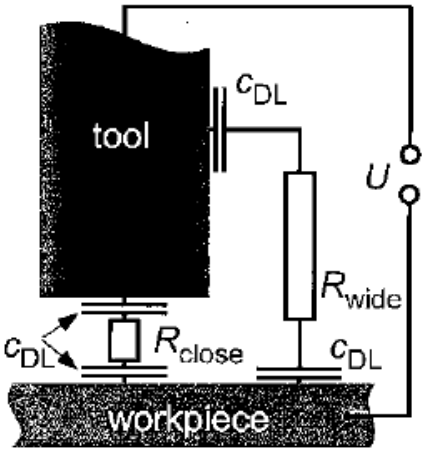

Fig. 1.15 Scheme of an electrochemical cell[49)]

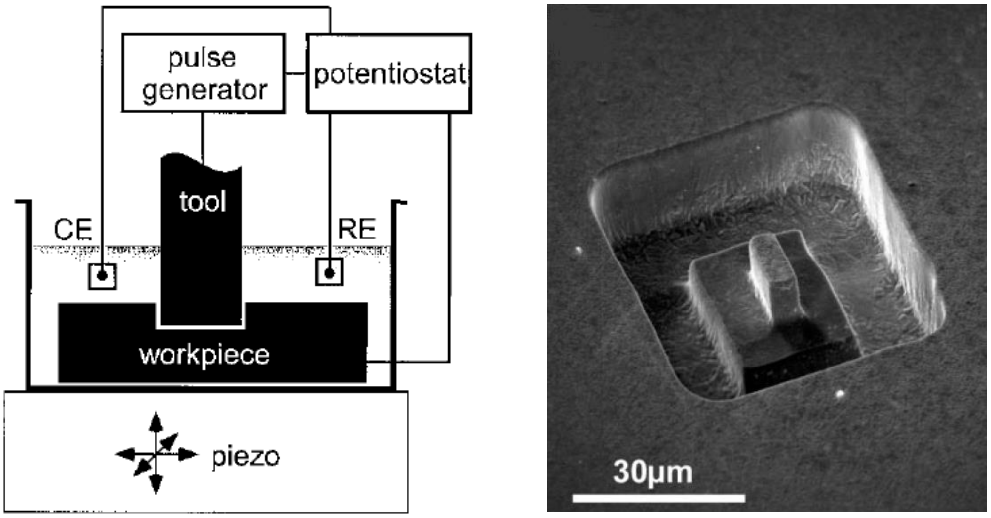

(a) Experiment setup (b) Micro structure

Fig. 1.16 Experiment for ultrashort voltage pulse ECM[49)]

1.6 Micro-electrochemical machining

The term micro-machining means the material removal of small dimension ranging from 1 to 999 μm[25, 47)]. Micro ECM is widely used in the biomedical, semiconductor and automobile industries. It primarily involves the use of micro tools with small working gaps in the order of 5～50 μm and the application of a pulse power supply [15, 19, 20, 21, 48)].The application of ultrashort pulse voltage of only nanosecond duration in ECM can localize the electrochemical dissolution in a submicrometer precision[49)]. The concept of

ultrashort pulse ECM can be illustrated by a simplified equivalent circuit of two electrodes immersed in electrolyte as shown in Fig. 1.15. The electric double layers are formed on the surfaces of the electrodes when the pulse power is applied. The time constant of charging can be expressed as $\tau=RC=\rho dC_{DL,}$ depending on the (local) gap width d between the electrodes, the electrolyte resistivity ρ, and the specific double layer capacity C_{DL}. Hence, with the ultrashort pulse voltage, the double layers will be charged quickly with a small d where the working gap is significantly small. In contrast, the double layers are not charged enough at the place with a large gap width d. The duty factor of the pulse is set to be significantly low, thereby the double layers are initialized during the pulse interval. Therefore, the electrochemical reaction will be sharply localized to the areas with small gap widths.

Table 1.1 General comparison between ECM and Micro-ECM[25)]

Major machining characteristics	Electrochemical machining (ECM)	Micro electrochemical machining (Micro-ECM)
Voltage	10-30 V	<10 V
Current	150-10000 A	<1 A
Power supply	Continuous/pulsed	Pulsed
Frequency	Hz-kHz range	kHz-MHz range
Electrolyte concentration	>20 g/l	<20 g/l
Size of the tool	Large to medium	Micro
Inter-electrode gap	100-600 μm	5-50 μm
Machining rate	0.2-10 mm/min	5 μm/min
Side gap	>20 μm	<10 μm
Accuracy	±0.1 mm	±0.02-0.1 mm
Surface finish	Good, 0.1-1.5 μm	Excellent, 0.05-0.4 μm
Problems due to waste disposal/toxicity	Low	Low to moderate

Experimental verification of the ultrashort pulse ECM was achieved when a Cu substrate was immersed in an electrochemical cell mounted on a piezo-driven x-y-z stage[49)] as shown in Fig. 1.16(a). The micro structure machined into a mechanically polished, electrochemically deposited Cu layer of an electronic board is shown in Fig. 1.16(b), in which a Pt cylinder (a polished Pt wire 10 μm in diameter) was used as tool electrode.

Micro-ECM using the ultrashort pulse appears to be a very promising micromachining technology due to its advantages that include high machining rate, better precision and control, no residual stress, excellent surface finish, and also because it permits machining of chemically resistant materials like titanium, copper alloys, super alloys, and stainless steel, which are widely used in biomedical, electronic and MEMS applications. A general comparison between ECM and Micro-ECM is presented in Table 1.1[25]. Based on the principle described above, the inter-electrode gap and side gap in micro-ECM are significantly small, resulting in higher accuracy. However, the material removal rate of micro ECM is significantly low, because the duty factor is low, as described above. Furthermore, narrow working surface area reduces the volumetric removal rate, as described in Section 1.5.

1.7 Electrical discharge machining[50, 51, 52]

1.7.1 Principle of EDM

Electrical discharge machining (EDM) is one of the non-traditional manufacturing processes, in which the material is removed by melting and/or evaporating of the workpiece due to a series of repeated discharges generated between two electrodes in a dielectric medium (oil, deionized water, air, etc.). By placing the tool electrode oppositely to the workpiece with a distance of several μm to several tens μm, when a high voltage between electrodes is applied, arc discharge with intense heat can be generated at a certain point by the breakdown of the dielectric. The temperature of the arc plasma (around 7000 K) of discharge is so high that the workpiece material can be melt and/or evaporated resulting in a discharge crater on the workpiece surface. The material is removed by accumulation of discharge craters. However, since the tool electrode is heated by the arc plasma while removing material from the workpiece, tool wear is one of the problems in EDM like the conventional machining processes.

In EDM, discharge is generally considered as arc discharge, and it is generated at one spot on electrode surfaces per pulse. Discharge current (current density approaching $10^8 \sim 10^9$ A/m^2) flows through the arc column formed by breakdown of dielectric medium. Super high heat flux, which is generated from the arc column, flows into the local areas on electrode surfaces where the arc column exists. The heat flux melts and/or evaporates the electrode materials. The melted electrode material is removed by and a discharge crater is generated on the electrode surfaces. The removal volume of single discharge is very small and the machining is accomplished by accumulating small discharge craters through rapidly repeated discharges. The formation of discharge and removal of material are illustrated in Fig. 1.17.

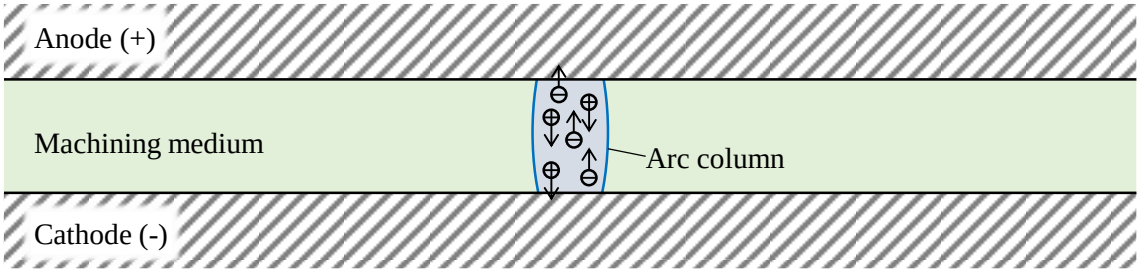

(a) Generation of arc discharge

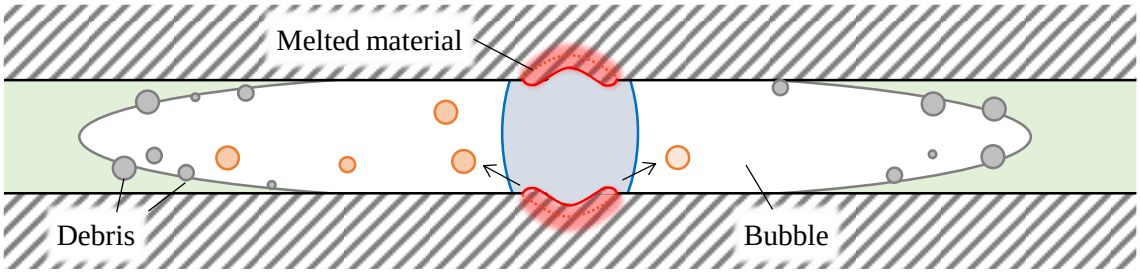

(b) Material removal and generation of bubble

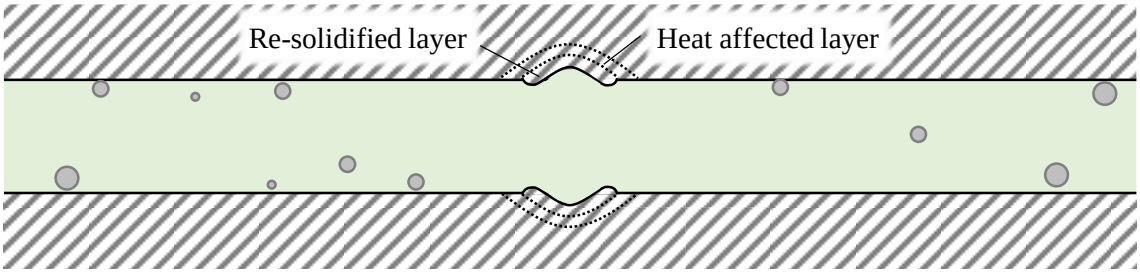

(c) Recovery of dielectric and formation of discharge crater

Fig. 1.17 Illustration of electrical discharge machining mechanism

1.7.2 Categories of EDM

In general, EDM is classified into two main categories, sinking EDM and wire EDM, based on their different specialty and application. Sinking EDM processes are generally used to machine a workpiece by utilizing a reversely shaped tool electrode as shown in Fig. 1.18. Therefore, sinking EDM is widely used in the mold industry and also for machining intricate shapes. On the other hand, wire EDM, as shown in Fig. 1.19, uses a metal wire (brass, zinc coated brass, zinc coated steel, tungsten, etc.)as the tool electrode to cut the workpiece, and the diameter of the wire is about 20 μm～300 μm. Wire EDM can cut extremely thin and flexible metal foils or thick metal plates precisely and easily. Micro EDM is a machining process based on material removal by melting and, partly vaporization[52]. Kawakami and Kunieda[53] studied on the side effect found in micro EDM.

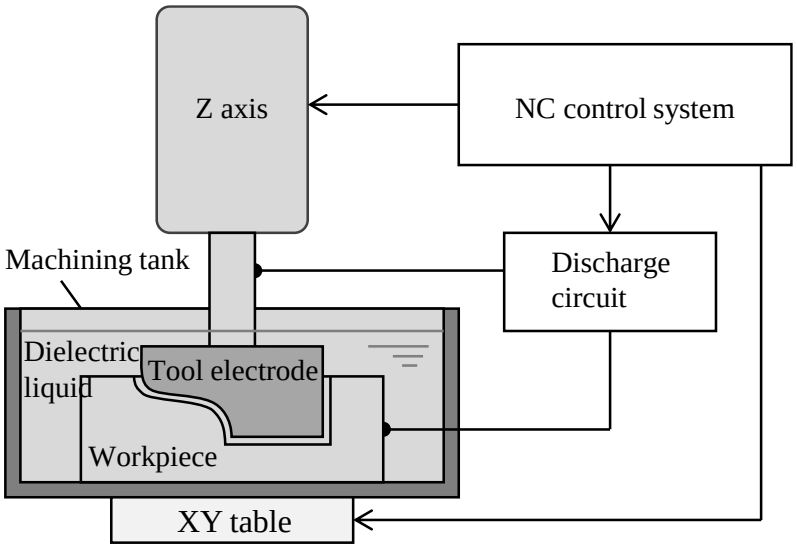

Fig. 1.18 Diagram of sinking electrical discharge machining

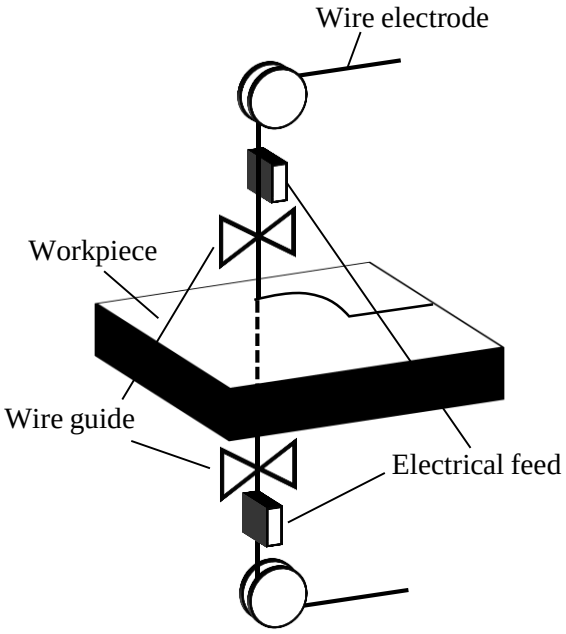

Fig. 1.19 Diagram of wire electrical discharge machining

1.8 Electrical machining using electrostatic induction feeding method

1.8.1 Electrostatic induction feeding EDM

Fig. 1.20[54, 55, 56, 57] shows the principle of the electrostatic induction feeding EDM. In the figure, C_1 is the feeding capacitance of a capacitor inserted in series between the pulse voltage and the tool electrode, or the feeding gap between the feeding electrode and tool

electrode in the case of non-contact electric feeding, and C_2 is the capacitance of the working gap. In this example, C_1 is assumed to be 10 times as large as C_2, and electric charge shown with ⊕ ⊖ is 10 times as large as those shown with + -. A pulse voltage E_0 is applied between the feeding electrode and work piece with a constant pulse duration.

When the voltage of the pulse generator becomes E_0, the capacitances of both the feeding gap C_1 and working gap C_2 are charged. In the working gap, the tool electrode and work piece are charged positive and negative respectively, resulting in a high electric field. Therefore, discharge occurs and electrons are transferred from the workpiece to the tool electrode. Since discharge duration is as short as several tens of nanoseconds, dielectric breakdown strength of the working gap can be recovered immediately after discharge. During the pulse off time, the voltage of the pulse generator becomes 0. Then electrons are displaced to balance the voltage of the feeding gap with the voltage of the working gap. The tool electrode and the work piece are charged negative and positive, respectively. Consequently, discharge occurs with polarity opposite to the previous one, and electrons are translated from the tool electrode to the work piece. Machining is carried out by repetition of the cycle above. Fig. 1.20(b) and (d) show that discharge is bipolar in this method.

Fig. 1.21(a) shows the influence of stray capacitance in the circuit of the relaxation type pulse generator. The stray current determines the minimum electric discharge energy, hence, the limit of miniaturization was difficult to be improved. On the other hand, when the electrostatic induction feeding method is used for micro EDM, the influence of stray current can be eliminated as shown in Fig. 1.21(b) [56]. Kimori et al.[57] were able to decrease the diameter of discharge craters to 0.4 μm with this method, smaller than that of the relaxation type pulse generator by 0.3 μm. Thus, the limit of miniaturization of micro-rod machined by WEDG[57] using this method was 0.8 μm in diameter, smaller than that of the relaxation type pulse generator by 0.1 μm[58]. X.D. Yang[59, 60] obtained a straight micro-beam of 3.8 μm in width and 100 μm in length as shown in Fig. 1.22, by micro WEDM using the electrostatic induction feeding method.

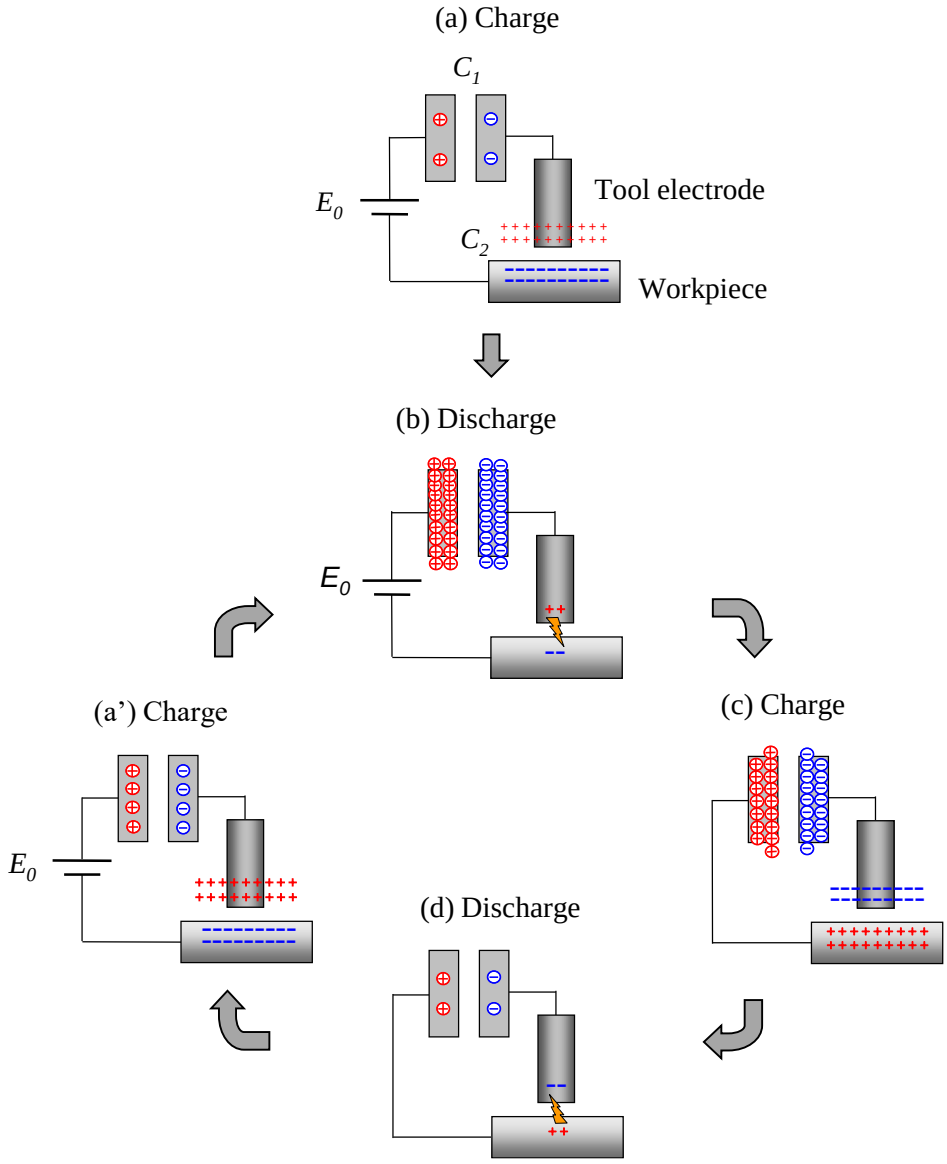

Fig. 1.20 Electrostatic induction feeding method[54, 55)]

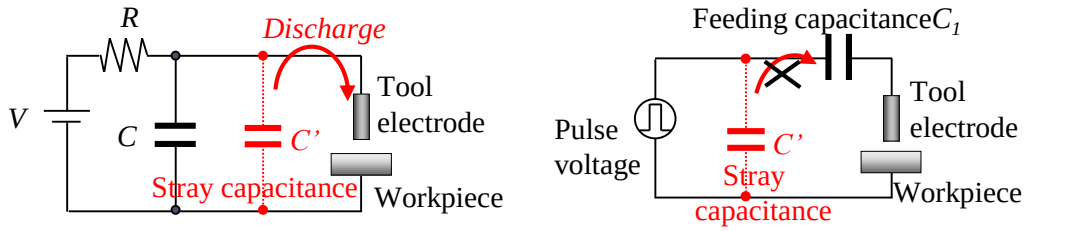

(a) RC discharge circuit (b) Electrostatic induction feeding method

Fig. 1.21 Influence of stray capacitance[56)]

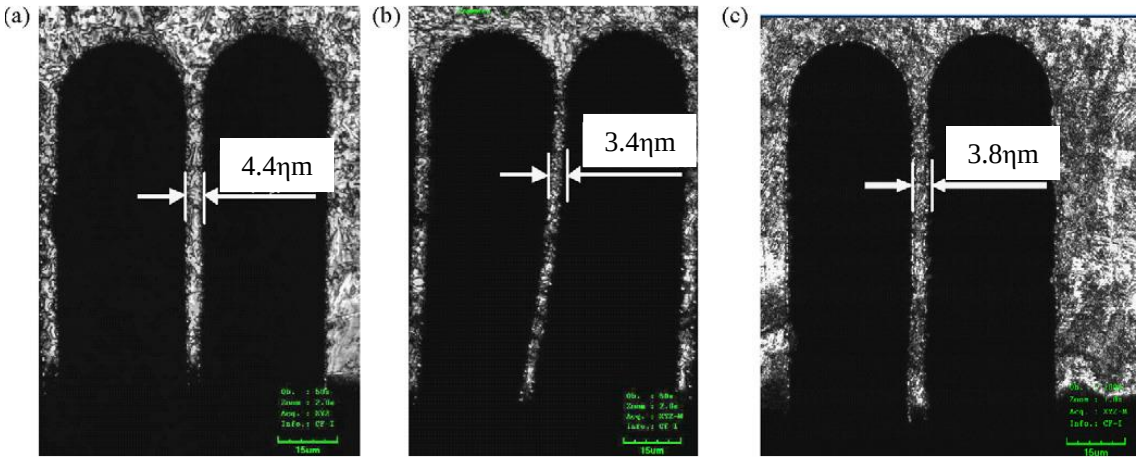

Fig. 1.22 Samples of beams machined by electrostatic induction feeding[59)]

1.8.2 Electrostatic induction feeding ECM

Koyano and Kunieda[61)] applied the electrostatic induction feeding method to ECM as shown in Fig. 1.23. The circuit construction is the same as that used in micro EDM. However, the equivalent circuit of the machining gap shown in Fig. 1.23 is different from that in electrostatic induction feeding EDM. C_{dl} is the capacitance of electric double layer formed on both electrodes, Z_f is the Faraday impedance, and R_g is the resistance of electrolyte in the machining gap.

The current can only flow through the working gap when the pulse voltage changes, because the pulse power supply is coupled to the electrode by the feeding capacitance C_1. Fig. 1.24 shows the waveforms of pulse voltage and current through the machining gap. In contrast to the electrostatic induction feeding EDM, where discharge occurs after an ignition delay time, electrolytic current flows immediately when the pulse voltage is applied to the machining gap. Since the pulse power supply is coupled to the tool electrode by the feeding capacitance C_1, current only flows at the instance when the pulse voltage changes to high or low. Hence, the current pulse duration is nearly equal to the rise and fall time regardless of the pulse on-time of the pulse voltage. In the transient periods, current flows with the polarity of positive of tool electrode when the output voltage of the pulse power supply changes to high in respect to the ground level. On the other hand, it flows with the opposite polarity when the output voltage changes to zero. Hence, electrolytic current is bipolar. In some cases, this may result in the dissolution of the tool electrode when the polarity of the tool electrode is positive. The electric charge q per each pulse is the same for both polarities, and can be expressed using the amplitude of pulse voltage E_0 and the feeding capacitance C_1 as $q=C_1E_0$[61)].

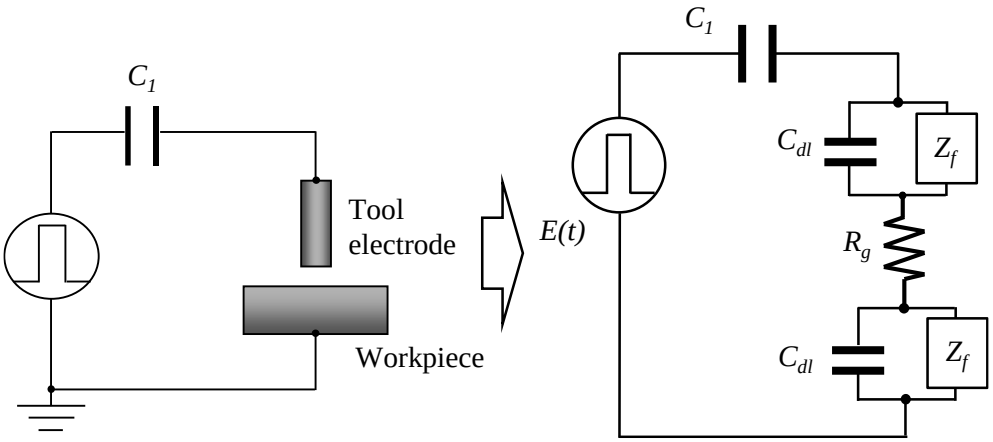

Fig. 1.23 Equivalent circuit of ECM

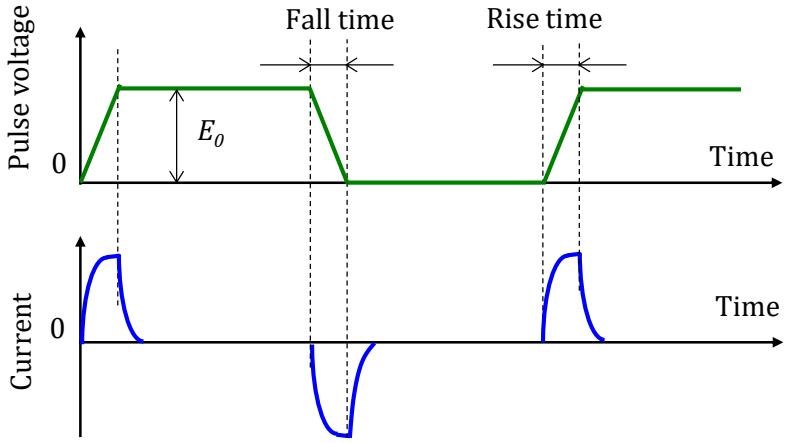

Fig. 1.24 Waveforms of pulse voltage and current

Koyano and Kunieda[61] investigated the influence of the current pulse duration on the machining gap, with the rise and fall time of pulse voltage varied at 20 ns, 40 ns, and 60 ns to change the current pulse duration. In addition, for the rise and fall time of 20 ns, 40 ns, and 60 ns, the amplitude of pulse voltage were varied at 8 V, 20 V, and 40 V, respectively to obtain the same peak current independent of the current pulse duration. Since the feed rate was the same for every pulse duration, it was necessary to equalize the averaged current i_{ave}, which can be expressed as $i_{ave}=qf=C_1E_0f$, where f is the frequency of the pulse voltage. For this reason, f was changed inversely proportionally to voltage amplitude to obtain constant i_{ave}. The machining conditions are shown in Table 1.2. Even though the averaged current and total machining times were the same, the gap width and the removal volume were less with shorter pulse duration, this is because with shorter pulse duration, the dissolution of workpiece could be localized to places where the gap width was smaller. The experimental results show that the machining accuracy increased with decreasing the pulse width, as shown in Fig. 1.25, because the electrochemical

dissolution was localized in a smaller working gap by the shorter pulse current. Here, it is noted that the removal volume was larger with large pulse duration, although the total charge was the same. This is because higher fraction of electric charge was used for charging the electric double layer with shorter pulse duration, resulting in lower current efficiency.

In order to control the narrow working gap of several micrometers, Koyano and Kunieda[61] developed a servo feed system based on the measurement of the gap voltage, using the control system shown in Fig. 1.26. Fig. 1.27 shows the cross sectional shape of a machined micro-hole with the inner diameter of 55 μm and depth of 50 μm using the developed servo feeding system.

Table 1.2 Experimental conditions to investigate the influence of pulse width

Pulse voltage			
Rise/fall time [ns]	20	40	60
Amplitude [V]	8	20	40
Frequency [kHz]	1250	500	250
Duty factor [%]	50		
Feeding capacitance C_1 [pF]	47		
Electrolyte	NaCl aq. 2wt%		
Tool electrode rotation [rpm]	3000		

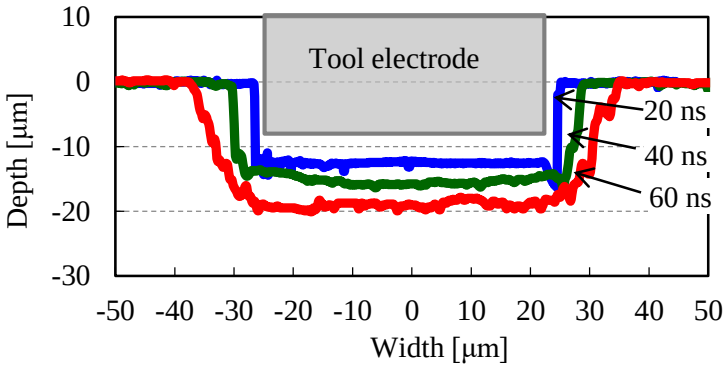

Fig. 1.25 Influence of pulse width on machining accuracy[61]

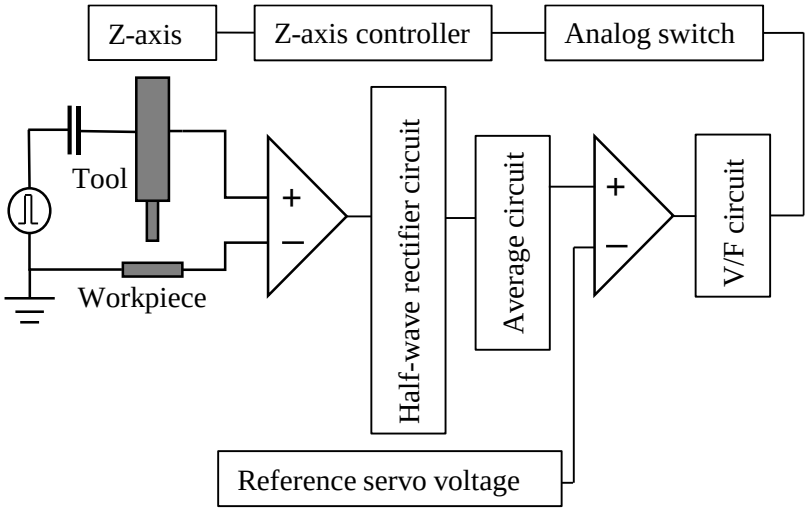

Fig. 1.26 Servo feed control system[61)]

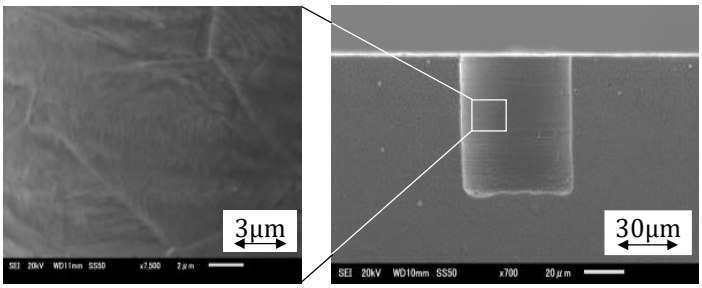

Fig. 1.27 Cross-sectional shape of machined micro-hole using servo feed control system[61)]

1.9 Research purpose

This thesis describes the fundamental research of the electrostatic induction feeding ECM through micro-holes and micro-rods machining. Based on the research results, a hybrid machining system combining the electrostatic induction feeding EDM and ECM in same electrolyte method was proposed to take full advantages of the two machining technologies with the different material removal mechanisms.

The electrochemical reaction can be localized in a gap width of several micrometers with the ultrashort pulse current supplied by the electrostatic induction feeding method. However, collision and discharge between electrodes easily occur, causing a damage on the electrodes. To control the gap width of the electrostatic induction feeding ECM, Koyano and Kunieda[61)] developed a servo feeding control system based on the monitoring of the average gap voltage. However, the average gap voltage was 200 mV or less due to the pulse duration of several tens of ns with significantly low duty ratio. Hence, the gap control accuracy was not sufficiently high with the average gap voltage because of the

low signal to noise ratio (S/N ratio). Subsequently, in this paper, a new servo feeding control system, which compares the peak of the gap voltage with the reference voltage, was developed to improve the response accuracy of the servo feeding control. Then, the machining results were compared with those of micro EDM.

Next, micro-rods were machined using electrostatic induction feeding ECM for the first time. Micro-rods have been widely used as micro tools in micro machining of 3D structures, micro probes in measuring systems, and micro dies/molds. Micro-rods are usually fabricated by wire drawing, turning, grinding, micro electrical discharge machining (micro EDM), laser machining, etc. However, significantly large residual stress is generated by the plastic deformation in the conventional mechanical processes. The thermal processes also suffer from drawbacks such as tool wear and heat affected zone (HAT) on the machined surfaces[53]. Electrochemical machining (ECM) removes material by anodic dissolution that does not produce any residual stress. Hence, ECM is a promising method to fabricate micro-rods.

With the machining of micro-rods, a rotating workpiece rod is fed to a tool electrode plate, in the radial or axial direction to remove the material and fabricate a micro-rod. There are two gaps formed during machining: the axial gap and radial gap. When the tool electrode is fed in the axial direction, the current should be confined in the axial gap for material dissolution, while the current in the radial gap should be eliminated because machining accuracy is deteriorated by the stray current in the radial gap, resulting in the pitting corrosion and tapered shape. Thus, the influences of the thickness and surface area of the tool electrode on the machining characteristics were investigated to improve the machining accuracy. In addition, the dependence of the machining characteristics on the feeding directions of the workpiece in axial and radial directions was also researched. So far, there are many reports on micromachining of micro-rods using EDM. However, there are few papers about micro ECM of micro-rods. It has been believed that the ability of micromachining of ECM cannot compete with that of EDM. Thus, the present research first investigated the machining characteristics of ECM of micro-rods in details, using the electrostatic induction feeding method and compared the results with those of micro EDM.

The workpiece rod used was cut from a reel of stainless steel wire. Considering the fabrication of the wire by drawing, there may exist some residual stress and some other defects in the micro structure, which may deteriorate the machining accuracy. Hence, the influence of annealing process of workpiece on the machining characteristics was investigated.

In addition, the electrolytes in ECM are classified into two categories: passivating electrolytes containing oxidizing anions such as sodium nitrate, sodium chlorate, and non-

passivating electrolytes containing relatively aggressive anions such as sodium chloride. Passivating electrolytes generally give better machining precision. Hence, the influences of different kinds of electrolyte, sodium chloride (NaCl) and sodium nitrate ($NaNO_3$) aqueous solution, on the accuracy and limit of miniaturization in rod machining were investigated. There are many papers which investigated the influence of the kinds of electrolyte on the machining characteristics of ECM. However, there are few reports on the dependence of machining characteristics on kinds of electrolyte in micro ECM.

Electrochemical reaction is significantly different depending on the kind of materials used for the workpiece. Therefore, there are some materials which are difficult to machine by ECM even though they are electrically conductive. For example, novel metals such as Au or Pt cannot be machined by ECM. Tungsten, niobium, and titanium are difficult to be machined because oxide film is generated on the surface. However, these materials are promising materials to be used for micro tools, micro-machines, micro-probes and so on. Hence, the influences of different kinds of materials on the machining characteristics were researched with the electrostatic induction feeding ECM. It is known that bipolar current is needed for the machining of tungsten using a neutral electrolyte[62]. However, the use of bipolar current results in the tool wear. Thus, the influences of machining parameters on the tool wear rate were investigated. Moreover, the machining characteristics of the high-speed steel (SKH51) and cemented tungsten carbide were also researched.

In addition, electrical discharge machining (EDM) is one of the most efficient machining processes for conductive materials. The process, based on the electro-thermal erosion of metallic materials, can be used for any difficult-to-machine material regardless of its density, toughness, or hardness. However, since EDM is a thermal process, the machined surface is characterized by recast layers, including cracks and residual tensile stresses. In contrast, electrochemical machining (ECM) relies on the mechanism of anode electrochemical dissolution to remove material, with the advantage that the machined surface has no recast layers and is free of residual stress and micro-cracks. Thereby, exploiting the advantages of these two processing technologies, a hybrid system of EDM and ECM, which can switch EDM and ECM modes using the same setup and electrolyte, was developed to achieve both high machining efficiency and high surface quality. There are some papers which tried to develop the hybrid machining system[63, 64]. However, they changed the working liquid or the condition of the electrolyte to switch between the EDM mode and ECM mode. It is noted that this research proposed a new hybrid system which can switch the modes using the same electrolyte. In Nguyen's research, the same machining medium was used for the hybrid machining method, and the working gap is filled with low-resistivity deionized water, which exhibits both characteristics of a

dielectric fluid and a slightly conductive electrolyte. Hence, when the working gap meets the critical value, the discharge takes place. However, because of the low conductivity of deionized water, the material removal rate in ECM process was significantly low with this method. With the method proposed in this thesis, the high conductivity electrolyte such as the $NaNO_3$ aqueous solution of 6wt% in concentration was used as the machining medium resulting in a high material removal rate in the ECM process.

1.10 Dissertation structure

This dissertation consists of eight chapters.

In Chapter 1, Introduction, the principle and gap phenomena of electrochemical machining (ECM) were introduced. The influences of many important factors, such as gap control and status monitoring, electrolyte, tool electrode manufacturing and so on, on the machining characteristics of the ECM process were explained. In addition, the electrostatic induction feeding methods developed for electrical machining processes: EDM and ECM, were introduced, and their principles were explained. The problems to be solved in micromachining technologies using the electrostatic induction feeding ECM were summarized and the research purposes were described.

In Chapter 2, Theory of electrostatic induction feeding micro-ECM is explained. The influences of fundamental parameters: gap width and feeding capacitance on the gap current are calculated to verify the theory. Then the experimental equipment used for the electrostatic induction feeding micro-ECM is explained.

In Chapter 3, a servo feed control system for electrostatic induction feeding micro-ECM is developed. It is shown that the servo feeding control system with the peak voltage method has higher control sensitivity of the working gap width compared with the conventional average voltage method, because of higher S/N ratio. The machining characteristics with different reference voltages are investigated. Then, through-holes of 50μm in diameter are machined on a stainless steel (SUS304) plate of 50μm in thickness to shown the availability of the system.

In Chapter 4, micro-rods are fabricated with the electrostatic induction feeding ECM. There are two methods to machine the micro-rod, according to the feeding of workpiece in axial or radial direction. With the feeding of workpiece in axial direction method, the influences of the thickness and surface area of the tool electrode are investigated, and the current distribution in the gap is calculated with the COMSOL Multiphysics. With the feeding of workpiece in radial direction method, the micro-rods with different feed distances in radial direction are machined and the material removal process is also simulated using the COMSOL Multiphysics. Then, the differences between the feeding

of workpiece in axial and radial direction methods are compared. At last, the machining characteristics of the electrostatic induction feeding ECM are compared with those of micro EDM.

In Chapter 5, to improve the machining accuracy of micro-rod, at first, the influence of the annealing process of the workpiece on the machining characteristics is investigated, considering that the workpiece rod was produced by wire drawing. Then, the machining characteristics of different electrolytes, NaCl and $NaNO_3$ aqueous solutions, are researched.

In Chapter 6, the influences of different workpiece materials on the machining characteristics are investigated, including the materials of tungsten, high-speed steel (SKH51) and tungsten carbide. The tool wear during the tungsten machining is researched, because bipolar current is needed with a neutral electrolyte to machine tungsten resulting in the wear of the tool electrode.

In Chapter 7, a hybrid micromachining system combining the electrostatic induction feeding EDM and ECM in the same electrolyte is proposed by utilizing the passive oxide layer formed on the surface of tungsten electrode. First, the principle to switch the EDM and ECM modes is explained. Then, a rough machining with the EDM mode and finishing machining with the ECM mode are conducted in sequence using the electrolyte of $NaNO_3$ aqueous solution of 6wt%.

In Chapter 8, the main achievements are summarized as the final conclusions of this thesis. The remaining research subjects and the perspective of future research work that are related to this thesis are discussed.

Chapter 2 Theory and experimental equipment of electrostatic induction feeding Micro-ECM

2.1 Introduction

In micro electrical discharge machining (EDM), one of the factors which determine the limits of miniaturization is the discharge crater size. In order to obtain smaller discharge craters, the electric discharge energy per pulse must be reduced as much as possible. In conventional micro EDM, the relaxation type pulse generator is generally used. If capacitance of the capacitor becomes closer to zero, the discharge energy is expected to decrease infinitesimally. In the actual EDM machine, however, stray capacitance exists between the electric feeders, between the tool electrode holder and work table, and between the tool electrode and work piece. Hence, even if the capacitor is not wired, machining can be conducted with the stray capacitance. This means that the minimum electric discharge energy per pulse is determined by the stray capacitance, indicating a limit to miniaturization[52, 53]. Therefore a new pulse generator using the capacity coupling method was developed[54, 55, 56, 57]. With this method, since the feeding capacitance can be placed closely to the discharge gap, the influence of the stray capacitance in the circuit can be eliminated, thereby realizing discharge craters of nanometer order. In addition, since non-contact electric feeding is possible, this method enables non-contact feeding to a high speed rotating spindle, air bearing spindle and magnetic bearing spindle without causing vibration of the spindles.

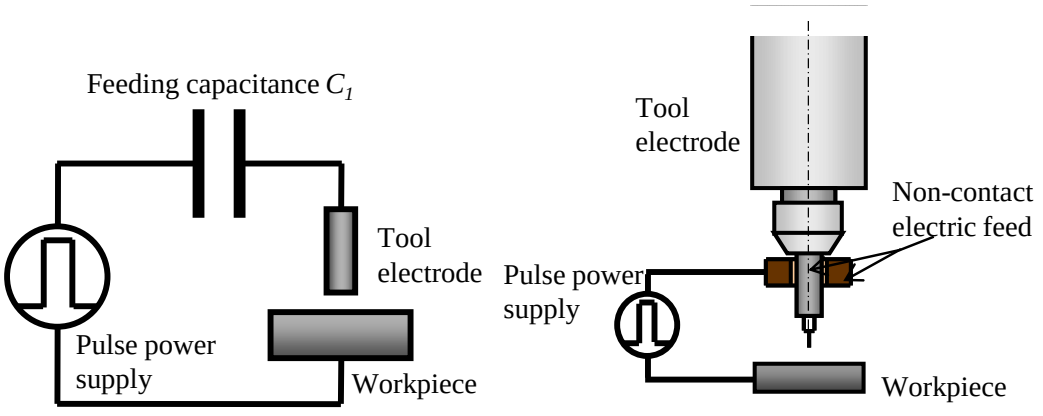

(a) Basic circuit (b) Non-contact electrostatic induction feeding ECM

Fig. 2.1 Electrostatic induction feeding ECM

Then, Koyano et al. [61] used the electrostatic induction feeding method to micro ECM. Fig. 2.1(a) shows the basic circuit of the electrostatic induction feeding ECM. Since the pulse power supply is coupled to the working gap by a feeding capacitance, the current can only flow through the working gap when the pulse voltage is changed. Ultra-short pulse current can be easily obtained by controlling the rise and fall time of the pulse power supply, and without considering the pulse duration time. If the capacitance C_1 is replaced by the gap between the ring shaped feeding electrode and the rotating spindle as shown in Fig. 2.1(b), the tool electrode can be rotated with a high rotation speed because of the non-contact feeding of electric charge to the tool electrode.

This chapter describes the theory of the electrostatic induction feeding ECM, including the influences of the gap resistance and feeding capacitance on the gap current. Then the experimental equipments were introduced.

2.2 Principle of electrostatic induction feeding method

2.2.1 Equivalent circuit

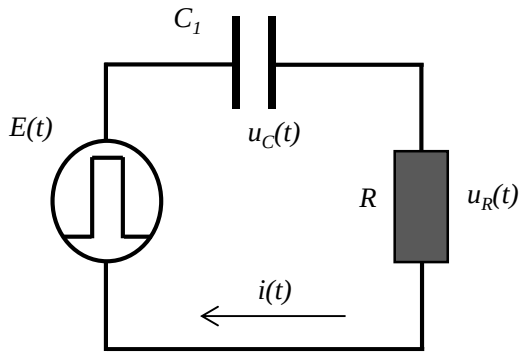

Fig. 2.2 Equivalent circuit used for calculation.

The electrostatic induction feeding method, as shown in Fig. 2.1, can be simplified as the equivalent circuit shown in Fig. 2.2[61]. Harada and Natsu[65] and Kadokura and Natus[66] reported that the gap width can be controlled using the peak current in the transient state of the current pulse because the capacitance of electric double layer C_{dl} and Faraday impedance Z_f can be ignored in the equivalent circuit as shown later in Fig. 3.14.The working gap is expressed by a gap resistance R, and $u_R(t)$ is the gap voltage as shown in Fig. 2.2. C_1 is the feeding capacitance, and $u_c(t)$ is the capacitance voltage. $E(t)$ is the pulse voltage supplied by a function generator. $i(t)$ is the current flowing through the working gap.

2.2.2 Influence of gap resistance

In ECM process, the gap resistance is determined by the gap width, and smaller gap width results in higher machining accuracy. Hence, the gap voltage and current depending on the gap resistance were calculated with the electrostatic induction feeding method. Since the current mainly flows during the rise/fall time of the pulse voltage and is cut off within the pulse duration time, the gap voltage was calculated in two steps. The pulse voltage used in this calculation is shown in Fig. 2.3. The total amplitude and rise/fall time were 20 V and 40 ns, respectively, as shown in Table 2.1.

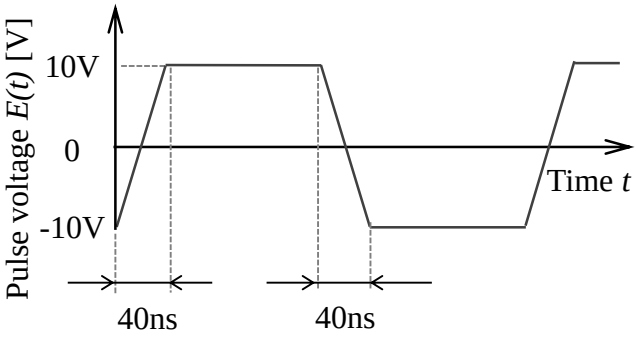

Fig. 2.3 Pulse voltage used for calculation

Table 2.1 Parameters of pulse voltage

Amplitude [V]	20
Frequency [Hz]	500k
Duty factor [%]	50
Rise/fall time [ns]	40

Step 1: At the rise/fall time of pulse voltage

According to the equivalent circuit in Fig. 2.2,

$$i(t) = C_1 \frac{d(u_c(t))}{dt} = C_1 \frac{d(E(t) - u_R(t))}{dt} = C_1 \frac{d(E(t))}{dt} - C_1 \frac{d(u_R(t))}{dt}$$

where, C_1 is the feeding capacitance.

At the rise and fall time of the pulse voltage, $\frac{d(E(t))}{dt}$ is a constant, and equals to A. Then

$$i(t) = AC_1 - C_1 \frac{d(u_R(t))}{dt}$$

In addition,

$$i(t) = \frac{u_R(t)}{R}$$

Then

$$\frac{u_R(t)}{R} = AC_1 - C_1\frac{d(u_R(t))}{dt}$$

The solution of the differential equation is

$$u_R(t) = AC_1R(1 - e^{-\frac{t}{C_1R}})$$

Step 2: within the pulse duration time

From the equivalent circuit

$$i(t) = C_1\frac{d(u_c(t))}{dt} = C_1\frac{d(E(t) - u_R(t))}{dt} = C_1\frac{d(E(t))}{dt} - C_1\frac{d(u_R(t))}{dt}$$

When, pulse voltage is constant, $\frac{d(E(t))}{dt}$ =0

Then

$$i(t) = -C_1\frac{d(u_R(t))}{dt}$$

In addition,

$$i(t) = \frac{u_R(t)}{R}$$

Then

$$-C_1\frac{d(u_R(t))}{dt} = \frac{u_R(t)}{R}$$

If *P(t)* is defined as,

$$P(t) = -\frac{1}{u_R(t)} \times \frac{d\big(u_R(t)\big)}{dt} = \frac{1}{C_1R}$$

The general solution of the differential equation is expressed as

$$u_R(t) = \mathrm{B}e^{-\int P(t)dt}$$

$$u_R(t) = \mathrm{B}e^{-\int\frac{1}{C_1R}dt} = \mathrm{B}e^{-\frac{t}{C_1R}}$$

When *t*=0

$$u_R(0) = \mathrm{B}$$

And $u_R(0)$ can be obtained in step 1, then the solution of the differential equation is

$$u_R(t) = u_R(0)e^{-\frac{t}{C_1R}}$$

The gap voltage $u_R(t)$ was calculated under the conditions: C_1=47 pF. The value of C_1 was selected so that the stray capacitance in the circuit, which is assumed to be around 10pF[56], can be ignored compared to C_1. The gap resistance *R* was calculated to be 250 Ω, 300 Ω, and 350 Ω[61, 62], assuming that the end of a rod tool electrode with a diameter of 50 μm was positioned over the workpiece at a gap width of 1.39 μm, 1.67 μm, and 1.94

μm, respectively, in NaCl aqueous solution of 2 wt% in concentration. Fig. 2.4 shows the calculated gap voltages and currents with different gap resistances. The gap voltage is higher and the gap current is lower with larger gap resistance. Based on this result, Koyano and Kunieda[61] developed a servo feed system for the eloectrostatic induction feeding ECM. Since the electric charge per pulse $q=C_1E_0$ is constant with the electrostatic induction feeding method, longer pulse duration results in lower peak value of gap current as shown in Fig. 2.4(b). Fig. 2.5 shows the gap current and voltage waveforms with the gap width of 3 μm, under the pulse voltage conditions shown in Table 2.1. It is found that the experimental results agree with the calculated gap current and voltage.

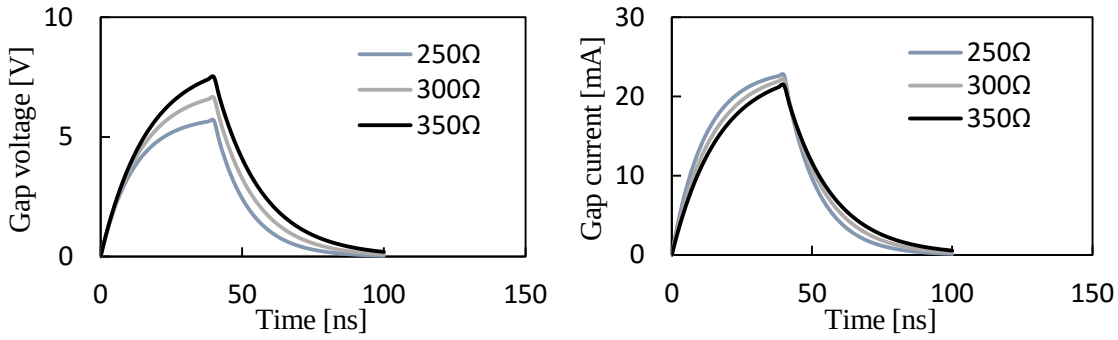

(a) Gap voltage (b) Gap current

Fig. 2.4 Gap voltage and current with different gap resistances

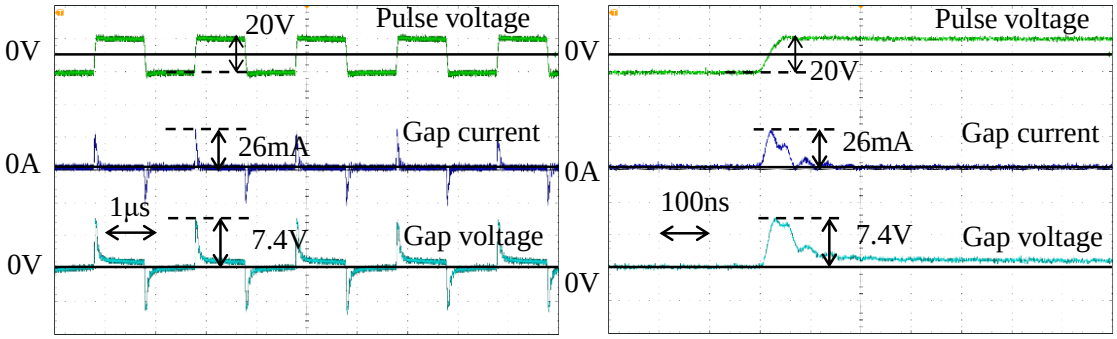

Fig. 2.5 Waveforms of gap current and voltage with gap width of 3 μm

2.2.3 Influence of feeding capacitance

Using the calculation method described in Section 2.2.2, the gap voltage and current with feeding capacitances of C_1=47 pF and 68 pF were calculated as shown in Fig. 2.6. It was assumed that the gap width is 1.67 μm, resulting in the gap resistance of 300 Ω. The gap voltage and current increased with increasing the feed capacitance C_1 because $q=C_1E_0$.

Fig. 2.7 shows the gap current and voltage measured with the feeding capacitance of 68 pF, which were similar with the calculated results shown in Fig. 2.6.

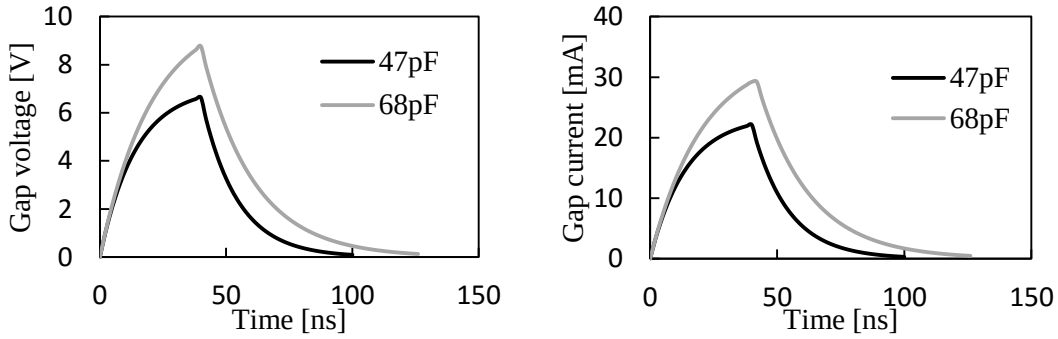

Fig. 2.6 Gap voltage and current with feeding capacitance C_1= 47 pF and 68 pF

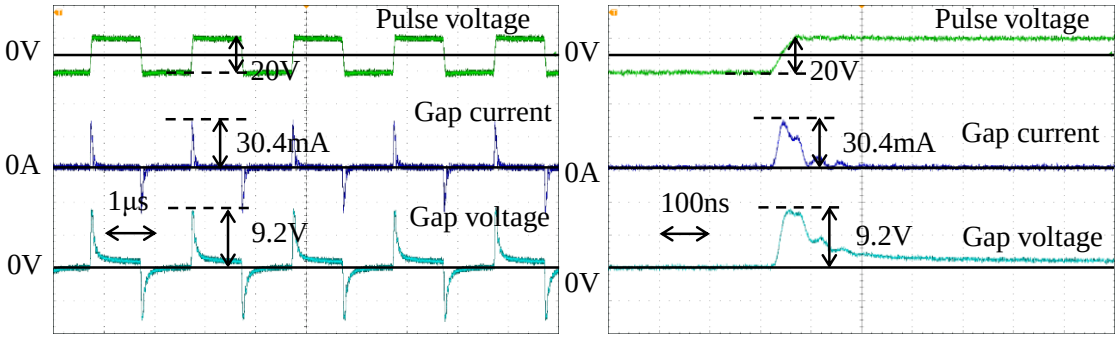

Fig. 2.7 Waveforms of gap current and voltage with feeding capacitance C_1= 68 pF

2.3 Experimental equipment of electrostatic induction feeding Micro-ECM

2.3.1 Machine tool

A micro EDM machine (Panasonic, MG-ED72W) shown in Fig. 2.8 was refitted to be used for electrochemical machining. Positioning of the table has a resolution of 0.1 μm in x, y and z axis direction, respectively. The feed speed of x, y and z axis is from 0.1 μm/s to 12 mm/s, driven by a ball screw and stepper motor.

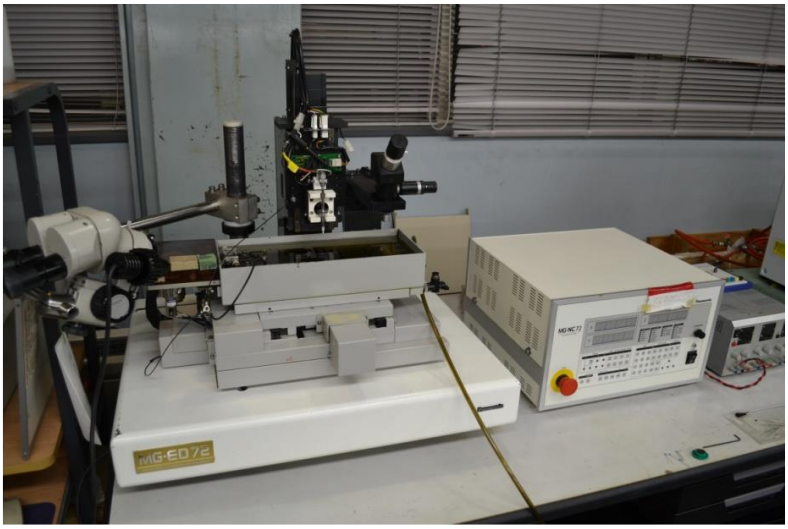

Fig. 2.8 Micro EDM machine MG-ED72W

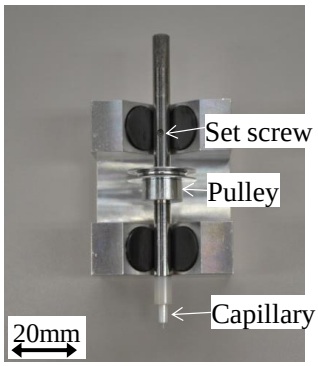

(a) Holder of rod electrode

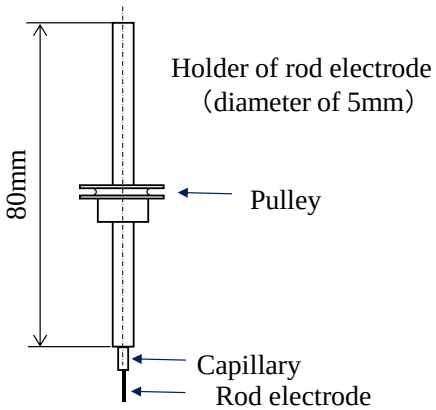

(b) Overview of rod electrode holder

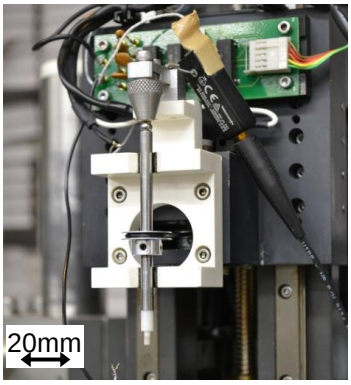

(c) Holding mechanism of rod electrode

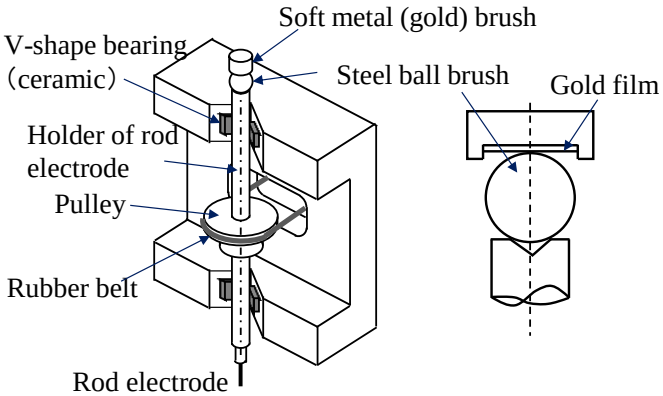

(d) Overview of rod holder and rotation mechanism

Fig. 2.9 Holder and rotation mechanism of tool electrode

2.3.1.1 Holding mechanism of tool electrode

Fig. 2.9 shows the holder and rotation mechanism of rod electrode. Fig. 2.9(a) and (b) show the holder of rod electrode. A capillary is inserted into the holder, and the inner diameter of the capillary is the same as the diameter of rod electrode. The rod electrode is precisely guided by the capillary at the rotation axis, which is fixed to the holder using the set screw shown in Fig. 2.9(a). Fig. 2.9(c) and (d) show the rotation mechanism of the rod electrode. The holder is supported by V-shape bearings of which the material is ceramic. The holder is rotated by a rubber belt hooked on the pulley attached to the holder. The holder can be rotated up to 4000 rpm with sufficiently small runout under 0.5 μm. The electric current is supplied to the rod electrode using a brush composed of a steel ball and soft metal made of gold as shown in Fig. 2.9(d).

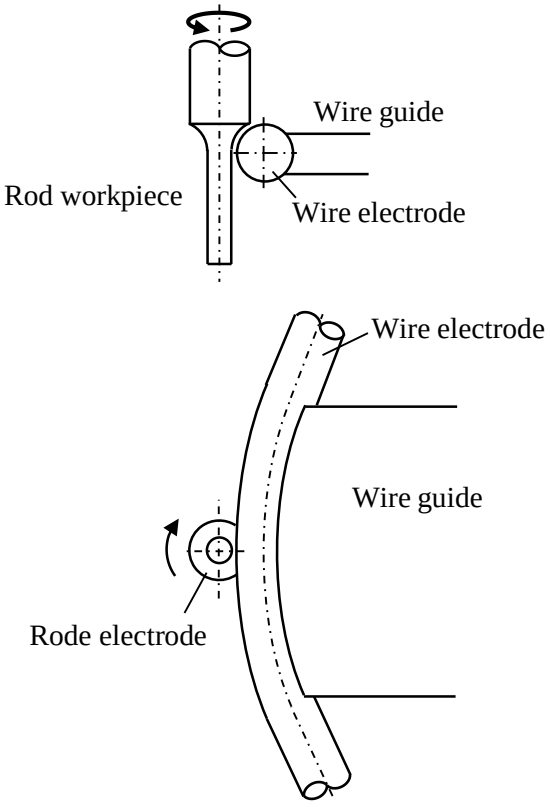

Fig. 2.10 WEDG method[58)]

2.3.1.2 WEDG method[58)]

In this research, the rod electrode was prepared by wire electro-discharge grinding (WEDG) method[58)] equipped on the micro EDM machine (Panasonic, MG-ED72W). The WEDG method shown in Fig. 2.10 was developed by Masuzawa et al. to machine very thin rods. Since the traveling wire is used as the tool electrode, influence of the tool wear on machining accuracy can be eliminated. Furthermore, since the wire electrode is guided

by the wire guide, there is no concern of wire vibration like the wire EDM, in which the wire electrode is stretched straight between the upper and lower wire guides as shown in Fig. 1.19. Very thin rods can be machined by WEDG without a skill of experienced operators. It is possible to fabricate a straight micro rod with a diameter smaller than 10 μm. Hence, it is suitable to prepare the tool electrode for drilling, and the workpiece used for rod machining described later in Chapter 4.

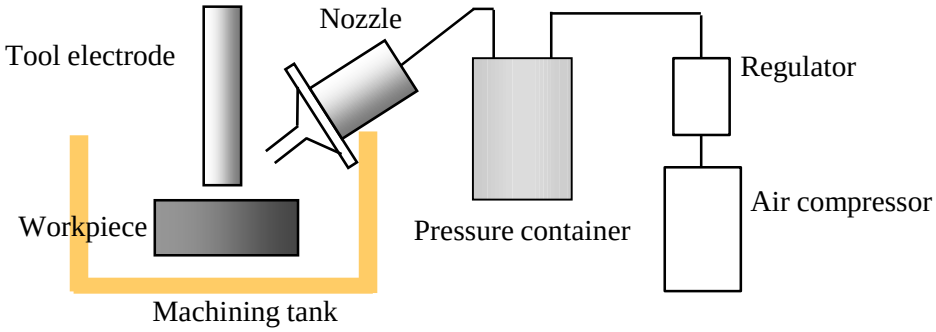

(a) Electrolyte supply

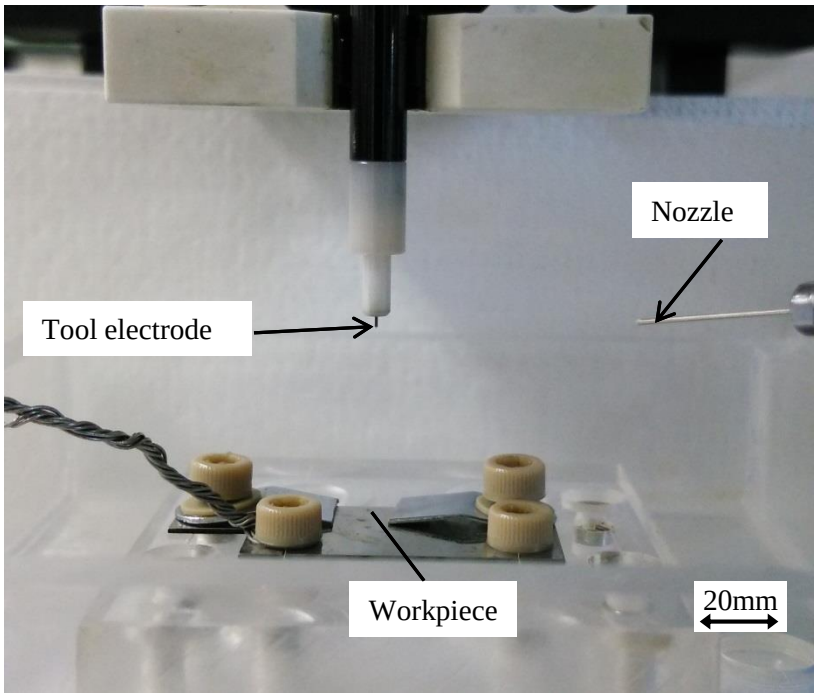

(b) Machining tank

Fig. 2.11 Electrochemical machining cell

2.3.2 Electrolyte supply

To refit the micro EDM machine (Panasonic, MG-ED72W) for electrochemical machining, an electrolyte supply was equipped as shown in Fig. 2.11. The electrolyte was

jetted into the working gap by a nozzle, of which the inner diameter was 200μm. When a micro hole is drilled, a micro rod tool electrode is held as mentioned above, and the workpiece is fixed on the bottom of the tank as shown in Fig. 2.11(b). The electrolyte is stored in a pressure container which is connected to the air compressor.

2.3.3 Power supply

2.3.3.1 Feeding capacitance C_1

The Feeding capacitance C_1 connects between the pulse voltage and tool electrode as shown in Fig. 2.1. Since it should work stably at a high frequency, a mica capacitance was used in this research. The selected mica capacitance and parameters are shown in Fig. 2.12 and Table 2.2.

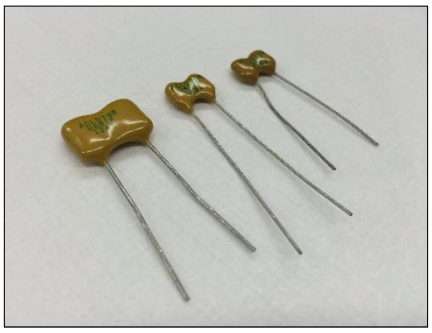

Fig. 2.12 Mica capacitance

Table 2.2 Parameters of feeding capacitance C_1

Capacitance tolerance	+-0.5 pF where C<50 pF
	+-1% where C>50 pF
Temperature range	-40 ℃ to 85 ℃
Maximum voltage	500 V DC
Insulation resistance	100 G for C<10000 pF

In addition, the current and voltage during machining were measured with the oscilloscope of Tektronix DPO4104, which has 1 GHz bandwidth and 5 GS/s sample rate on all channels. The 10X passive probe of P6139A (Tektronix production) was used to measure the voltage signal, and its system bandwidth (-3 dB) was 500MHz. The AC current probe CT1 (Tektronix production) was used to measure the current, and its bandwidth was 25 kHz to 1 GHz and rise time was 350 ps.

2.3.3.2 Function generation

The function/ arbitrary waveform generator (Agilent, 33250A) was used to generate pulse voltage for the electrostatic induction feeding method. Pulse waveforms, like sinusoidal, square, ramp, etc. can be output from the function generator. Since the

maximum amplitude of the output voltage is 10 V, the output was amplified by the bipolar amplifier. The key parameters of the function generator are listed in Table 2.3.

Table 2.3 Parameters of function generator 33250A

Standard	Sine, Square, Pulse, Ramp, Noise Sin(x)/x, Exponential rise, Exponential Fall, Cardiac, DC volts
Bandwidth	1 μHz～80 MHz
Output voltage	$10mV_{pp}$～$10V_{pp}$

2.3.3.3 Bipolar amplifier

Since the maximum amplitude of the output voltage with the function generator (Agilent, 33250A) cannot satisfy the requirement of the experiment, a high speed bipolar amplifier (NF Corporation HSA4101), as shown in Fig. 2.13, was used to amplify the pulse signal from the function generator. The highest bandwidth of the high speed bipolar amplifier is 10MHz, and other key parameters are listed in Table 2.4.

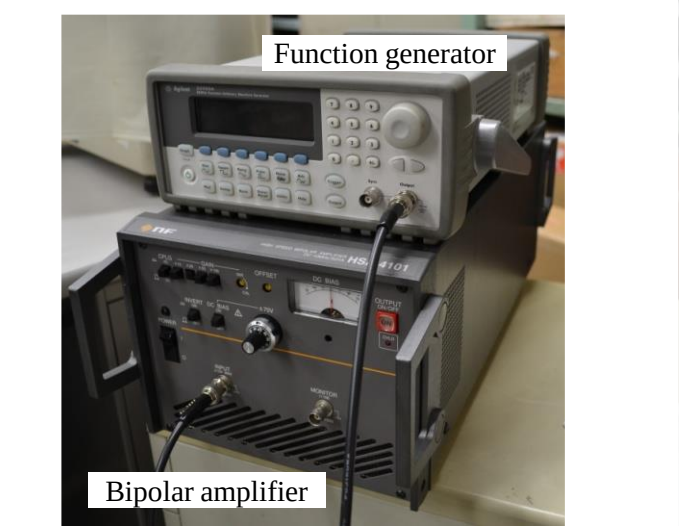

Fig. 2.13 Function generator and bipolar amplifier

Table 2.4 Parameters of bipolar amplifier HSA4101

Bandwidth	DC-10 MHz
Maximum voltage	±71 V ($142V_{pp}$)
Maximum current	±1.4 A
Conversion rate	5000 V/μs

2.4 Example of micro-hole machining

A preliminary experiment of micro-hole machining was conducted using tungsten rod electrode of 50 µm in diameter. The machining conditions are shown in Table 2.5. The tool electrode was positioned over the workpiece with an initial gap width of 3 µm by using the contact sensing function of the micro EDM machine used. The servo feed system with the average gap voltage method, which is described later in Chapter 3, was used. The reference voltage was 140 mV, and feed distance was 50 µm from the surface of the workpiece. The machined hole and cross section are shown in Fig. 2.14. The cross section shape was measured using a laser confocal microscope (Olympus, OLS3000). Although the side surface was not measured correctly, the depth of the hole was measured precisely. Since the depth of the hole was 55 µm, it is found that the working gap width on the bottom surface was about 5 µm. The z-axis displacement of the tool electrode during machining is shown in Fig. 2.15. The total machining time was 23 minutes, and average feed speed was 0.038 µm/s.

Table 2.5 Machining conditions used for micro-hole machining

Pulse voltage	Amplitude [V]	20
	Frequency [Hz]	500 k
	Duty factor [%]	50
	Rise/fall time [ns]	40
Feeding capacitance C_1 [pF]		47
Electrolyte		NaCl aq. 2wt%
Tool electrode rotation [rpm]		3000

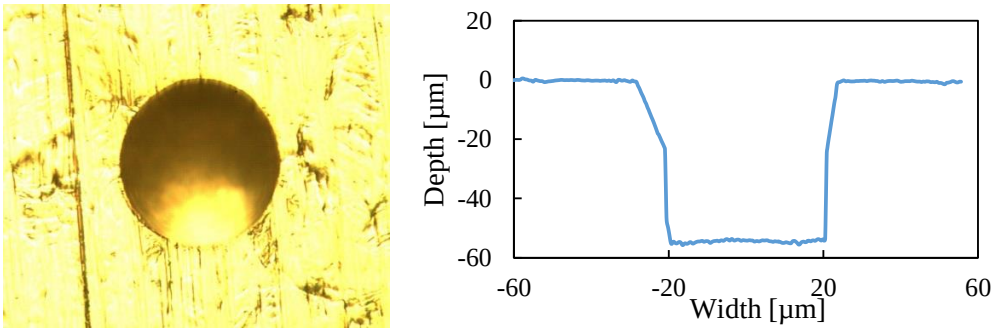

(a) Micro hole (b) Cross section shape

Fig. 2.14 Micro hole and cross section shape measured using laser confocal microscope

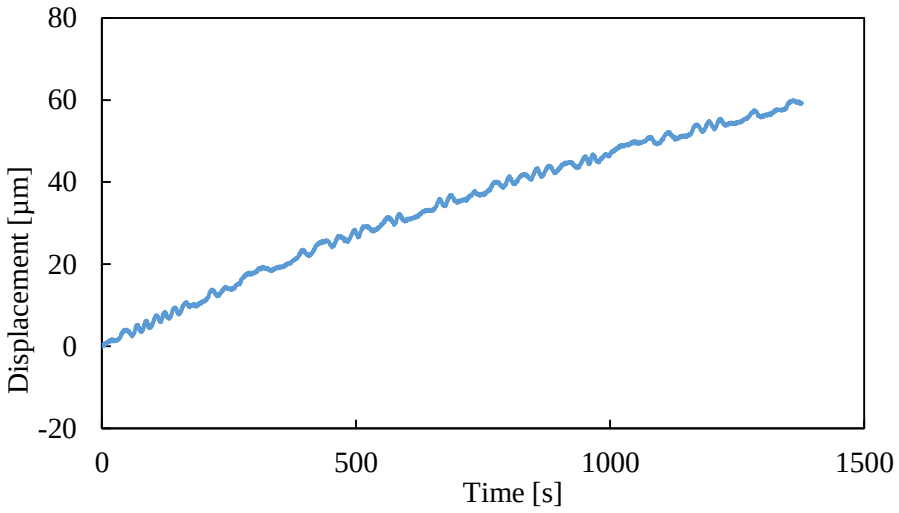

Fig. 2.15 Feed displacement of tool electrode in z-axis

2.5 Conclusions

In this chapter, the theory of the electrostatic induction feeding ECM and the experimental equipments were introduced. The gap current with different gap widths and feeding capacitances were calculated, and compared with the waveforms measured in the experiment. The calculation results verified that the gap current decreases with larger gap width due to the larger gap resistance. The gap current increases with increasing the feeding capacitance because the electrical charge per pulse $q=C_1E_0$ is constant. Then, the experimental equipments of electrostatic induction feeding ECM was introduced, including machine tools, feeding capacitance and power supply. In addition, a micro-hole was drilled with the electrostatic induction feeding ECM as a preliminary experiment. The bottom gap width was 5 μm, which is equivalent but not less compared to that of micro EDM.

Chapter 3 Servo feed control of electrostatic induction feeding micro-ECM

3.1 Introduction

Electrochemical machining (ECM) has many advantages over traditional machining methods such as applicability regardless of material hardness, no tool wear, high material removal rate, smooth and bright finish, and good machinability of complex geometries. Hence, ECM is an effective method for producing turbine blades, engine castings, dies and molds, etc., compared with many other traditional machining methods. However, further research needs to be carried out on the improvement of this machining method. The electrochemical dissolution in the side gap cannot be easily prevented, which generates taper shapes deteriorating accuracy. Furthermore, the generation of dissolution products and bubbles, and temperature rise due to Joule heating result in non-uniform electrochemical dissolution in the frontal gap. The improvement of the machining accuracy is thus a challenging task. Pulse ECM is an effective method for improving the machining accuracy[3, 19, 22, 48, 67]. In recent years, the machining accuracy of micro-ECM continues to improve with the use of ultra-short voltage pulses ranging from several ns to several tens of ns, achieving machining precision in the micrometer order[18, 49]. This technique utilizes the electric double layers formed on the surface of the electrodes. The electrochemical reaction can be confined to a significantly narrow gap between the tool electrode and workpiece, where the time for charging the double layers is very short. With large gap widths, since the gap resistance is large, the large time constant of charging the double layers delays the electrochemical dissolution. Hence, the EC machining can be confined to small gap widths by turning off the pulse voltage before the electric double layers are formed in the large gap width.

To control the gap width of several micrometers with the electrostatic induction feeding ECM, Koyano and Kunieda[61] developed a servo feed control system based on the measurement of the gap voltage. It is difficult to servo feed the tool electrode in normal ECM processes because the change in the gap voltage is insensitive to the gap width. In normal ECM processes, where DC current or comparatively long pulse duration is used, the ohmic voltage drop in the electrolyte is not dominant in the total potential drop in the ECM gap as shown in Fig. 1.3, because the influences of the over potentials are significant. On the other hand, in the electrostatic induction feeding ECM, they found that the gap voltage is proportional to the gap width. Thus, they made a success to servo control the

gap width by comparing the average gap voltage with the reference voltage. However, the average gap voltage was 200 mV or less due to the pulse duration of several tens of ns with significantly low duty ratio as shown in Fig. 3.1. Hence, the gap control accuracy was not sufficiently high with the average gap voltage because of the low signal to noise ratio (S/N ratio). Subsequently, in this research, a new servo feed control system, which compares the peak of the gap voltage with the reference voltage, was developed to improve the response accuracy of the servo feed control.

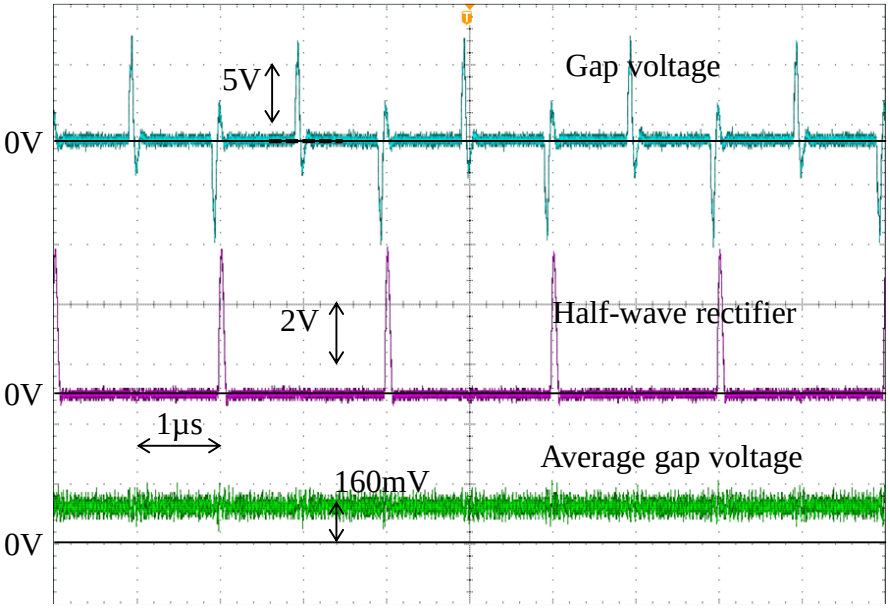

Fig. 3.1 Half-wave rectifier and average gap voltage

This chapter describes the control methods of the working gap with the electrostatic induction feeding ECM, the conventional average gap voltage method and peak voltage method newly proposed. The availability of the control method was verified by drilling micro-holes on stainless steel using a tungsten tool electrode.

3.2 Servo feed control methods

In this section, two servo feed control methods, the average and peak voltage methods, are introduced. As mentioned above, the average voltage was firstly developed for the electrostatic induction feeding ECM to control the gap width. However, the gap control accuracy was not sufficiently high due to the low average value of gap voltage. Then, the peak voltage method was proposed to improve the gap control sensitivity through increasing the S/N ratio.

3.2.1 Average voltage method

In the previous research, a servo feed control system for the electrostatic induction feeding ECM was developed by Koyano[61] to control the gap width and avoid short circuit. The servo feed system controls the gap width by monitoring the average gap voltage. This method compares the average value of the gap voltage and the reference voltage to control the gap width, because the calculation of the average gap voltage shows that it is proportional to the gap resistance with the electrostatic induction feeding method. It is well know that the gap resistance is proportional to the gap width during EC machining. Thereby, it is possible to control the gap width by monitoring the average value of the gap voltage. The difference of the average of gap voltage and reference voltage was converted to a pulse signal to control the feeding of the tool electrode. The tool electrode was fed when the average voltage was larger than the reference voltage, and it was retreated when the peak average was smaller than the reference voltage.

3.2.2 Peak voltage method

The gap control accuracy of the average gap voltage method was not sufficiently high, because the signal to noise ratio (S/N ratio) was low due to the pulse duration of several tens of ns with significantly low duty ratio. In order to solve this problem and improve the gap control accuracy, a new method with monitoring the peak gap voltage was put forward. The analysis of the electrostatics induction feeding method shows the peak value of the gap voltage increases with increasing the gap width as shown in Fig. 2.4. With this method, the peak of the gap voltage was detected by a peak detection circuit, in which the detected peak voltage was reset in every pulse period to obtain a high response. The difference of the average value of the peak voltage from the reference voltage was converted to a pulse signal to control the feeding of the tool electrode. The tool electrode will be fed when the peak voltage was larger than the reference voltage, and it will be retreated when the peak voltage was smaller than the reference voltage.

3.2.3 Comparison of average and peak voltage methods

In order to compare the average and peak voltage methods, the average and peak of the gap voltages were measured under the experimental conditions shown in Table 3.1. The tool electrode was a tungsten rod with a diameter of 50 μm and the workpiece was stainless steel (SUS304). The tool electrode was positioned on the workpiece with a fixed gap width of 3 μm to 12 μm using the contact sensing function of the micro EDM machine. The pulse voltage was applied for several seconds, and the average and peak voltage were

measured by the developed servo feed control system. It is noted that the measured peak voltage was the average of the captured peak voltage, which was sampled, held, and reset at every pulse period as shown later in Fig. 3.17.

The average and peak voltage measured are shown in Fig. 3.2. It is found that both voltages increase with increasing the gap width. Since the peak voltage was much higher than the average voltage resulting in a higher S/N ratio, the gap control sensitivity of the peak voltage can be increased compared with the average voltage method. The experiments about the material removal rate with different feed control methods are discussed in the following sections.

Table 3.1 Experimental conditions used to compare average and peak voltage methods

Pulse voltage	Amplitude [V]	20
	Frequency [Hz]	500 k
	Duty factor [%]	50
	Rise/fall time [ns]	40
Feeding capacitance C_1 [pF]		47
Electrolyte		NaCl aq. 2wt%
Tool electrode rotation [rpm]		3000
Tool electrode		Φ50μm tungsten

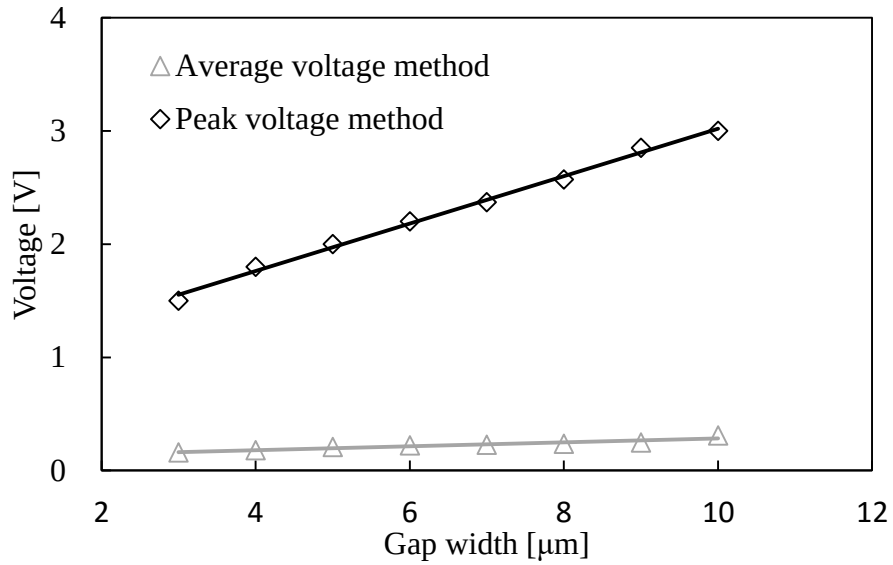

Fig. 3.2 Comparison between average and peak voltage methods

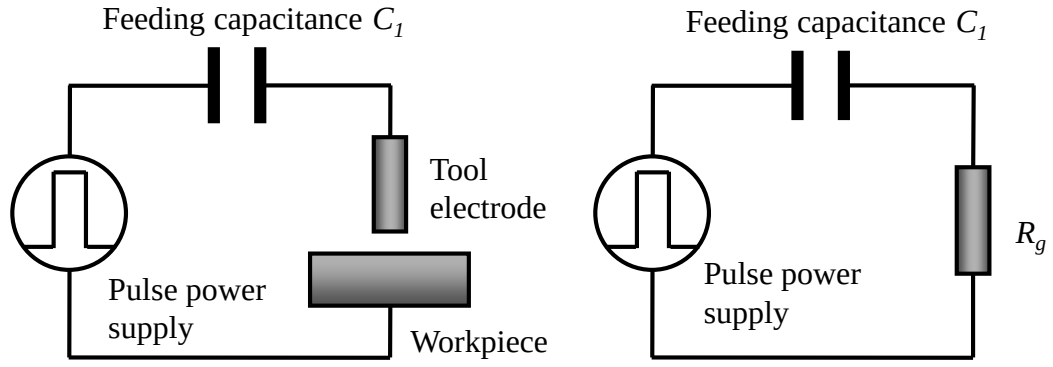

(a) Electrostatic induction feeding ECM (b) Equivalent circuit

Fig. 3.3 Gap voltage calculation with electrostatic induction feeding ECM

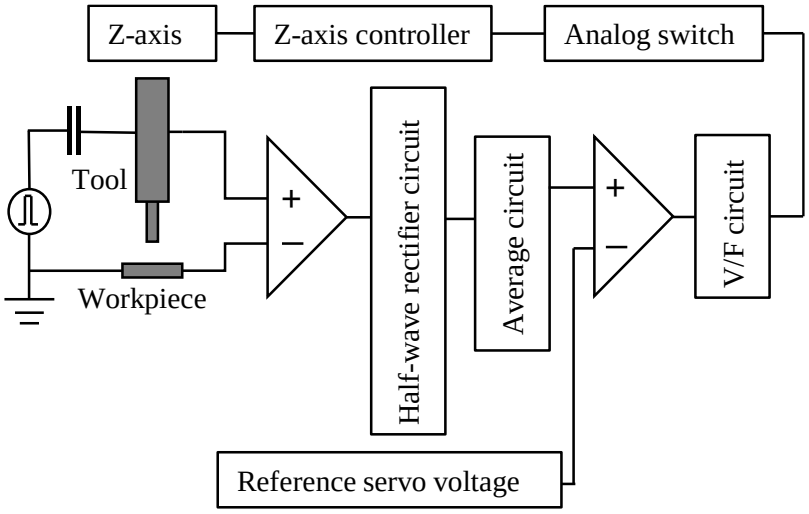

Fig. 3.4 Schematic of servo feed control system with average gap voltage method

3.3 Average gap voltage method

3.3.1 Principle

In the equivalent circuit shown in Fig. 3.3, the machining gap is simplified as a resistance R_g. When the gap voltage is half-wave rectified, the average working gap voltage V_{ave} can be expressed as

$$V_{ave} = \frac{R_g}{T}\int_0^T idt = \frac{R_g q}{T} \tag{3.1}$$

where T is the period of the pulse voltage.

In electrostatic induction feeding method, the electric charge q per each current pulse is constant regardless of the gap width. The q can be expressed using the amplitude of pulse voltage E_0 and the feeding capacitance C_1 as $q=C_1E_0$. Since R_g is proportional to the gap width, the above equation indicates that V_{ave} increases with increasing the gap width. Fig. 3.4 shows the schematic of the servo feed control system. The half-wave rectified gap voltage was smoothened to obtain the average gap voltage V_{ave}. The difference between V_{ave} and the reference servo voltage was converted to pulse signal by the *V/F* circuit to control the feeding of the tool electrode.

3.3.2 Machining with different reference voltages

3.3.2.1 Experimental conditions

There are many applications of micro-holes, such as micro molds, fuel injection nozzles, spinneret holes, MEMS and so on[68]. In the aerospace industry, micro-holes are the most critical structures used in film-cooling technology, and they are extensively used and located all over the surfaces of blades and vanes[69]. The blades and vanes are made of nickel based alloy, of which the composition is similar to stainless steel. Hence, micro-holes were machined with the stainless steel to investigate the gap control characteristics of the electrostatic induction feeding ECM.

Table 3.2 Experimental conditions used to investigate influence of reference voltage

Pulse voltage	Amplitude [V]	20
	Frequency [Hz]	500 k
	Duty factor [%]	50
	Rise/fall time [ns]	40
Feeding capacitance C_1 [pF]		47
Electrolyte		NaCl aq. 2wt%
Tool electrode rotation [rpm]		3000

The experimental conditions used to perform micro drilling are shown in Table 3.2. The tool electrode was a tungsten rod of 50 μm in diameter fabricated by the wire electrical discharge grinding (WEDG) method[58], and the workpiece was a stainless steel (SUS304) plate. Tungsten was used as tool electrode because of high erosion resistance, good electrical and thermal conductivity, and high stiffness. Stainless steel was used as workpiece material because it has been widely used for food production and storage, architecture, building and construction, and the composition is similar to nickel based alloys which are widely used as blades and vanes in aero-engines. The tool electrode was

positioned on the workpiece with an initial gap width of 5 μm using the contact sensing function of the micro EDM machine. The feed distance of tool electrode in the axial direction was 20 μm. The reference voltage was changed as 90 mV, 110 mV, 130 mV, 150 mV, 170 mV and 200 mV.

3.3.2.2 Inlet side gap width

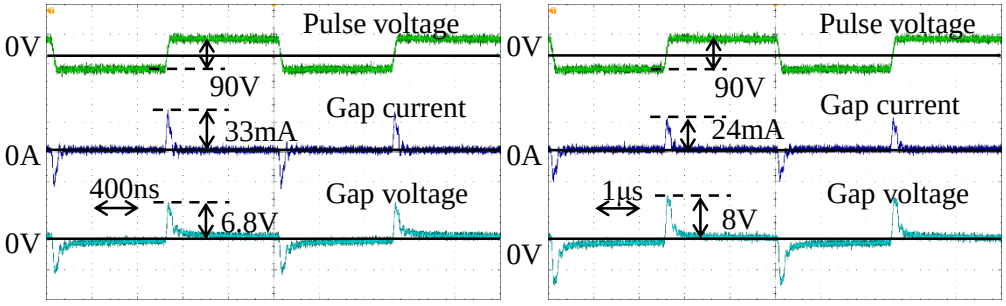

(a) Reference voltage of 110 mV (b) Reference voltage of 200 mV

Fig. 3.5 Waveforms of gap current and voltage with reference voltages of 110 mV and 200 mV

Fig. 3.5 shows the waveforms of gap current and voltage with the reference voltages of 110 mV and 200 mV. Since the gap width is smaller with lower reference voltage, the gap current increased with decreasing the reference voltage. Fig. 3.6 shows the micro-holes machined with different reference voltages. The grain boundaries were observed with low reference voltages. Since the working gap was small with low reference voltage resulting in high current density, the better surface finish was obtained. This result is common in the normal electrochemical machining processes. Fig. 3.7 shows the cross section shapes of micro-holes with the reference voltages of 90 mV and 130 mV. The cross section was measured using a laser confocal microscope (Olympus, OLS3000). The diameter of micro-hole became larger with higher reference voltage because the electrochemical reaction occurred in a larger gap width resulting in more material dissolution in the side gap. The electrochemical reaction was mainly localized at the narrow bottom gap resulting in less material dissolution in the side gap. The increase in the reference voltage by 44.5% from 90 mV to 130 mV caused only a small increase in the bottom gap width by 20% from 3.2 μm to 3.8 μm, which shows the gap control accuracy was not sufficiently high with the average gap voltage method. Fig. 3.8 shows the inlet side gap widths with different reference voltages, which increased with increasing the reference voltage.

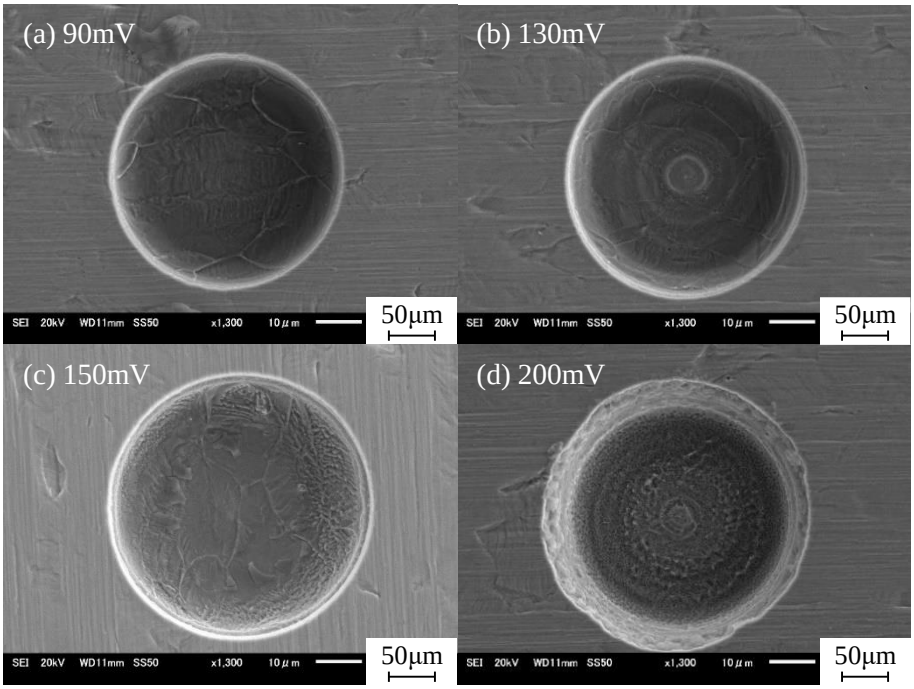

Fig. 3.6 Micro-holes machined with different reference voltages

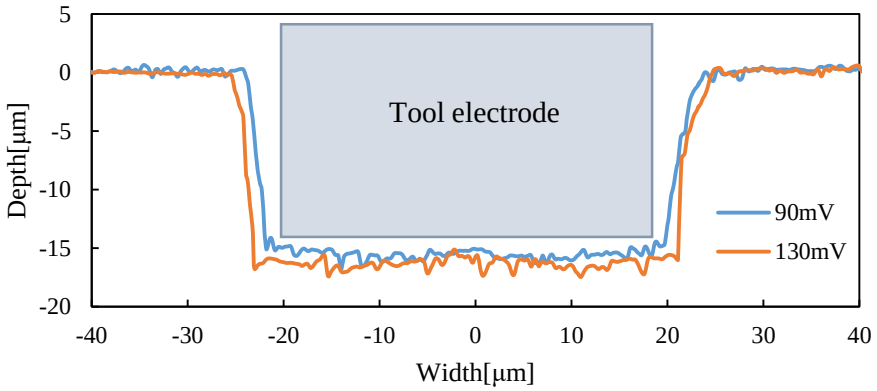

Fig. 3.7 Cross section shape with reference voltages of 90 mV and 130 mV

In addition, the inlet side gap width with different feed distances was also investigated using the conditions shown in Table 3.3. In this experiment, the tool electrode was a tungsten rod of 50 μm in diameter fabricated by the wire electrical discharge grinding (WEDG) method, and the workpiece was a stainless steel (SUS304) plate. The tool electrode was positioned on the workpiece with an initial gap width of 5 μm using the contact sensing function of the micro EDM machine. The reference voltage was 140 mV based on the above experimental results. The experimental conditions are shown in Table 3.3. The feed distances of tool electrode were 5 μm, 15 μm, 25 μm, 35 μm and 45 μm.

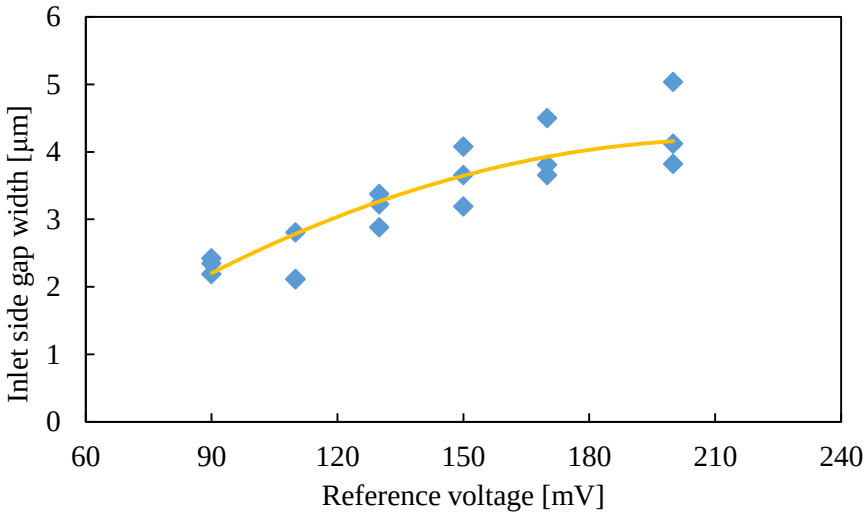

Fig. 3.8 Inlet side gap widths with different reference voltages

Table 3.3 Experimental conditions used to investigate influence of feed distance

Pulse voltage	Amplitude [V]	20
	Frequency [Hz]	500 k
	Duty factor [%]	50
	Rise/fall time [ns]	40
Feeding capacitance C_1 [pF]		47
Electrolyte		NaCl aq. 2wt%
Tool electrode rotation [rpm]		3000
Feed distance [μm]		5, 15, 25, 35, 45
Reference voltage		140mV

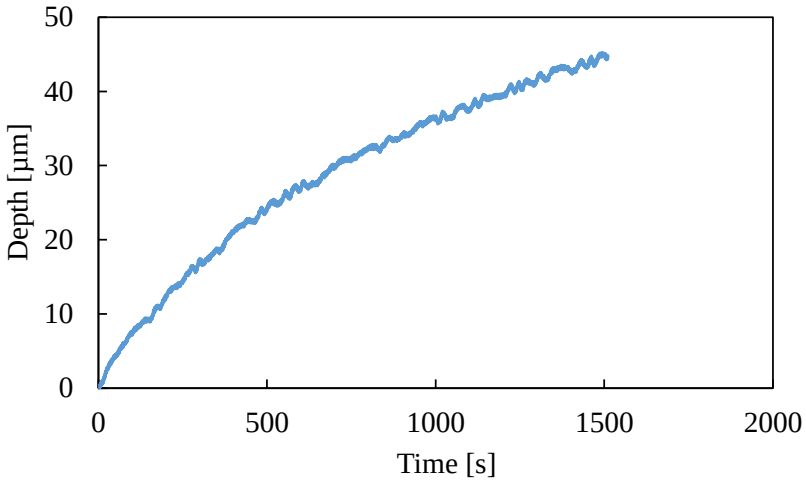

Fig. 3.9 Displacement of tool electrode with feed distance of 45 μm

Fig. 3.9 shows the displacement of tool electrode with the feed distance of 45 μm. Fig. 3.10 shows the micro-holes machined with the feed distances of 25 μm, 35 μm and 45 μm. It is found that the bottoms were significantly smooth because of the low reference voltage of 140 mV. However, the centre of the micro-hole was not as smooth as other areas, this is because the flushing of electrolyte was not sufficiently effective in the centre area. Thereby the sludge and bubbles were difficult to be flushed out of the working gap. Shimasaki and Kunieda[70] observed the ECM gap with a rotating tool electrode using a transparent electrode and found that bubbles are collected at the rotation center due to the centrifugal force.

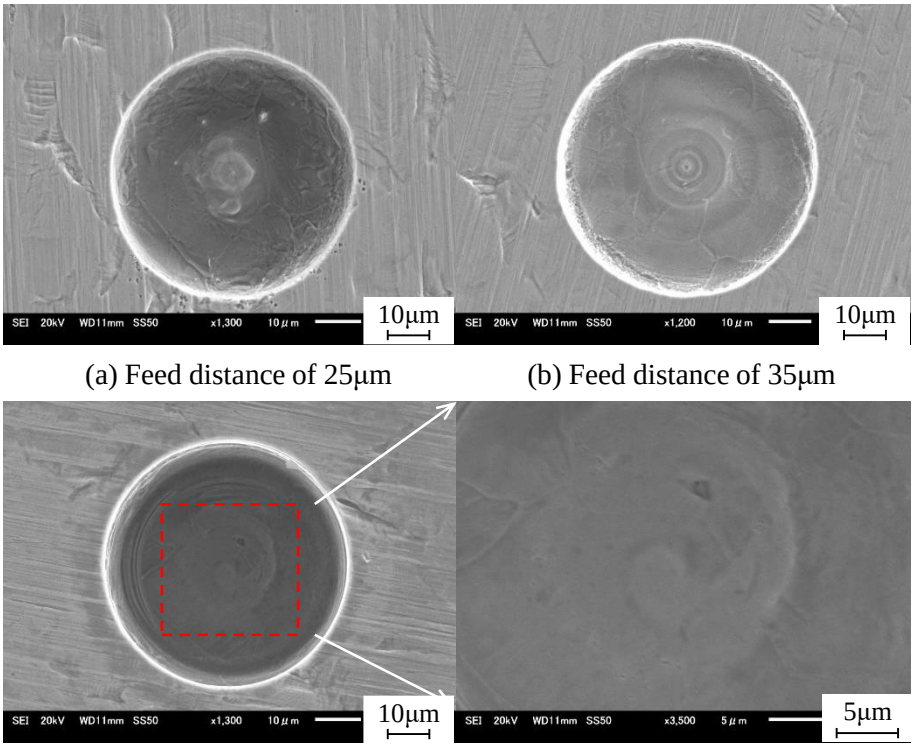

(a) Feed distance of 25μm (b) Feed distance of 35μm

(c) Feed distance of 45μm

Fig. 3.10 Micro-hole machined with different feed distances

Fig. 3.11 shows the inlet side gap width with different feed distances. It is found that the inlet side gap width increased with increasing the feed distance, because the inlet side gap width was not only increased by the reference voltage but also the machining time. The machining time was longer with increasing the feed distance resulting in the increase of the material removal volume in the side gap.

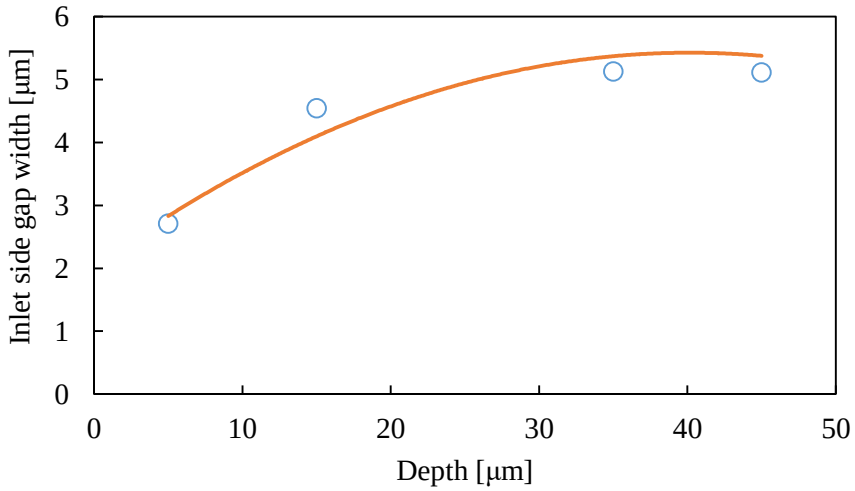

Fig. 3.11 Inlet side gap widths with different feed distance

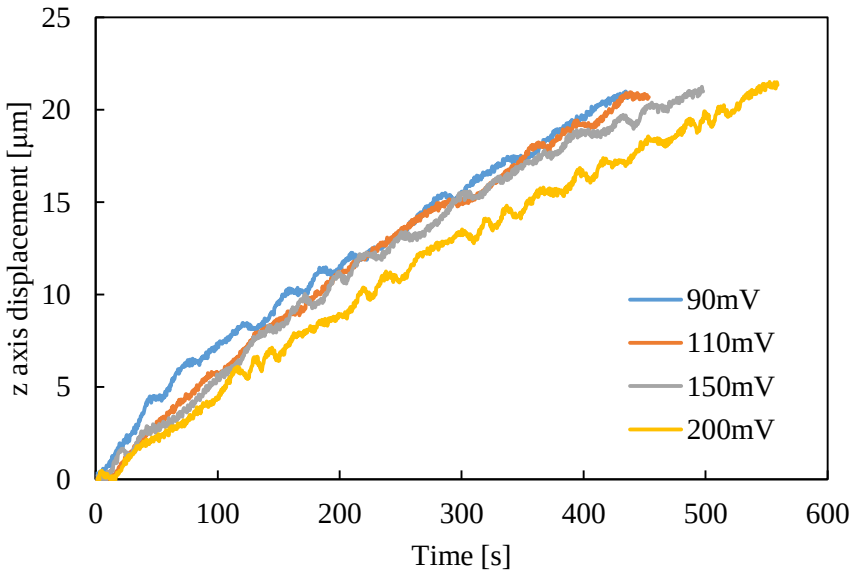

Fig. 3.12 Displacements of tool electrode with different reference voltages

3.3.2.3 Material removal rate

Fig. 3.12 shows the displacements of tool electrode with different reference voltages. It is noted that the difference was slight with different reference voltages. The material removal rate was defined as the material removal volume divided by the machining time. Fig. 3.13 shows the material removal rate with different reference voltages. It slightly decreased with increasing the reference voltage, because the current density was decreased with a higher reference voltage resulting in lower material removal rate. The change of the material removal rate was not obvious because the gap control sensitivity was not sufficiently high due to the low S/N ratio.

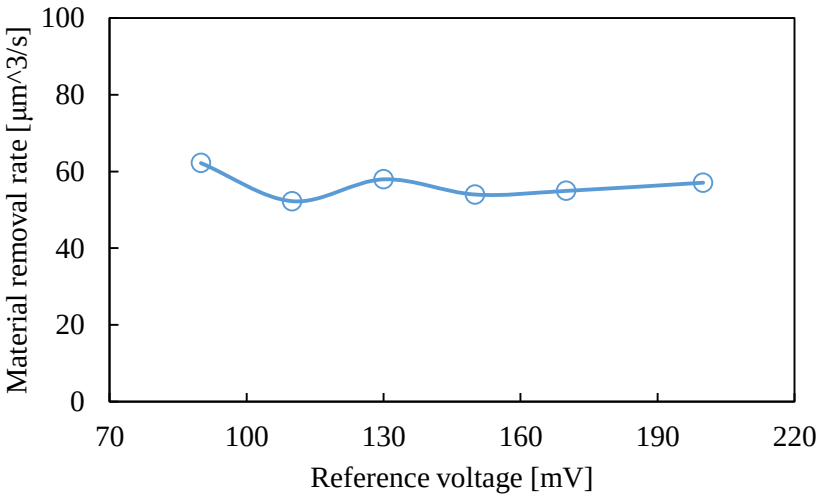

Fig. 3.13 Material removal rate with different reference voltages

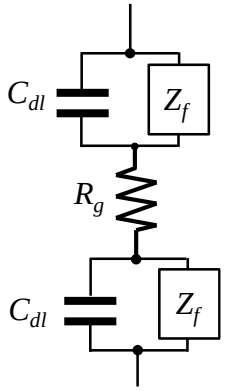

Fig. 3.14 Equivalent circuit of ECM gap

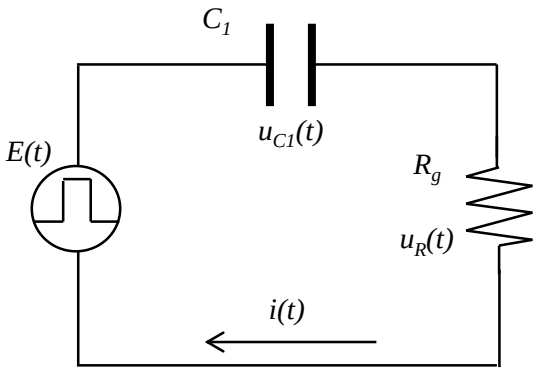

Fig. 3.15 Equivalent circuit of electrostatic induction feeding ECM

3.4 Peak gap voltage method

3.4.1 Principle

Harada and Natus[65] and Kadokura and Natsu[66] reported that the gap width can be measured using the peak current in the transient state of the current pulse because the C_{dl} and Z_f can be ignored in the equivalent circuit shown in Fig. 3.14. Thus, they controlled the feeding of the tool electrode in pulse ECM based on the measurement of the peak current of normal pulse ECM. Since the pulse duration of the electrostatic induction feeding ECM is significantly short, the equivalent circuit of the electrostatic induction feeding ECM (Fig. 1.22) can be simplified as Fig. 3.15. The current *i(t)* flowing through the working gap can be expressed as

$$i(t) = C_1 \frac{d\big(u_{c1}(t)\big)}{dt} = C_1 \frac{d\big(E(t) - u_R(t)\big)}{dt} \tag{3.2}$$

$$i(t) = \frac{u_R(t)}{R_g} \tag{3.3}$$

Here, R_g is the resistance of the working gap. Thus

$$C_1 \frac{d(E(t))}{dt} - C_1 \frac{d(u_R(t))}{dt} = \frac{u_R(t)}{R_g} \tag{3.4}$$

Solving the differential equation (3.4), the gap voltage $u_R(t)$ was calculated under the conditions: C_1=47 pF, pulse voltage rising and falling time of 40 ns, and pulse voltage amplitude of 20 V. The value of C_1 was determined so that the stray capacitance in the circuit, which is assumed to be around 10 pF[56], can be ignored compared to C_1. The gap resistance R_g was calculated to be 250 Ω, 300 Ω, and 350 Ω, assuming that the end of a rod tool electrode with a diameter of 50 μm was positioned over the workpiece at a gap width of 1.39 μm, 1.67 μm, and 1.94 μm, respectively, in NaCl aqueous solution of 2 wt%[71]. The calculated gap voltages and currents with different gap resistances were already shown in Fig. 2.4. The peak of the gap voltage increases from 6 V to 8 V with increasing the gap resistance from 250 Ω to 350 Ω. Hence, it is possible to control the gap width based on the measurement of the peak gap voltage.

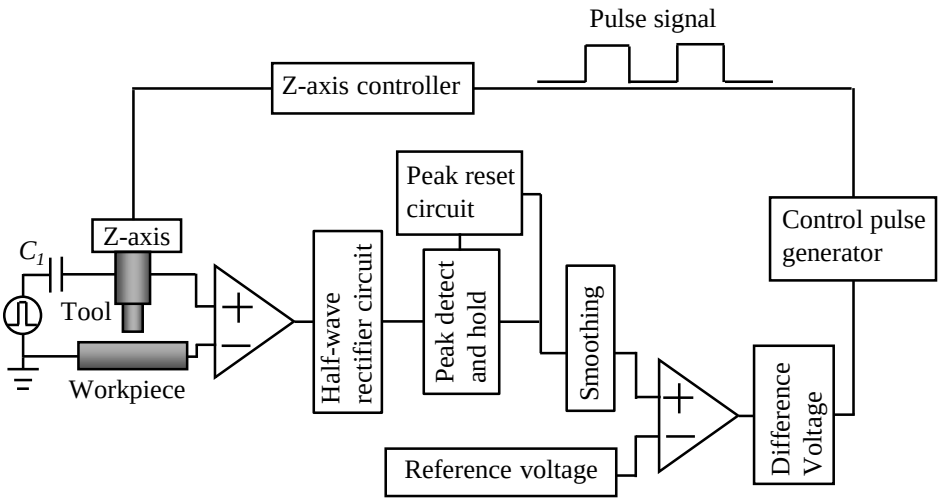

Fig. 3.16 Servo feed control system using peak voltage

Fig. 3.16 shows the servo feed control system using the peak voltage. Since the gap voltage is bipolar, the half-wave rectifier circuit is used. Fig. 3.17 shows the waveforms obtained from the circuit. The rectified gap voltage becomes unipolar with the help of the half-wave rectifier circuit. The peak of the rectified gap voltage is detected using a peak detect and hold circuit, and smoothened to obtain the average peak voltage. The difference between the average peak voltage and reference voltage is converted to a pulse signal to control the tool electrode feed. The tool electrode is fed when the average peak voltage is larger than the reference voltage, and it will be retreated when opposite.

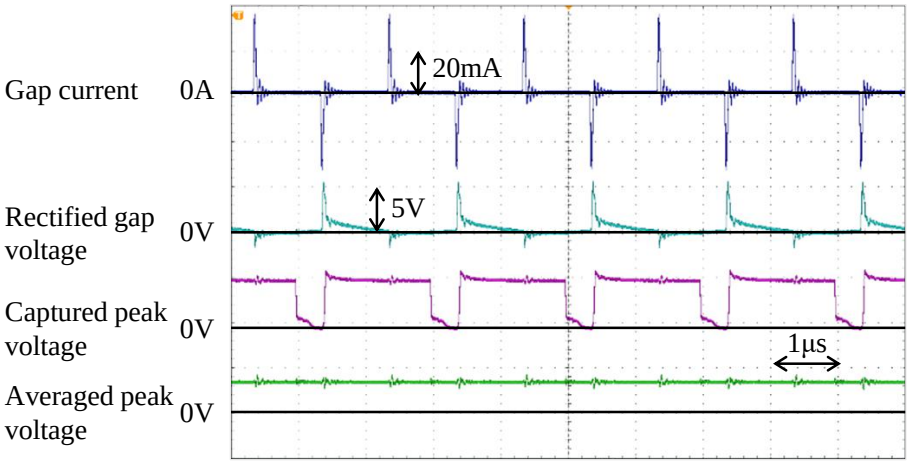

Fig. 3.17 Waveforms obtained from servo feeding control circuit

The held peak voltage is reset at every pulse period to obtain a quick response which is realized by a peak hold and reset circuit as shown in Fig. 3.18. The gap voltage was filtered using the half-wave rectifier circuit to get the unipolar voltage, when the

workpiece was positive polarity. The schematic of peak detection is shown in Fig. 3.18(a). The peak voltage is detected through the capacitance charge. However, when the input voltage decreases to 0 V, the electric charge in the capacitance cannot discharge in time and the detected peak would be kept for some time. Hence a reset circuit is needed to provide a discharge circuit for the electric charge in the capacitance when the peak voltage decreases to 0 V as shown in Fig. 3.18(b).

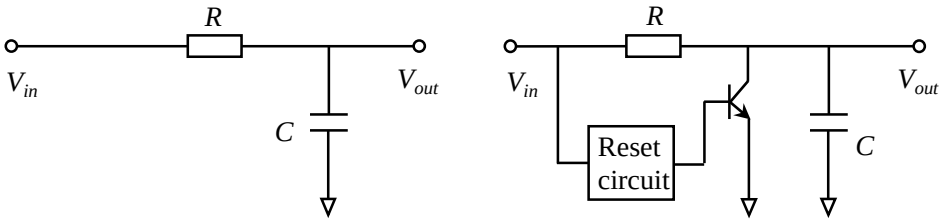

(a) Peak detection (b) Peak detection with reset circuit

Fig. 3.18 Schematic of peak detection

The schematic of reset is shown in Fig. 3.19. The peak hold signal is triggered by gap voltage and the detected peak voltage is held for time T_1. Then the peak reset signal is triggered by the hold signal. During the reset time T_2, the electric charge in the capacitance C in Fig. 3.18 is discharged. Hence the detected peak is reset. Fig. 3.20 shows the waveform from the reset circuit.

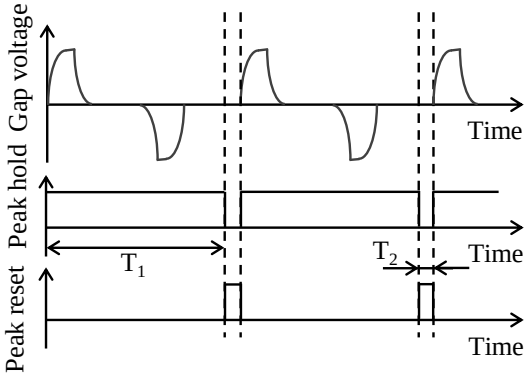

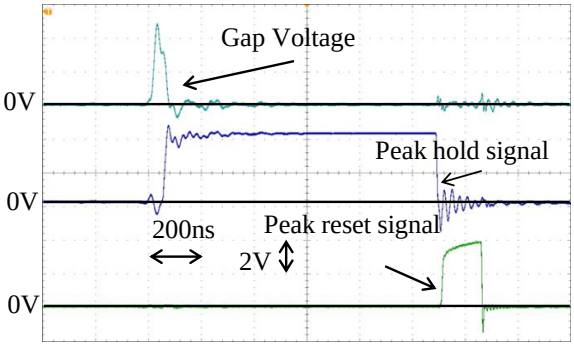

Fig. 3.19 Principle of reset circuit Fig. 3.20 Waveform of peak reset circuit

3.4.2 Experimental verification

Before making the new servo feed control system, a series of fundamental experiments were performed to verify the feasibility. The peak gap voltage with different gap widths was measured without feeding of the tool electrode. Then, micro holes were machined

using a manual control method to keep the same peak voltage and imitate the servo feed control.

Table 3.4 Experimental conditions to measure peak voltage

Pulse voltage	Amplitude [V]	20
	Frequency [Hz]	500 k
	Duty factor [%]	50
	Rise/fall time [ns]	40
Feeding capacitance C_1 [pF]		47
Electrolyte		NaCl aq. 2wt%
Tool electrode rotation [rpm]		3000

3.4.2.1 Peak gap voltage measurement

The peak gap voltage was measured under the experimental conditions shown in Table 3.4. The tool electrode was a tungsten rod with the diameter of 47 μm, and the workpiece was a stainless steel (SUS304) plate. The tool electrode was positioned on the workpiece with an initial gap width of 4 μm and 5 μm between the end surface of the tool electrode and the workpiece surface using the contact sensing function of the micro EDM machine, respectively. The gap current and voltage peak were measured in the machining process without feeding of the tool electrode using an oscilloscope. The experimental results are shown in Fig. 3.21.

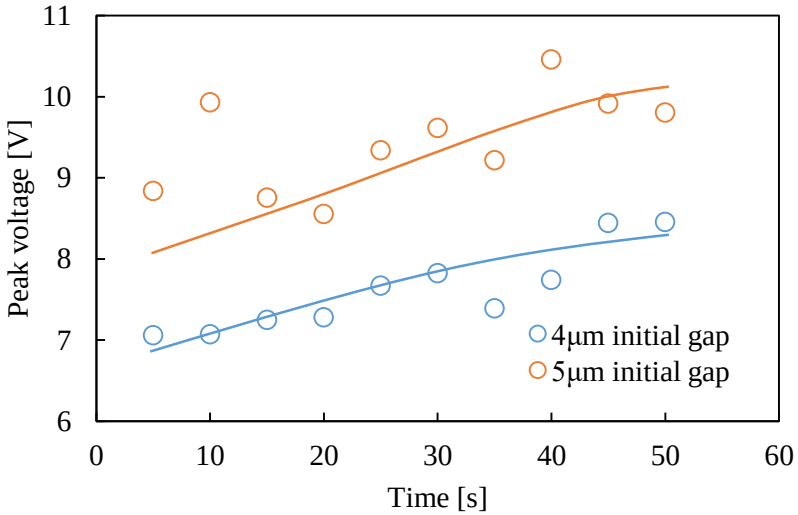

Fig. 3.21 Peak gap voltage with initial gap of 4 μm and 5 μm

The peak of the gap voltage increased with the passage of time, because the gap width increased due to the material dissolution.

3.4.2.2 Peak gap voltage with different gap widths

The quantitative relationship between the peak of the gap voltage and the gap width was obtained from the following experiment. The experimental conditions were the same as in Table 3.4. The tool electrode was tungsten rod of 48.5 μm in diameter, and the workpiece was a stainless steel (SUS304) plate. The tool electrode was positioned on the workpiece with an initial gap width of 3 μm using the contact sensing function of EDM machining. 18 holes were machined by changing the machining time from 10 s to 180 s, incrementally with a step of 10 s without feeding of the tool electrode in the axial direction. The gap current and voltage peak were measured at the end of machining for each hole. The depth of machined hole was measured using a laser confocal microscope (Olympus OLS3000). Since the tool electrode was not fed, the gap width at the end of machining was the sum of 3 μm initial gap and the depth of the machined hole. Hence, the relationship between the gap width and gap current and voltage peak could be obtained quantitatively as shown in Fig. 3.22.

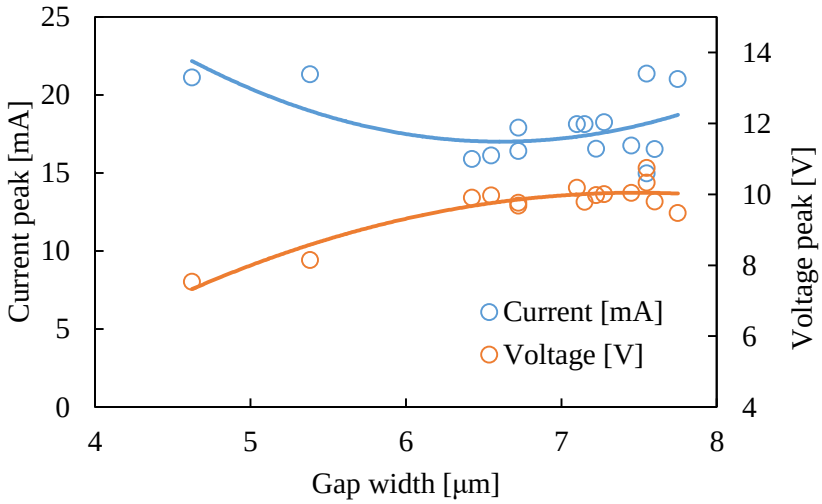

Fig. 3.22 Gap current and voltage peak with different gap widths

When the gap width was larger than 6 μm, the gap current and voltage peak hardly changed. Since the bottom gap resistance was very large with a larger bottom gap, the current density in the bottom gap decreased. Since the electric charge in each pulse $q=C_1E_0$ is constant as described in the previous section, the current density in the side gap increased. Hence, when the bottom gap width larger than 6 μm, the peak current did not increase significantly.

3.4.2.3 Micro-hole machining by manual feed control

To check the functionality of the servo feed control circuit developed, micro holes were machined by a manual feed control. In this experiment, the tool electrode was fed

manually to maintain the constant peak gap voltage. The experimental conditions were the same as in Table 3.4. The tool electrode was a tungsten rod of 48.5 μm in diameter, and the workpiece was a stainless steel (SUS304) plate. The tool electrode was positioned on the workpiece with an initial gap width of 3 μm using the contact sensing function of the EDM machine. The minimum feeding distance was 0.1 μm for every push of the feeding button for the z-axis of the machine tool. The peak gap voltage was kept constant at 7 V and 9 V, respectively, and the feeding distance was 15 μm in total from the surface of the workpiece. The machined holes are shown in Fig. 3.23 (a). From the cross sectional shapes with the voltage peak of 7 V and 9 V in Fig. 23 (b), it was found that the bottom gap width increased by 34% with increasing the gap voltage by 28.6%.

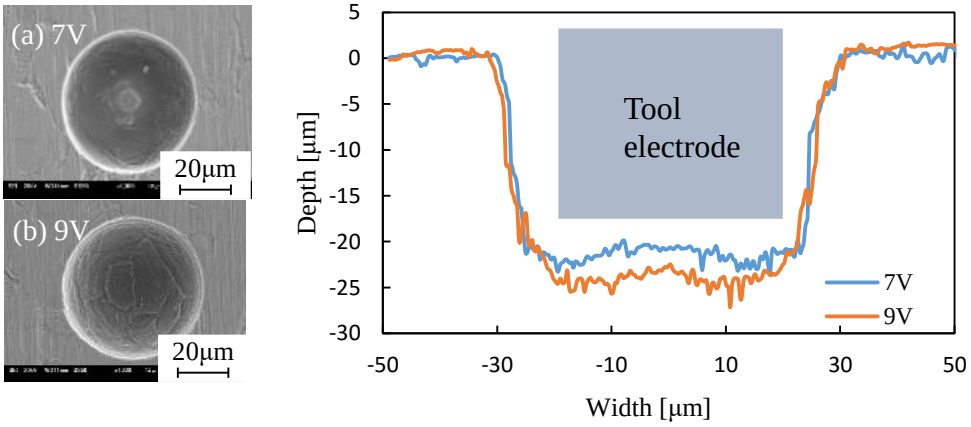

(a) Micro holes (b) Cross sectional shapes

Fig. 3.23 Micro holes and cross sectional shapes

Table 3.5 Experimental conditions with peak gap voltage method

Pulse voltage	Amplitude [V]	20
	Frequency [Hz]	500 k
	Duty factor [%]	50
	Rise/fall time [ns]	40
Feeding capacitance C_1 [pF]		47
Electrolyte		NaCl aq. 2wt%
Tool electrode rotation [rpm]		3000
Reference voltage [V]		1.5, 2, 2.5, 3
Tool electrode		Φ50μm tungsten
Workpiece		Stainless steel (SUS) plate

3.4.3 Machining with different reference voltages

Micro-holes were drilled with different reference voltages using the electrostatic induction feeding method, and the influence of the reference voltage on the machining characteristics was investigated with the developed servo feed control system.

3.4.3.1 Experimental conditions

The influences of servo reference voltage on the material removal rate (MRR) and machining accuracy of the micro-holes were investigated under the machining conditions shown in Table 3.5. The tool electrode was a tungsten rod 50μm in diameter fabricated by the wire electro-discharge grinding method (WEDG)[58]. The workpiece was a stainless steel (SUS304) plate. NaCl aqueous solution of 2 wt% was used as the electrolyte, and jetted from a nozzle with an inner diameter of 200 μm, which was set close to the machining gap, at a flow rate of 10 ml/min. The servo reference voltage was varied at 1.5 V, 2 V, 2.5 V, and 3 V. The tool electrode was positioned over the workpiece with an initial gap width of 10 μm, and the feeding distance of the tool electrode was set as 40 μm. The material removal volume was measured by a laser confocal microscope (Olympus, OLS3000), and the inlet side diameter of the micro-hole was measured by SEM.

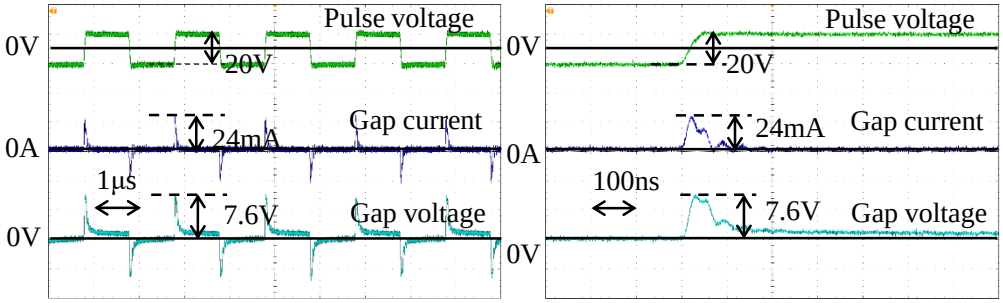

Fig. 3.24 Waveforms of pulse voltage, gap current and voltage at C_1=47 pF

3.4.3.2 Inlet side gap width

Fig. 3.24 shows the waveforms of the pulse voltage, gap current and voltage with a reference voltage of 2 V at the moment of the feeding distance of 30 μm. It was found that the current is bipolar with the electrostatic induction feeding method. Fig. 3.25 (a) and (b) show the micro-holes machined with the reference voltage of 2 V and 3 V, respectively. The bottom surface of the micro-hole machined with the reference voltage of 2 V was significantly smooth, enabling clear observation of the grain boundary of the crystal structure. However, at the reference voltage of 3 V, the micro-holes show a pore structure at the bottom. This is because the current density is low with the larger working gap width when the reference voltage is 3 V. This result agrees with the well-established

fact that higher current density results in smoother surface roughness in ECM. Fig. 3.26 shows the inlet side gap width of the micro-holes machined with different reference voltages. Since the current density in the side gap decreases with decreasing reference voltage, the material dissolution in the side gap decreased, resulting in a smaller inlet side gap width. Thus, at the reference voltage where the MRR peaks, the side gap width is tolerably narrow. This conclusion can be verified in the next section.

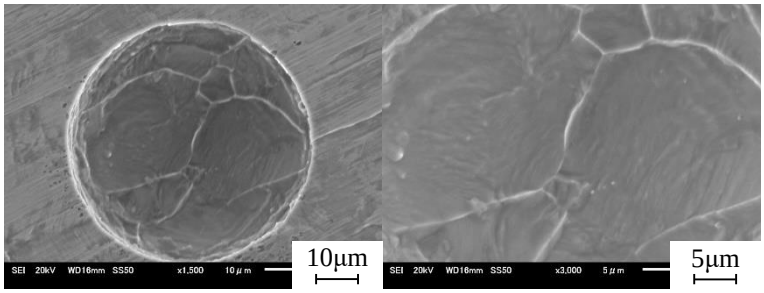

(a) Reference voltage of 2V

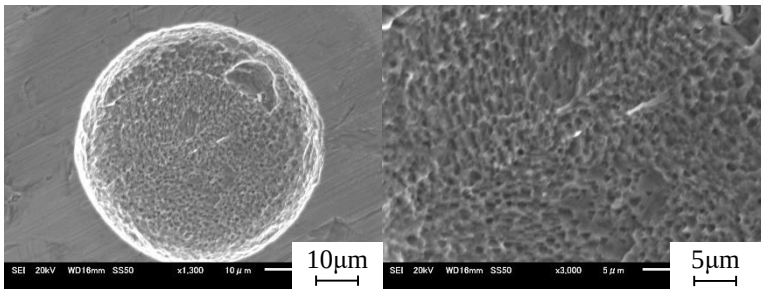

(b) Reference voltage of 3V

Fig. 3.25 Micro-holes with different reference voltages at C_1=47 pF

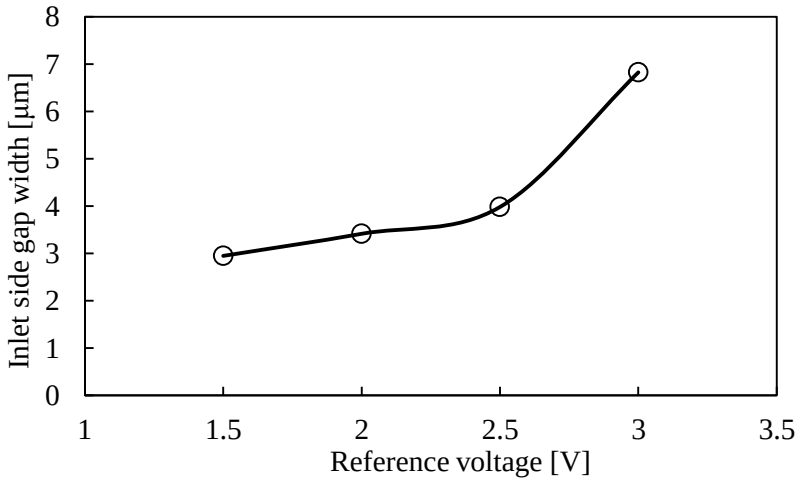

Fig. 3.26 Inlet side gap width with different reference voltages at C_1=47 pF

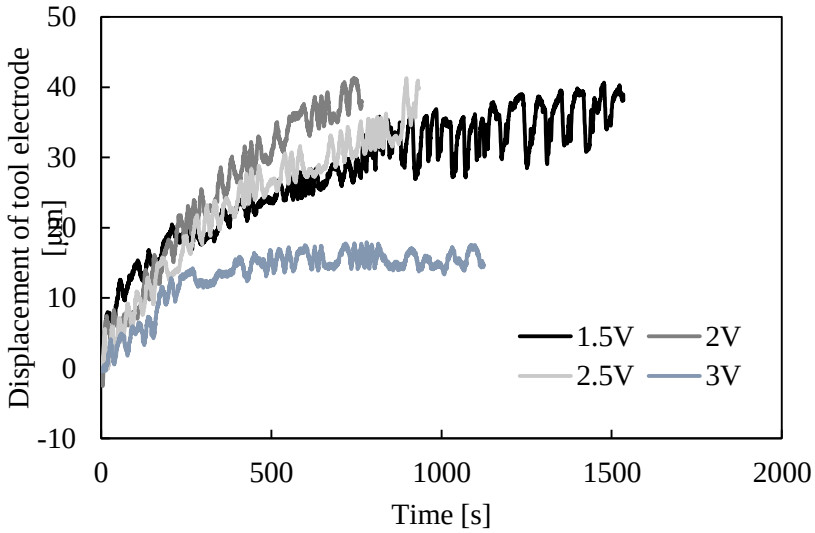

Fig. 3.27 Displacement of tool electrode with different reference voltages at C_1=47 pF

3.4.3.3 Material removal rate

The displacement of the tool electrode with different reference voltages is shown in Fig. 3.27. The electric charge per each pulse period q flowing through the working gap can be expressed as $q=C_1E_0$ using the amplitude of pulse voltage E_0 and the feeding capacitance C_1. Hence, the material removal rate should be the same with the same feeding capacitance C_1 using the electrostatic induction feeding method. However, it can be seen from Fig. 3.27 that lower reference voltage results in faster feeding speeds. This is because higher current density can be obtained in a smaller working gap width which is proportional to the reference voltage. Hence, the electrochemical dissolution is mainly confined to the bottom gap, resulting in a lower stray current in the side gap and on the un-machined workpiece surface. However, it was found that the machining time with the reference voltage of 1.5 V was longer than that with the reference voltage of 2 V. This is because the tool electrode is frequently retracted due to short circuiting as a result of the significantly small working gap. After the gap width is widened, many bubbles and electrochemical products are generated, thereby the electrochemical conductivity of the gap is decreased. Thus, the tool electrode is fed forward to decrease the gap width. Therefore, the degree of machining instability can be measured from the amplitude of oscillation in the displacement of the tool electrode. On the other hand, the machining could not be completed with the reference voltage of 3 V, because the current efficiency was significantly low under the conditions of low current density with large working gap width. In addition, many bubbles and electrochemical productions were generated in the narrow working gap during the ECM process, which can cause the short circuit between

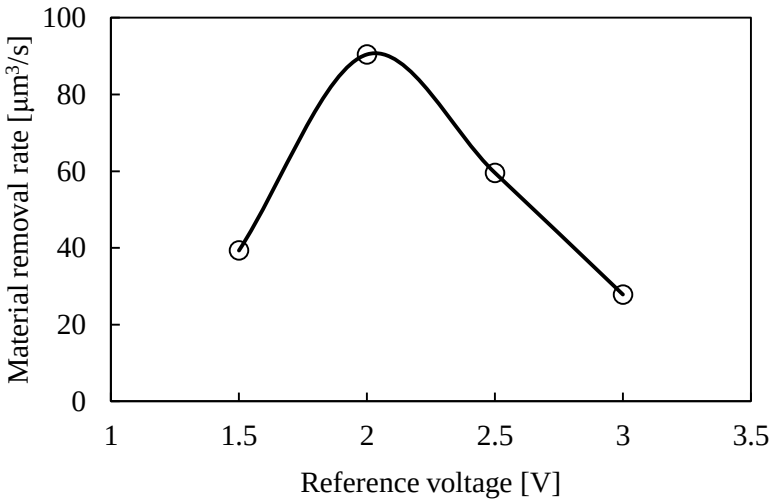

Fig. 3.28 Material removal rate with different reference voltages at C_1=47 pF

Table 3.6 Experimental conditions for electrostatic induction feeding EDM

Pulse voltage	Amplitude [V]	70
	Frequency [Hz]	100 k, 1 M
	Duty factor [%]	50
Feeding capacitance C_1 [pF]		470
Tool electrode		Tungsten (Φ150 μm)
Tool electrode rotation [rpm]		3000
Machining medium		Discharge oil
Workpiece		Stainless steel (SUS) plate
Polarity		Workpiece: +

electrodes. Hence, the tool electrode is quickly retreated when the servo feed system detects the short circuit resulting in the vibration of displacement of tool electrode as shown in Fig. 3.27. The material removal rate was defined as the material removal volume divided by the machining time. The material removal rates at different reference voltages are summarized in Fig. 3.28. As described above, the stray current reduces the MRR. In addition, the current efficiency depends on the current density. Hence, the MRR peaked at the reference voltage of 2 V under the feeding capacitance C_1=47 pF. With the experimental conditions in Table 3.6, Koyano[72)] investigated the material removal rate with the electrostatic induction feeding EDM as shown in Fig. 3.29, which was much higher compared with the electrostatic induction feeding ECM shown in Fig. 3.28. In EDM, the discharge occurs only at a single discharge location per each pulse, hence, volumetric removal rate is constant. As a result, the volumetric removal rate of ECM is

significantly high, compared with EDM when the machining area is large. In Micro ECM, however, the advantage of the high removal rate is lost, because the machining area is small.

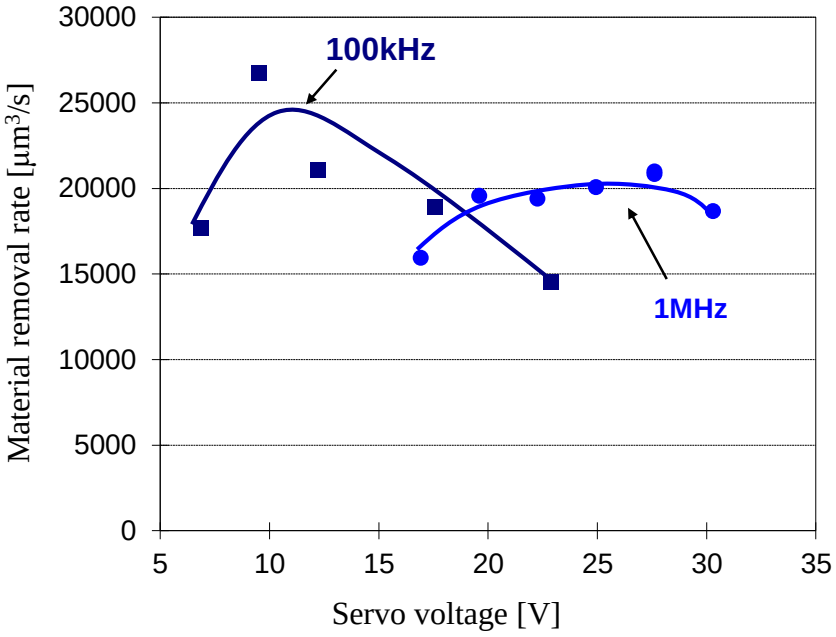

Fig. 3.29 Material removal rate with electrostatic induction feeding EDM[72)]

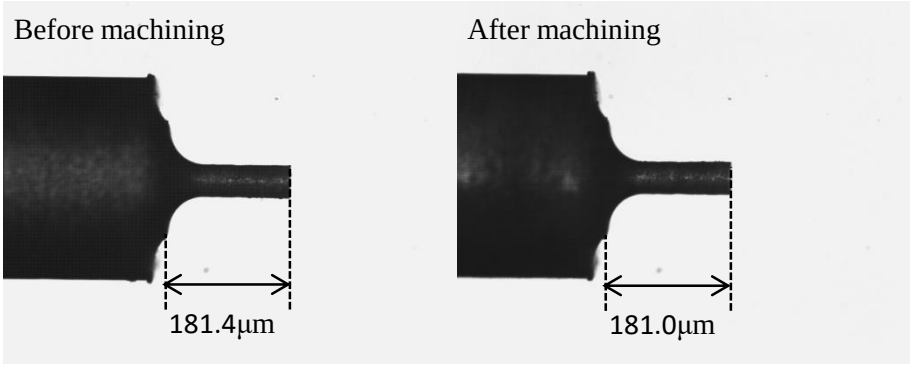

Fig. 3.30 Tool electrodes before and after machining

3.4.3.4 Tool wear

Moreover, at the end of experiment, the wear of the tool electrode was measured as shown in Fig. 3.30. Almost no tool wear was observed, even though the current was bipolar with the electrostatic induction feeding method. This result agrees with the report by Manabe and Kunieda[73)] who found that the temperature rise in the thin rod tool electrode, which is higher than that in the plate workpiece, prevents the wear of the thin rod tool electrode.

3.4.4 Machining with different feeding capacitances

The electric charge per each pulse q can be expressed as $q=C_1E_0$. Hence the material removal rate should be increased by increasing the feeding capacitance C_1. Using the calculation method described in Section 2.2, the gap voltage and current with feeding capacitances of C_1=47 pF and 68 pF were calculated as shown in Fig. 3.31, assuming that the gap resistance is 300 Ω. The gap voltage and current increased with increasing feed capacitance C_1. Fig. 3.32 shows the voltage and current waveforms measured with C_1=68 pF and the reference voltage of 2.5 V. Compared with Fig. 3.24 where C_1=47 pF and the reference voltage is 2.5 V, the gap voltage and current peak increased with larger C_1. However, the pulse duration time was the same for both C_1=47 pF and 68 pF because the pulse duration is determined by the rising and falling time of the pulse voltage.

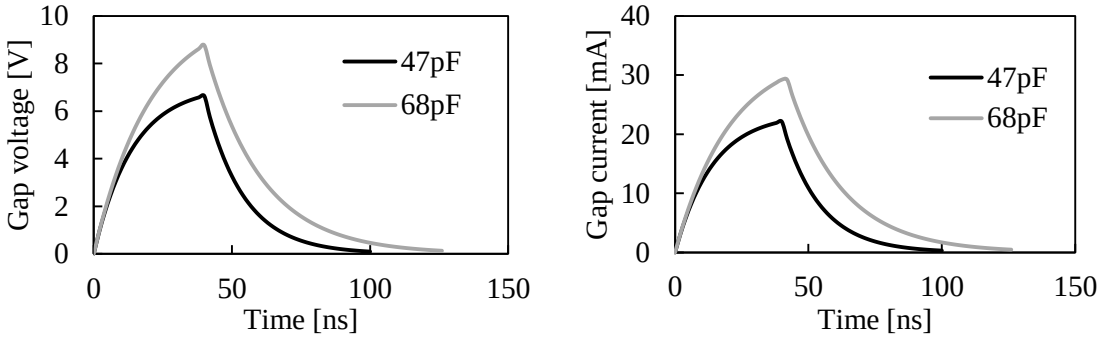

Fig. 3.31 Gap voltage and current with feeding capacitance C_1= 47 pF and 68 pF

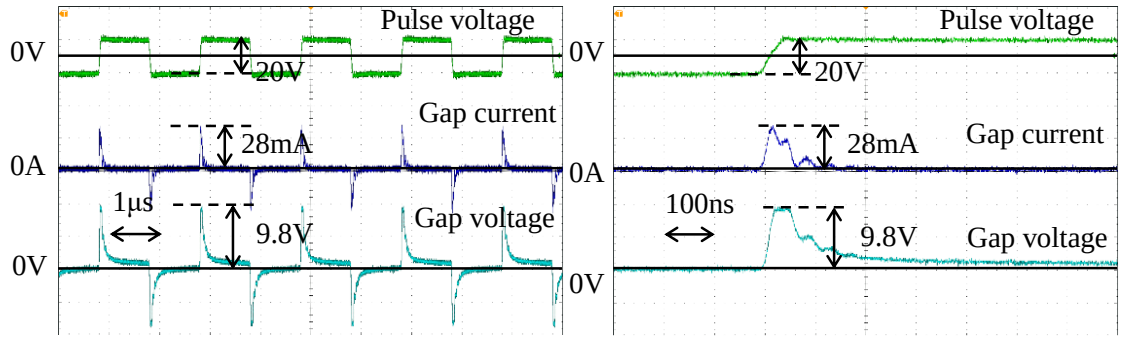

Fig. 3.32 Waveforms of pulse voltage, current and gap voltage with feeding capacitance C_1= 68 pF

3.4.4.1 Experimental conditions

The tool electrode was a tungsten rod 50 μm in diameter fabricated by the wire electro-discharge grinding method (WEDG). The workpiece was a stainless steel (SUS304) plate.

NaCl aqueous solution of 2 wt% was used as the electrolyte, and jetted from a nozzle with an inner diameter of 200 μm, which was set close to the machining gap, at a flow rate of 10 ml/min. The tool electrode was positioned over the workpiece with an initial gap width of 10 μm. Micro-holes were machined with C_1= 68 pF under the conditions shown in Table 3.7. The reference voltage was varied at 2 V, 2.5 V, 3 V and 3.5 V. The initial gap width and feeding distance of the tool electrode were set as 10 μm and 40 μm, respectively, which were the same as Section 3.4.3.

Table 3.7 Experimental conditions used with large feeding capacitance

Pulse voltage	Amplitude [V]	20
	Frequency [Hz]	500 k
	Duty factor [%]	50
	Rise/fall time [ns]	40
Feeding capacitance C_1 [pF]		68
Electrolyte		NaCl aq. 2 wt%
Tool electrode rotation [rpm]		3000
Reference voltage [V]		2, 2.5, 3, 3.5
Tool electrode		Φ50 μm tungsten
Workpiece		Stainless steel (SUS) plate

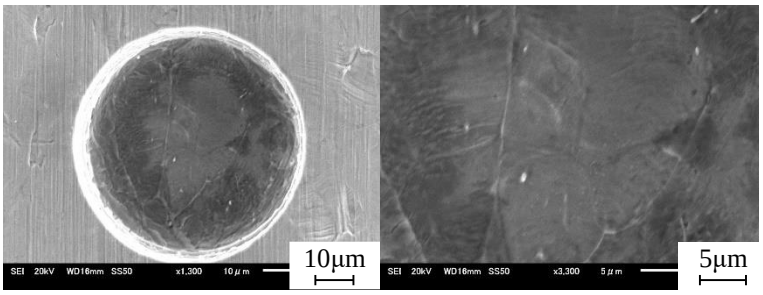

(a) Reference voltage of 2.5 V

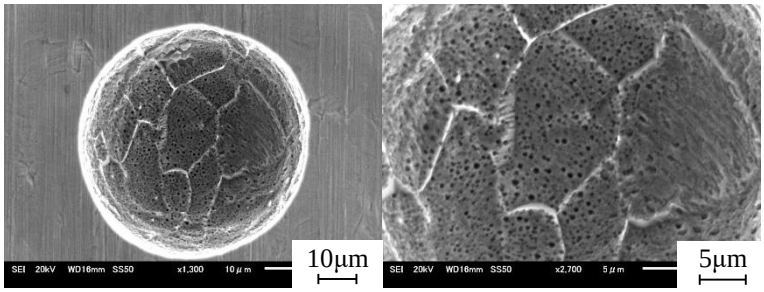

(b) Reference voltage of 3.5 V

Fig. 3.33 Micro-holes with different reference voltages at C_1=68 pF

3.4.4.2 Inlet side gap width

Micro-holes machined with the reference voltages of 2.5 V and 3.5 V are shown in Fig. 3.33. The surface finish was smoother with the lower reference voltage in the same way as that in Fig. 3.25.

Inlet side gap widths with different reference voltages are shown in Fig. 3.34. The inlet side gap widths when C_1= 68 pF were nearly equal to those in Fig. 3.26 when C_1=47 pF under the same reference voltage.

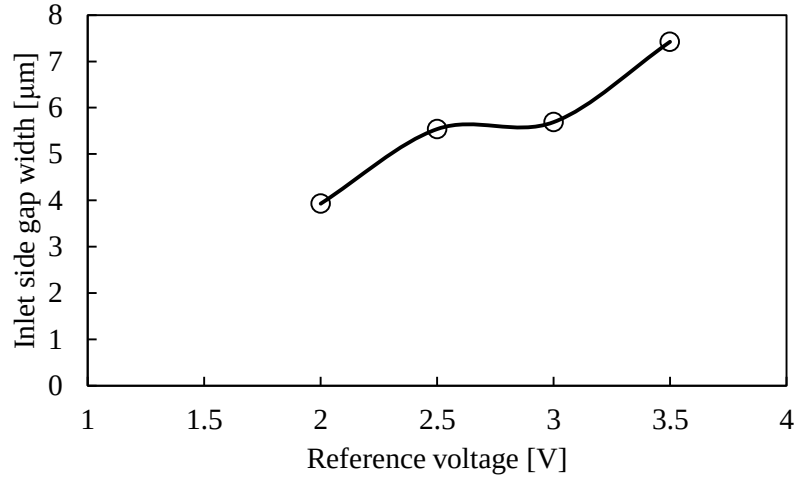

Fig. 3.34 Inlet side gap width with different reference voltages at C_1=68 pF

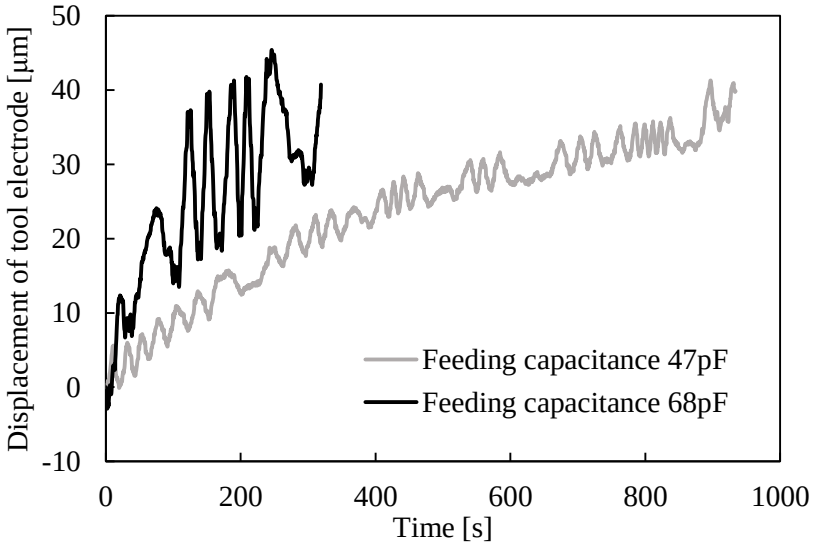

Fig. 3.35 Material removal rate with different feeding capacitances at C_1=68 pF

3.4.4.3 Material removal rate

Fig. 3.35 shows the displacements of the tool electrode at different feeding capacitance of C_1=47 pF and 68 pF when the reference voltage was 2.5 V. Higher material removal

rate could be obtained with the larger feeding capacitance of 68 pF. It was also found that the amplitude of feeding back and forth the tool electrode was much larger than that with C_1=47 pF. More metal sludge and bubbles are thought to be generated from the electrochemical reaction with the higher material removal rate in the working gap. The electrolyte temperature is higher due to higher Joule heating, resulting in boiling of the electrolyte. Hence, it may be difficult to keep the average peak voltage equal to the reference voltage without a large retraction motion of the tool electrode.

Material removal rates at different reference voltages are shown in Fig. 3.36. The material removal rates are significantly higher compared with Fig. 3.28 where C_1= 47 pF. As shown in Fig. 3.31, larger C_1 results in higher gap voltage under the same gap width. Hence, the frontal gap width should be narrower when C_1=68 pF than when C_1=47 pF under the same reference voltage. Thus, the reference voltage at which the MRR peaks was 2.5 V when C_1=68 pF, higher than that when C_1=47 pF.

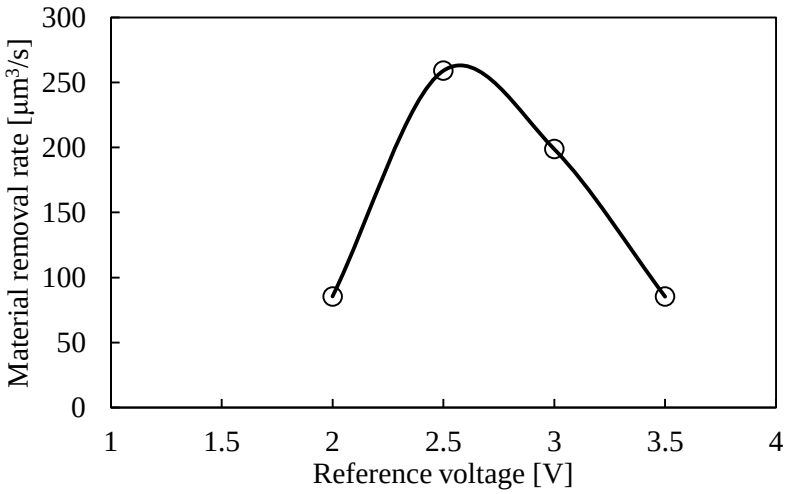

Fig. 3.36 Material removal rate with different reference voltages

3.4.5 Through-holes machining

Through-holes were machined to investigate the straightness of the holes machined with different reference voltages.

3.4.5.1 Experimental conditions

The tool electrode was a tungsten rod 50 μm in diameter fabricated by the wire electro-discharge grinding method (WEDG). The workpiece was a stainless steel (SUS304) plate of 50 μm in thickness. NaCl aqueous solution of 2 wt% was used as the electrolyte, and jetted from a nozzle with an inner diameter of 200 μm, which was set close to the machining gap, at a flow rate of 10 ml/min. The tool electrode was positioned over the

workpiece with an initial gap width of 10 μm. The machining conditions are shown in Table 3.8. A feeding capacitance of 47 pF was used to obtain higher accuracy.

Table 3.8 Experimental conditions used to machine through-holes

Pulse voltage	Amplitude [V]	20
	Frequency [Hz]	500 k
	Duty factor [%]	50
	Rise/fall time [ns]	40
Feeding capacitance C_1 [pF]		47
Electrolyte		NaCl aq. 2 wt%
Tool electrode rotation [rpm]		3000
Reference voltage [V]		2, 2.5
Tool electrode		Φ50 μm tungsten
Workpiece		Stainless steel (SUS) plate 50 μm in thickness

3.4.5.2 Straightness of through-holes

Fig. 3.37 shows machined through-holes at different reference voltages. It took 15.64 min and 14.28 min with the reference voltage of 2 V and 2.5 V, respectively. Since the machining process at last stage became not as stable as initial machining process with a small working gap, the lower reference voltage of 2 V, which results in a smaller working gap, took a little longer time to complete the machining. The inlet side gap width and outlet side gap widths are shown in Fig. 3.38. Both the inlet and outlet side gap widths were smaller with the lower reference voltage of 2 V, because the working gap is smaller with lower reference voltage. The taper of through-hole can be evaluated by the difference between the inlet and outlet side gap widths. However, there was no significant difference between the reference voltages of 2 V and 2.5 V in taper, as shown in Fig. 3.38. This is because the taper angle was determined not only by the gap width, which is controlled by the reference voltage, but also by the total time during which the stray current flows in the gap. In addition, the side wall of the reference voltage of 2 V was smoother than the 2.5 V. This is because the current density is higher in the smaller gap width with lower reference voltage. However, it should be noted that the side walls were significantly rough compared with the bottom surfaces shown in the previous sections. This is because the side surface was roughened under the low current density in the large gap.

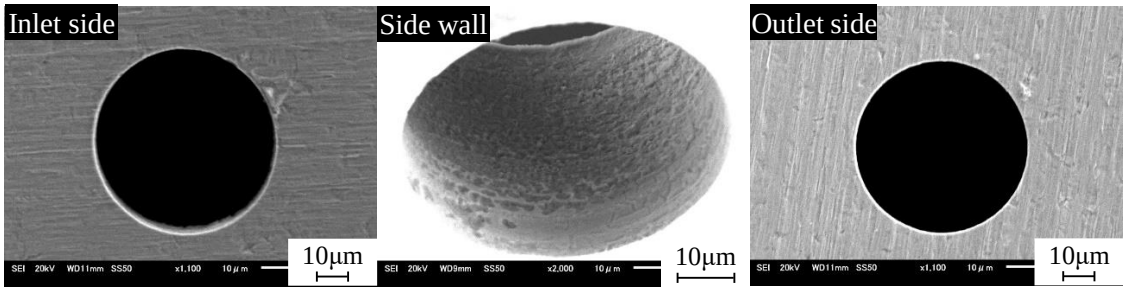

(a) Reference voltage of 2V

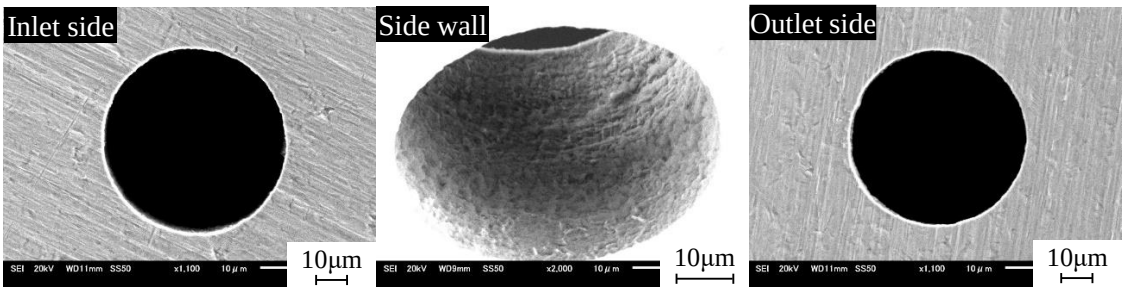

(b) Reference voltage of 2.5V

Fig. 3.37 Machined through-holes with different reference voltages

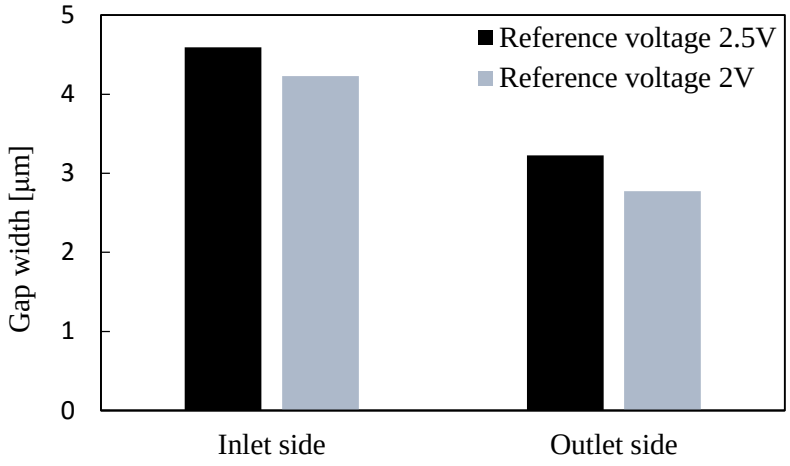

Fig. 3.38 Inlet and outlet side gap width of through-holes with different reference voltages

3.4.5.3 Machining accuracy comparison with micro-EDM

Micro-EDM using the electrostatic induction feeding method shows the highest ability to obtain minimum machinable size in EDM[74]. Koyano[72] investigated the influence of rotation speed of the tool electrode on the machining accuracy of micro-holes as shown in Fig. 3.39. The experimental conditions are shown in Table. 3.8. The diameter of tool electrode was 80 μm and the thickness of workpiece (SUS304) was 100 μm. It is found

that the inlet side gap width of EDM was about 3-4 μm, which was 3.75%-5% of the diameter of the tool electrode. In the present ECM process, the inlet side gap width was about 4 μm, which was 8% of the diameter of the tool electrode. On the other hand, the outlet side gap width was smaller than 1μm with the EDM process, which was smaller than 1.25% of the diameter of the tool electrode. With the ECM process, the outlet side gap width was about 3μm, which was 6% of the diameter of the tool electrode. Hence, the gap width of the electrostatic induction feeding ECM was larger than the electrostatic induction feeding EDM process. However, order is almost the same. Thus, it can be concluded that the machining accuracy of the present ECM can compete with that of micro-EDM.

Table 3.8 Experimental conditions to investigate the influence of tool rotation speed

Pulse voltage	Amplitude [V]	140
	Frequency [Hz]	800 k
	Duty factor [%]	50
Dielectric		EDM oil
Feeding capacitance C_1 [pF]		16
Tool electrode		Tungsten (Φ80 μm)
Workpiece		Stainless steel (SUS304)
Rotation [rpm]		1000, 50000

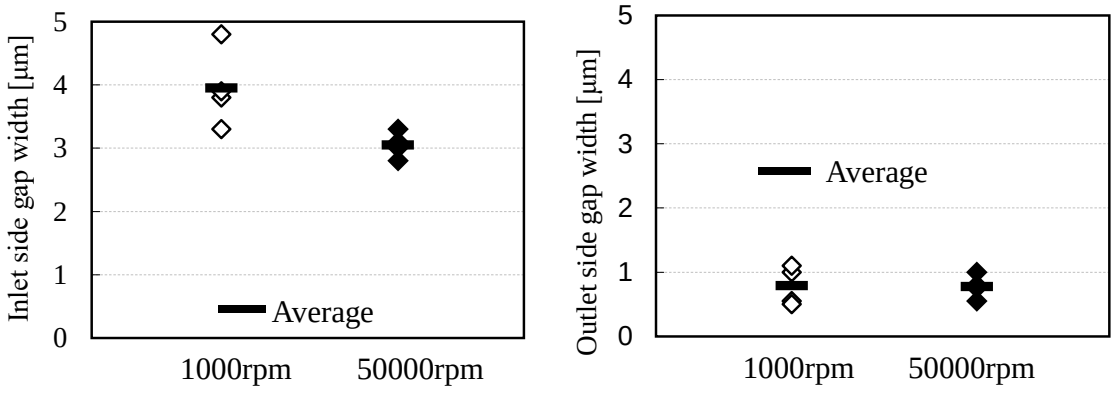

(a) Inlet side gap width (b) Outlet side gap width

Fig. 3.39 Inlet and outlet side gap width with different rotation speeds[72)]

3.5 Conclusions

Since the working gap was significantly small with the electrostatic induction feeding ECM, collision between electrodes easily occurred between electrodes. In order to avoid

the collision and improve the machining accuracy, servo feed control system was developed based on the characteristics of electrostatic induction feeding ECM. The machining characteristics of the servo feed control were investigated.

Using the conventional servo feed control system by monitoring the average gap voltage, the machining characteristics were investigated. Micro-holes with smooth bottom surface were successfully drilled using the average gap voltage method. The inlet side gap width increased with increasing the reference voltage, because the electrochemical reaction occurred in the larger gap width with the higher reference voltage. However, the material removal rate did not change obviously with different reference voltages. It is considered that the average gap voltage was 200 mV or less due to the pulse duration of several tens of ns with significantly low duty ratio. Hence, the gap control accuracy was not sufficiently high with the average gap voltage method because of the low S/N ratio. In order to solve the problem of low S/N ratio and improve the gap control accuracy, a new method with monitoring the peak gap voltage was developed. The peak voltage was detected and held to obtain a high input voltage for the servo feed control system, and it was reset in every period to keep a high response. Compared with the average gap voltage method, the gap control sensitivity was improved by increasing the S/N ratio. With the peak voltage method, lower reference voltage resulted in higher material removal rate, because of the smaller working gap, leading to higher current density on the bottom surface. Thus, current is concentrated on the bottom surface, and furthermore the current efficiency is increased. However, the material removal rate decreased with a significantly small reference voltage because the tool electrode frequently retracted due to the collision between electrodes with a significant small working gap. Hence, the material removal rate peaks at an optimum reference voltage. In addition, the material removal rate was higher with larger feeding capacitance C_1. This is because the electric charge per each pulse is proportional to C_1. The inlet side gap width was nearly the same independent of C_1. With the peak gap voltage method, through-holes of 50 μm in diameter were machined on a stainless steel (SUS304) plate of 50 μm in thickness with different reference voltages. The diameter of the hole was smaller and the surface roughness on the side wall was smoother with the reference voltage of 2 V than that with 2.5 V.

Comparison of the straightness and side gap width of the holes drilled by the present ECM method with those of micro EDM shows that the machining accuracy of the present method can compete with that of micro EDM. Furthermore, the material removal rate of the electrostatic induction feeding EDM was much higher than the ECM. In EDM, the discharge occurs only at a single discharge location per each pulse, hence, volumetric

removal rate is constant. As a result, the volumetric removal rate of ECM is significantly high, compared with EDM when the machining area is large. In micro ECM, however, the advantage of the high removal rate is lost, because the machining area is small. Considering that ECM has advantages of no heat affected zone, no crack, and good surface equality, there is a possibility that the electrostatic induction feeding ECM can be used in place of micro EDM preferably in the finish machining.

Chapter 4 Fabrication of micro-rods

4.1 Introduction

Chapter 3 investigated the influence of working gap on machining accuracy in the electrostatic induction feeding ECM, and developed a servo feed control system to control the small working gap. Based on the research results in Chapter 3, micro-rods with a high machining accuracy were machined utilizing the small working gap.

Recent changes in demands from society have gradually led to the introduction of accurate and precise micro-tools for the micromachining of complex micro features in a wide range of engineering materials. Micro-rods have been widely used as tools in micro drilling and micro machining of 3D structures[52], probes in measuring system, and micro emitters for electrons and ions. When they are used for micro tools, there are many applications in various industries such as aerospace, biomedical, automobile, healthcare and consumer electronics. For the fabrication of micro tools with small dimensions, the available machining methods are those used in the integrated circuits industry such as lithography, electroforming, LIGA, and focused ion beam machining[75]. However, special costly machining equipments required for these methods lead to high costs and complex processes. On the other hand, micro tools have been successfully fabricated by micro electrical discharge machining (micro EDM). However, drawbacks such as the wear of the tool electrode and heat-affected zones below the machined surface exist due to the thermal effect of this process. Spur et al.[76] discovered that thin fins cut by wire EDM may bend due to the residual stress caused by the EDM process when fin thickness is smaller than 0.1mm in rough cutting. Sundaram and Rajurkar[77] analyzed the causes of surface cracks and material exfoliation after machining of micro rods by WEDG. Therefore, it is necessary to find alternative processes that can avoid the above mentioned drawbacks to fabricate micro rods. Electrochemical machining (ECM) is an anodic electrochemical dissolution process[78]. It has such advantages as no generation of burrs, cracks, nor heat-affected zones on the machined surface. Schuster et al.[18] found that use of ultra-short pulse in the order of several tens of ns realizes micro interelectrode gap which is equivalent to micro EDM. 3D features were machined on stainless plate with a platinum electrode of 10μm in diameter[17]. Hence, ECM is a potential method for fabricating precision micro tools. Mathew and Sundaram[79] fabricated micro-rods using a long pulse duration of 5ms as shown in Fig. 4.1, and the machining accuracy was deteriorated by an obvious taper at the root of the micro-rod as shown in the red ellipse.

This is because the electrochemical reaction cannot be localized in a small working gap with the long pulse duration of 5ms, and the material dissolution occurred in a large working gap. Hence, it is difficult to machine a precise micro-rod with a shape stage at the root area of the micro-rod. Therefore, the electrostatic induction feeding method was used to generate an ultra-short pulse duration of several tens of ns to localize the electrochemical dissolution in a small working gap. It is possible to machine a micro-rod with straight side surface and a shape stage at the root area due to the significantly small working gap.

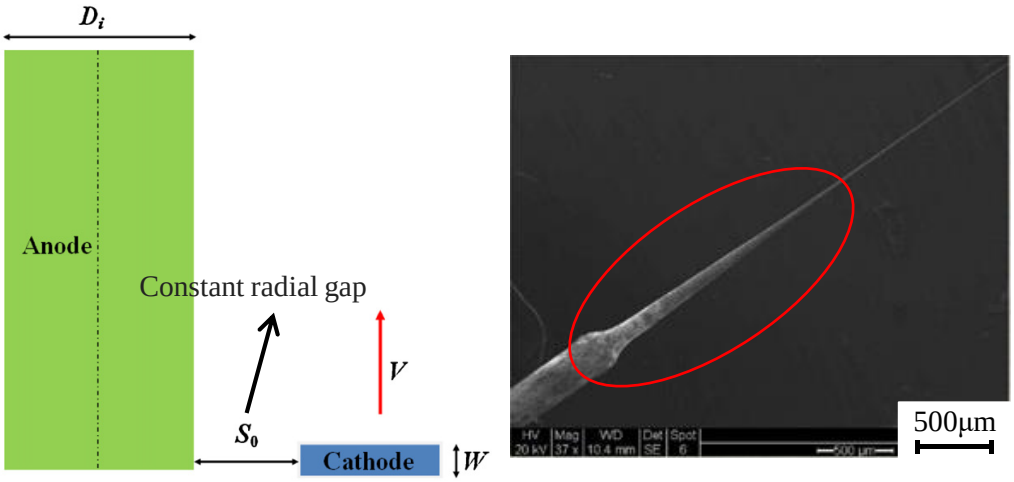

Fig. 4.1 Micro-rod machining using current in radial gap

This chapter describes the micro-rods machining with the electrostatic induction feeding ECM. The machining characteristics with the two different machining methods: the feeding of workpiece in axial direction and feeding of workpiece in radial direction, were investigated using the sodium chloride (NaCl) aqueous solution as electrolyte.

4.2 Machining methods of micro-rod

Fig. 4.2 shows the machining method of micro-rods used in this research. The pulse power is supplied by the electrostatic induction feeding method. The workpiece can be fed in axial and radial direction and there are two gaps formed during machining, axial gap and radial gap. A stainless steel (SUS304) rod of 200µm in diameter was fabricated by wire electro discharge grinding (WEDG) method[58] and used as the workpiece of micro ECM. The tool electrode was a tungsten plate. Stainless steel was used as the rod material because stainless steel is a widely used material. ECM is often used to machine mechanical parts, bearings, medial parts, micro needles, micro probes, hydraulic channels and pipes, because complicated shapes can be machined with higher MRR than milling

and mirror like finishing. Considering these applications, stainless steel is a suitable material to investigate machining characteristics using ECM. There are many applications of stainless micro rods such as micro needles for medical use, micro pipes for micro fluidics and reactors, micro dispensors in electronics industries, and micro probes. Stainless micro rods are also useful as micro tool electrodes in ECM because there is no tool wear in ECM.

The electrolyte was sodium chloride aqueous solution. It is reported that the working gap width can be decreased using lower concentration of electrolyte in micro ECM[68, 80]. Hence, the sodium chloride aqueous solution with low concentration of 2wt% was selected. During machining, the electrolyte was supplied from a nozzle with the inner diameter of 200μm to the machining gap at the flow rate of 10ml/min.

In order to obtain the pulse voltage of the electrostatic induction feeding method, the output of a function generator (Agilent, 33250A) was amplified by a bipolar amplifier (NF Corporation, HSA4101). As mentioned Section 1.8.2, the bipolar current of electrostatic induction feeding method may result in the tool wear when the polarity of the tool electrode is positive. Hence, a diode was attached in parallel to the working gap to avoid the wear of the tool electrode as shown in Fig. 4.3.

The servo feed control system developed in Chapter 3 was used in Chapter 4 to machine micro-rods, and the experimental results were shown in Section 4.3.4. However, the machining process was not as stable as the constant feed speed method. In addition, the constant feed speed method is more suitable for the fundamental research to get a deep insight into the process. Hence, the constant feed speed method was mainly used in Chapter 4.

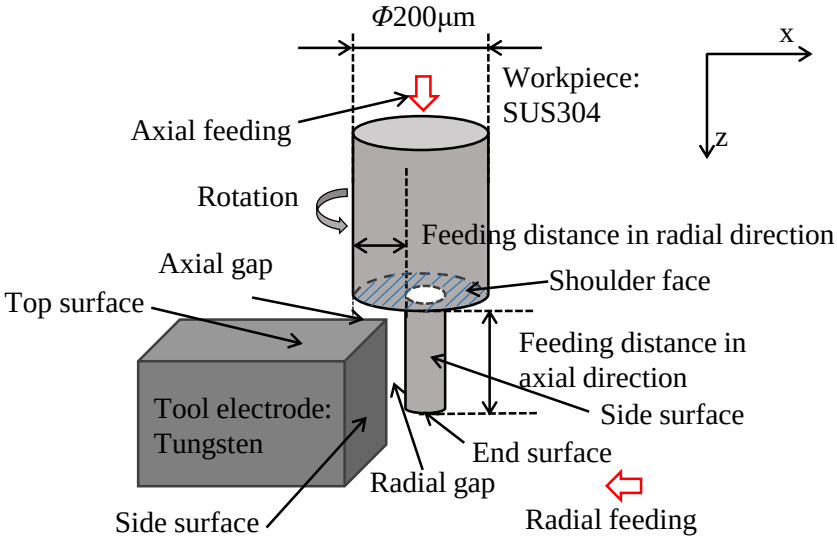

Fig. 4.2 Micro-rod machining method

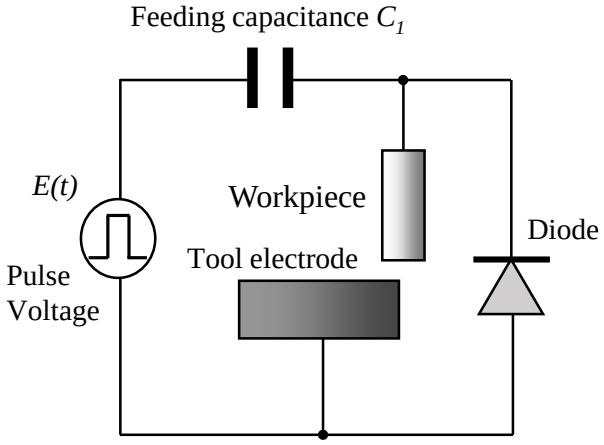

Fig. 4.3 Diode was used to avoid tool wear

4.3 Micro-rod machining with feeding of workpiece in axial direction

4.3.1 Influence of voltage amplitude

In order to investigate the influence of voltage amplitude on machining characteristics, the total amplitude of voltage was set as 90V, 100V and 110V, respectively.

4.3.1.1 Experimental conditions

The materials and size of electrodes are shown in Fig. 4.4. The materials of workpiece and tool electrode were stainless steel (SUS304) and tungsten, respectively. Stainless steel was used as rod material, because there are many applications of stainless micro rods such as micro needles for medical use, micro pipes for micro fluidics and reactors, micro dispersors in electronics industries, and micro probes. Tungsten was used as tool electrode because of the same reason described in Chapter 3. The workpiece rod was cut off from the reel of the stainless steel wire with diameter of 300μm and reshaped by the wire electro discharge grinding (WEDG) method to make it sufficiently straight, resulting in a reshaped size of 200μm in diameter and 300μm in length as shown in Fig. 4.5(b). The workpiece rod was positioned over the tool electrode with an initial axial gap width of 5μm before machining. The depth of cut in the radial direction was set at various values, and kept constant during machining. The feed distance in the axial direction was increased at a constant feed speed. Hence, the depth of cut in the radial direction and the feed distance in the axial direction determine the diameter and length of micro-rod machined, respectively. As shown in Fig. 4.4, two gaps are formed during machining, axial gap and

radial gap. The current should mainly flow through the axial gap, while the current in the radial gap should be limited because it would deteriorate the machining accuracy.

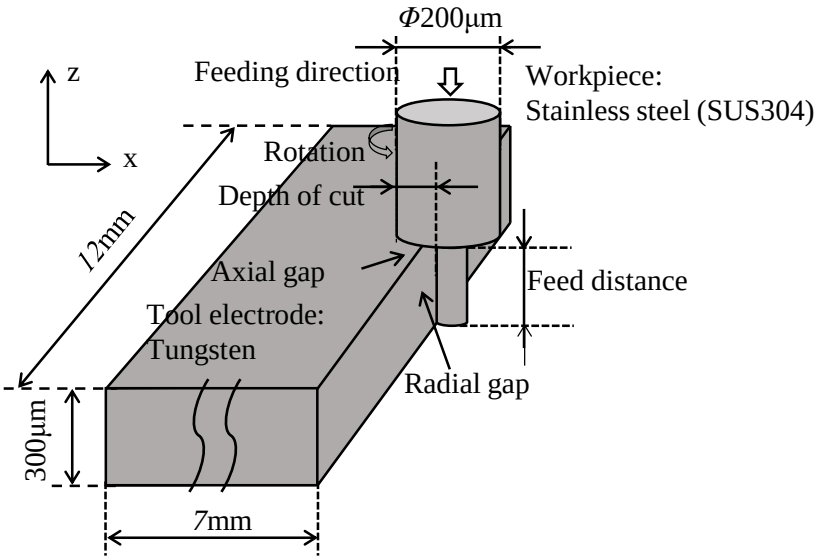

Fig. 4.4 Micro-rod machining with feeding of workpiece in axial direction

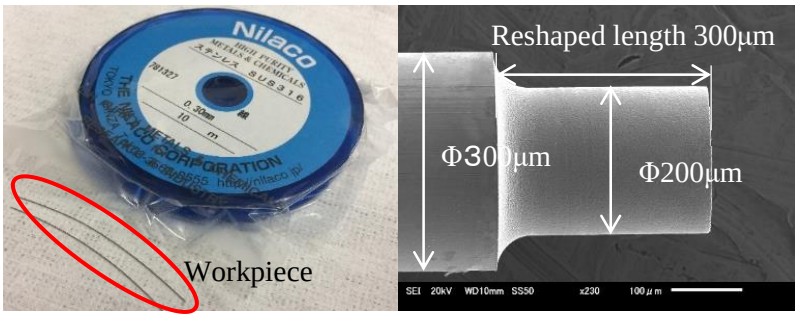

(a) Stainless steel (SUS304) wire (b) Reshaped workpiece by WEDG

Fig. 4.5 Reshaped workpiece by WEDG

Table 4.1 Experimental conditions used for feeding of workpiece in axial direction method

Pulse voltage	Amplitude [V]	90, 100, 110
	Frequency [Hz]	500k
	Duty factor [%]	50
	Rise/fall time [ns]	40
Feeding capacitance C_1 [pF]		47
Electrolyte		NaCl aq. 2wt%
Tool electrode rotation [rpm]		3000
Feed speed [μm/s]		0.2, 0.3, 0.4, 0.5, 0.6, 0.7, 0.8, 0.9, 1.0, 1.1

The experimental conditions are shown in Table 4.1. The total amplitude of pulse voltage was 90V, 100V and 110V, and the tool electrode was a tungsten plate with the surface size of 7mm×12mm, and the thickness of 300μm. The depth of cut in the radial direction was set as 50μm. The feed speed was set between 0.2μm/s and 1.1μm/s with an increment of 0.1μm/s.

4.3.1.2 Machinable length limitation

Fig. 4.6 shows the gap current and voltage waveforms with the pulse voltage amplitude of 90V and feed speeds of 0.4μm/s and 0.7μm/s. The gap current increased and voltage decreased due to the smaller gap width and gap resistance with the higher feed speed. Figs. 4.7(a) and (d) show micro-rods with feed speeds of 0.2μm/s and 0.8μm/s, respectively. With the significantly low feed speed of 0.2μm/s, many corrosion pits, which were generated by pitting corrosion, are observed on the side and shoulder surfaces of the micro-rod. Since the end surface is dissolved completely, it is difficult to obtain long micro rods with significantly low feed speeds. It is known that pitting corrosion occurs more easily with lower current density[81]. Furthermore, since the current density in the axial gap is low, the remaining current flows through the side and end surfaces because q is constant independent of the feed speed. Hence, the radial gap width increases, and pitting corrosion may occur not only on the shoulder surface but also on the side and end surfaces. With the higher feed speed of 0.8μm/s, the pitting corrosion is almost invisible on the shoulder surface, because of the small gap width in the axial gap. However, scratches were observed over the shoulder surface caused by collision between electrodes. This is because the gap width was significantly small with the feed speed of 0.8μm/s. The probability of collision increases with increasing feed distance because the stray current in the radial gap area is increased, resulting in decreased current density in the axial gap.

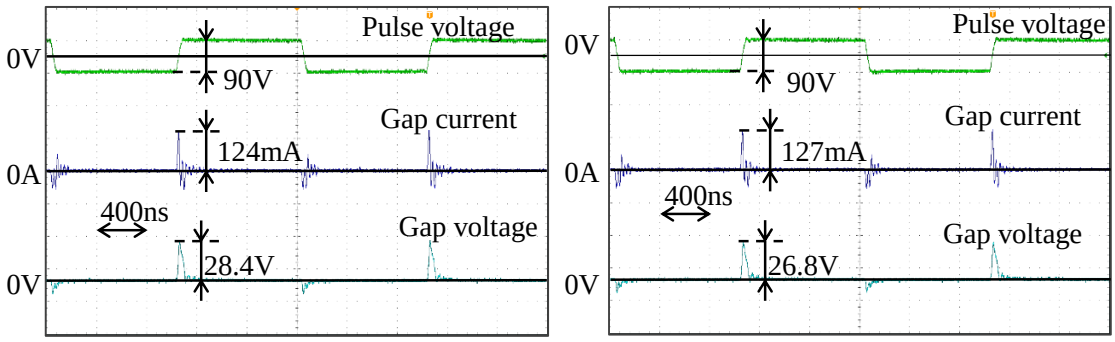

(a) Feed speed 0.4μm/s (b) Feed speed 0.7μm/s

Fig. 4.6 Waveforms with voltage amplitude of 90V

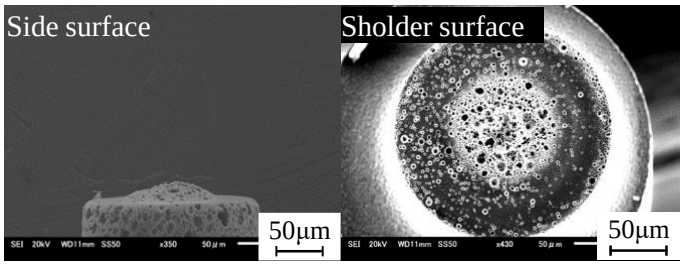

(a) Feed speed of 0.2μm/s

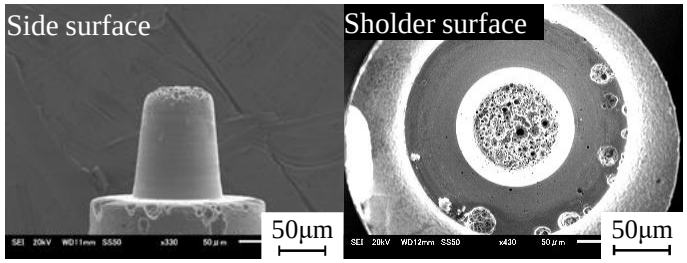

(b) Feed speed of 0.4μm/s

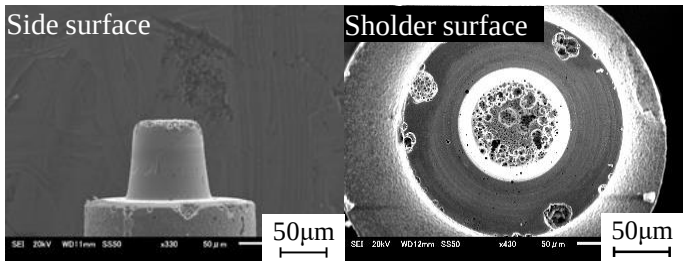

(c) Feed speed of 0.5μm/s

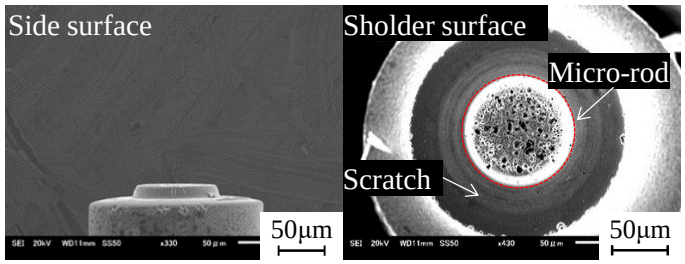

(d) Feed speed of 0.8μm/s

Fig. 4.7 Micro-rods with voltage amplitude of 90V and feed speeds of 0.2, 0.4, 0.5 and 0.8μm/s

To machine micro rods with high aspect ratio, the change in the machinable length limitations with different feed speeds was measured, and the experimental results are shown in Fig. 4.8. When the feed speed is low, pitting corrosion is likely to occur, and its probability increases with increasing the feed distance, because the increased radial gap area decreases the current density in the axial gap furthermore. Hence, the machinable length limitation is determined by the occurrence of pitting corrosion with lower feed speeds. Thus, with increasing feed speed, the limit increases. On the other hand, with

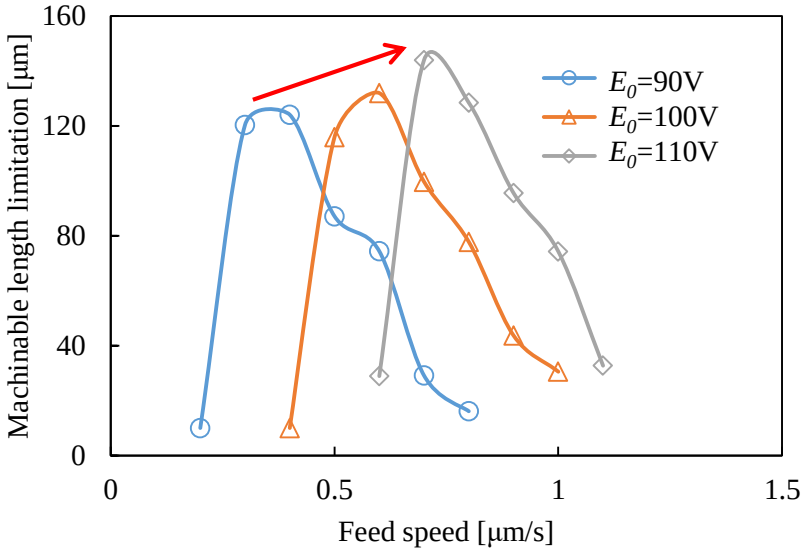

Fig. 4.8 Machinable length limitations with different feed speeds

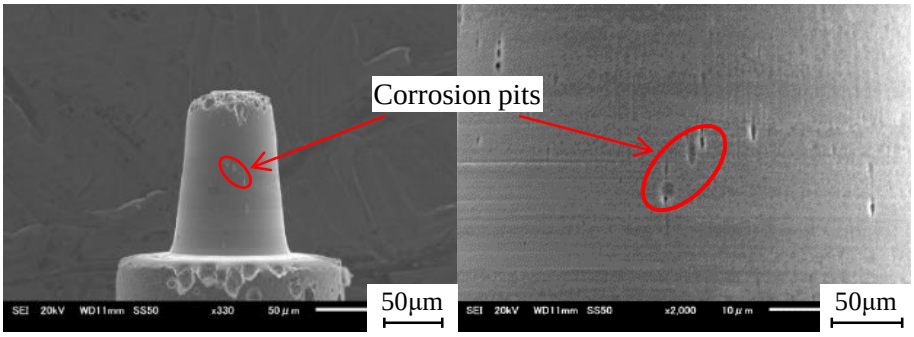

(a) SEM of micro-rod

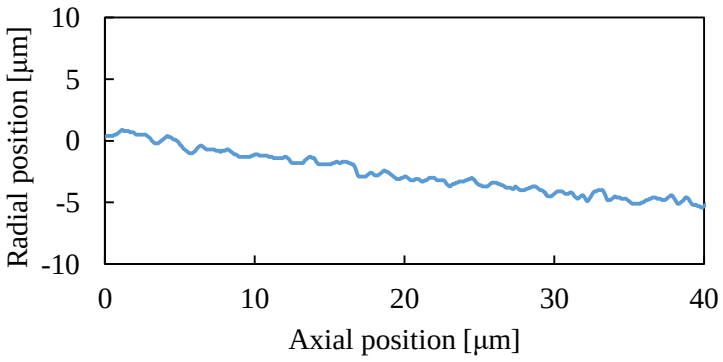

(b) Profile of micro-rod

Fig. 4.9 Corrosion pits on micro-rod and profile with voltage amplitude of 100V and feed speed of 0.6μm/s

higher feed speed, the probability of collision increases with increasing feed speed. Figs. 4.7(b) and (c) show micro-rods with machinable length limitations at the feed speeds of

0.4μm/s and 0.5μm/s, respectively. The length was decreased with feed speed of 0.5μm/s because the probability of collision increased with higher feed speed. Hence, the machinable length limitation peaks at a certain feed speed which is named the optimum feed speed. The peak is called the maximum length of micro-rod for a specific pulse voltage E_0. The optimum feed speed increases with increasing E_0, because $q=C_1E_0$. It is also found that the maximum length of micro-rod increases with increasing E_0.

4.3.1.3 Surface finish

The surface finish of micro-rod was smooth, as shown in Fig. 4.9, because the ECM is an anodic electrochemical dissolution process. However, some corrosion pits were generated by pitting corrosion on the side surface resulting in deterioration of the surface finish. To investigate the influence of machining conditions on pitting corrosion, the total number of corrosion pits generated on the side surface of micro-rod was measured. To obtain the total number, SEM photos of both sides were taken. Then the total number divided by the area of side surface was named the number of corrosion pits per unit area in this research. Fig. 4.10 shows the number of corrosion pits per unit area with different voltage amplitudes. It was found that the number of corrosion pits per unit area is minimum at the optimum feed speed at which the maximum length of micro-rod was obtained. This is because the electrochemical dissolution rate is in best balance with the feed speed, resulting in higher current efficiency in the axial gap and fewer corrosions in the radial gap.

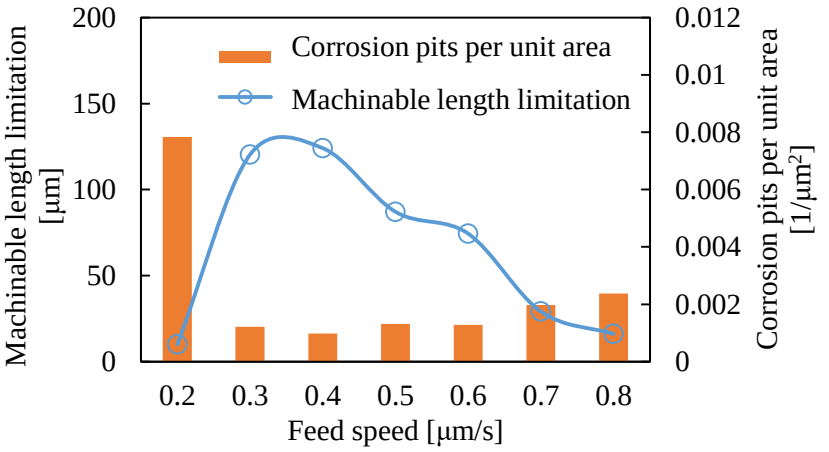

(a) Voltage amplitude 90V

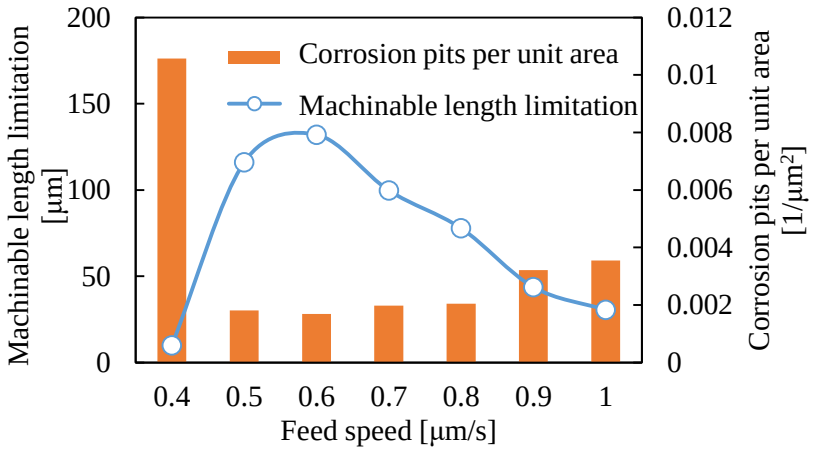

(b) Voltage amplitude 100V

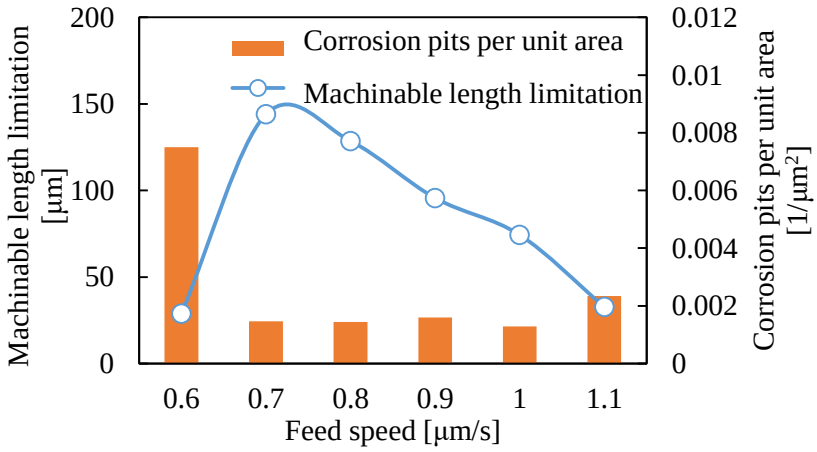

(c) Voltage amplitude 110V

Fig. 4.10 Corrosion pits per unit area with different voltage amplitudes

4.3.1.4 Straightness of micro-rod

It is noted that the side surface of micro-rod was not sufficiently straight as shown in Figs. 4.7(b) and (c), and a taper was generated after machining. This is because the material was removed not only in the axial gap, but also in the radial gap. In this experiment, the taper angle θ was defined as the included angle between the side surface and rod axis as shown in Fig. 4.11. In order to measure the taper angle θ of the micro-rod, diameters were measured with the same interval Δx by SEM as shown in Fig. 4.11. Then least squares fit was used to simulate the side surface of the micro-rod and calculate the taper angle θ. With the voltage amplitude of 90V and the feed speeds of 0.4μm/s and 0.6μm/s, the equations of the side surface were:

$$y = -35.487 + 0.355x \qquad \text{feed speed } 0.4\mu m/s$$
$$y = -40.368 + 0.034x \qquad \text{feed speed } 0.6\mu m/s$$

The above equations are shown in Fig. 4.12, where θ_1 and θ_2 are the taper angles.

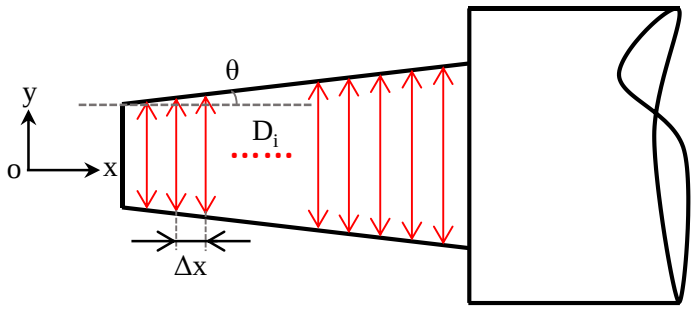

Fig. 4.11 Diameter measuring for calculating taper angle

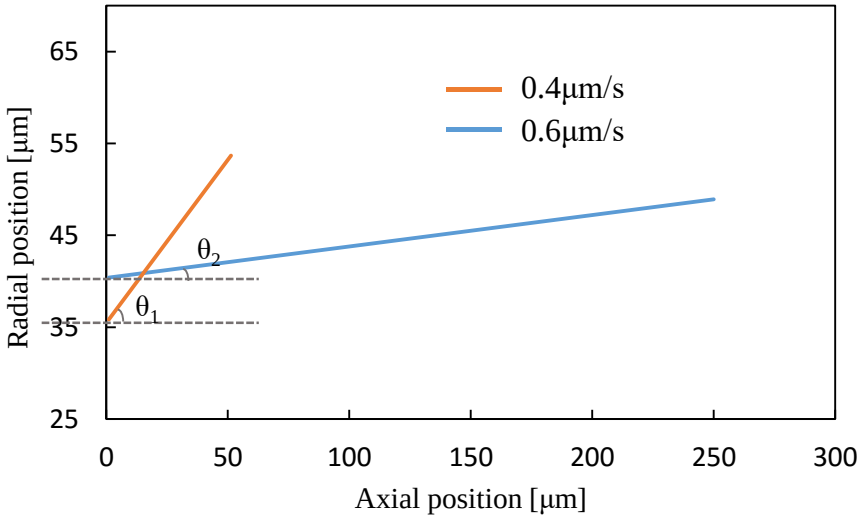

Fig. 4.12 Taper angle calculation with the feed speeds of 0.4μm/s and 0.6μm/s

The θ with different voltage amplitudes and feed speeds is shown in Fig. 4.13. With the same feed speed, the taper angle was larger with increasing the voltage amplitude. This is because the gap width was increased with increasing the voltage amplitude. With the same voltage amplitude, the taper angle decreased with increasing feed speed. Since the current in the axial gap increased due to the smaller gap width with higher feed speed, the stray current in the radial gap decreased because of constant $q=C_1E_0$ per pulse. Hence, the taper angle decreased with higher feed speed.

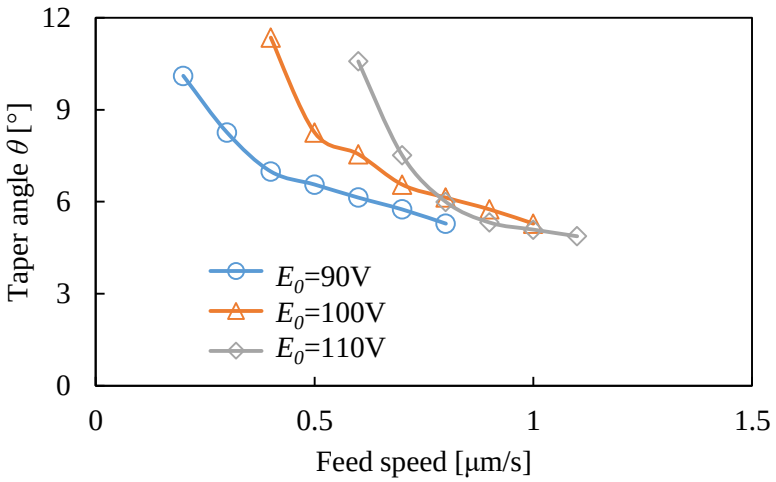

Fig. 4.13 Taper angle with different voltage amplitudes and feed speeds

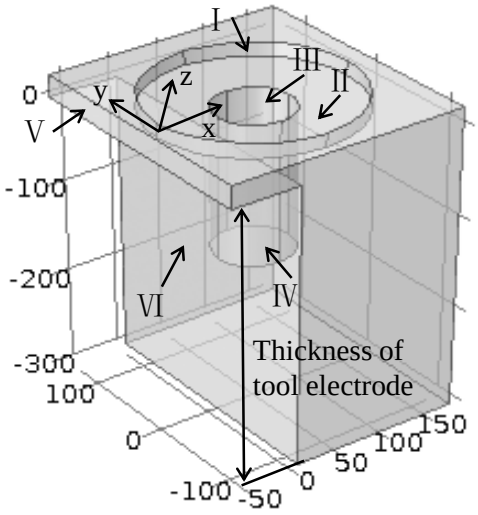

Fig. 4.14 Model of current density calculation

4.3.1.5 Gap current simulation corresponding to different feed speeds

In order to verify the result of small taper angle with higher feed speed, a 3D model was built to calculate the current density distribution using COMSOL Multiphysics as

shown in Fig. 4.14. Since the electric charge per pulse $q=C_1E_0$ is constant with the electrostatic induction feeding method, the constant current of 95mA during the pulse duration of 40ns was assumed based on the experimentally obtained waveforms. Hence, the total current flowing through the workpiece surfaces Ⅰ (radial surface of workpiece rod un-machined), Ⅱ (shoulder surface), Ⅲ (radial surface) of micro rod machined by ECM and Ⅳ (end surface) was set at 95mA and the potential of the tool electrode surfaces Ⅴ and Ⅵ was set as ground. Then, other surfaces were assumed as electrically insulative. The mesh size was a user-controlled mesh with extra fine element size. The axial gap width was varied at 2μm, 4μm, 6μm, 8μm and 10μm, which corresponds to the change in the feed speed, while the radial gap width was assumed to be constant at 12μm independent of the axial gap width. The electrolyte was sodium chloride (NaCl) aqueous solution with concentration of 2wt%. Fig. 4.15 shows the simulation results of the current density distribution on the workpiece surface. The current density on the side surface of the workpiece was averaged along y=0 and plotted in the graph with the axial gap width. It is found that the smaller axial gap width results in lower current density in the radial gap. This can well explain why the taper angle decreased with increasing feed speed as shown in Fig. 4.13.

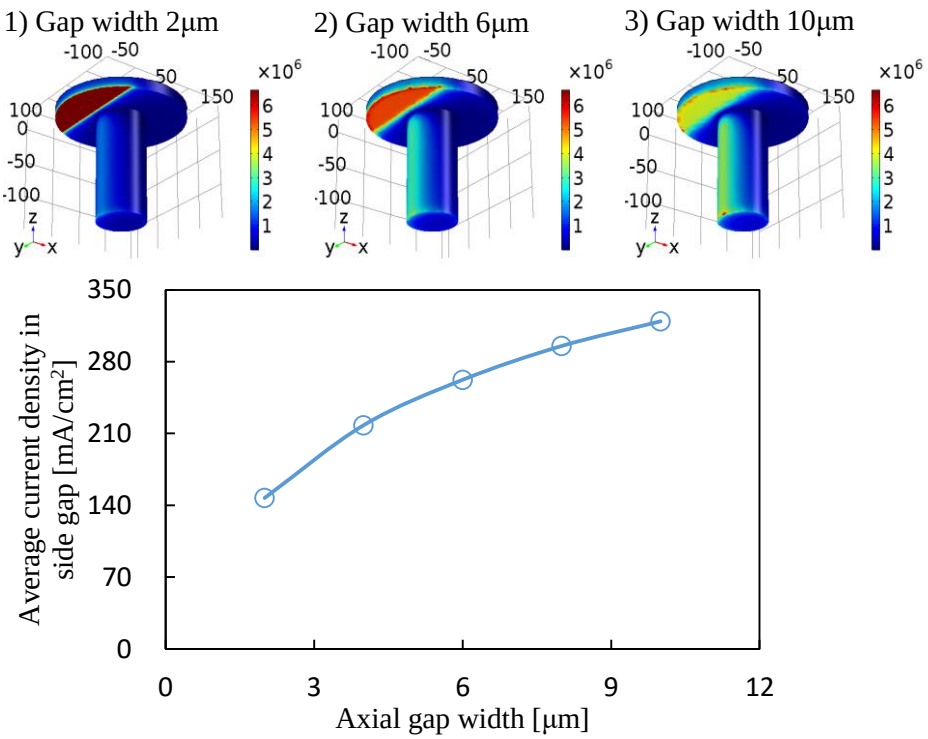

Fig. 4.15 Simulation of influence of axial gap width on current density distribution on workpiece surface

4.3.2 Influence of thickness of tool electrode

` The taper and corrosion pits were generated by the stray current flowing through the radial gap during machining. Hence, it is considered that decreasing the influence of stray current plays an important role in improving machining accuracy. Thus, the thickness of tool electrode was changed to decrease the area of radial gap and current flowing through it.

4.3.2.1 Experimental conditions

The experimental conditions are shown in Table 4.2. The total amplitude of pulse voltage was 90V. The materials of workpiece and tool electrode were stainless steel (SUS304) and tungsten, respectively. The workpiece was prepared in the same way as shown in Fig. 4.5. The tool electrode was a tungsten plate with surface area of 7×12mm^2. Thickness was varied at 25μm, 50μm and 300μm. The workpiece was positioned over the tool electrode with an initial axial gap width of 5μm. The depth of cut in the radial direction was set as 50μm, and the feed distance in axial direction was continued until the machinable length limitation corresponding to each feed speed. The feed speed was changed from 0.2μm/s to 1μm/s with an increment of 0.1μm/s.

Table 4.2 Experimental conditions used to investigate influence of thickness of tool electrode

Pulse voltage	Amplitude [V]	90
	Frequency [Hz]	500k
	Duty factor [%]	50
	Rise/fall time [ns]	40
Feeding capacitance C_1 [pF]		47
Electrolyte		NaCl aq. 2wt%
Tool electrode rotation [rpm]		3000
Feed speed [μm/s]		0.2, 0.3, 0.40.5, 0.6, 0.7, 0.8, 0.9, 1.0
Thickness of tool electrode [μm]		25, 50, 300

4.3.2.2 Machinable length limitation

Fig. 4.16 shows the waveforms of gap current and voltage with tool electrode of 25μm in thickness and feed speeds of 0.6μm/s and 0.7μm/s. Compared with Fig. 4.6, where the thickness of tool electrode was 300μm and the feed speed was 0.7μm/s, the peak of gap current decreased from 127mA to 96mA with decreasing the thickness of tool electrode. This is because the gap resistance increased due to the decrease in the gap area with decreasing thickness of the tool electrode. Fig. 4.17 shows the micro-rods machined with

a tool electrode of 25μm in thickness and feed speeds of 0.6μm/s and 0.7μm/s, of which the machined length limitation was 250μm and 179μm, respectively.

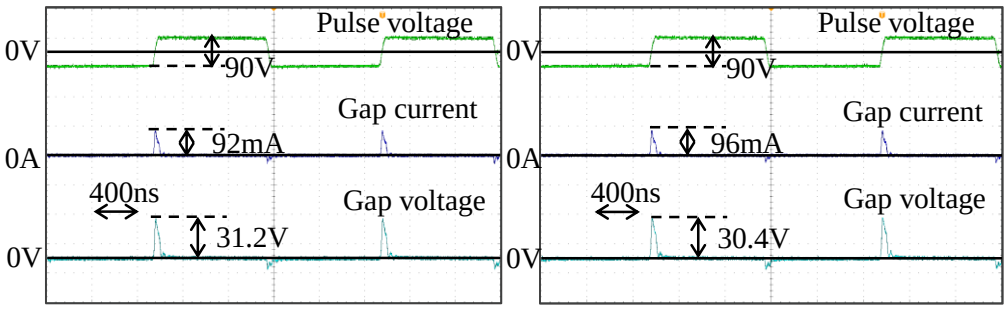

(a) Feed speed 0.6μm/s (b) Feed speed 0.7μm/s

Fig. 4.16 Waveforms with tool electrode of 25μm in thickness and feed speeds of 0.6μm/s and 0.7μm/s

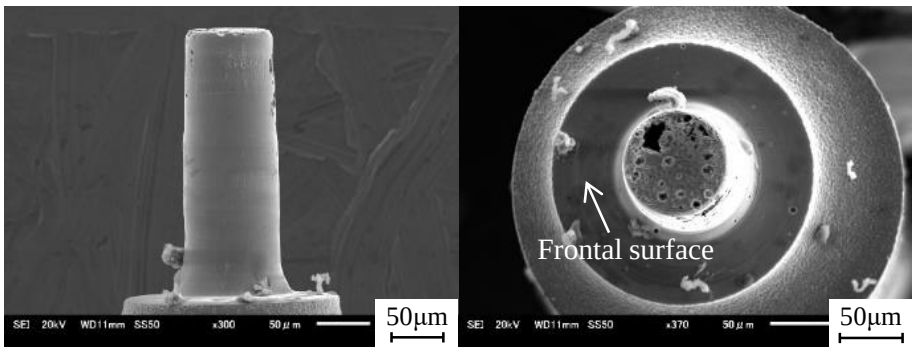

(a) Feed speed of 0.6μm/s

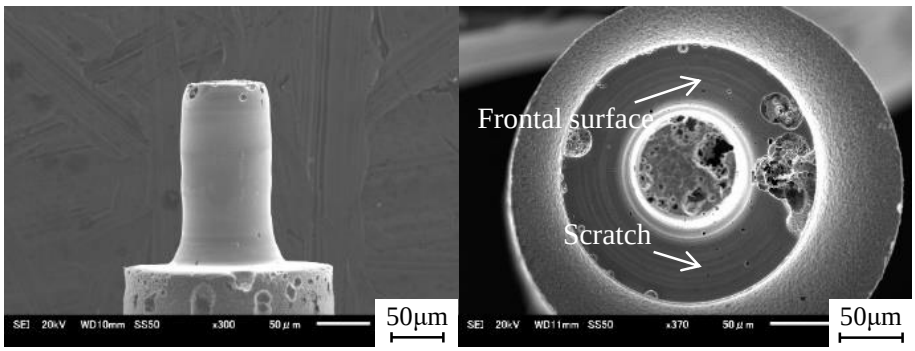

(b) Feed speed of 0.7μm/s

Fig. 4.17 Micro-rods with tool electrode of 25μm in thickness and feed speeds of 0.6μm/s and 0.7μm/s

Fig. 4.18 shows the machinable length limitations with different thicknesses of tool electrode. For each thickness, the maximum length of micro-rod was obtained at the optimum feed speed. It is found that the maximum length of the micro-rod increased with

decreasing thickness of the tool electrode. When the thickness of the tool electrode was decreased, the stray current flowing through the radial gap decreased due to the decrease in the gap area. Furthermore, since the electric charge $q=C_1E_0$ is constant with the electrostatic induction feeding method, the current in the axial gap increased, resulting in the increase in the maximum length of micro-rod.

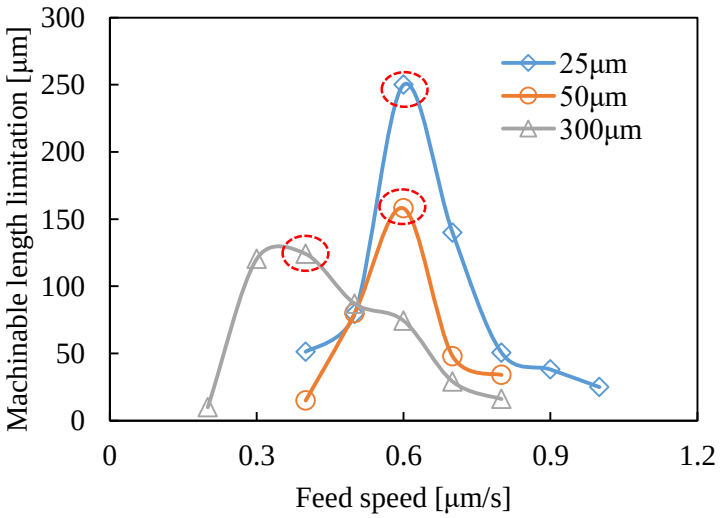

Fig. 4.18 Machinable length limitations with different thicknesses of tool electrode

4.3.2.3 Gap current simulation corresponding to different tool thicknesses

In order to study the change in the gap current with decreasing thickness of the tool electrode, a 3D model was built in COMSOL Multiphysics. The model was almost the same as in Fig. 4.14, except that the gap width of the axial gap was constant at 8μm and the thickness of tool electrode was varied at 25μm, 50μm, 100μm, 147μm, 200μm and 300μm, respectively. A constant current of 95mA was set on the working surface. Fig. 4.19 shows the simulation results of the current density distribution on the workpiece surface. The current density on the shoulder gap was averaged along y=0 and plotted in the graph with the tool electrode thickness. The average current density in the axial gap increased with decreasing thickness of the tool electrode. Hence, it is found that longer micro-rod can be machined with smaller thickness. The difference in the current density was small between the thickness of 200μm and 300μm, because the length of the micro-rod was set as 150μm shorter than the thickness of the tool electrode in the model, resulting in a smaller change in the current density with increasing thickness.

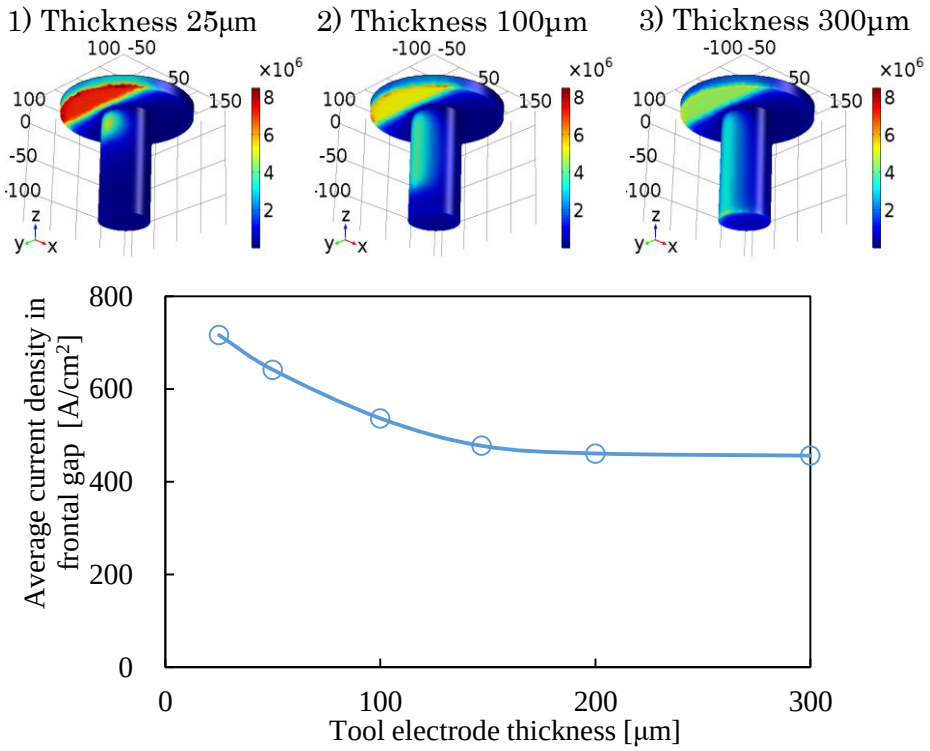

Fig. 4.19 Simulation of influence of tool electrode thickness on current density on workpiece surfaces

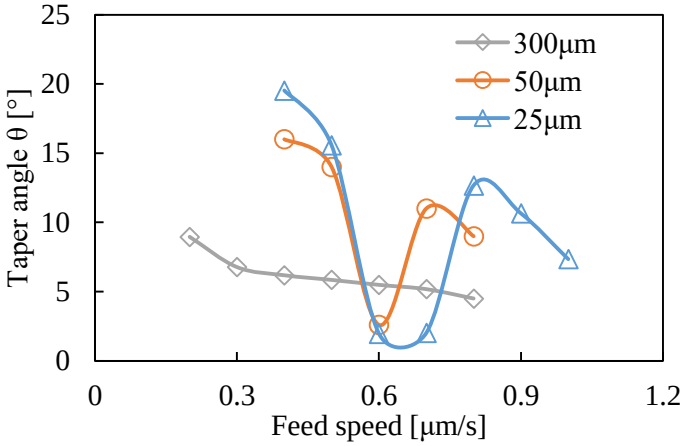

Fig. 4.20 Influence of thickness of tool electrode on taper angle

4.3.2.4 Straightness of micro-rod

Fig. 4.20 shows the taper angle θ with different thicknesses of the tool electrode. The taper angle was minimum at the optimum feed speed at which the maximum length of the micro-rod was obtained, when tool electrodes of 25μm and 50μm in diameters were used. This is because the influence of the stray current in the side surface of the workpiece can be decreased using tool electrodes with thickness thinner than the length of the micro-rod

as shown in Fig. 4.19 (1) and (2). The minimum taper angle was smaller with thinner tool electrodes. This is because the current mainly flows in the root area, whereas on the side surface of the workpiece, the current density is significantly low.

4.3.2.5 Surface finish

Fig. 21 shows the influence of thickness of the tool electrode on pitting corrosion, when the rod workpiece was fed with the same distance and the same feed speed of 0.5μm/s. It is found that the corrosion pits per unit area decreased with decreasing the thickness of the tool electrode especially at the edge of the end surface. Since some stray current flew through the end of micro-rod during machining, the corrosion at the edge of the end surface was serious.

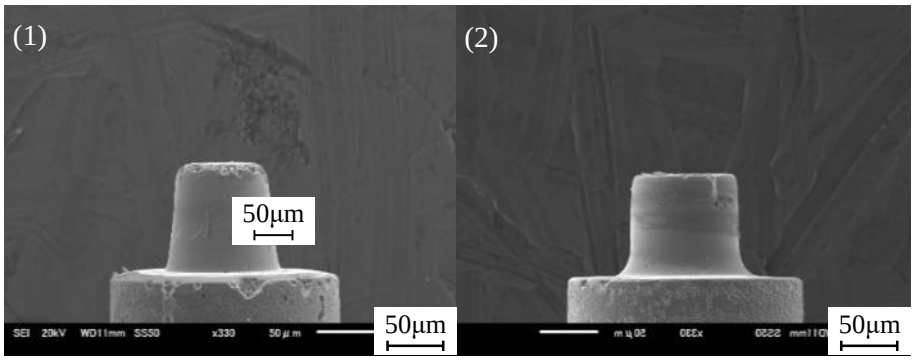

(a) Micro-rods with different thicknesses of tool electrode: (1) 300μm and (2) 25μm

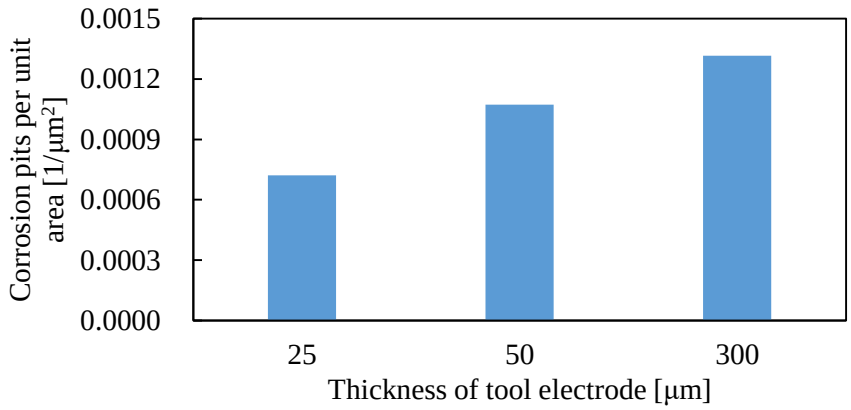

(b) Corrosion pits per unit area with different thicknesses of tool electrode

Fig. 4.21 Corrosion pits with different thicknesses of tool electrode

Fig. 4.22 shows the surface finish before and after machining with the thickness of the tool electrode of 25μm. The surface before machining was prepared by WEDG with the discharge capacitance of 10pF. Compared with the EDM surface, the surface finished by ECM was much smoother. Fig. 4.23 shows the corresponding profiles measured using a laser confocal microscope (Olympus, OLS3000). Despite the smoother surface after

machining, it is noted that there is a larger taper angle generated compared with the EDM surface.

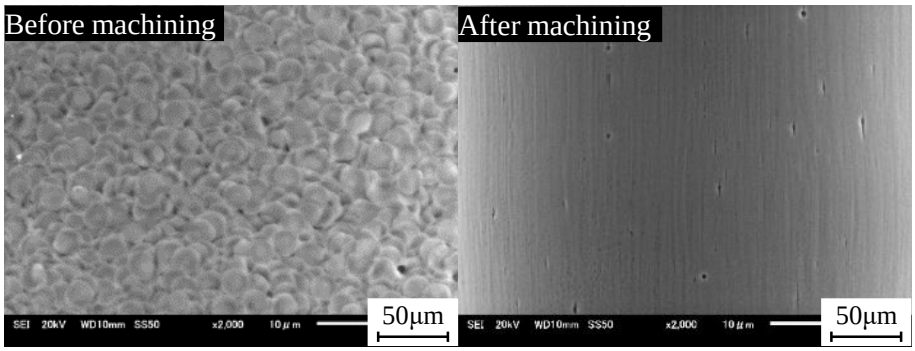

Fig. 4.22 Surface finish before and after machining with thickness of tool electrode of 25μm

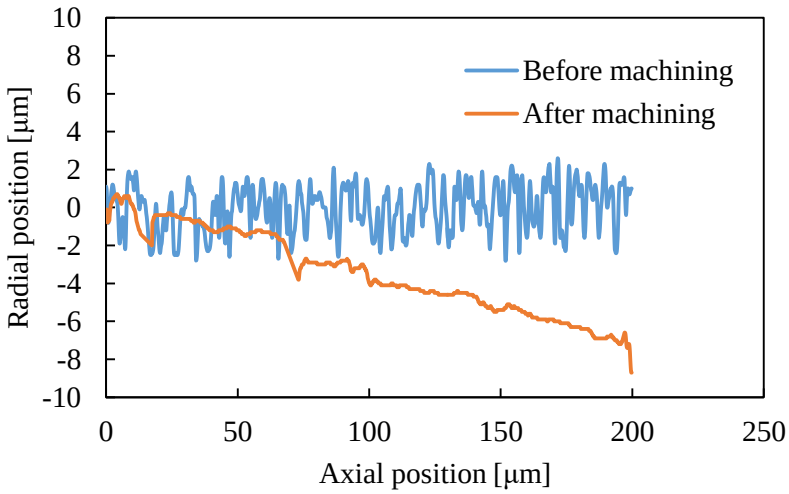

Fig. 4.23 Profiles before and after machining with thickness of tool electrode of 25μm

4.3.3 Influence of surface area of tool electrode

Stray current may flow over the top surface of the tool electrode where the distance from the axial gap is even far, which decreases the current density in the axial gap, because the electric charge per pulse $q=C_1E_0$ is constant. In addition, the current in the radial gap may also increase with increasing top surface area of the tool electrode, because the radial gap area increases. Hence, there is a necessary to investigate the influence of the top surface area of tool electrode on the machining characteristics.

4.3.3.1 Experimental conditions

The experimental conditions are shown in Table 4.3. In order to investigate the influence of the top surface area of the tool electrode on the machining characteristics, tool electrodes of two sizes were used in the experiment as shown in Fig. 4.24, which were named as large area and small area tool electrodes. The workpiece was positioned over the tool electrode with an initial axial gap width of 5μm. The depth of cut in the radial direction was set as 50μm, and the feed in the axial direction was continued until the machinable length limitation corresponding to each feed speed. The feed speed was changed from 0.4μm/s to 1μm/s with an increment of 0.1μm/s.

Table 4.3 Experimental conditions used to investigate surface area of tool electrode

Pulse voltage	Amplitude [V]	90
	Frequency [Hz]	500k
	Duty factor [%]	50
	Rise/fall time [ns]	40
Feeding capacitance C_1 [pF]		47
Electrolyte		NaCl aq. 2wt%
Tool electrode rotation [rpm]		3000
Feed speed [μm/s]		0.4, 0.5, 0.6, 0.7, 0.8, 0.9, 1.0

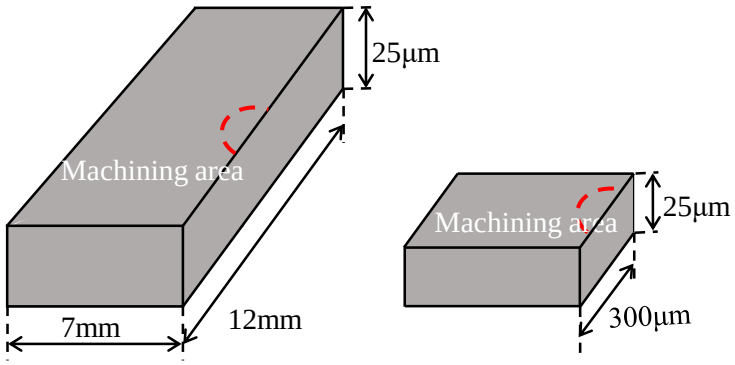

(a) Large area tool electrode (b) Small area tool electrode

Fig. 4.24 Tool electrodes with different top surface areas

4.3.3.2 Machinable length limitation

Fig. 4.25 shows the micro-rods machined with the small area tool electrode and feed speeds of 0.7μm/s, which was the optimum feed speed, and 0.9μm/s. Fig. 4.26 shows the comparison of the machinable length limitation between the small and large tool electrodes. The optimum feed speed of the small area tool electrode was slightly higher, however, the difference in the maximum machinable length was small.

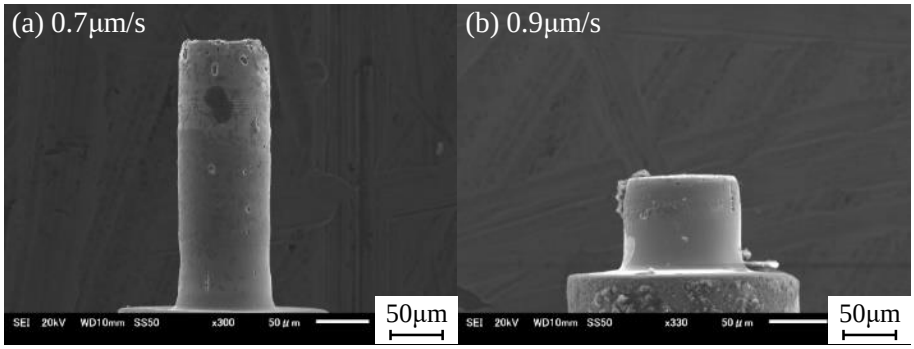

Fig. 4.25 Micro-rods with small area tool electrode and feed speeds of 0.7μm/s and 0.9μm/s

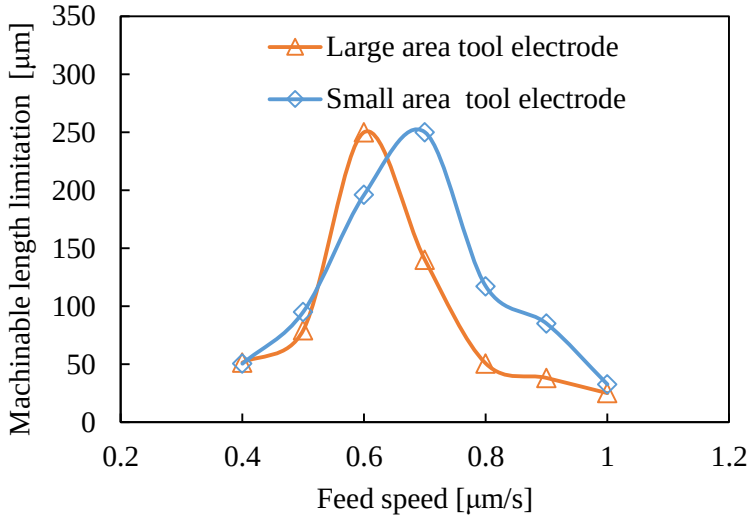

Fig. 4.26 Influence of top surface area of tool electrode on machinable length limitation

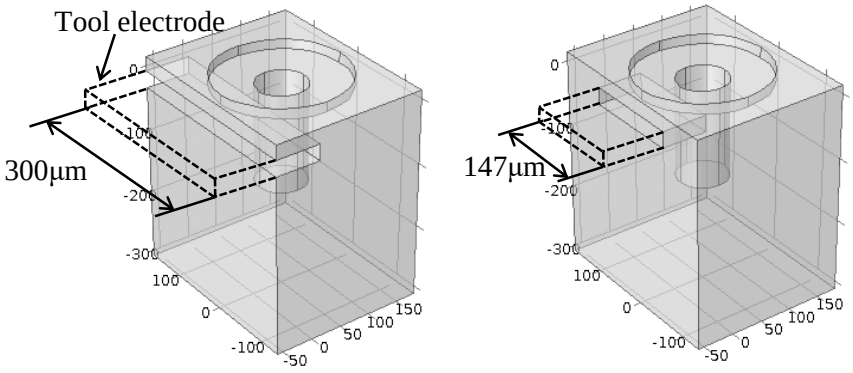

(a) Width of tool electrode 300μm (b) Width of tool electrode 147μm

Fig. 4.27 Simulation model with different top surface areas of tool electrodes

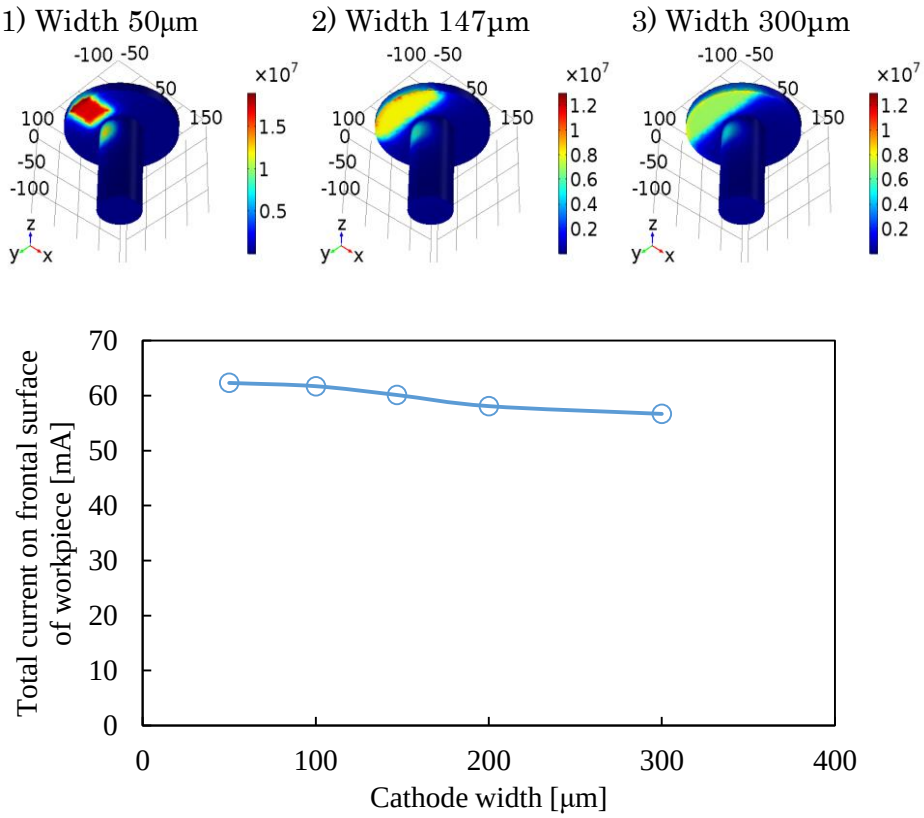

Fig. 4.28 Influence of top surface area of tool electrode on current density distribution

4.3.3.3 Gap current simulation corresponding to different tool surface area

In order to investigate the slight difference between large and small area tool electrodes as shown in Fig. 4.26, a simulation model was built up in COMSOL Multiphysics as shown in Fig. 4.27, in which the current density distribution was calculated with changing the top surface area of tool electrode. The width of the tool electrode was changed at 50μm, 100μm, 147μm, 200μm and 300μm, respectively. The gap widths of the surface and radial gaps were 8μm and 12μm, respectively. Constant current 95mA was set in the working gap and the boundary conditions were the same as Fig. 4.14. Fig. 4.28 shows the simulation results of current density distribution. There is a significant difference in the current density depending on the top surface area. However, since the machining area is different, the material removal rate in the axial gap is not determined by the current density, but by the total current flowing in the axial gap. Hence, the total current on the shoulder gap of workpiece was calculated with different widths of tool electrodes. The results in the graph show that the total current in the axial gap was obviously increased with decreasing width of the tool electrode, however, the difference in the total current on the shoulder gap of the workpiece was insignificant resulting in a small difference in

MRR. Thereby, it was found that the influence of the top surface area of the tool electrode on the maximum machinable length was small as shown in Fig. 4.28.

4.3.3.4 Surface finish

Fig. 4.29 shows the corrosion pits per unit area with the small and large area tool electrodes. Since the difference in the total current in the axial gap between the small and large area tool electrodes was small as shown in Fig. 4.28, the difference in the total current in the radial gap was also small. Hence, the difference in the corrosion pits per unit area with small and large area tool electrodes was insignificant as shown in Fig. 29.

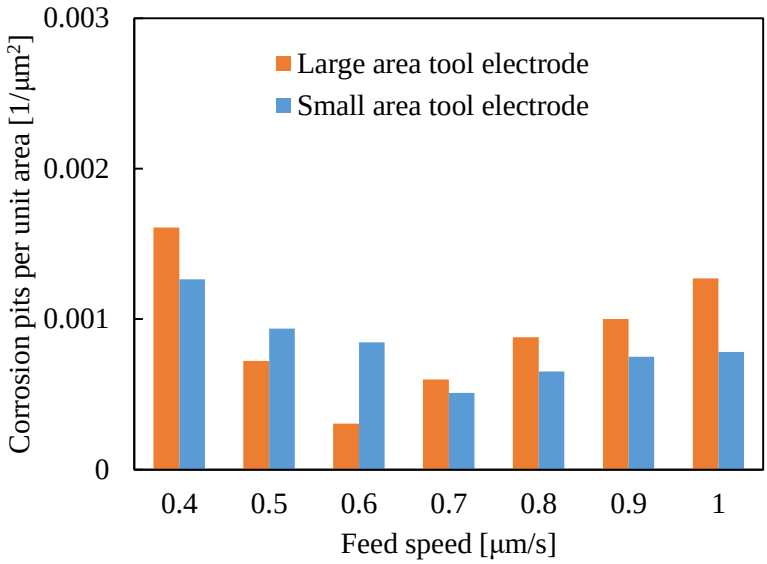

Fig. 4.29 Corrosion pits per unit area with large and small area tool electrode

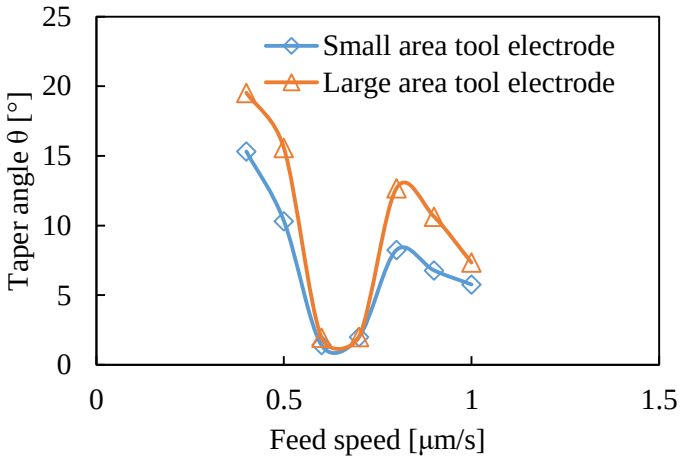

Fig. 4.30 Taper angle with small and large area tool electrodes

4.3.3.5 Straightness of micro-rod

Fig. 4.30 shows the taper angle with the small and large area tool electrodes. Since the difference in the total current in the axial gap between the small and large area tool electrodes was small as shown in Fig. 4.28, the difference in the total current in the radial gap was also small. Hence, the difference in the taper angle with small and large area tool electrodes was insignificant as shown in Fig. 4.30.

4.3.4 Micro-rod machining with servo feed control

In this section, the servo control characteristics of rod machining were investigated using the servo feeding control system developed, by which the gap width was controlled by monitoring the peak of gap voltage. Since the peak voltage was about 30V in the experiment which was much higher than the maximum input voltage of 15V with the circuit for the servo feed control shown in Fig. 3.16, in which the maximum input voltage of the used IC is 15V, the gap voltage was attenuated to 1/3 of the original value, which was then input to the servo control circuit.

Table 4.4 Experimental conditions used for micro-rods machining with servo feeding control

Pulse voltage	Amplitude [V]	90
	Frequency [Hz]	500k
	Duty factor [%]	50
	Rise/fall time [ns]	40
Feeding capacitance C_1 [pF]		47
Electrolyte		NaCl aq. 2wt%
Tool electrode rotation [rpm]		3000

The relationship between the gap width and the average peak voltage was measured under the experimental conditions shown in Table 4.4. The tool electrode was positioned on the workpiece with a fixed gap width of 3μm to 12μm. The feed distance in radial direction was 50μm. The materials of workpiece and tool electrode were stainless steel (SUS304) and tungsten, respectively. The diameter of the tool electrode was 200μm as shown in Fig. 4.5. The size of the tungsten plate electrode is shown in Fig. 4.31. When the pulse voltage was applied for several seconds, the averaged peak voltage was measured by the servo feeding control system developed. Fig. 4.32 shows waveforms of the averaged peak voltages with gap widths of 3μm and 9μm. The results are summarized in Fig. 4.33. It can be found that peak voltage increases with increasing the gap width.

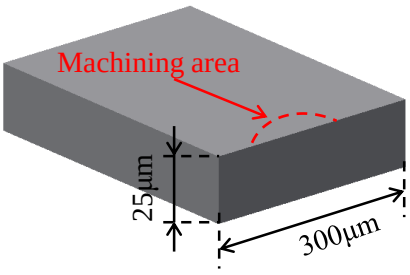

Fig. 4.31 Size of tungsten plate electrode

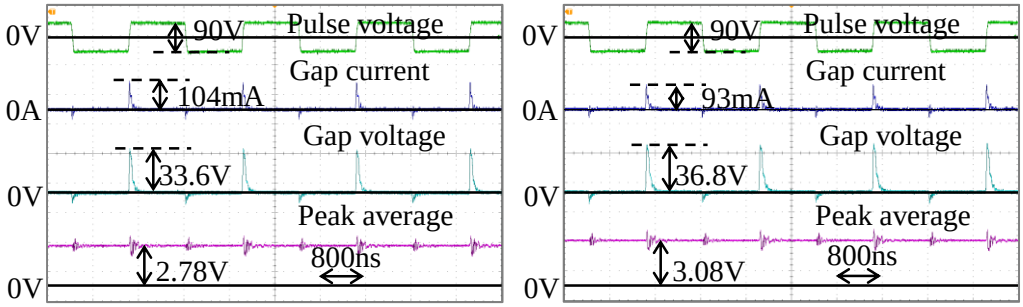

(a) Gap width 3μm (b) Gap width 9μm

Fig. 4.32 Waveforms with gap widths of 3μm and 9μm

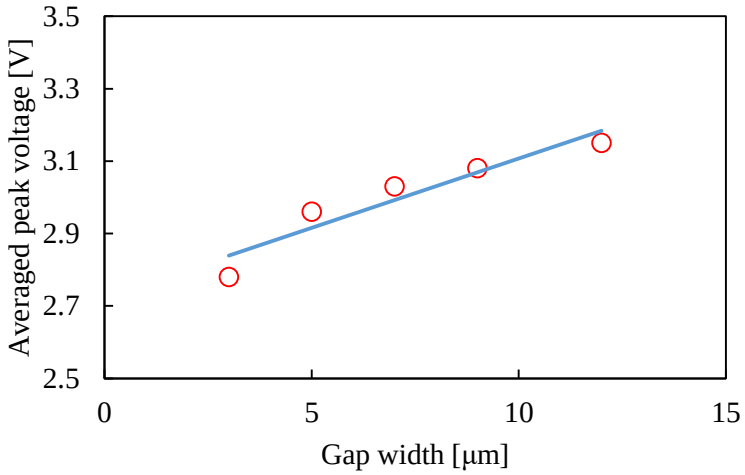

Fig. 4.33 Relationship between gap width and averaged peak voltage in rod machining with axial feeding method

4.3.4.1 Experimental conditions

In order to investigate the influence of the servo reference voltage, micro-rods were machined with different reference voltages using the developed servo feed control system. The experimental conditions are shown in Table. 4.5. The materials of workpiece and tool electrode were stainless steel (SUS304) and tungsten, respectively. The diameter of the

workpiece was 200μm. The size of the tungsten plate is shown in Fig. 4.31. The workpiece was positioned over the tool electrode, at the position as shown in Fig. 4.31, with an initial gap width of 5μm. The cut depth in radial direction was set as 50μm, and the feed distance in axial direction was set as 100μm. The reference voltages were 2.4V to 3.0V with an increment of 0.2.

Table 4.5 Experimental conditions used to investigate the influence of reference voltage

Pulse voltage	Amplitude [V]	90
	Frequency [Hz]	500k
	Duty factor [%]	50
	Rise/fall time [ns]	40
Feeding capacitance C_1 [pF]		47
Electrolyte		$NaNO_3$ aq. 2wt%
Tool electrode rotation [rpm]		3000
Reference voltage [V]		2.4, 2.6, 2.8, 3.0

4.3.4.2 Material removal rate

Fig. 4.34 shows the waveforms of gap current and voltage with the reference voltages of 2.4V and 3.0V. Fig. 4.35 shows the displacements of tool electrode with different reference voltages. The collision between electrodes interrupted the machining quickly with the significantly low reference voltage of 2.4V at the beginning of machining. This is because the corresponding narrow gap width was too small. The machining could not be completed, either, with the highest reference voltage of 3.0V as shown in Fig. 4.35. This is because the current density in the gap was significantly low with the highest reference voltage because of large axial gap width.

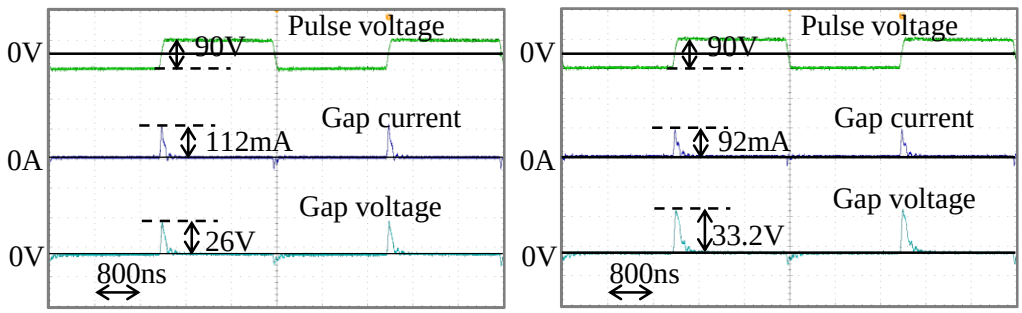

(a) Reference voltage 2.4V (b) Reference voltage 3.0V

Fig. 4.34 Waveforms with reference voltages of 2.4V and 3.0V in rod machining with axial feeding method

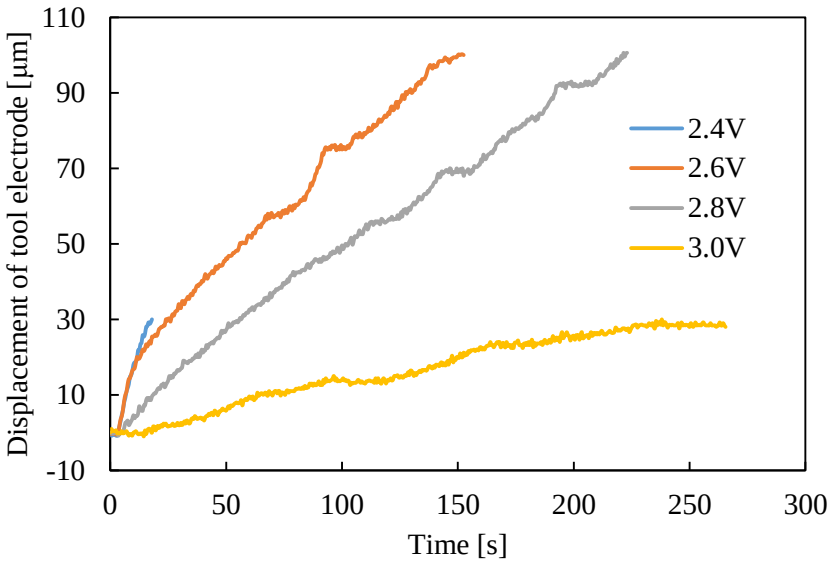

Fig. 4.35 Displacement of tool electrode with different reference voltages

Fig. 4.36 shows the micro-rods machined with the different reference voltages. The rod diameter was larger with smaller reference voltage, because of the smaller gap width in the axial gap, resulting in lower current density in the radial gap.

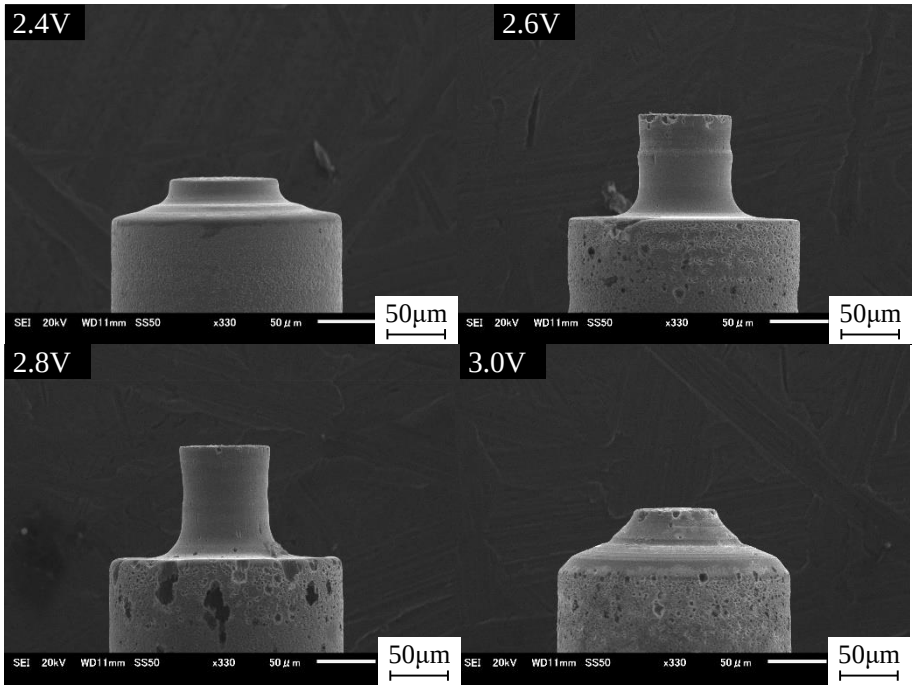

Fig. 4.36 Micro-rods with different reference voltages

Fig. 4.37 shows the material removal rate with different reference voltages. The material removal rate increased with decreasing the reference voltage, because the current

density in the axial working gap was higher with the lower reference voltage and smaller gap width, resulting in higher current efficiency of electrochemical dissolution in the axial gap.

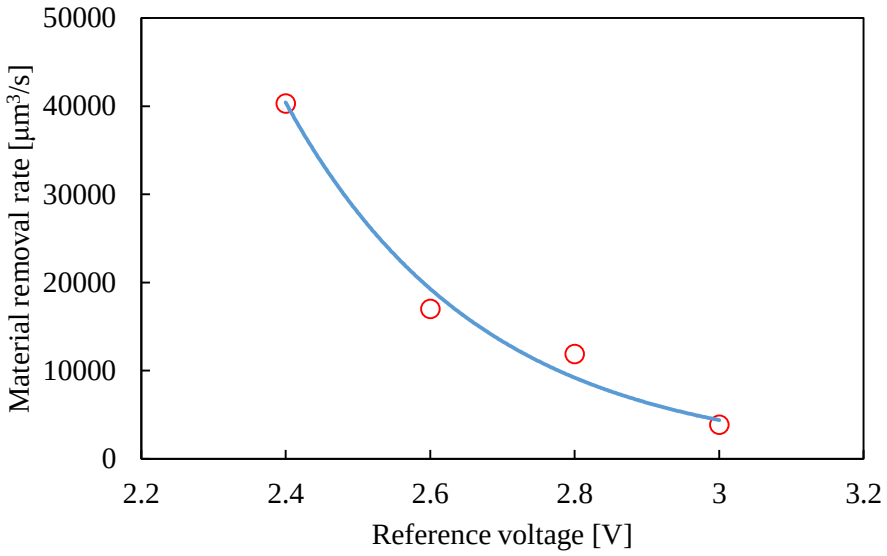

Fig.4.37 Material removal rates with different reference voltages

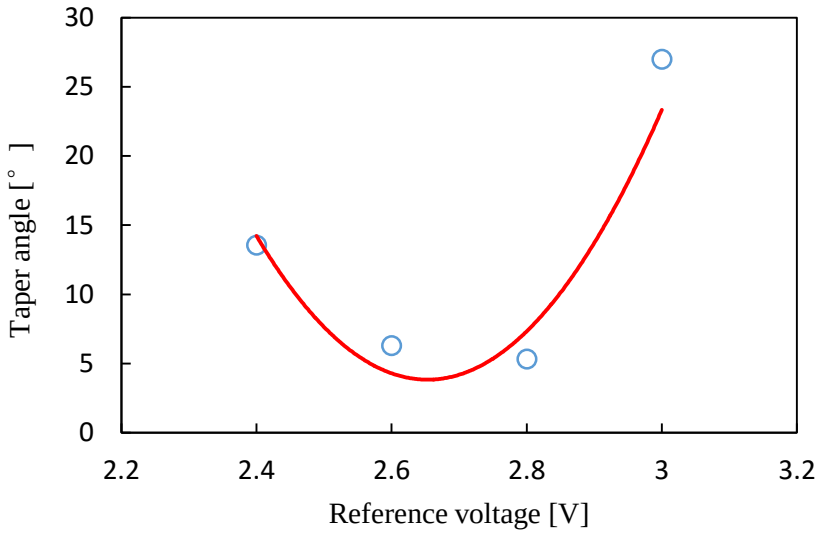

Fig. 4.38 Taper angle with different reference voltages

4.3.4.3 Straightness of micro-rod

Fig. 4.38 shows the taper angle with different reference voltages. The taper angle should increase with increasing the reference voltage, because of the large radial gap width. However, compared with the reference voltage of 2.4V, the taper angles were significantly smaller with the reference voltages of 2.6V and 2.8V as shown in Fig. 4.38.

This is because longer micro-rods were machined under the optimum reference voltage, where the influence of the corner radius at the root of the micro-rod on the taper angle was negligibly small. The corner at the root of the micro rod is rounded with a radius equivalent to the axial gap and radial gap.

4.3.4.4 Surface finish

Fig. 4.39 shows the corrosion pits per unit area with different reference voltages. It increased with increasing the reference voltage. The gap width and resistance were larger with the higher reference voltages. Hence, the current density in the gap decreased with increasing the reference voltage. As a result, pitting corrosion easily occurred with the low current density. The top surface of the tungsten plate tool electrode before and after machining was observed as shown in Fig. 4.40. Scratch was found on the top surface of tungsten plate tool electrode after machining, which was caused by the collision with the shoulder surface of the rod workpiece.

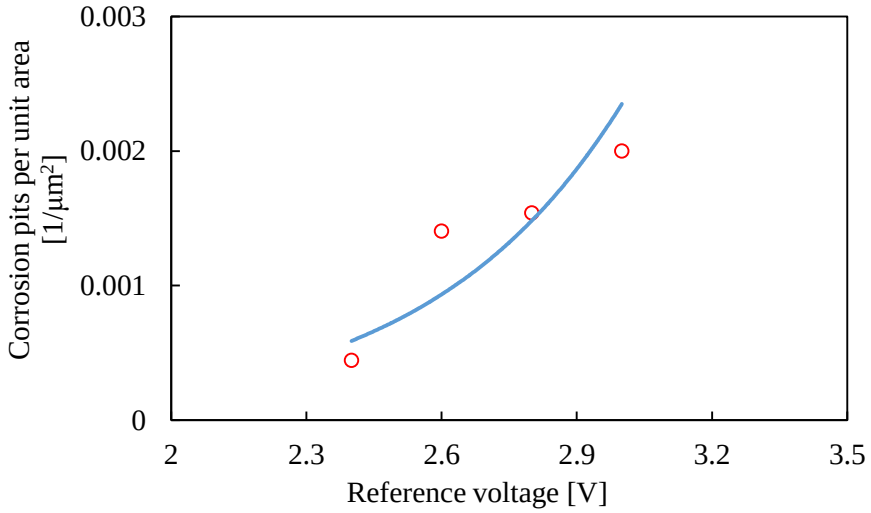

Fig. 4.39 Corrosion pits per unit area with different reference voltages

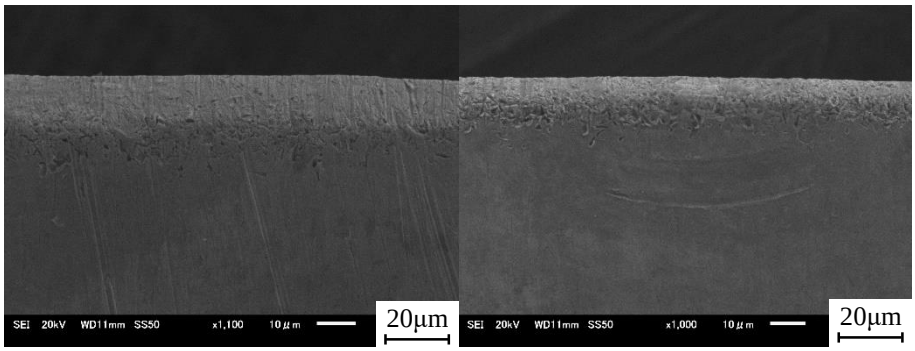

(a) Before machining (b) After machining

Fig. 4.40 Top surface of tungsten tool electrode before and after machining

4.4 Micro-rod machining with feeding workpiece rod in radial direction

As shown in Fig. 4.2, it is also possible to feed the workpiece in radial direction to machine a micro-rod. In this section, the machining characteristics of this method were investigated.

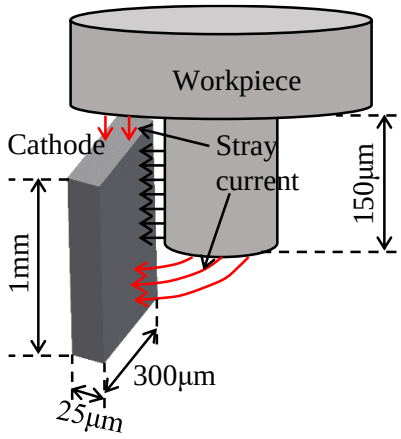

Fig. 4.41 Schematic of micro-rod machining

Table 4.6 Experimental conditions used for feeding of workpiece in radial direction method

Pulse voltage	Amplitude [V]	140
	Frequency [Hz]	500k
	Duty factor [%]	50
	Rise/fall time [ns]	40
Feeding capacitance C_1 [pF]		47
Electrolyte		NaCl aq. 2wt%
Tool electrode rotation [rpm]		3000
Feed speed [μm/s]		0.2

4.4.1 Micro-rods machining with different feed distances in radial direction

4.4.1.1 Experimental conditions

The size of the cathode electrode used in this method is shown in Fig. 4.41. Different from the axial feeding method, the feeding distance in axial direction is kept constant during machining, and the machining current mainly flows through the radial gap. The machining conditions are shown in Table 4.6. The voltage amplitude was 140V which

was much higher than the axial feeding method. This is because the machining area was large compared with the axial feeding method. The machining length in axial direction was set as 150μm, and the feeding distance in radial direction were varied at 30μm, 40μm, 45μm and 52μm, respectively. For the preliminary experiment to obtain the fundamental machining characteristics, the servo feed control was not used, and the workpiece rod was fed at the feed speed of 0.2μm/s.

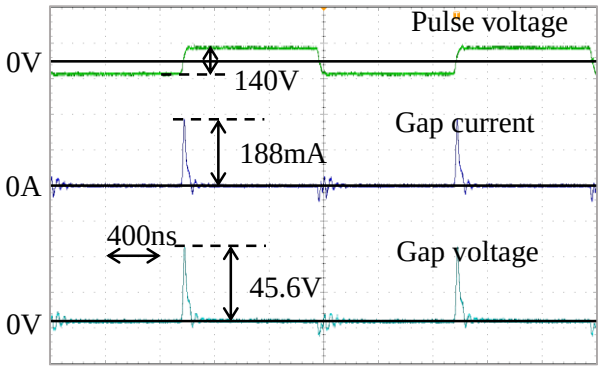

Fig. 4.42 Gap current and voltage with radial feeding method

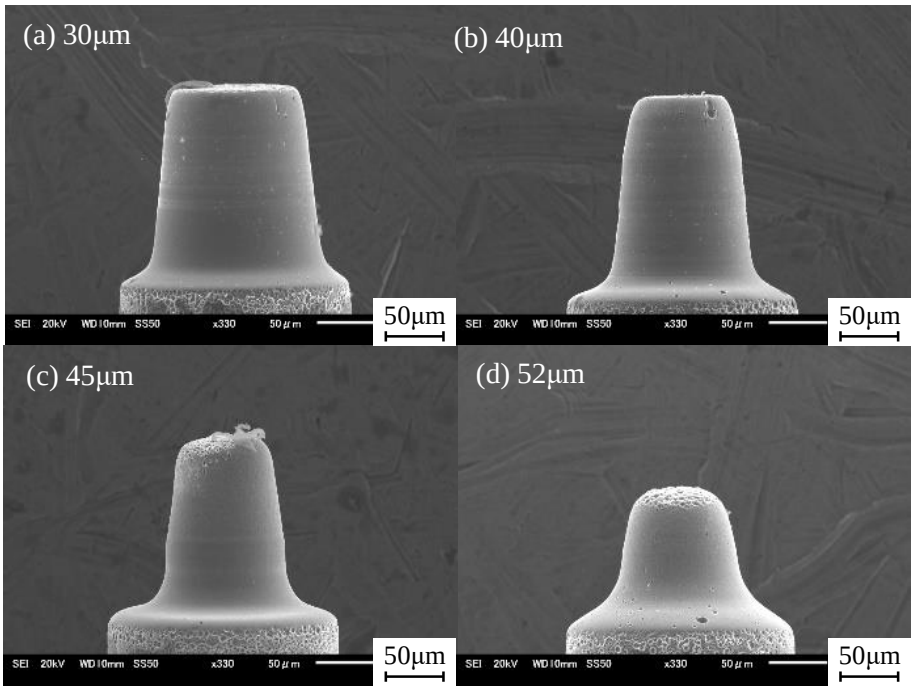

Fig. 4.43 Micro-rods machined with different feeding distances in radial direction

4.4.1.2 Surface finish

The gap current and voltage waveforms with the radial feeding method are shown in Fig. 4.42. The gap current and voltage were much higher than that in Fig. 4.16 with the axial feeding method, because higher voltage amplitude was needed for the large

machining area under the same feed speed. The micro-rods machined are shown in Fig. 4.43. The end of micro-rod was rounded with the feeding distance of 45μm. Furthermore, the end of the micro-rod started to be dissolved when the feeding distance was increased to 52μm, and the length of the micro-rod was shortened to 83.7μm, much shorter than the set value of 150μm for the machining length. In the case of radial feed machining, the feed speed should be increased inversely proportional to the radius of the rod machined. Since the feed speed was constant, the gap width increased with the decrease in the radius. Thus, the stray current flowed on the end surface significantly. As shown in Fig. 4.41, the machining process was influenced by not only the stray current flowing through the axial gap, but also the current flowing through the end surface of micro-rod. Since the thickness and height of tool electrode were 25μm and 1mm, respectively, as shown in Fig. 4.41, the stray current flowed mainly through the end of micro-rod. This is the reason why the micro-rod started to be dissolved from the end as shown in Fig. 4.43(d). Fig. 4.44 shows that the corrosion pits per unit area increased with increasing the feeding distance in radial direction. This is mainly because corrosion pits increased in the vicinity of the end surface as shown in Fig. 4.43.

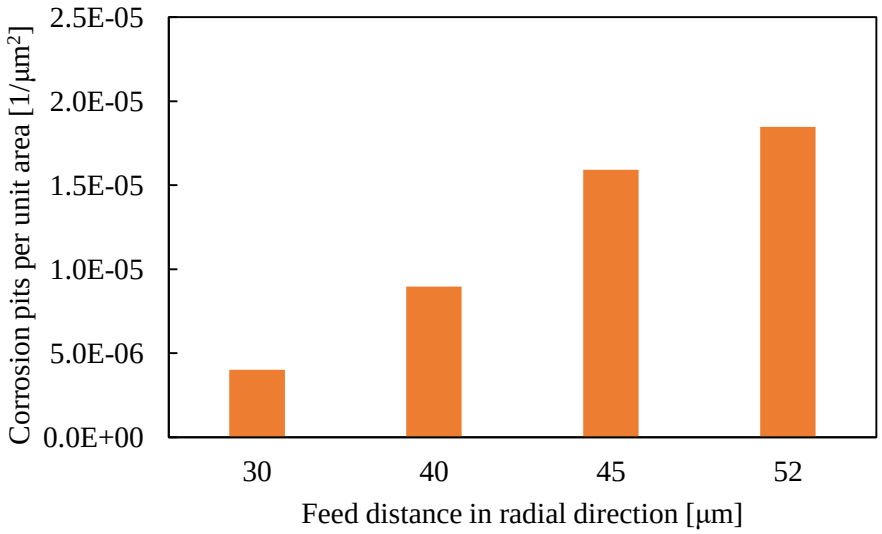

Fig. 4.44 Corrosion pits per unit area with different feeding distances in radial direction

4.4.1.2 Straightness of micro-rod

The taper angles with different feeding distances in radial direction are shown in Fig. 4.45. The taper angle increased with increasing the feeding distance. Since the gap width increased with increasing the feeding distance in radial direction, the taper angle was increased.

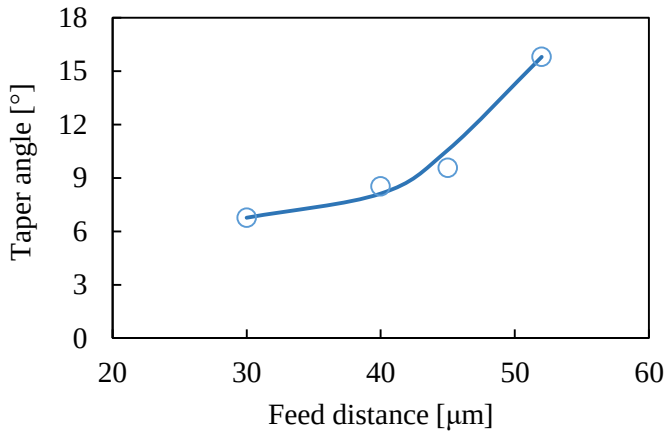

Fig. 4.45 Taper angle with different feeding distances in radial direction

4.4.2 Simulation of material removal process without rotation of workpiece

The material removal process was simulated with the COMSOL Multiphysics when the workpiece was fed in radial direction. To understand the reason why the micro-rod was shortened with increasing the feed distance in radial direction, the current density distribution was calculated and the material removal process was simulated. First, for simplicity, the layer thickness of the removal on the workpiece surface was calculated assuming that the workpiece is not rotated. Then, considering the rotation of workpiece, change in the workpiece rod was calculated.

4.4.2.1 Model and boundary conditions

The 3D model is shown in Fig. 4.46(a). There are three parts, the workpiece, tool electrode and electrolyte. The diameter of workpiece was 1×10^{6}μm and the working gap on the side surface was 5μm. Tungsten was chosen for the domain of the tool electrode and stainless steel was chosen for the workpiece. So the domains of tool electrode and workpiece had an electrical conductivity of 13.89×10^{6}S/m and 4.032×10^{6}S/m, respectively. The domain of the electrolyte was assigned to NaCl aqueous solution with concentration of 2wt%, and its conductivity was 3.02S/m. Hence, the potential drop inside the metallic electrodes is negligibly small. A feed speed of 200μm/s was added to the tool electrode, which was determined by the method described in Section 4.4.3.1. The mesh size was set as normal size, as shown in Fig. 4.46(b), and the end surface of workpiece was refined to obtain a higher mesh quality.

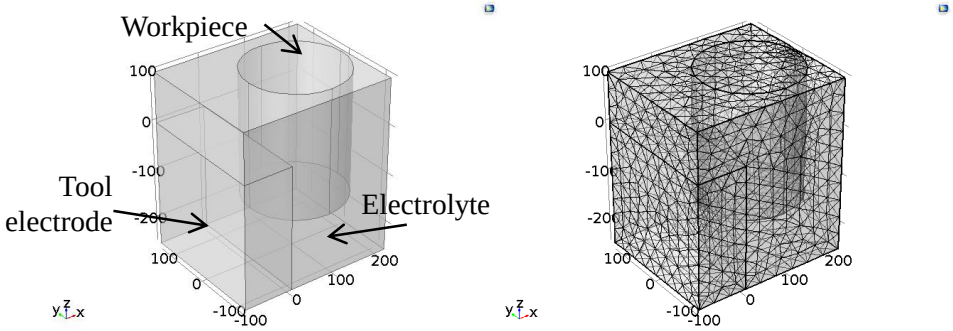

(a) Model (b) Mesh

Fig. 4.46 Simulation model and mesh

The calculations of the electric current density and deform action of the geometries were coupled. The boundary conditions used in the electric current calculation are electric potential and electric insulation. The workpiece was applied electric potential 20V, and tool electrode was set as ground. Then other boundaries were set as electric insulation. About the deformable geometry interfaces, the side surface of workpiece was given a prescribed normal mesh velocity, based on the Faraday's law (equation (4.1)). The Faraday's law describes the functional principle of ECM.

$$V = \frac{M}{\rho . Z_A . F} . Q = V_{sp} . Q \tag{4.1}$$

V is the dissolved volume which depends on the molar mass M, the density ρ, electrochemical valence Z_A of the material of the workpiece. F is the Faraday constant and Q is the electric charge transport. The first term can be converted to equation (4.2), which is the velocity of material removal in normal direction $\vec{v}_n$ as a function of the current density in normal direction $\vec{J}_n$. The used values to calculate the specific dissolve volume V_{sp} are listed in Table 4.7.

$$\vec{v}_n = V_{sp} . \vec{J}_n \tag{4.2}$$

Table 4.7 Values used to calculate V_{sp}

Symbol	Name	Value
M	Molar mass	55.06g/mol
Z_A	Valence	3.436
ρ	Mass density	7.76g/cm^3
F	Faraday constant	96.49×10^{3}C/mol

4.4.2.2 Gap current

Fig. 4.47 shows the current densities at different times of 0.2s, 0.4s, 0.6s and 0.8s observed from horizontal and vertical slices, respectively. The change of the current density in the working gap was small due to the small change in the gap width with feeding of the tool electrode.

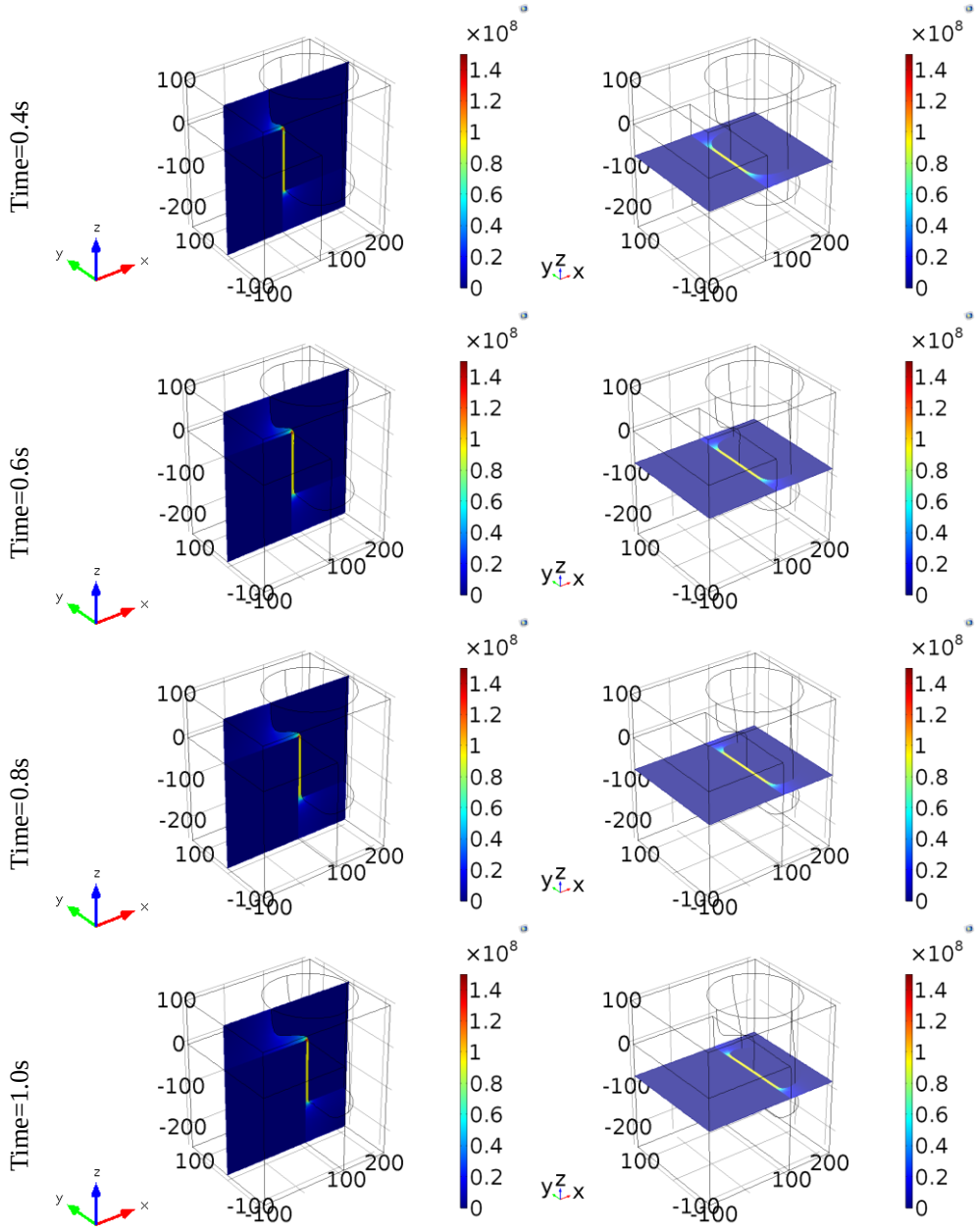

Fig. 4.47 Simulation results of current density at 0.4s, 0.6s, 0.8s and 1.0s

4.4.2.3 Shape of workpiece

Fig. 4.48 shows the cross sections of micro-rod in the horizontal plane at z=-90 according to the coordinate shown in Fig. 4.47 and at times 0.4s, 0.6s, 0.8s, and 1.0s. The

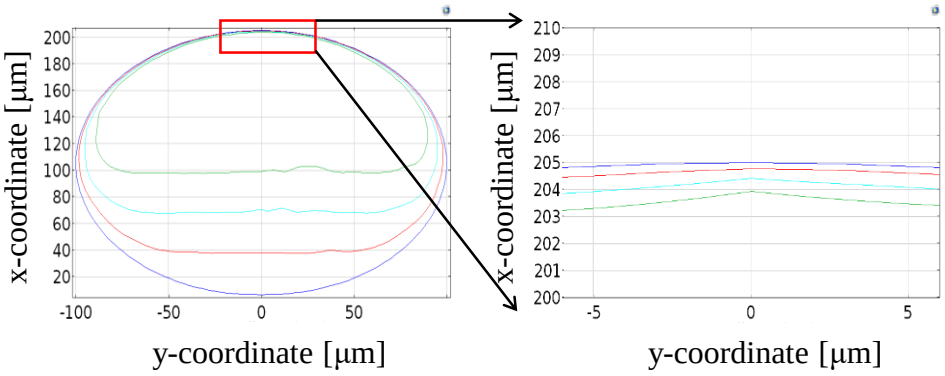

Fig. 4.48 Shape of micro-rod at 0s, 0.2s, 0.4s, 0.6s and 0.8s

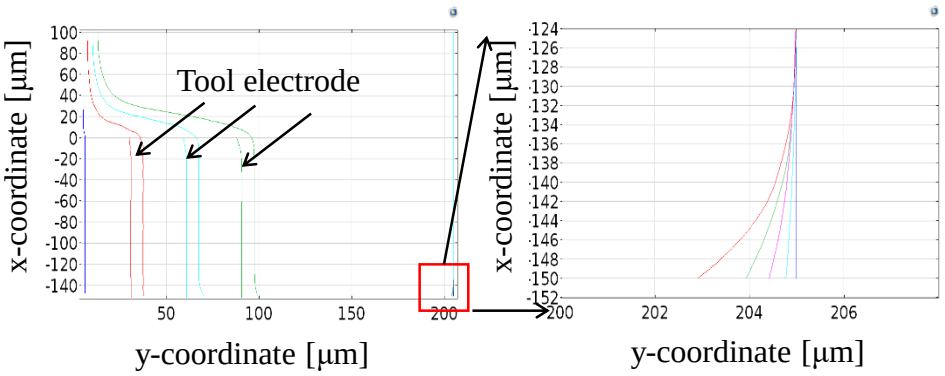

Fig. 4.49 Side surface of micro-rod at 0s, 0.2s, 0.4s, 0.6s and 0.8s

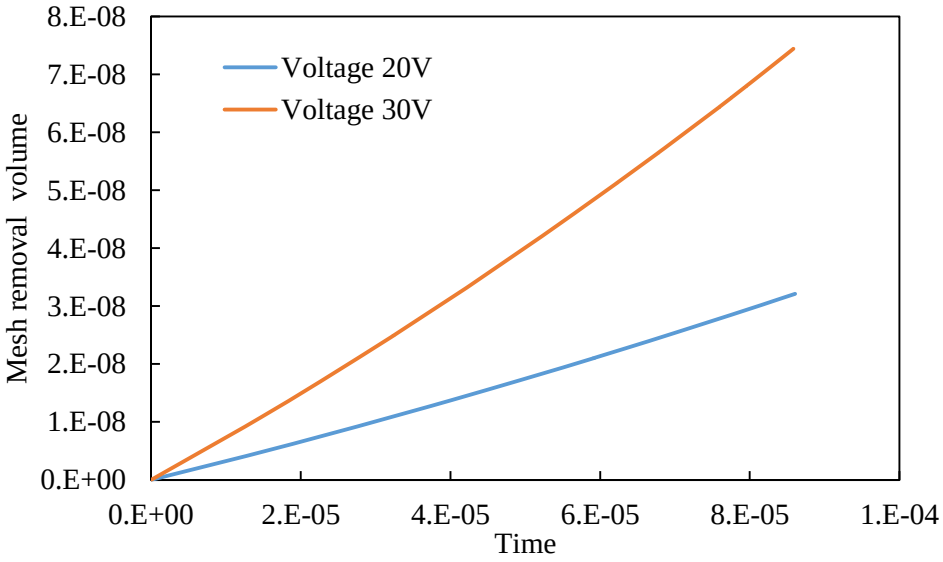

Fig. 4.50 Material removal volume with electric potential 20V and 30V

material removal volume was much lower on the opposite surface of working gap than that on the shoulder gap. This is because the workpiece did not rotate resulting in the current density significantly low on the opposite surface of the working gap. Fig. 4.49 shows the cross section of micro-rod in the vertical plane at y=0 according to the coordinate in Fig. 4.47 and at time of 0s, 0.2s, 0.4s, 0.6s and 0.8s and 1.0s.

4.4.2.4 Material removal rate

Fig. 4.50 shows the material removal volume with the electric potential of 20V and 30V, and the feed speed of 1×10^6μm/s. The material removal rate increased with increasing the electric potential because the current density in the working gap increased.

4.4.3 Simulation of material removal process considering rotation of workpiece

In this section, the material removal process was simulated with rotation of the workpiece. The rotation method of the workpiece was based on the simulated results in Section 4.4.2 without rotation of workpiece.

4.4.3.1 Model and boundary conditions

The model and boundary conditions were the same as Section 4.4.2. In the deformed geometry interface, the side and end surfaces of workpiece was given a prescribed normal mesh velocity to simulate the material removal process, which was relied on the Faraday's law (equation (4.1)). The Faraday's law describes the functional principle of ECM.

$$V = \frac{M}{\rho . z . F} . Q = V_{sp} . Q \tag{4.3}$$

V is the dissolved volume which dependents on the molar mass M, the density ρ, electrochemical valence z of the material of the workpiece. F is the Faraday constant and Q is the electric charge transport. These parameters are listed in Table 4.7.

The feed speed of the tool electrode was determined by a simulation result with fixed tool electrode. According to the cross sections of micro-rod at y=0 at different times, as shown in Fig. 4.51, in which the tool electrode was fixed, the increase rates of gap width could be calculated at the times t=0s, t=0.2s, t=4s, t=0.6s, t=0.8s and 1.0s. Then the average of the increase rates of gap width determined the feed speed of tool electrode as 200μm/s.

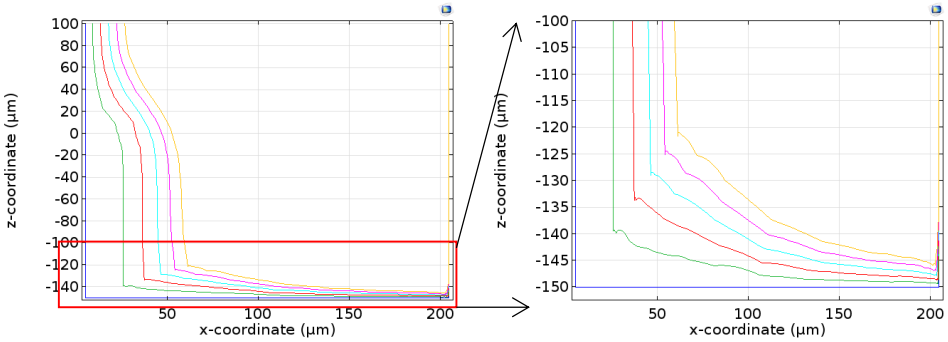

Fig. 4.51 Cross sections of micro-rod at y=0 at times 0s, 0.2s, 0.4s, 0.6s, 0.8s and 1.0s

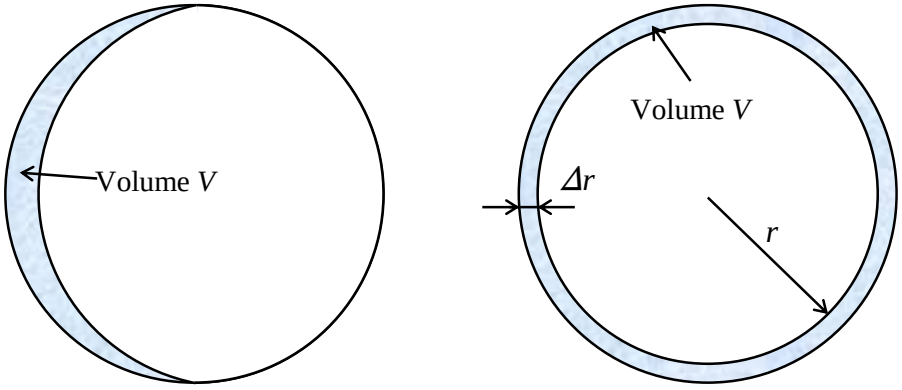

(a) No rotation (b) Rotation

Fig. 4.52 Determination of feed speed v_2 of tool electrode

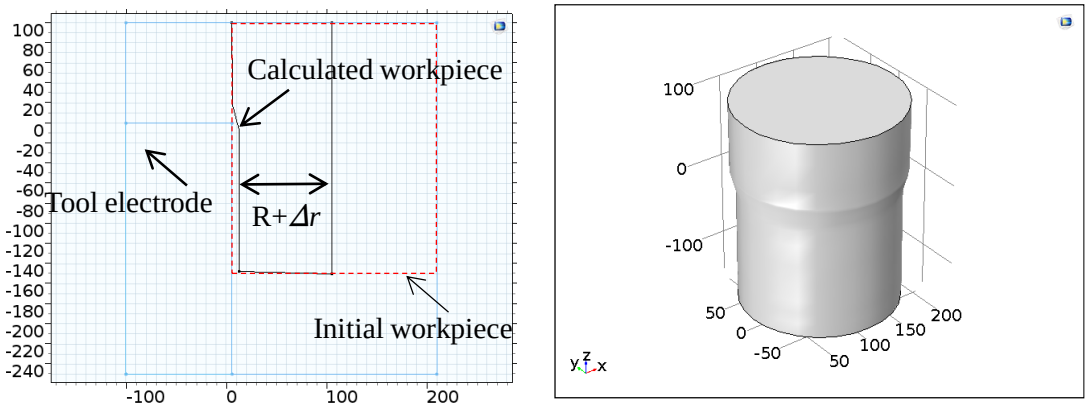

(a) Cross section shape of workpiece (b) Rebuilt geometry of workpiece

Fig. 4.53 Rotation method of workpiece

4.4.3.2 Method to obtain workpiece rotation

The program was calculated at every short time step Δt without the rotation of the workpiece. Then the material removal volume V as shown in Fig. 4.52(a) was obtained at

the end of the time step. Considering the rotation of the workpiece, the decreased radius Δr of the workpiece with rotation could be calculated by following equation.

$$\Delta r = \frac{V}{2\pi r} \tag{4.4}$$

Where r is the initial radius of workpiece at every time step.

Thereby, the geometry of workpiece with rotation could be formed by rotating the calculated cross section shape of workpiece as shown in Fig. 53(a). The new geometry of workpiece, as shown in Fig. 53(b), was used as the initial condition of the next time step. Hence, the rotation of the workpiece in the simulation was realized with this method.

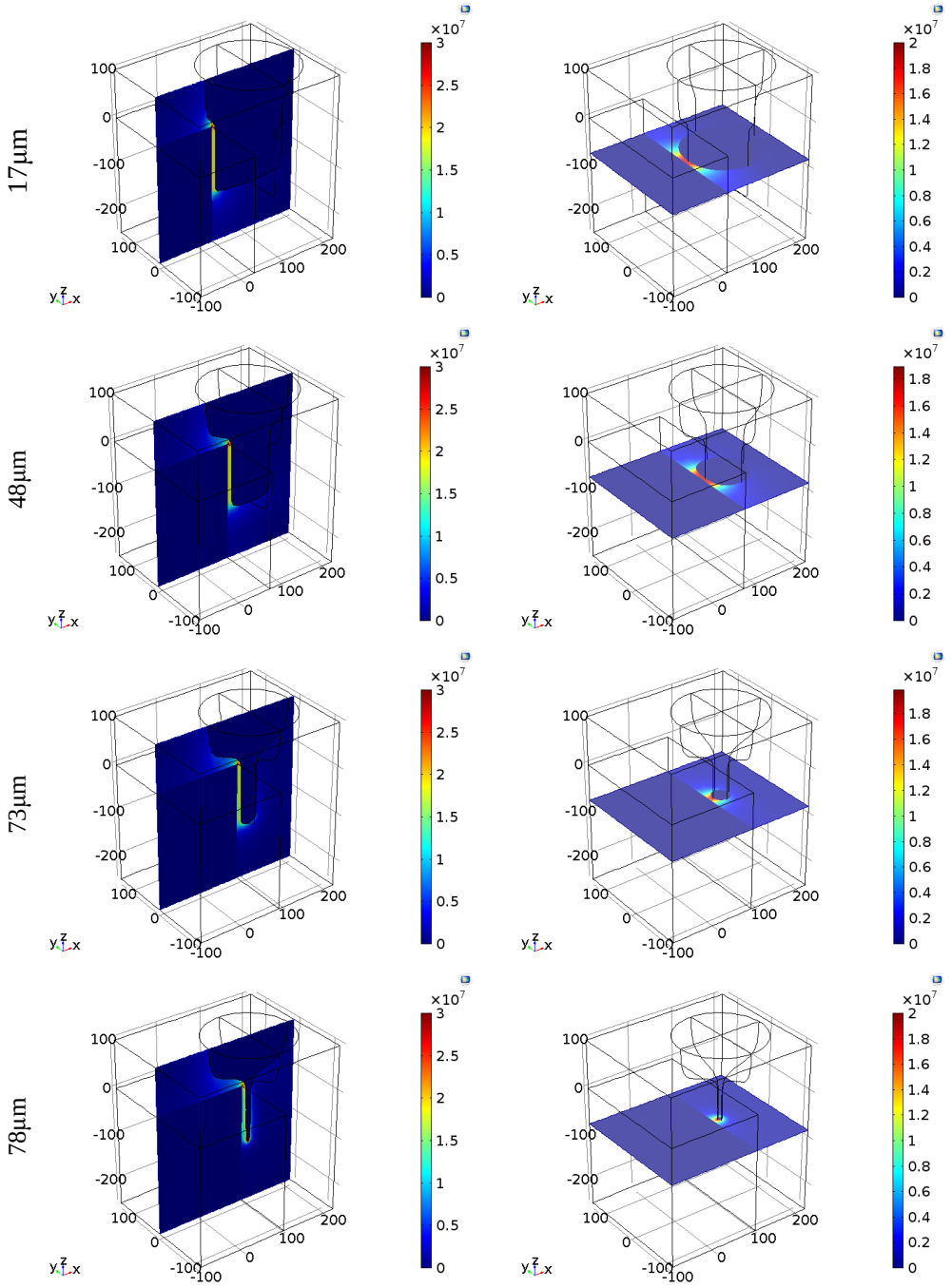

Fig. 4.54 Current density with feed distances of 17μm, 48μm, 73μm and 78μm

4.4.3.3 Gap current

Fig. 4.54 shows the current density in the working gap with the feed distances of 17μm, 48μm, 73μm and 78μm in radial direction. The current density decreased with increasing the feed distance, because the gap resistance was increased with the diameter of the workpiece decreasing.

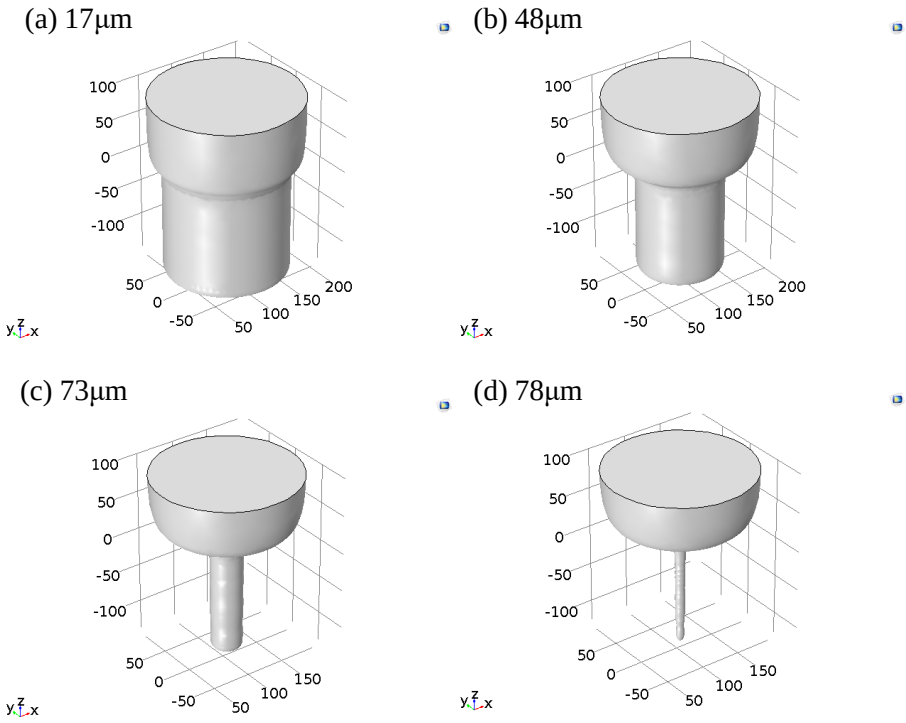

Fig. 4.55 Workpiece with feed distances of 17μm, 48μm, 73μm and 78μm in radial direction

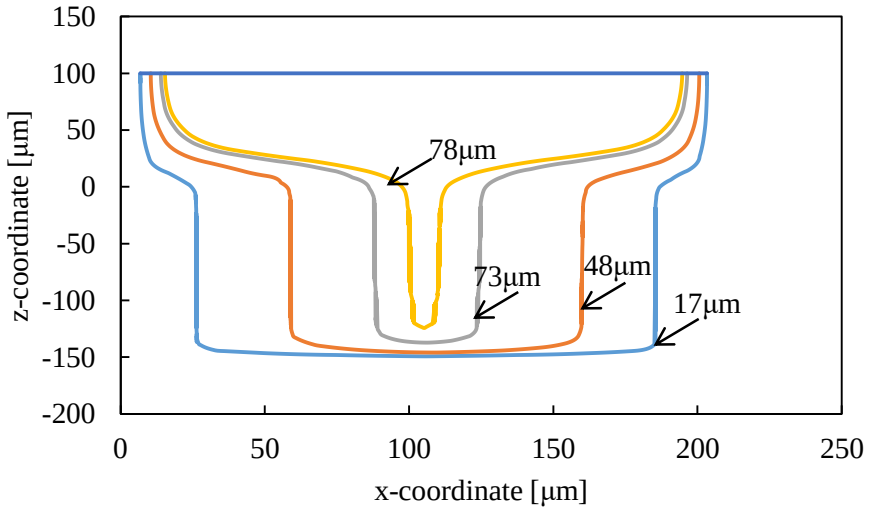

Fig. 4.56 Cross section shapes of workpiece with feed distances of 17μm, 48μm, 73μm and 78μm in radial direction

4.4.3.4 Shape of workpiece

Fig. 4.55 and Fig. 4.56 show the simulated geometries and cross section shapes of workpiece with feeding distances of 17μm, 48μm, 73μm and 78μm in radial direction,

respectively. It is noted that the micro-rod was shortened with decreasing the diameter, which was qualitatively in agreement with the experimental results.

4.5 Comparison between axial and radial feeding methods

The corrosion pits per unit area in Fig. 4.29 was about 0.0005 to 0.0013[1/μm^2] with the axial feeding method using a small area tool electrode, whereas, it was about 4×10^{-6} to 19×10^{-6}[1/μm^2] with the radial feeding method as shown in Fig. 4.44. This is because the current flowing through the radial gap is used for machining with the radial feeding method, and pitting corrosion only occurs on the end surface where current density is low. Since the current flowing through the axial gap is used for machining with the axial feeding method, stray current with low current density is generated in the radial gap. Hence, the side surface of micro-rod is more easily influenced by pitting corrosion due to the low current density. In addition, compared with the radial feeding method, the taper angle of the axial feeding method was significantly small where the thickness of the plate tool electrode was small with the optimum feed speed.

Compared with the axial feeding method, the machining area was much larger with the radial feeding method. Hence, higher voltage amplitude was needed to keep the same feed speed with this method. Furthermore, it is noted that a micro-rod with the length more than 200μm can be machined with the axial feeding method. However, it was difficult to obtain micro-rods longer than 150μm with the radial feeding method. This is because the stray current dissolves the end surface of the micro-rod.

4.6 Conclusions

Micro-rods were machined with the electrostatic induction feeding ECM. Two machining methods were investigated in this chapter: the feeding of workpiece in axial and radial direction methods. The following conclusions were obtained.

With the feeding of workpiece in axial direction method, the machinable length limitation peaks at an optimum feed speed, because lower feed speed results in higher current density in the radial gap and higher feed speed causes collision between the tool electrode and workpiece. The maximum length of micro-rod was increased with increasing voltage amplitude. However, the taper was smaller with lower voltage. The corrosion pits per unit area was minimum at the optimum feed speed at which the maximum length of the micro-rod was obtained, because of the high current efficiency resulting in low influence of stray current in the radial gap. The taper angle was minimum at the optimum feed speed at which the maximum length of micro-rod can be obtained,

because the influence of the root of the micro-rod on the taper angle was decreased with longer rod length. The maximum length of the micro-rod increased and the corrosion pits per unit area decreased with decreasing thickness of tool electrode, because the current flowing through the side surface decreased. The influences of top surface area of tool electrode on machining accuracy were insignificant, because the difference in the total current on the shoulder gap of micro-rods was small, resulting in small difference in MRR. The influences of axial gap width, tool electrode thickness, and top surface area of tool electrode on the current density distribution on the workpiece surfaces were calculated with COMSOL Multiphysics. The results explained the machining results successfully.

With the feeding of workpiece in radial direction method, the number of corrosion pits per unit area increased with increasing the feeding distance in radial direction, because of the stray current around the end surface. The taper angle was increased with increasing the feeding distance because the gap width increases with the decrease in the workpiece diameter, resulting in increased stray current on the end surface. Due to the same reason the micro-rod started to be shortened by the stray current flowing through the end, when the feeding distance in radial direction was increased. The simulation results of the material removal process was qualitatively in agreement with the experiment results.

Compared with the axial feeding method, the influence of pitting corrosion was smaller with the radial feeding method, because the current flowing through the radial gap was used for machining. Because of the larger machining area with the radial feeding method, higher voltage amplitude was needed to keep the same feed speed compared with the axial feeding method. Longer length of micro-rod was more easily machined with the axial feeding method. This is because the stray current dissolves the end surface of the micro-rod with increasing the feed distance in radial direction.

Chapter 5 Improvement of machining accuracy of micro-rod

5.1 Introduction

The previous research shows that the machining accuracy of micro-rod was deteriorated by the influences of pitting corrosion, taper angle and so on with the axial feed method. The pitting corrosion was mainly caused by the low current density in the side gap, and the probability of pitting corrosion increased with lower current density. Since the material dissolution occurred not only in the axial gap but also in the side gap, the taper angle is mainly determined by the material removal volume in the side gap. The taper angle can be decreased by decreasing the gap width in the axial gap, because the material dissolution in the side gap is decreased. Use of small thickness of the plate electrode is one of the solutions, as described in Section 4.3.2. In order to improve the machining accuracy furthermore, the influences of annealing process and different electrolytes on the machining characteristics were investigated in this chapter. In the previous experiment, corrosion pits formed on the side surface of micro-rod showed anisotropic feature. The corrosion pits were elongated in the axial direction because the stainless steel wire used as the workpiece was produced by wire drawing. Hence, the influence of annealing process of workpiece was investigated. The annealing process may eliminate the residual stress due to the drawing process and improve the micro structure of the workpiece. In addition, it is reported that the sodium nitrate ($NaNO_3$) aqueous solution has a lower current efficiency compared with the sodium chloride (NaCl) aqueous solution. The machining gap can be decreased with the $NaNO_3$ aqueous solution compared with the NaCl aqueous solution. Furthermore, for neutral electrolyte, the passivating electrolytes (such as $NaNO_3$) is more advantageous than the non-passivating electrolytes (such as NaCl) due to its probability to increase the machining accuracy. Hence, the influence of different electrolytes on the machining accuracy of micro-rod was investigated.

This chapter describes the influences of different kinds of electrolytes, the NaCl and $NaNO_3$ aqueous solutions, on the machining accuracy of micro-rods fabrication, when the stainless steel and tungsten were used as workpiece and tool electrode, respectively. The targets of micro-rods machining is to have an aspect ratio of higher than 10, and high machining accuracy with negligible influences of taper, pitting corrosion and so on. In addition, it is aimed that a micro-rod with a diameter smaller than 10μm can be machined.

5.2 Influence of annealing process

Fig. 5.1 shows that the corrosion pits are formed anisotropically, and elongated along the axial direction. Considering the workpiece wire was cut from a reel of stainless steel wire produced by drawing, a residual stress may exist inside the wire. Hence, the influence of the annealing process of the workpiece was investigated in this section, because the micro structure of workpiece can be changed by the annealing process. In the experiment, the workpiece was annealed at different temperatures, and the machining characteristics were analyzed, and also compared with the workpiece machined without the annealing process.

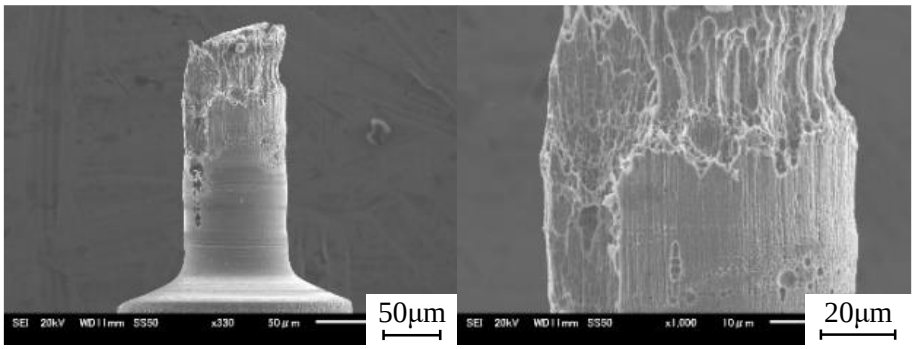

Fig. 5.1 Influence of pitting corrosion

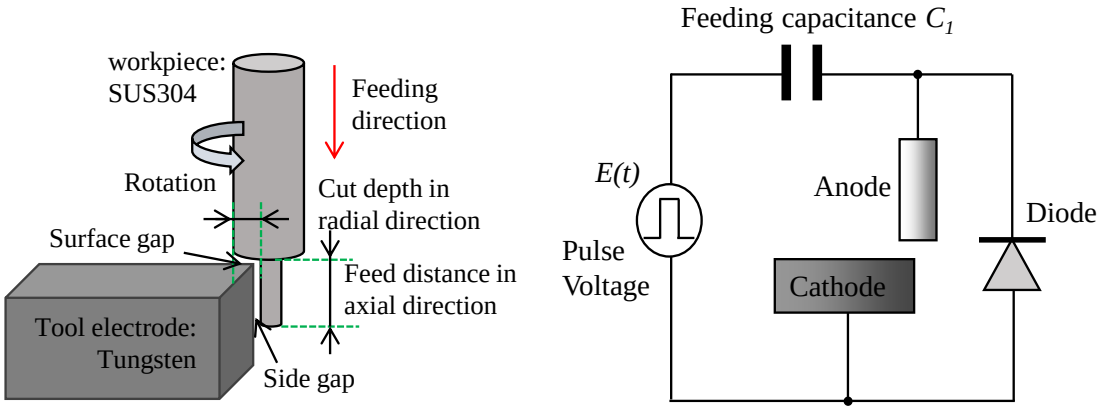

(a) Machining method (b) Diode was used to avoid tool wear

Fig. 5.2 Method of machining micro-rod and circuit

5.2.1 Influence of annealing temperature

In this experiment, the feed distance was equal to the initial gap width of 5μm to avoid the formation of the side gap and the influence of the stray current in the side gap. The

influence of corrosion on the frontal surface of micro-rod with different annealing temperatures was investigated.

5.2.1.1 Experimental conditions

The experimental method is shown Fig. 5.2. The materials of stainless steel (SUS304) and tungsten were used as workpiece and tool electrode, respectively. The workpiece rod was annealed at 1000 K, 1100 K, 1200 K and 1300 K for 0.5 h as shown in Table 5.1. The furnace used was FUW220PA (ADVANTEC company). The atmosphere of annealing was in air. The diameter of the workpiece was 200 μm as shown in Fig. 5.3(a), and the surface size and thickness of the tool electrode are shown in Fig. 5.3(b). The experimental conditions are shown in Table 5.2. The total amplitude and frequency of power supply were 90 V and 500 kHz, respectively, and the rise/fall time was 40 ns. The electrolyte was NaCl aqueous solution of 2 wt% in concentration. The workpiece was positioned over the top surface of tool electrode with an initial gap width of 5 μm. Then the feed distance in axial direction was set as 5 μm, and the cut depth in radial direction was set as 50 μm.

Table 5.1 Annealing conditions

Temperature [K]	1000	1100	1200	1300
Time [h]	0.5	0.5	0.5	0.5

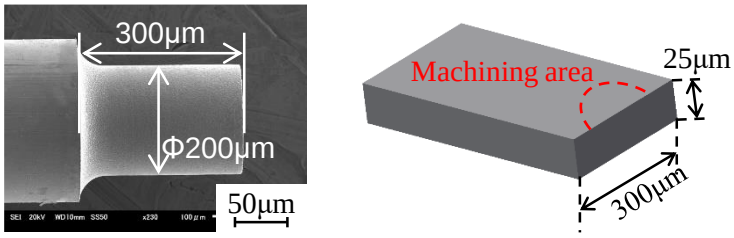

(a) Workpiece (b) Tool electrode

Fig. 5.3 Workpiece and tool electrode

Table 5.2 Experimental conditions

Pulse voltage	Amplitude [V]	90
	Frequency [Hz]	500 k
	Duty factor [%]	50
	Rise/fall time [ns]	40
Feeding capacitance C_1 [pF]		47
Electrolyte		NaCl aq. 2 wt%
Tool electrode rotation [rpm]		3000
Feed speed [μm/s]		0.7
Feed distance [μm]		5

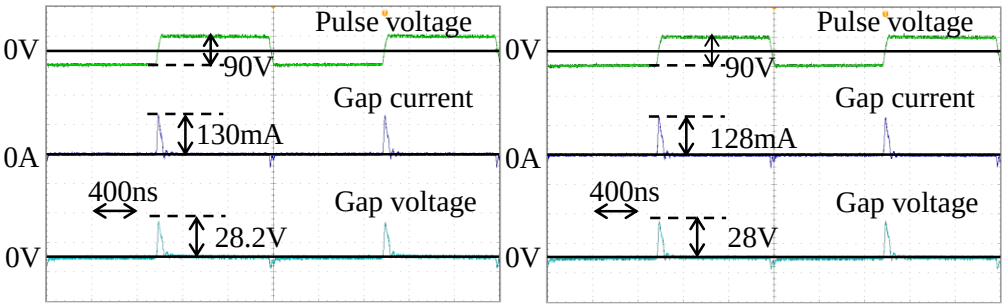

(a) Anneal temperature 1000 K (b) Anneal temperature 1200 K

Fig. 5.4 Waveforms with annealing temperatures of 1000 K and 1200 K

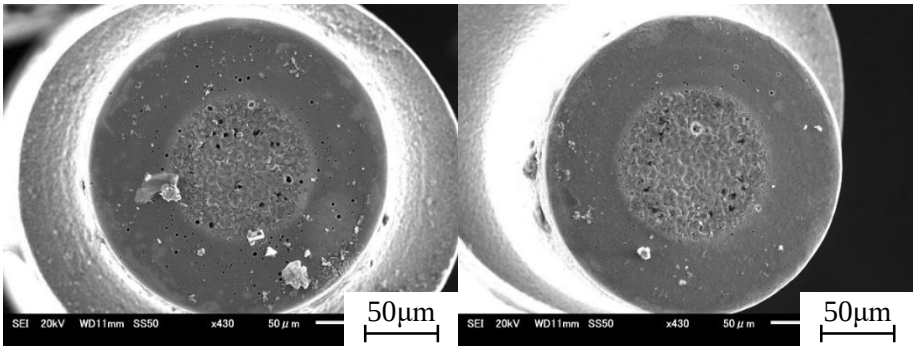

(a) Without annealing process (b) Annealing temperature 1000 K

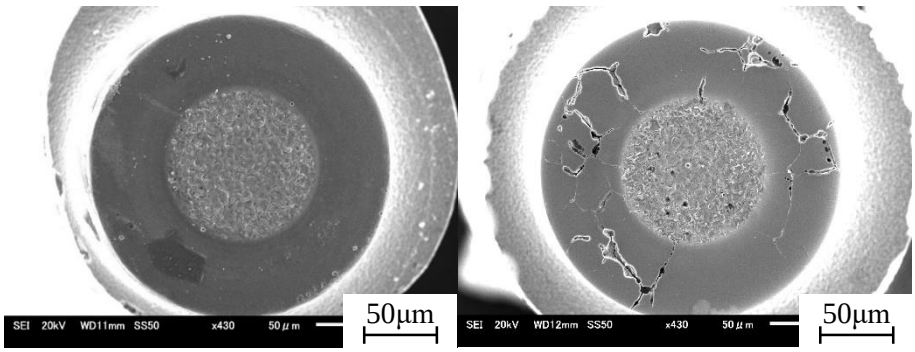

(c) Annealing temperature 1100 K (d) Annealing temperature 1200 K

Fig. 5.5 Experimental results with different kinds of workpiece

5.2.1.2 Surface finish

Fig. 5.4 shows the gap current and voltage waveforms obtained with the workpieces annealed at 1000 K and 1200 K. The difference of the waveforms between different annealing temperatures was insignificant. Fig. 5.5 shows the experimental results with different kinds of workpieces. Many corrosion pits were generated on the frontal surface of workpiece without annealing process as shown in Fig. 5.5(a). When the workpiece was annealed at 1000 K, a few of corrosion pits were generated on the frontal surface. There

was almost no corrosion pits on the frontal surfaces of workpieces with the annealing temperatures of 1100 K. However, crevice corrosion was observed over the workpiece annealed at 1300 K as shown in Fig. 5.5(d), which is much severer than the pitting corrosion.

5.2.2 Comparison of machining characteristics between with and without annealing process

When the feed distance was equal to the initial gap width of 5 μm, the above experimental results show that the corrosion pits were least with the annealing temperature of 1100 K. Then, the machining characteristics of the workpieces with and without annealing process were investigated with increasing the feed distance in the axial direction.

Table 5.3 Experimental conditions

Pulse voltage	Amplitude [V]	90
	Frequency [Hz]	500 k
	Duty factor [%]	50
	Rise/fall time [ns]	40
Feeding capacitance C_1 [pF]		47
Electrolyte		NaCl aq. 2 wt%
Tool electrode rotation [rpm]		3000
Feed speed [μm/s]		0.7
Feed distance [μm]		25, 35, 45, 55

5.2.2.1 Experimental conditions

The workpiece annealed at 1100 K for 0.5 h was used for machining according to the above experimental results. The machining method and electrodes were the same as Fig. 5.2 and Fig. 5.3. The experimental conditions are shown in Table 5.3. The electrolyte was NaCl aqueous solution of 2 wt% in concentration. The total amplitude and frequency of power supply were 90V and 500 kHz, respectively, and the rise/fall time was 40 ns. The workpiece was positioned on the top surface of tool electrode with an initial gap width of 5 μm. The feed distance in radial direction was set as 50 μm, and the feed distance in axial direction was set as 25 μm, 35 μm, 45 μm and 55 μm, respectively.

5.2.2.2 Machinable length with and without annealing process

Fig. 5.6 shows the annealed workpiece with feed distance of 25 μm. Some corrosion pits were generated on the frontal surface of micro-rod, however, a short micro-rod was successfully machined.

Fig. 5.7 shows the micro-rods machined with the feed distances of 35 μm, 45 μm and 55 μm. The micro-rod started to be dissolved with increase ng the feed distance to 35 μm because of corrosion as shown in Fig. 5.7(a). At last, the micro-rod was dissolved completely with the feed distance of 55 μm in axial direction as shown in Fig. 5.7(c).

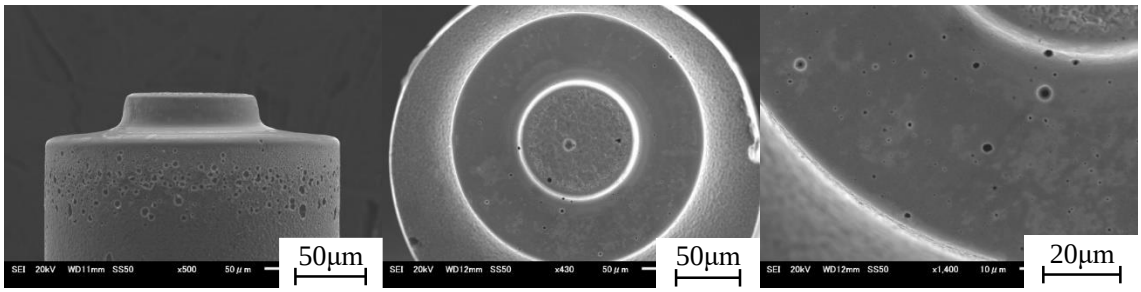

Fig. 5.6 Annealed workpiece with feed distance of 25 μm

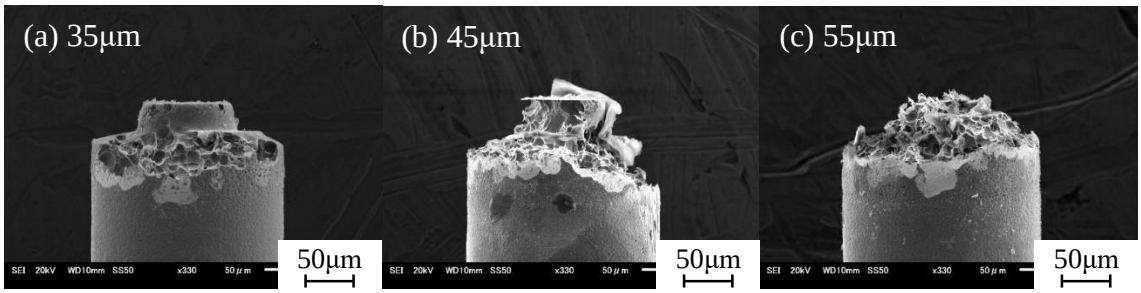

Fig. 5.7 Micro-rods machined with different feed distance in axial direction (a) 35 μm (b) 45 μm, (c) 55 μm

With the workpiece without annealing process, micro-rods machined in the same experimental conditions are shown in Fig. 5.8. The feed distances in axial direction were 105 μm and 205 μm. Compared with the annealed workpiece in Fig. 5.7, a much longer micro-rod could be machined using the workpiece without annealing process. Hence, the annealing process of workpiece cannot eliminate the influence of pitting corrosion, and the machinable length limitation of micro-rod was decreased compared with the workpiece without annealing process. It is considered that the annealing process in air resulted in oxidation of the material. Thus, annealing should be conducted in a protective gas atmosphere.

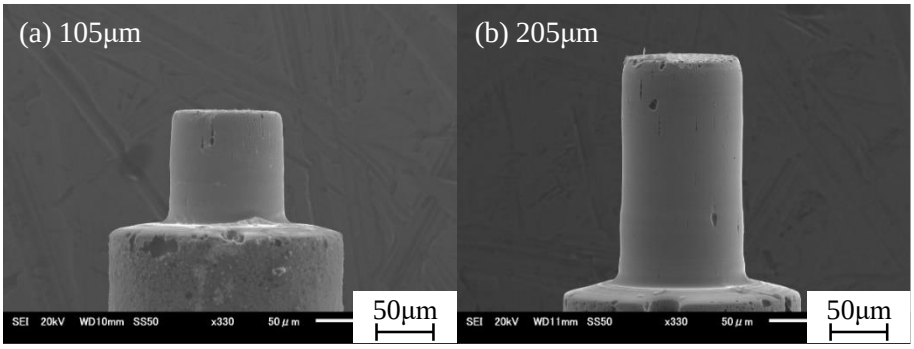

Fig. 5.8 Micro-rods machined with workpiece without anneal process: (a) Feed distance of 100 μm, (b) Feed distance of 200 μm

5.3 Influence of different electrolytes

In the previous experiments, where the NaCl aqueous solution was used as electrolyte, the machining accuracy was deteriorated more or less by corrosion pits, taper and so on. It is reported that passivating electrolytes (such as $NaNO_3$ aqueous solution) generally give better machining precision compared with non-passivating electrolytes (such as NaCl aqueous solution). For neutral electrolyte, $NaNO_3$ is more advantageous than the NaCl due to its higher probability to increase the machining accuracy. Hence, the machining characteristics of $NaNO_3$ aqueous solution were investigated and compared with those using NaCl aqueous solution. The machining method and the tool electrodes used are shown in Fig. 5.2 and Fig. 5.3, respectively.

Table 5.4 Experimental conditions

Pulse voltage	Amplitude [V]	90
	Frequency [Hz]	500 k
	Duty factor [%]	50
	Rise/fall time [ns]	40
Feeding capacitance C_1 [pF]		47
Electrolyte		NaCl/$NaNO_3$ aq. 2 wt%
Tool electrode rotation [rpm]		3000
Feed speed [μm/s]		0.4, 0.5, 0.6, 0.7, 0.8, 0.9

5.3.1 Machining characteristics with different feed speeds

5.3.1.1 Experimental conditions

The materials of stainless steel (SUS304) and tungsten were used as workpiece and tool electrode, respectively. The diameter of the workpiece was 200 μm as shown in Fig.

5.3(a), and the surface size and thickness of the tool electrode are shown in Fig. 5.3(b). Table 5.4 shows the experimental conditions. The NaCl and $NaNO_3$ aqueous solution of 2 wt% in concentration were used as electrolyte. The voltage amplitude and rise/fall time of pulse power supply were 90 V and 40ns, respectively. The workpiece was positioned on the top surface of tool electrode with an initial gap width of 5 μm. The cut depth in radial direction was set as 50 μm. The feed speed was increased from 0.4 μm/s to 0.9 μm/s with an increment of 0.1. The feed distances in axial direction was 100 μm.

5.3.1.2 Length of micro-rod machined

Fig. 5.9 shows the gap current and voltage waveforms with the feed speed of 0.7 μm/s using different electrolytes. The difference in gap current was insignificant. Fig. 5.10 shows the lengths of micro-rods machined at different feed speeds with the electrolytes of NaCl and $NaNO_3$ aqueous solution. When the electrolyte of NaCl aqueous solution was used, the given feed distance of 100 μm in axial direction not completed with the feed speeds of 0.4 μm/s and 0.5 μm/s. This is because the micro-rod started to be dissolved before the feed distance reached 100 μm due to the influence of pitting corrosion. However, the micro-rods of 100 μm in length were successfully machined under the same conditions when the electrolyte of $NaNO_3$ aqueous solution was used, and there was no corrosion pits generated. When the electrolyte of $NaNO_3$ aqueous solution was used, however, the micro-rod of 100 μm in length could not be obtained with the feed speed of 0.8 μm/s because of the collision between electrodes. This is because the current density in the axial gap decreased with increasing the feed distance in axial direction. The area of side gap increased with increasing the feed distance resulting in the lower current density in the axial gap. However, micro-rod of 100 μm in length was successfully machined with the feed speed of 0.8 μm/s using the electrolyte of NaCl aqueous solution. This is because of the higher current efficiency with NaCl aqueous solution, compared with $NaNO_3$ aqueous solution.

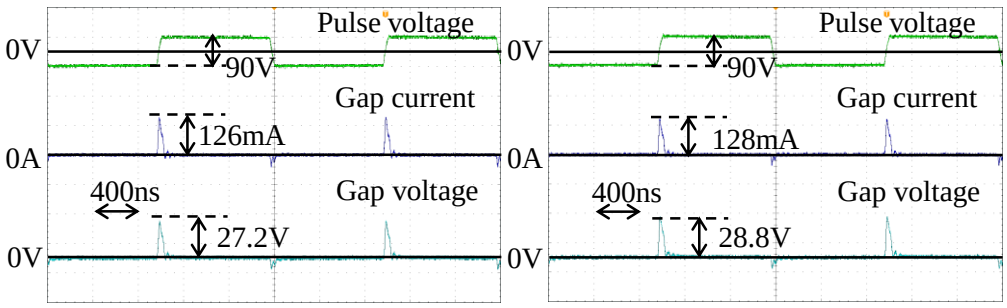

(a) NaCl aqueous solution (b) $NaNO_3$ aqueous solution

Fig. 5.9 Waveforms of gap current and voltage with feed speed of 0.7 μm/s

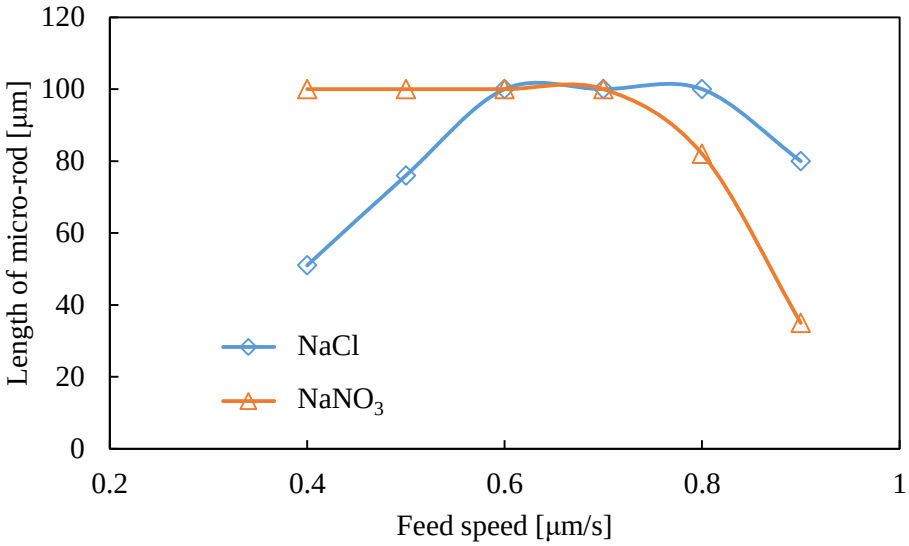

Fig. 5.10 Length of micro-rod machined with different feed speeds

Fig. 5.11 shows micro-rods machined with the feed speeds of 0.4 μm/s, 0.6 μm/s, 0.7 μm/s and 0.8 μm/s using electrolytes of NaCl and $NaNO_3$ aqueous solution. It is noted that the corrosion pits were eliminated with the electrolyte of $NaNO_3$ aqueous solution as shown in Fig. 5.11(b), while, there were many corrosion pits generated on the surface of micro-rods machined with the electrolyte of NaCl aqueous solution, especially with lower feed speeds.

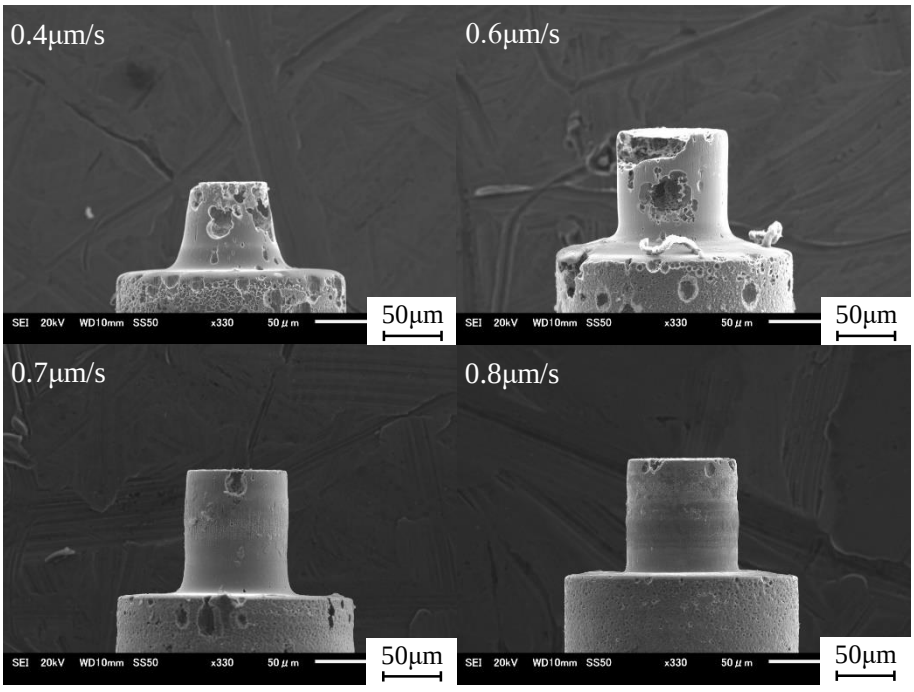

(a) NaCl aqueous solution

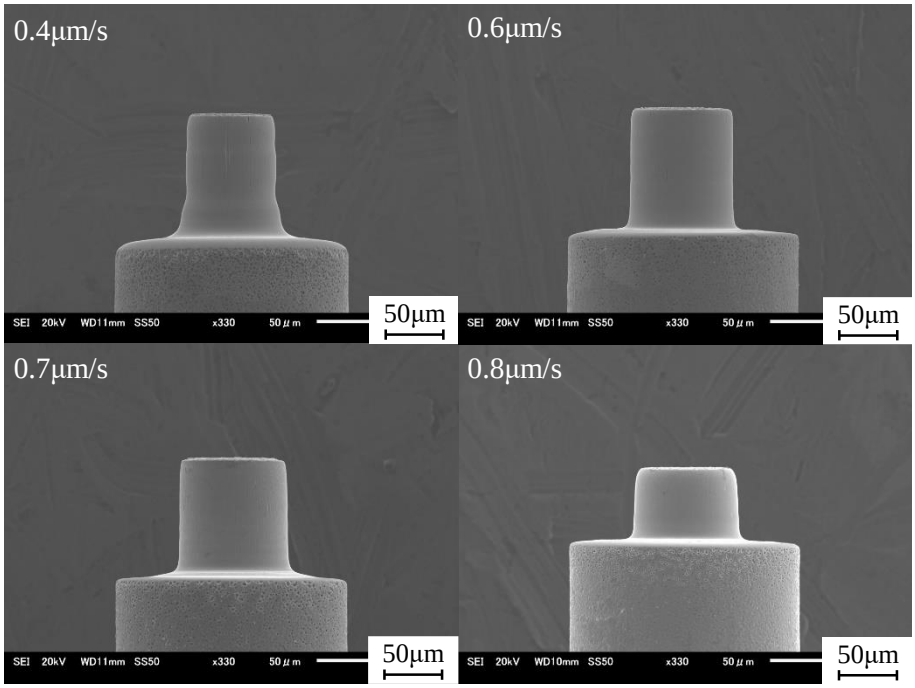

(b) $NaNO_3$ aqueous solution

Fig. 5.11 Micro-rods machined with different feed speeds

5.3.1.3 Gap width

As shown in Fig. 5.2(a), there are two working gaps during machining, the axial gap and side gap. The axial gap width can be calculated as

$$d_f = H - h + g \tag{5.1}$$

where, H is the length of the micro-rod, h is the feed distance and g is the initial gap width. The length of the micro-rod was measured by a scanning electron microscope. When the depth of cut in radial direction is 50 μm, the side gap width can be calculated as

$$d_s = \frac{1}{2}(D - d)\text{-}50 \tag{5.2}$$

where, D is the diameter of workpiece rod and d is the diameter of micro-rod machined. Both of them were measured by a scanning electron microscope.

Fig. 5.12 shows the axial gap width at different feed speeds with electrolytes of NaCl and $NaNO_3$ aqueous solution. The gap width decreased with increasing the feed speed. The axial gap width with the electrolyte of NaCl aqueous solution was larger than that of the electrolyte of $NaNO_3$ aqueous solution, because the electrochemical dissolution can occur at the large gap width with a lower current density due to the higher current efficiency of NaCl aqueous solution. Fig. 5.13 shows the side gap width at different feed speeds with electrolytes of NaCl and $NaNO_3$ aqueous solution. It was decreased with increasing the feed speed, and the side gap width of the electrolyte of $NaNO_3$ aqueous

solution was also smaller compared with the electrolyte of NaCl aqueous solution for the mentioned reason.

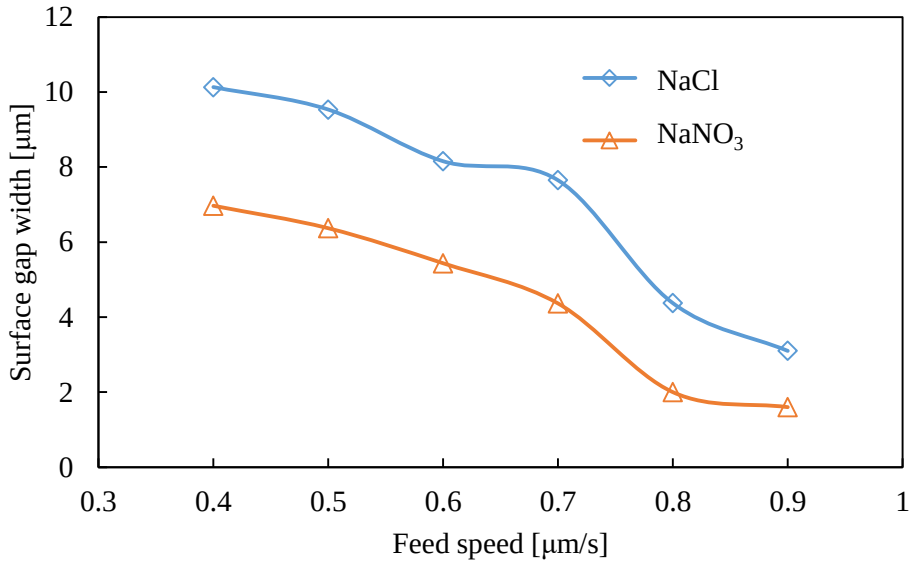

Fig. 5.12 Axial gap widths with electrolytes of NaCl and $NaNO_3$ aqueous solution

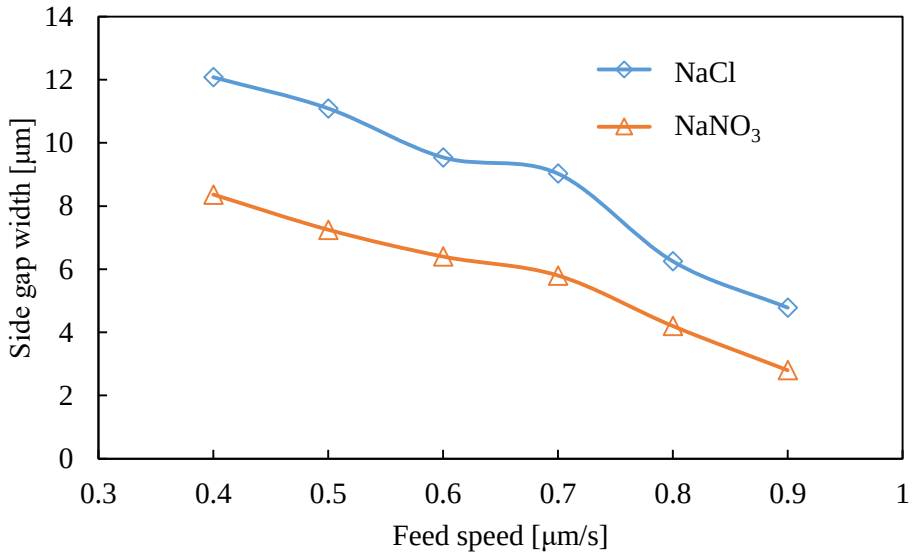

Fig. 5.13 Side gap widths with electrolytes of NaCl and $NaNO_3$ aqueous solution

5.3.1.4 Straightness of micro-rod

Fig. 5.14 shows the taper angle of micro-rod at different feed speeds with electrolytes of NaCl and $NaNO_3$ aqueous solution. The taper angle decreased with increasing the feed speed, because the gap width was decreased resulting in less material remove volume in the side gap. In addition, the taper angle was smaller with the electrolyte of $NaNO_3$

aqueous solution, because of the smaller gap width compared with the electrolyte of NaCl aqueous solution.

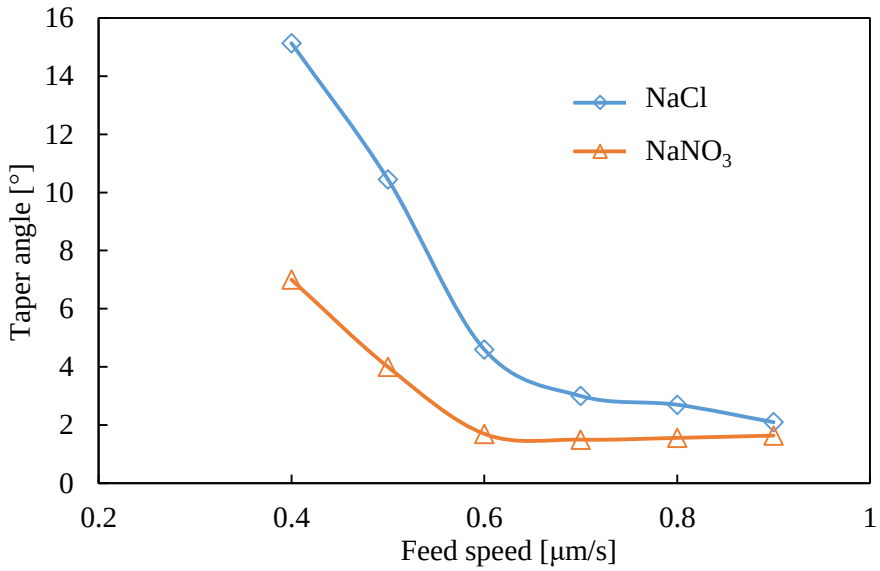

Fig. 5.14 Taper angle of micro-rod with electrolytes of NaCl and $NaNO_3$ aqueous solution

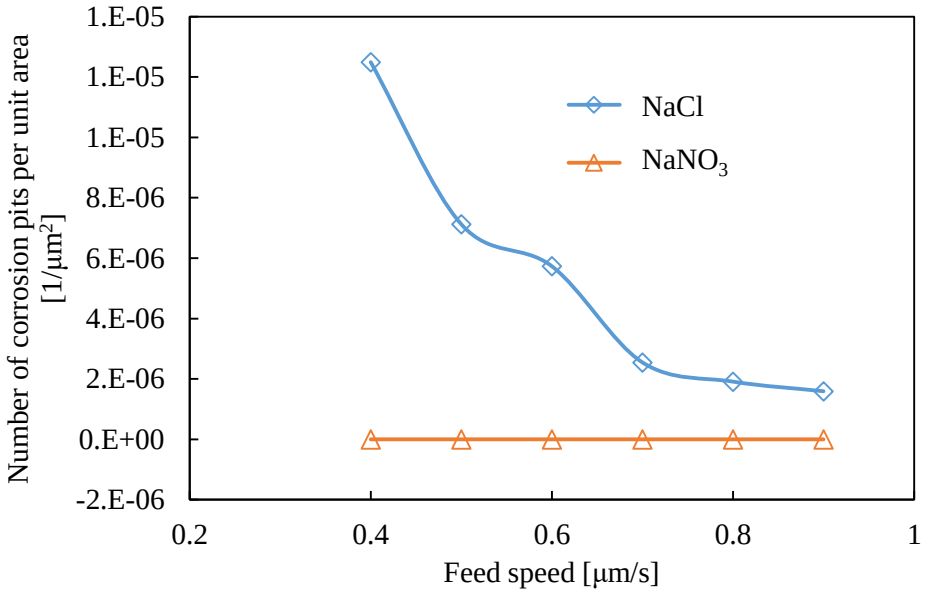

Fig. 5.15 Number of corrosion pits per unit area with electrolytes of NaCl and $NaNO_3$ aqueous solution

5.3.1.5 Surface finish

Fig. 5.15 shows the number of corrosion pits per unit area with different feed speeds using the electrolytes of NaCl and $NaNO_3$ aqueous solution. When the electrolyte of NaCl

aqueous solution was used, the influence of pitting corrosion was decreased with increasing the feed speed, because the current density was increased in the axial gap with higher feed speed resulting in lower probability of pitting corrosion. When the electrolyte of $NaNO_3$ aqueous solution was used, the influence of pitting corrosion was eliminated under any feed speeds. The reason can be explained as the following paragraph.

There is a layer of oxide passive film on the surface of metal as shown in Fig. 5.16, which protects it from the damage of the corrosion[81]. It is well known that the corrosion easily occurs when the oxide passive film is damaged. The chloride ion is tiny and aggressive compared with the nitrate ion, and therefore easily permeates the oxide passive film and triggers the occurrence of pitting corrosion. Hence, compared with the electrolyte of NaCl aqueous solution, the $NaNO_3$ effectively eliminate the influence of pitting corrosion as shown in Fig. 5.15.

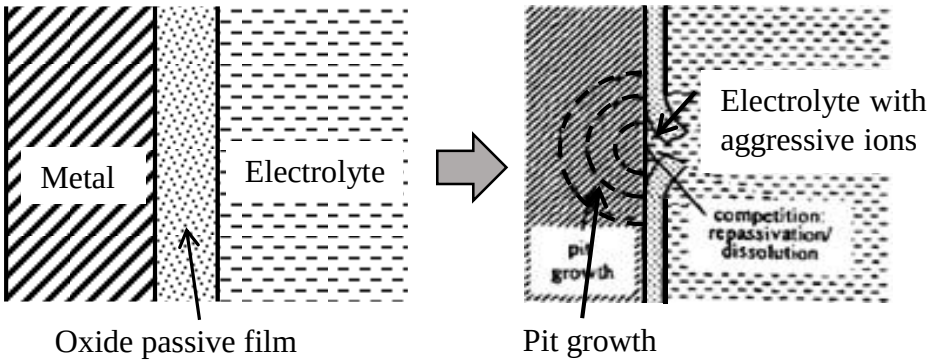

Fig. 5.16 Process of pitting corrosion[81]

5.3.2 Machinable length limitations with different electrolytes

The machinable length limitation was investigated with different electrolytes of NaCl and $NaNO_3$ aqueous solution. The machining method is shown in Fig. 5.2, and the tool electrode is shown in Fig. 5.3(b). The feed distance in axial direction was set as 850 μm. When the machining process was completed without a collision between electrodes or dissolution by pitting corrosion, it is considered that a limitless length of micro-rod can be fabricated, because the feed distance of 850 μm is 34 times of the thickness of the tool electrode. The influence of pitting corrosion and collision between electrodes would not limit the machinable length of the micro-rod, because the stray current in the side gap will not be changed significantly with increasing the feed distance further.

5.3.2.1 Experimental conditions

The stainless steel (SUS304) and tungsten were used as workpiece and tool electrode, respectively. The diameter of the workpiece was 200 μm as shown in Fig. 5.3(a), and the surface size and thickness of the tool electrode are shown in Fig. 5.3(b). The experimental

conditions are shown in Table 5.5. The NaCl and $NaNO_3$ aqueous solution of 2 wt% in concentration were used as electrolyte. The voltage amplitude and rise/fall time of pulse power supply were 90 V and 40 ns, respectively. The workpiece was positioned on the top surface of tool electrode with an initial gap width of 5 μm. The cut depth in radial direction was set as 50 μm. The feed speed was increased from 0.4 μm/s to 0.9 μm/s with an increment of 0.1.

Table 5.5 Experimental conditions

Pulse voltage	Amplitude [V]	90
	Frequency [Hz]	500 k
	Duty factor [%]	50
	Rise/fall time [ns]	40
Feeding capacitance C_1 [pF]		47
Electrolyte		NaCl/$NaNO_3$ aq. 2 wt%
Tool electrode rotation [rpm]		3000
Feed speed [μm/s]		0.4, 0.5, 0.6, 0.7, 0.8, 0.9

5.3.2.2 Machinable length limitations

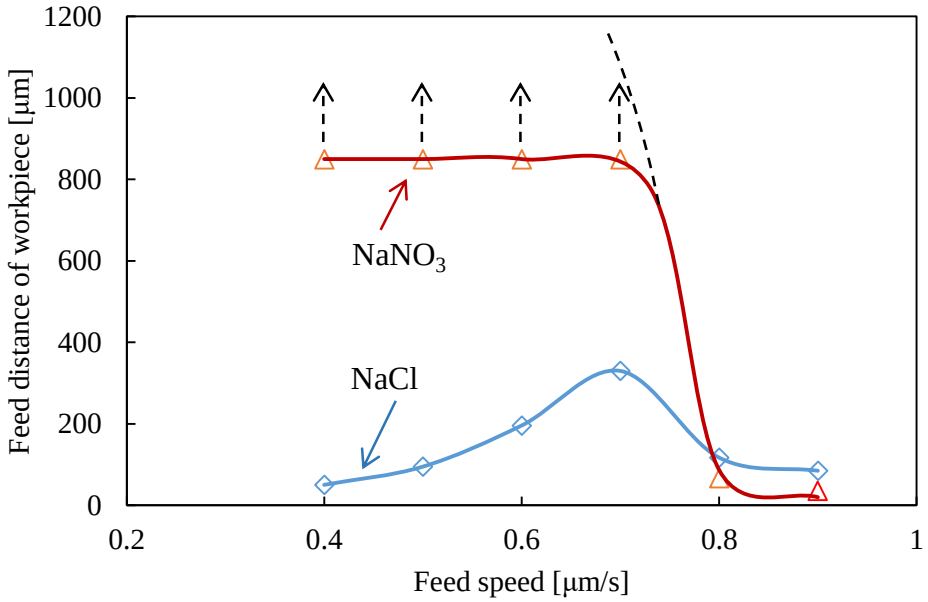

Fig. 5.17 Feed distances of workpiece with different electrolytes

Fig. 5.17 shows the feed distances with different electrolytes. The dotted line means that the machining process can be continued furthermore and even micro-rods longer than the feed distance of 850 μm can be obtained. With the electrolyte of $NaNO_3$ aqueous solution, there was no machinable length limitation with the feed speed from 0.4 μm/s to

0.7 μm/s. This is because the influence of pitting corrosion was eliminated. In addition, with the feed speeds of 0.8 μm/s and 0.9 μm/s, the machining process was interrupted by collision between electrodes, because the influence of stray current in the side gap was increased with increasing the feed distance in axial direction. With the electrolyte of NaCl aqueous solution, the machinable length was limited by corrosion with low feed speed, and by collision between electrodes with high feed speed. The maximum length of micro-rod was obtained at the optimum feed speed of 0.7 μm/s. Fig. 5.18 shows the micro-rods machined with different feed distances and electrolytes at the optimum feed speed of 0.7 μm/s. The number of corrosion pits were increased with increasing the feed distance using the electrolyte of NaCl aqueous solution. This is because the influence of stray current in the side gap increased with increasing the feed distance. However, there was no corrosion pits generated with the electrolyte of $NaNO_3$ aqueous solution. Fig. 5.19 shows the corrosion pits per unit area with different feed distances. The influence of pitting corrosion was eliminated with the electrolyte of $NaNO_3$ aqueous solution due to the reason mentioned above.

When the feed distance was increased to about 330 μm, the micro-rod started to be dissolved with the electrolyte of NaCl aqueous solution due to pitting corrosion. Fig. 5.20 shows the micro-rods machined with different electrolytes, the feed distances were 330 μm and 380 μm corresponding to the electrolytes of NaCl and $NaNO_3$ aqueous solution, respectively. It is found that the micro-rod started to be dissolved by pitting corrosion with the electrolyte of NaCl aqueous solution, while, there was no corrosion pits with the electrolyte of $NaNO_3$ aqueous solution.

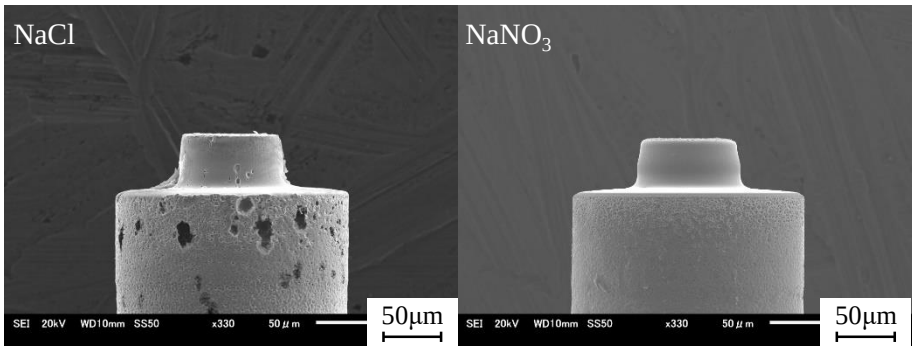

(a) Feeding distance 40 μm

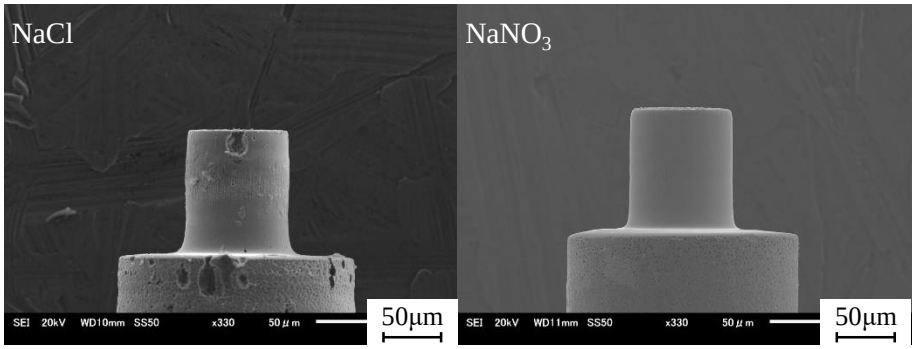

(b) Feeding distance 100 μm

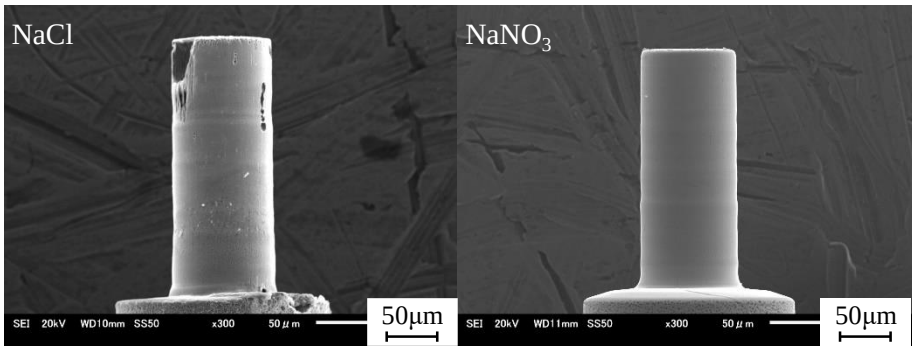

(c) Feeding distance 230 μm

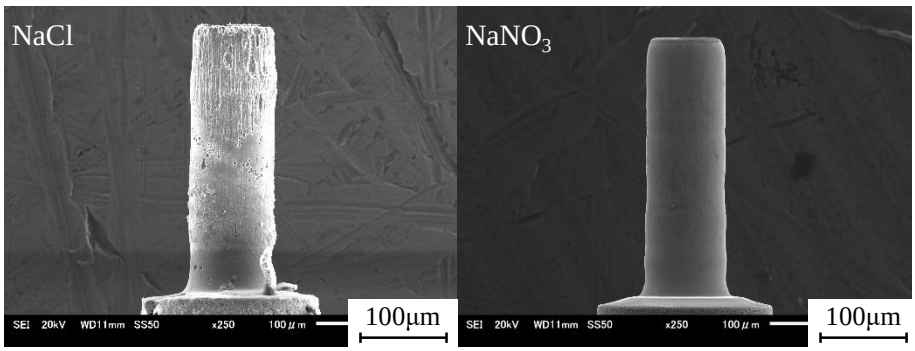

(d) Feeding distance 300 μm

Fig. 5.18 Micro-rods machined with different feed distances in axial direction: (a) 40 μm, (b) 100 μm, (c) 230 μm and (d) 300 μm

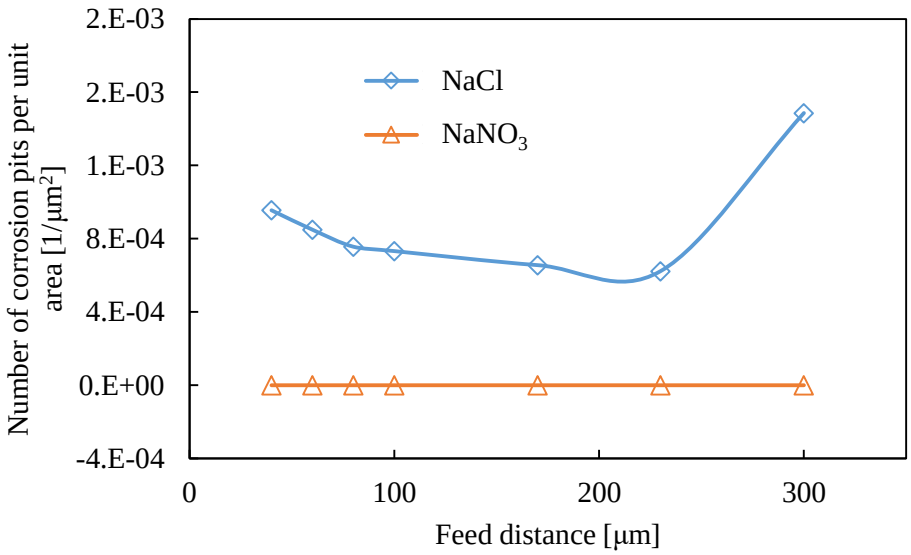

Fig. 5.19 Number of corrosion pits per unit area with different feed distances

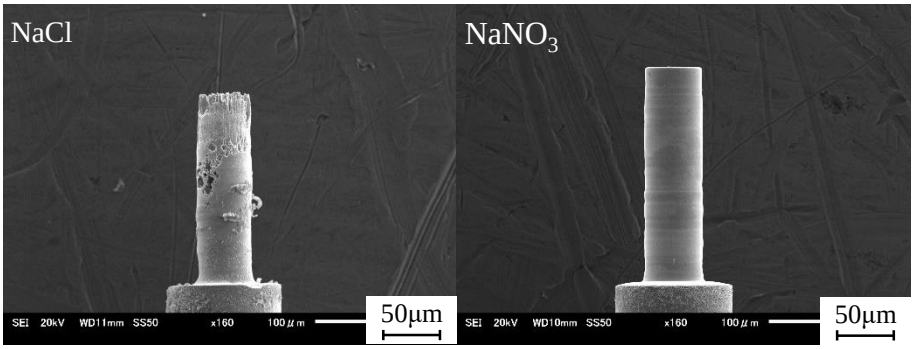

Fig. 5.20 Micro-rods machined with different electrolytes

Fig. 5.21 shows the micro-rods machined using the electrolyte of $NaNO_3$ aqueous solution with the feed distance of 850 μm. The workpiece was cut from a reel of stainless steel wire, as shown in Fig. 4.5(a). In order to make it straight enough, it was reshaped by the WEDG method, resulting the diameter of 200 μm as shown in Fig. 4.5(b). The EDM surface can be observed clearly on the workpiece surface prior to ECM machining, as shown in Fig. 5.21. Compared with the EDMed surface, the ECMed surface was much smoother.

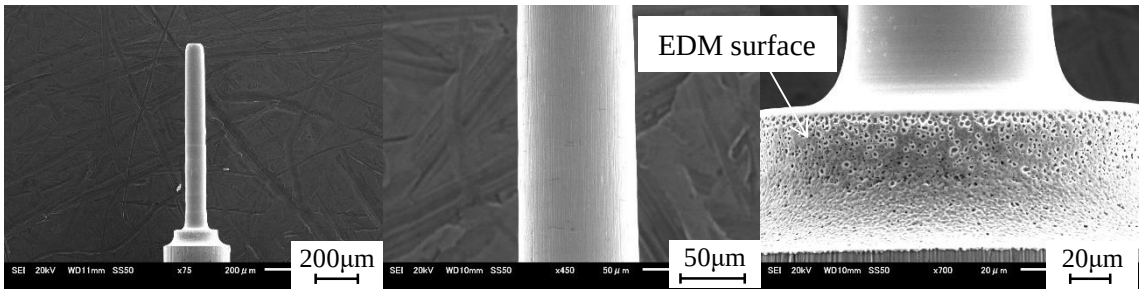

(a) Feed speed of 0.4 μm/s

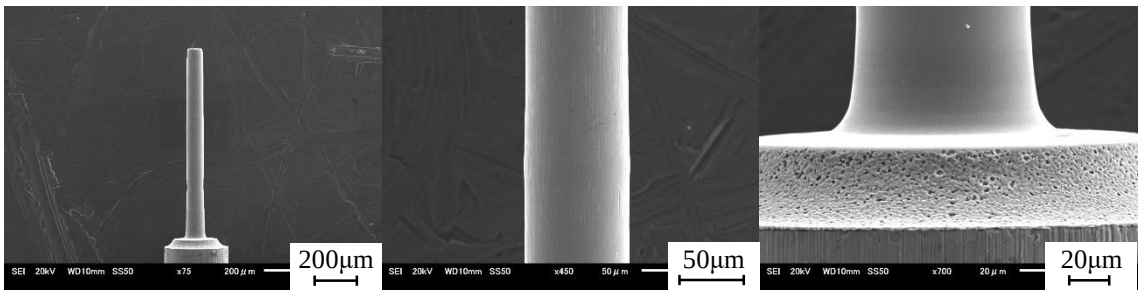

(b) Feed speed of 0.5 μm/s

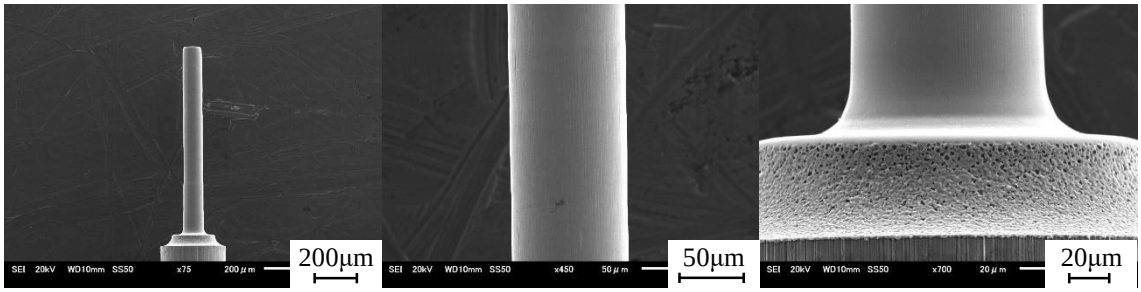

(c) Feed speed of 0.6 μm/s

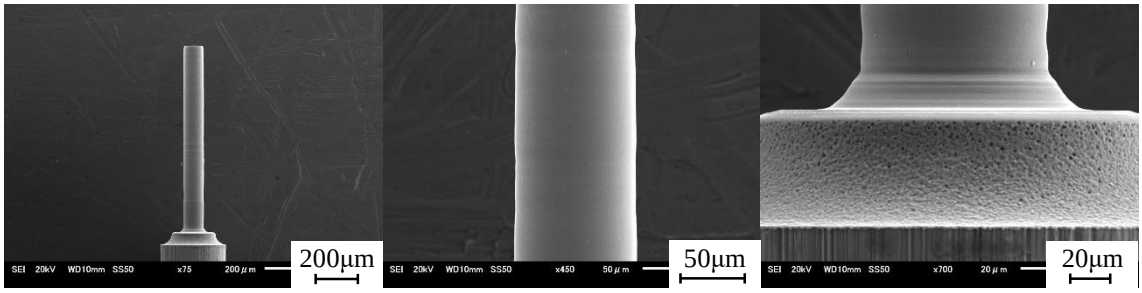

(d) Feed speed of 0.7 μm/s

Fig. 5.21 Micro-rods machined with feed distances of 850 μm

5.3.3 Machining of micro-rods with high aspect ratio

In this experiment, micro-rods of high aspect ratio were machined with the electrolyte of $NaNO_3$ aqueous solution. The length of micro-rod machined was 2 mm which was 20 times of the target rod diameter of 100 μm.

5.3.3.1 Experimental conditions

The experimental conditions are shown in Table 5.6. The voltage amplitude and rise/fall time of pulse power supply were 90 V and 40ns, respectively. The feed speed was 0.6 μm/s and 0.7 μm/s, respectively, which was determined according to the experimental results shown in Fig. 5.17. The electrolyte was $NaNO_3$ aqueous solution in concentration of 2 wt%. The workpiece was positioned on the top surface of tool electrode with an initial gap width of 5 μm. The cut depth in radial direction was set as 50 μm. The feed distances in axial direction was 2 mm which was 20 times of the targeted diameter of micro-rod machined. Fig. 5.22 shows the workpiece reshaped by WEDG method. Because of the thermal process of WEDG, the workpiece was bended.

Table 5.6 Experimental conditions used for micro-rods machining with high aspect ratio

Pulse voltage	Amplitude [V]	90
	Frequency [Hz]	500 k
	Duty factor [%]	50
	Rise/fall time [ns]	40
Feeding capacitance C_1 [pF]		47
Electrolyte		$NaNO_3$ aq. 2 wt%
Tool electrode rotation [rpm]		3000
Feed speed [μm/s]		0.6, 0.7

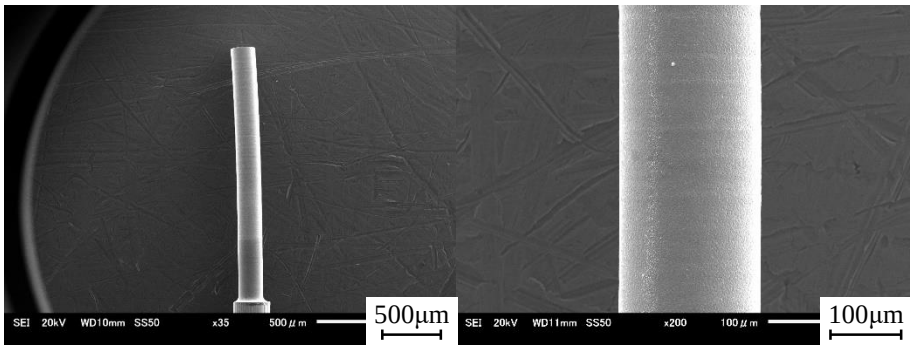

Fig. 5.22 Workpiece reshaped by WEDG

5.3.3.2 Micro-rod machined

Fig. 5.23(a) shows the micro-rod machined with high aspect ratio of 20 using the feed speed of 0.6 μm/s. The diameter of micro-rod near the end surface was smaller than that near the root, this is because the workpiece was not sufficiently straight after it was reshaped by WEDG as shown in Fig. 5.22. Fig. 5.23(b) shows the micro-rod machined with the feed speed of 0.7 μm/s. Some scratch can be seen on the surface of micro-rod,

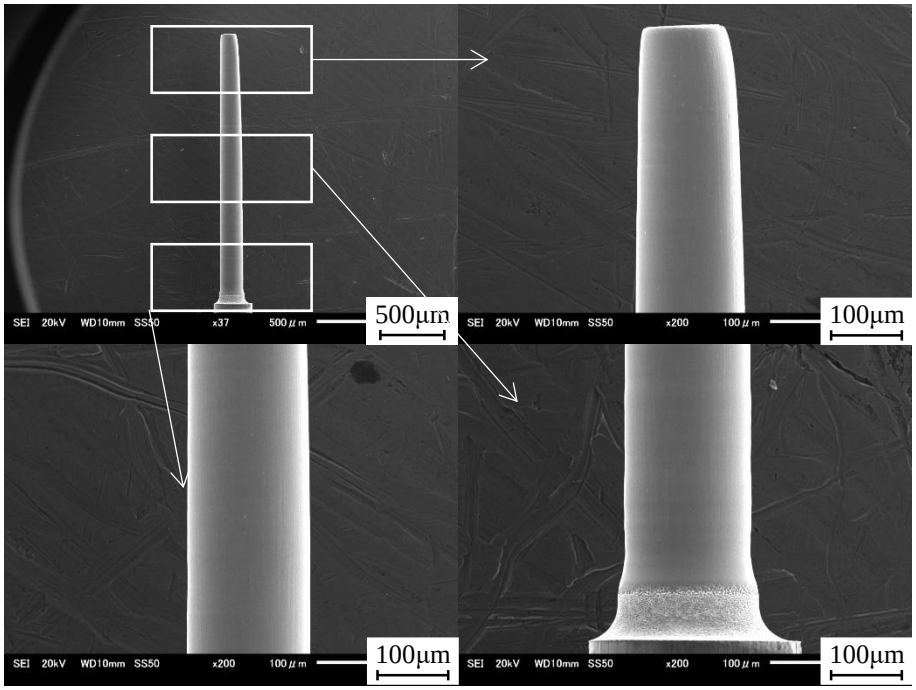

(a) Feed speed of 0.6 µm/s

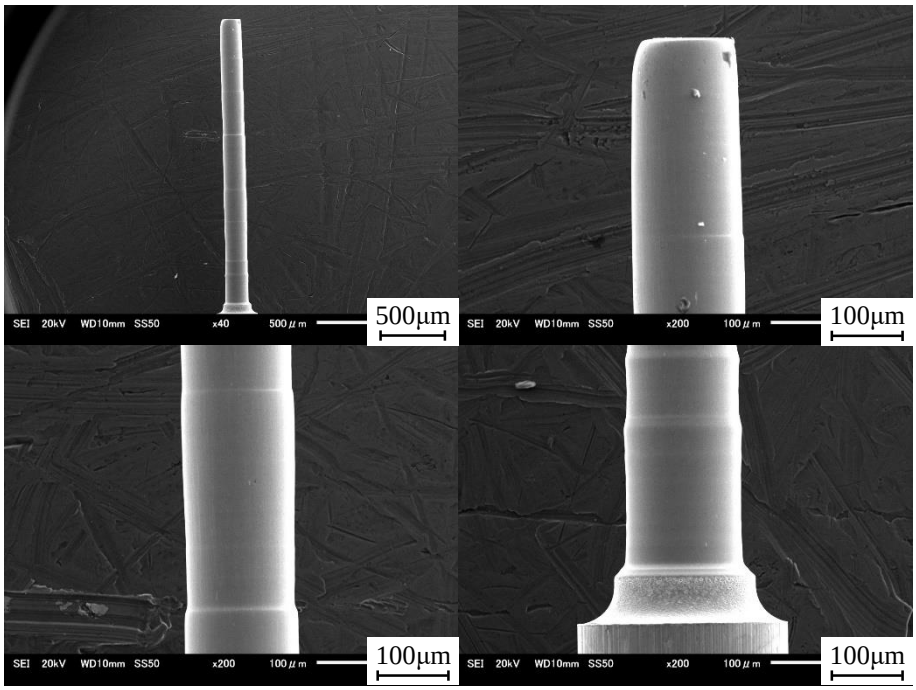

(b) Feed speed of 0.7 µm/s

Fig. 5.23 Micro-rods machined with feed distance of 2 mm

because the feed speed was high resulting in collision between electrodes. The gap width was significantly small with a high feed speed, therefore the flushing of the electrolyte in the working gap was not sufficient. In addition, there were existed a lot of and bubbles

during the electrochemical machining process, which hinders the refresh of the electrolyte in the machining gap. However, it is noted that the micro-rod became straight after the ECM process compared with that after the EDM process as shown in Fig. 5.22. This is because the ECM process is an anodic dissolution process without thermal influence.

5.3.3.3 Tool wear

At last, the tool wear was observed after machining, Fig. 5.24 shows the tool electrode before and after machining. There was almost no tool wear after machining, because unipolar current was used with the help of the diode, as shown in Fig. 5.2(b).

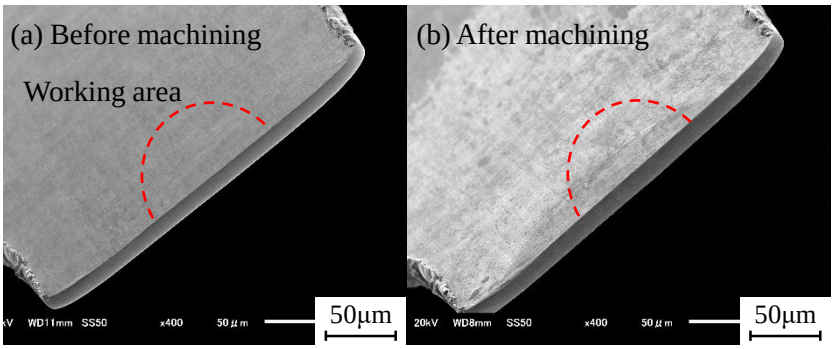

Fig. 5.24 Tool electrode before and after machining

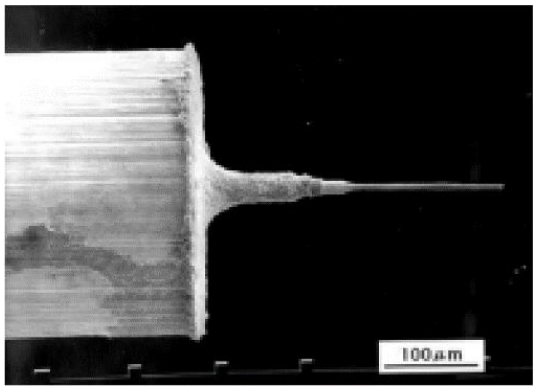

Fig. 5.25 A Φ4.5 μm micropin fabricated by WEDG[82, 83)]

5.3.4 Fabrication of minimum micro-rod

5.3.4.1 Fabrication of micro-rods with different cut depths in radial direction

To obtain the minimum machinable diameter of micro-rods, materials of stainless steel (SUS304) and tungsten were used as workpiece and tool electrode, respectively. The experimental conditions are shown in Table 5.7. The workpiece was positioned over the top surface of tool electrode with an initial gap width of 5 μm, and the feed speed was 0.5

μm/s. The feed distance in axial direction was set as 100 μm. The cut depth in axial direction were 40 μm, 50 μm, 70 μm, 90 μm and 92 μm.

Table 5.7 Experimental conditions used to fabricate minimum micro-rod

Pulse voltage	Amplitude [V]	90
	Frequency [Hz]	500 k
	Duty factor [%]	50
	Rise/fall time [ns]	40
Feeding capacitance C_1 [pF]		47
Electrolyte		$NaNO_3$ aq. 2 wt%
Tool electrode rotation [rpm]		3000
Feed speed [μm/s]		0.4
Cut depth in radial direction [μm]		40, 50, 70, 90, 92

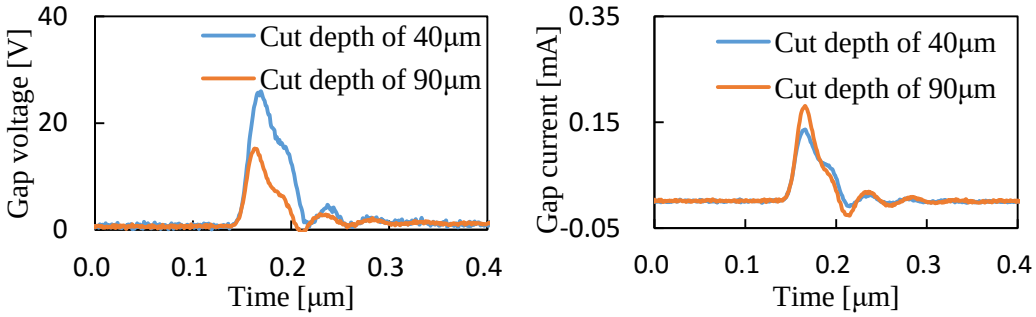

(a) Gap voltage waveforms (b) Gap current waveforms

Fig. 5.26 Waveforms with different cut depths in radial direction

Fig. 5.26 shows the waveforms with the cut depths of 40 μm and 90 μm in radial direction. Since the machining area increased with increasing the cut depth in radial direction, the gap resistance decreased resulting in higher gap current and lower gap voltage as shown in Fig. 5.26. In addition, since the electric charge per pulse $q = E_0C_1$ is constant, the current pulse duration slightly decreased with increasing the cut depth in radial direction as shown in Fig. 5.26(b). Fig. 5.27 shows the micro-rods machined with the cut depths of 40 μm, 70 μm, 90 μm, 92 μm in radial direction. With the cut depth of 40 μm in radial direction, the micro-rod machined was shortened as shown in Fig. 5.27(a). This is because the gap width was significantly large with a small cut depth in radial direction resulting in the increase in the influence of the stray current flowing through the radial gap and end of micro-rod. Hence, the micro-rod was shortened by the stray current outside of the axial gap. Micro-rods were successfully machined with the cut depths of 70 μm and 90 μm as shown in Figs. 5.27(b) and (c). However, the micro-rod was shortened with increasing the cut depth in radial direction to 92 μm as shown in Fig.

5.27(d). Since the target radius of the micro-rod was 8 μm with the cut depth of 92 μm in radial direction, it is considered that the radial gap width was larger than 8μm. Hence, the radial gap widths were plotted together with different cut depths in radial direction as shown in Fig. 5.28. The dotted line means the measurement of the radial gap width failed because the micro-rods were shortened as shown in Figs. 5.27(a) and (d). The radial gap width decreased with increasing the cut depth in radial direction, because the machining area increased, under the same axial feed speed. Furthermore, it is found that the radial gap width was larger than 8 μm with the cut depth of 92 μm in radial direction. Hence, the micro-rod was shortened as shown in Fig. 5.27(d).

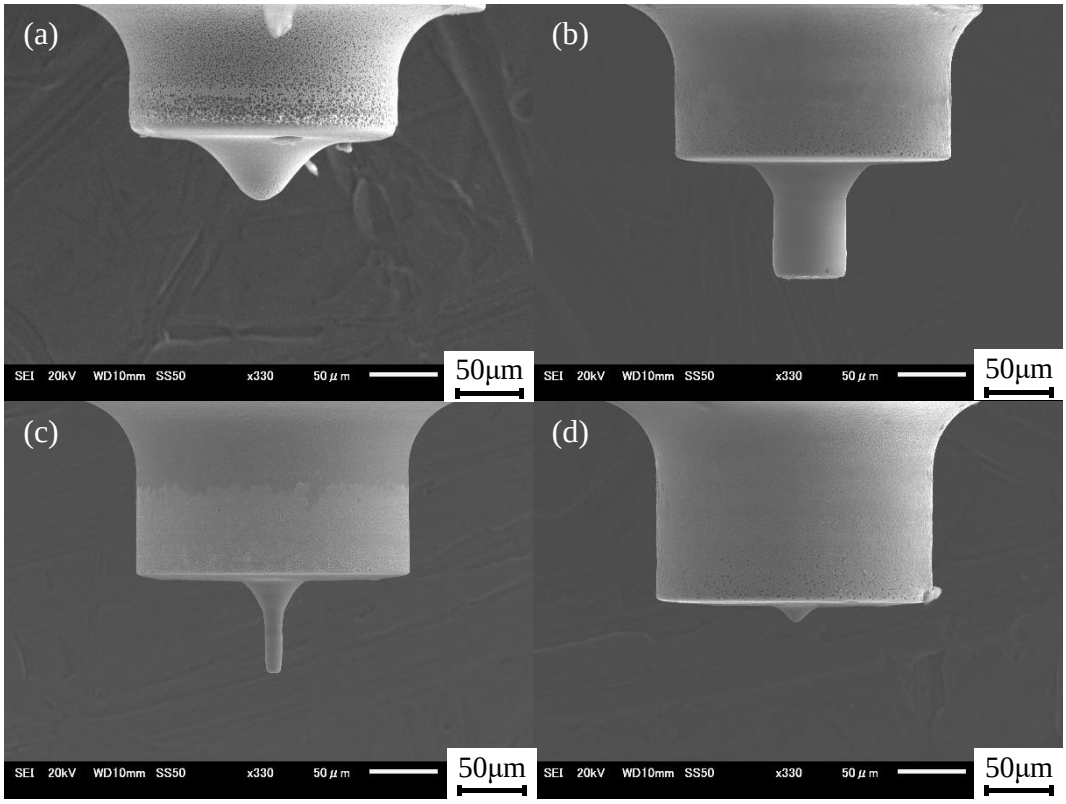

Fig. 5.27 Micro-rods machined with different cut depth in radial direction (a) 40 μm, (b) 70 μm, (c) 90 μm, (d) 92 μm

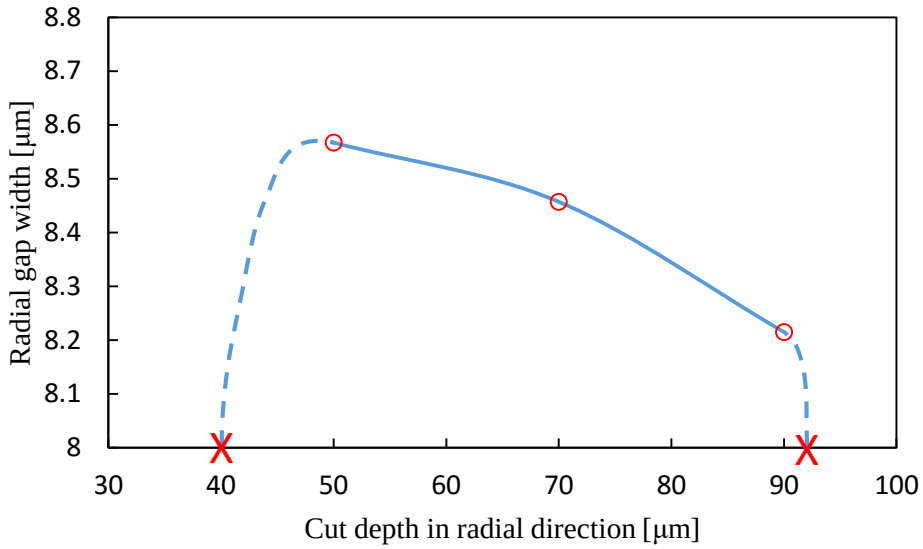

Fig. 5.28 Radial gap widths with different cut depths in radial direction

5.3.4.2 Fabrication of micro-rods with different feed speeds

It is considered that it is difficult to machine micro-rods of which diameter is smaller than the radial gap width. In the previous experiment however, the radial gap width was larger than 8 μm. Hence, the feed speed of the workpiece was increased with the same cut depth of 92 μm in radial direction, because the working gap width in both the axial and radial gaps can be decreased with increasing the feed speed of workpiece.

The experimental conditions are shown in Table 5.8. The workpiece was positioned over the top surface of tool electrode with an initial gap width of 5 μm, and the feed distance in axial direction was set as 100 μm. The cut depth in radial direction was 92 μm. The feed speeds were 0.4 μm/s, 0.5 μm/s, 0.6 μm/s and 0.7 μm/s.

Table 5.8 Experimental conditions used for micro-rods machining with different feed speeds

Pulse voltage	Amplitude [V]	90
	Frequency [Hz]	500 k
	Duty factor [%]	50
	Rise/fall time [ns]	40
Feeding capacitance C_1 [pF]		47
Electrolyte		$NaNO_3$ aq. 2wt%
Tool electrode rotation [rpm]		3000
Feed speed [μm/s]		0.4, 0.5, 0.6, 0.7

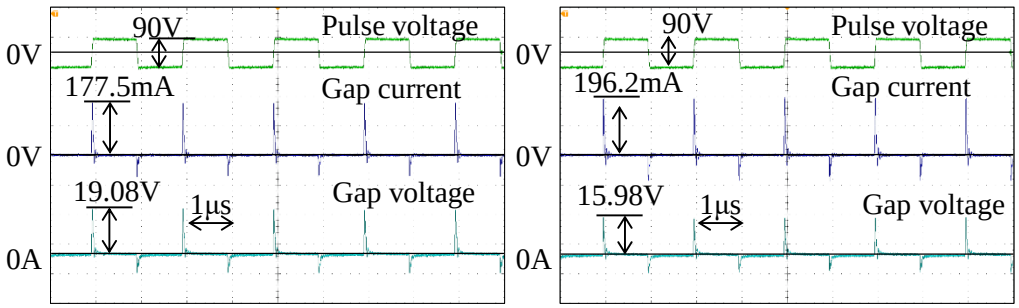

(a) Feed speed of 0.5 μm/s (b) Feed speed of 0.7 μm/s

Fig. 5.29 Waveforms of gap current and voltage with different feed speeds

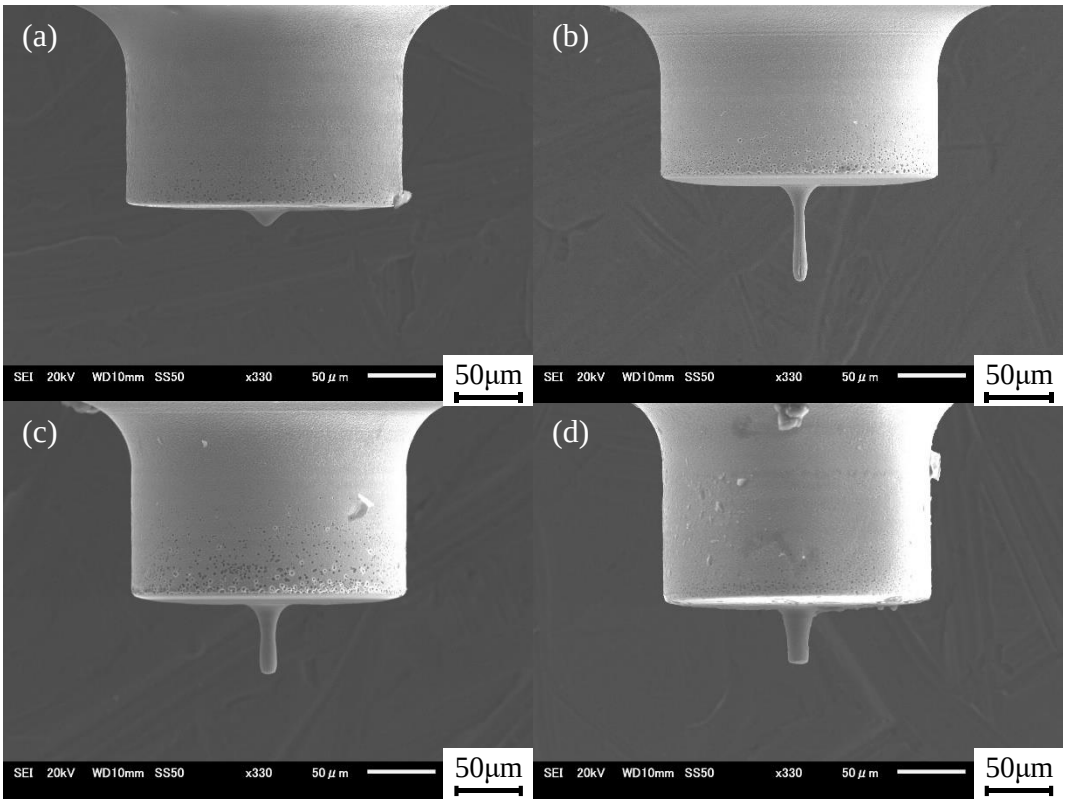

Fig. 5.30 Micro-rods machined with different feed speeds direction (a) 0.4 μm/s, (b) 0.5 μm/s, (c) 0.6 μm/s, (d) 0.7 μm/s

Fig. 5.29 shows the waveforms with the feed speeds of 0.5 μm/s and 0.7 μm/s. The gap current increased with increasing the feed speed due to the smaller gap width and resistance. Micro-rods machined with different feed speeds are shown in Fig. 5.30. Micro-rod was not obtained with the low feed speed of 0.4 μm/s because of the influence of stray current described above. Micro-rods were machined with other higher feed speeds. However, the lengths were shorter than the preset feed distance of 100 μm in axial direction. Fig. 5.31 shows the feed distances and lengths of micro-rods with different feed

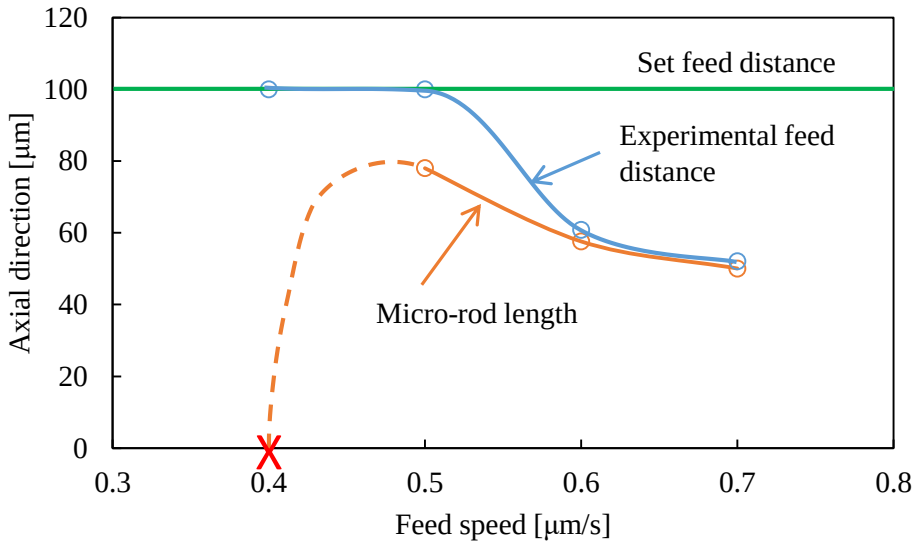

Fig. 5.31 Feed distances and micro-rods length with different fed speeds

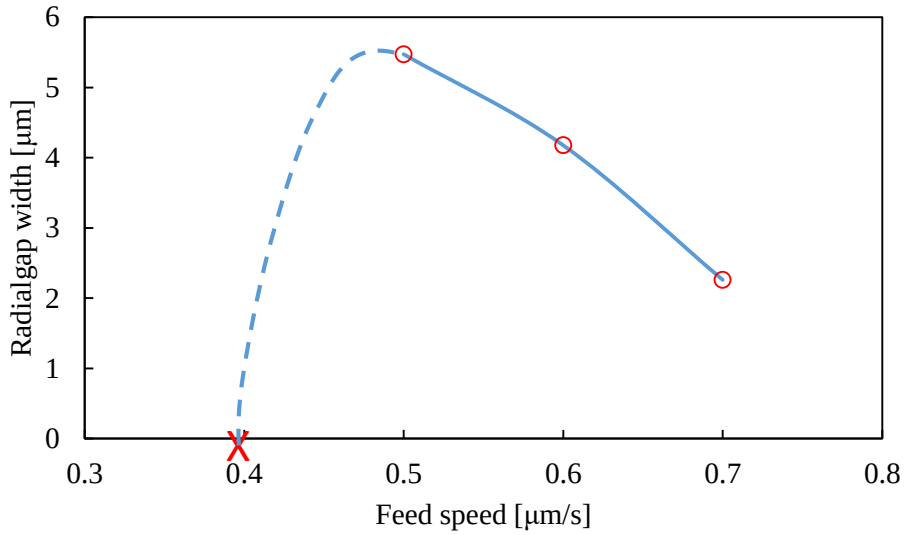

Fig. 5.32 Radial gap widths with different feed speeds

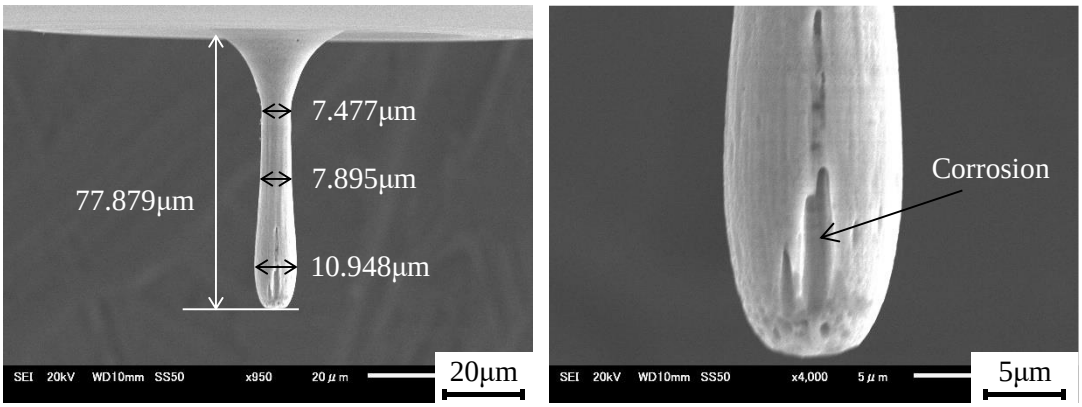

Fig. 5.33 Amplification of micro-rod machined with feed speed of 0.5 μm/s

speeds. The dotted line means the micro-rod machined disappeared completely due to dissolution as shown in Fig. 5.30(a). The machining processes were completed with the fed speeds of 0.4 μm/s and 0.5 μm/s. The length of micro-rod obtained was longest at the feed speed of 0.5 μm/s. Thereby, the influence of stray current on the machining accuracy was decreased with increasing the feed speed by comparing the experimental results with feed speeds of 0.4 μm/s and 0.5 μm/s. This is because the current was more localized in the axial gap with the higher feed speed of 0.5 μm/s, resulting in the decrease in the stray current in the radial gap. On the other hand, the machining process was interrupted by collision between electrodes with the higher feed speeds of 0.6 μm/s and 0.7 μm/s as shown in Fig. 5.31. Fig. 5.32 shows the radial gap widths with different feed speeds. It can be found that the radial gap can be decreased with increasing the feed speed. Since the radial gap width can be decreased, a micro-rod with smaller diameter can be machined more easily. The photo of the micro-rod machined with the feed speed of 0.5 μm/s in Fig. 5.30 was magnified as shown in Fig. 5.33. It is found that dissolution occurred preferentially in the axial direction due to the anisotropical micro structure existent prior to machining. This is probably because the stainless rod is produced by the drawing process.

5.4 Discussion

Masuzawa[82, 83)] fabricated micro-rods with high aspect ratio as shown in Fig. 5.25 using the wire electro-discharge grinding method. The diameter was 4.5 μm, which was much smaller than the miniaturization size of Φ9 μm obtained with the electrostatic induction feeding ECM. The electrochemical reaction was difficult to be localized in a small working gap with the ECM method resulting in the low machining accuracy. Therefore, the EDM has an obvious advantage in the miniaturization size compared with the electrostatic induction feeding ECM. However, there is no residual stress and cracks generated in ECM and the surface roughness is better, there is a possibility that the machining accuracy and miniaturization limit of ECM will be able to exceed EDM in the future.

5.5 Conclusions

Chapter 5 investigated the influences of the annealing process of the workpiece and different kinds of electrolytes on the machining characteristics. The experimental results show that the machinable length limitation was decreased using the annealed workpiece. It is considered that since the annealing process was performed in air, the workpiece

material was damaged due to oxidation. In addition, the machining characteristics with electrolytes of NaCl and $NaNO_3$ aqueous solution were investigated. The experimental results show that the influence of pitting corrosion was eliminated with the electrolyte of $NaNO_3$ aqueous solution. This is because chloride ion is a tiny and aggressive ion compared with nitrate ion, and therefore easily permeates the oxide film and triggers the occurrence of pitting corrosion. In addition, the gap width and taper angle was decreased with the electrolyte of $NaNO_3$ aqueous solution compared with that of the electrolyte of NaCl aqueous solution, because the electrochemical reaction can occur in a larger working gap with the NaCl aqueous solution due to the higher current efficiency. Furthermore, the machinable length of micro-rod was increased with the electrolyte of $NaNO_3$ aqueous solution compared with that of the NaCl aqueous solution, because the influence of pitting corrosion was eliminated. Then, a long micro-rod with diameter of 100 μm and aspect ratio of 20 was machined using the electrolyte of sodium nitrate aqueous solution. Furthermore, through optimizing the cut depth in radial direction and feed speed, micro-rod with the average diameter of 9 μm and length of 78 μm was machined successfully. Since the target diameter of micro-rod was significantly small, the radial gap width should be as small as possible to reduce the stray current in the radial gap.

Compared with the EDM, the machining accuracy and miniaturization limit were still lower with the electrostatic induction feeding ECM. However, since there are no residual stresses and cracks generated in ECM and the surface roughness is better, there is a possibility that the accuracy and miniaturization limit of ECM may become equivalent to those of EDM with the future development.

Chapter 6 Influence of kinds of workpiece materials

6.1 Introduction

Micro-rods have been widely used as tool electrodes in micro machining of 3D structures, fuel jet nozzle, spinning nozzle, cooling channels of turbine blade, measuring system, and micro die/mold. Kim et al.[84] machined 3D micro structures on stainless steel using a micro-rod as tool electrode. In general, the micro-rods should have properties of high erosion resistance, good electrical and thermal conductivity, and high stiffness[85]. Tungsten is usually fabricated to obtain micro-rod using micro EDM, laser machining, etc., and used as tool electrode for EDM and ECM. Compared with the above machining methods, ECM is a promising method to fabricate micro-rods because the material is removed by anodic dissolution that does not produce any residual stress[4, 6, 9] which is generally caused by the thermal processes of the above mentioned methods. Lim et al.[86] used KOH aqueous solution as electrolyte and DC current to etch the tungsten rod. They found that the geometry effect would affect the form of microelectrode. Zhi-Wen Fan et al.[87] fabricated a cylindrical tungsten microelectrode with the pulsed ECM, and the influences of working parameters (such as applied voltage, pulse period, duty factor, and temperature) on the fabrication of microelectrode were discussed. Yong-Mo Lim and Soo Hyun Kim[88] machined a slender tungsten micropin with the electrochemical etching, and derived a mathematical model to control the diameter of micropin. Zhenlong Wang et al.[89] designed a suitable micro electrochemical machining system and fabricated tungsten micro-rod with diameter of 30μm and tip radius of 100nm and compared the surface property and machining capability with the microelectrode fabricated by EDM. In their research, the sodium hydroxide (NaOH) or potassium hydroxide (KOH) were often used as electrolytes, because of generation of tungsten oxide on the workpiece surface, which hinders the electrolytic dissolution, should be avoided. However, these electrolytes are not environmentally friendly because of high toxicity. In addition, the alkaline solution easily corrodes experimental equipments. Hence, in this chapter, tungsten micro-rods are fabricated with the neutral electrolytes such as $NaNO_3$ and NaCl aqueous salt solutions using the electrostatic induction feeding ECM. The influences of feeding capacitance, concentration of electrolyte and different electrolytes on the machining characteristics were investigated. Because of the bipolar current required for the machining principle with neutral electrolyte, the tool occurred and investigated. In addition, in order to investigate the influences of different workpiece materials on the machining

characteristics, the materials of high speed steel (SKH51) and tungsten carbide were also used as workpieces to machine a micro-rod.

This chapter describes the influences of different kinds of workpiece materials on the machining characteristics of micro-rods fabrication, including the tungsten, high speed steel, tungsten carbide.

6.2 Fabrication of tungsten micro-rod

Tungsten has been widely used as tool electrode in micro machining. Some researchers have machined it using ECM method, however, most of the electrolytes were the alkaline aqueous solutions, such as potassium hydroxide (KOH), sodium hydroxide (NaOH) and so on, which are not environmentally friendly and corrosive to experimental equipments. In this research, therefore neutral electrolytes were used to machine tungsten rods.

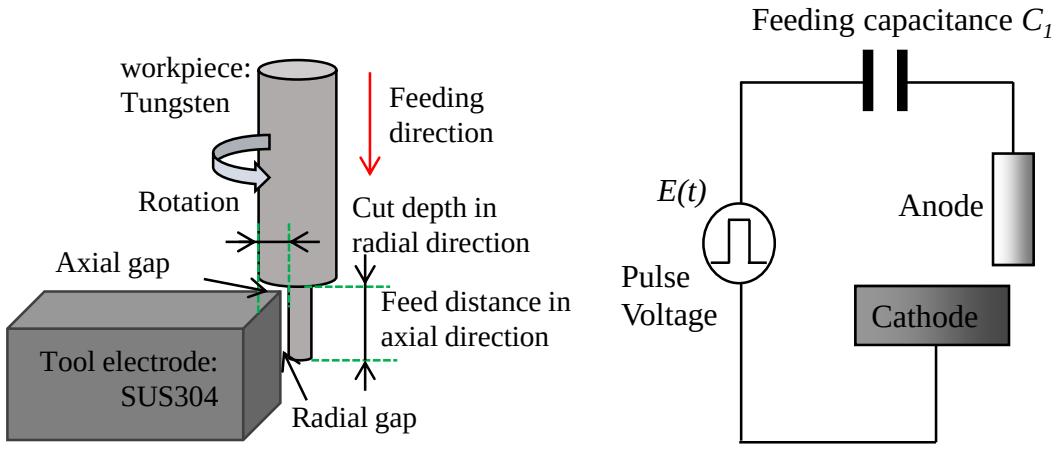

(a) Machining method of micro-rod (b) Diode was used to avoid tool wear

Fig. 6.1 Machining method of micro-rod and circuit

6.2.1 Principle of tungsten rod machining

6.2.1.1 Micro-rods machining method

The micro-rods machining method using the electrostatic induction feeding method is shown in Fig. 6.1(a). The workpiece was positioned on the top surface of tool electrode, and fed in axial direction. The workpiece was tungsten rod with diameter of 300 μm and reshaped by the wire electrical discharge grinding (WEDG)[58] method to make it sufficiently straight, resulting in a reshaped size of 200 μm in diameter and 300 μm in length as shown in Fig. 6.2(a). The tool electrode was a stainless steel (SUS304) plate, and the size is shown in Fig. 6.2(b). The electrolyte was sodium nitrate ($NaNO_3$) or sodium chloride (NaCl) aqueous solution. During machining, the electrolyte was supplied

from a nozzle with the inner diameter of 200 μm to the working gap at the flow rate of 10 ml/min. In order to obtain the pulse voltage of the electrostatic induction feeding method, the output of a function generator (Agilent, 33250A) was amplified by a bipolar amplifier (NF Corporation, HSA4101).

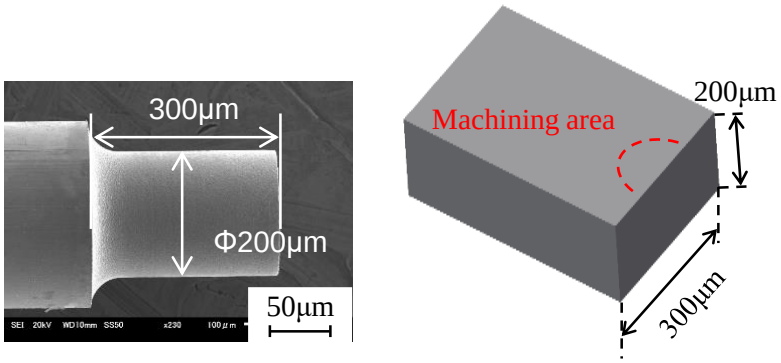

(a) Workpiece (b) Tool electrode

Fig. 6.2 Workpiece and tool electrode

6.2.1.2 Electrochemical reaction

With the bipolar current and electrolyte of $NaNO_3$ aqueous solutions, Maeda et al.[62] and Mazuzawa et al.[90] found that the following electrochemical reaction occurs when the tool electrode (tungsten) is positive.

$$2Na^{+}+2H_2O+2e \rightarrow 2NaOH+H_2 \quad (6.1)$$

Because of the NaOH, the tungsten oxide (WO_3), which is generated on the surface of tungsten rod, can be dissolved as

$$WO_3+2NaOH \rightarrow Na_2WO_4+H_2O \quad (6.2)$$

Hence, the tungsten can be machined with neutral electrolytes. In this research, sodium nitrate ($NaNO_3$) and sodium chloride (NaCl) aqueous solutions were used as electrolytes and the tungsten rod was used as workpiece and bipolar current was supplied by the electrostatic induction feeding method.

Table 6.1 Experimental conditions with comparatively longer pulse durations

Pulse voltage	Amplitude [V]	30
	Frequency [Hz]	200 k, 500 k, 1 M, 2 M, 3 M
	Duty factor [%]	50
Electrolyte		$NaNO_3$ aq. 6 wt%
Tool electrode rotation [rpm]		3000
Feed speed [μm/s]		0.5

6.2.1.3 Machining experiment with comparatively longer pulse durations

The experimental conditions are shown in Table 6.1. Fig. 6.3 shows the bipolar voltage used in the experiments with the frequency varied at 200 kHz, 500 kHz, 1 MHz, 2 MHz and 3 MHz. This pulse voltage was directly applied to the ECM gap without a feeding capacitance. Hence, like normal ECM, electrolytic current waveforms similar to the voltage waveforms can be obtained. The neutral electrolyte of $NaNO_3$ of 6 wt% in concentration was used. The cut depth in radial direction and feed distance in axial direction were set as 50 μm and 100 μm, respectively.

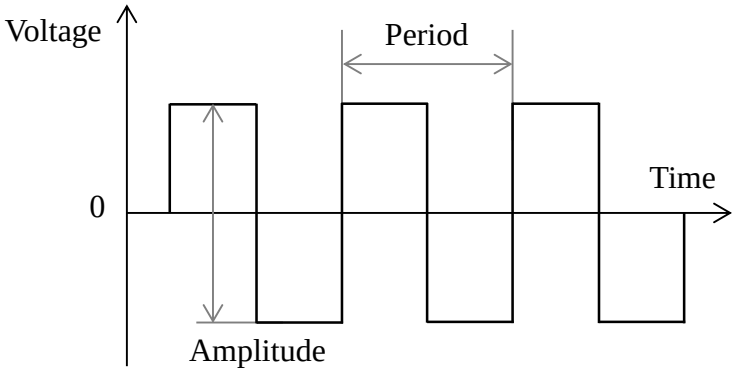

Fig. 6.3 Bipolar voltage

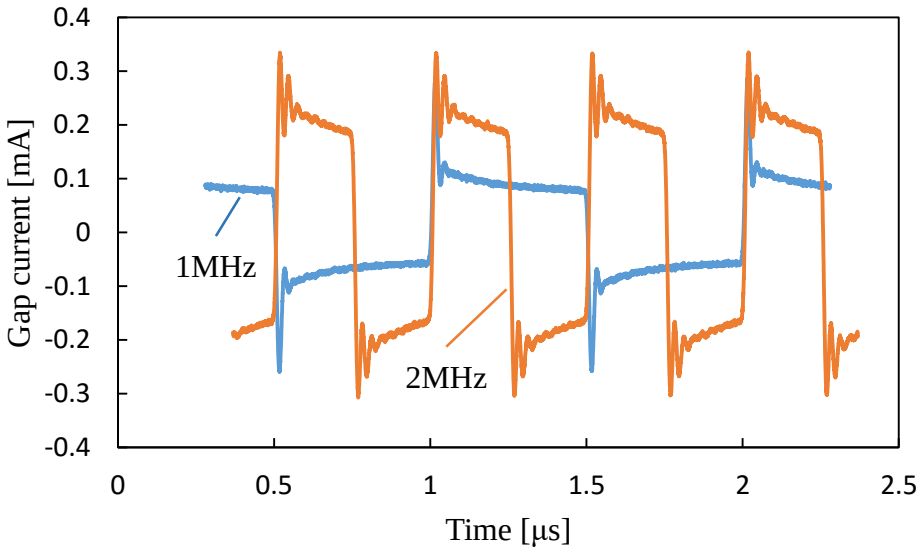

Fig. 6.4 Gap current waveforms with the frequencies of 1 MHz and 2 MHz

Fig. 6.4 shows the gap current waveforms with the frequencies of 1 MHz and 2 MHz. Since the electrochemical reaction was localized in a smaller working gap based on the

theory related to the electric double layer. Hence, the gap current increased with higher frequency of 2 MHz due to the smaller axial gap resistance as shown in Fig. 6.4.

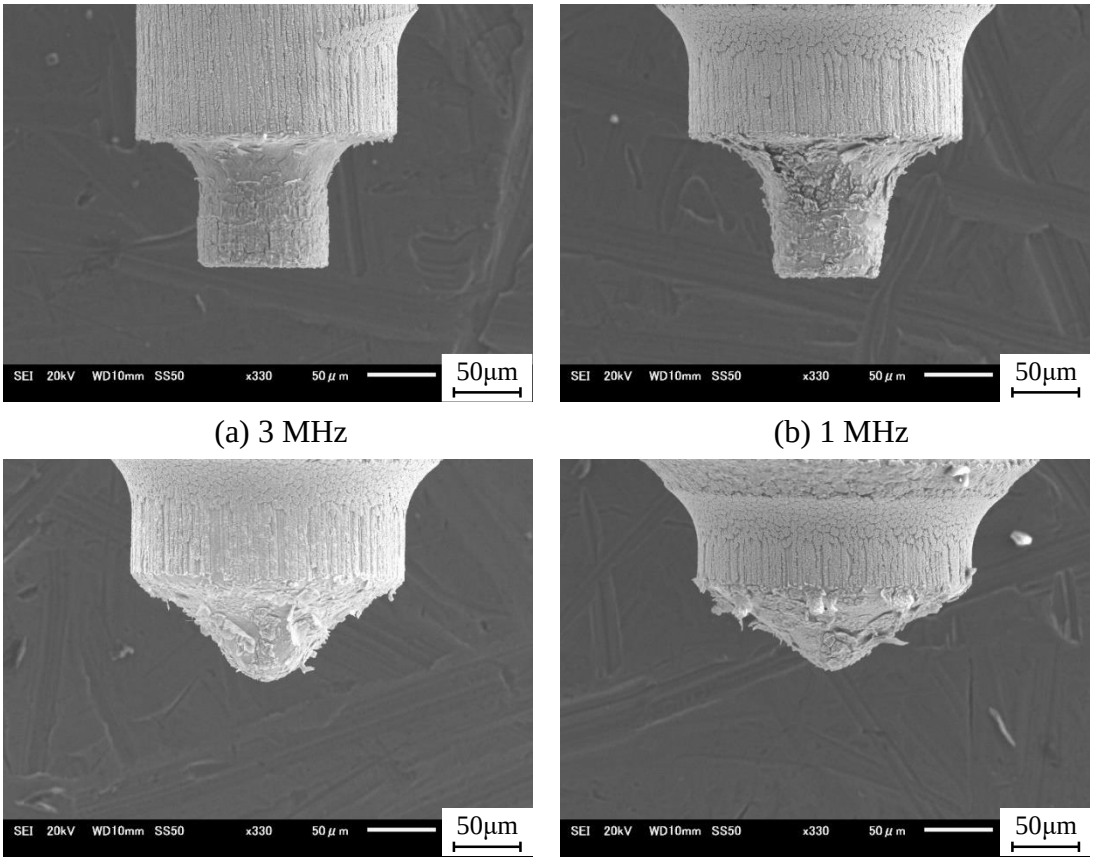

(a) 3 MHz (b) 1 MHz

(c) 500 kHz (d) 200 kHz

Fig. 6.5 Micro-rods machined with different frequencies of pulse voltage

Fig. 6.5 shows the micro-rods machined with the frequencies of 200 kHz, 500 kHz, 1 MHz and 3 MHz. It is found that the micro-rods were shortened with decreasing the frequency of pulse voltage. This is because the electrochemical dissolution occurred in a large working gap with long pulse duration resulting in the increase in the material dissolution from the radial gap and end of micro-rod. However, the target length of micro-rod, which was set as 100 μm in this experiment, was successfully achieved with the higher frequencies of 1 MHz, 2 MHz and 3 MHz because the electrochemical reaction mainly occurred in the narrow axial gap. Fig. 6.6 shows the length of micro-rods machined with different frequencies of pulse voltage, and the green dotted line is the target length of micro-rod. The experimental results show that the machining accuracy was increased with increasing the frequency of pulse voltage.

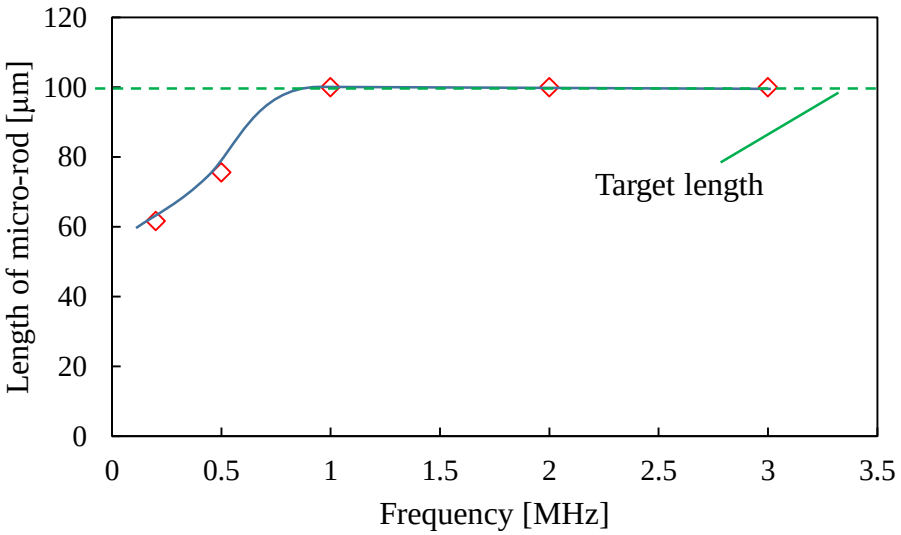

Fig. 6.6 Length of micro-rods with different frequencies

It was found that a layer of unknown material was adhered on the surface of micro-rods as shown in Fig. 6.5. The material compositions analyzed by EDS are shown in Fig. 6.7. There existed 13.25% of oxygen element and 63.6% of tungsten element. It is considered that the oxygen element results from the rapid oxidation of the tungsten, and the unknown material should be tungsten oxide. Fig. 6.8 shows the distribution of tungsten element and oxide element.

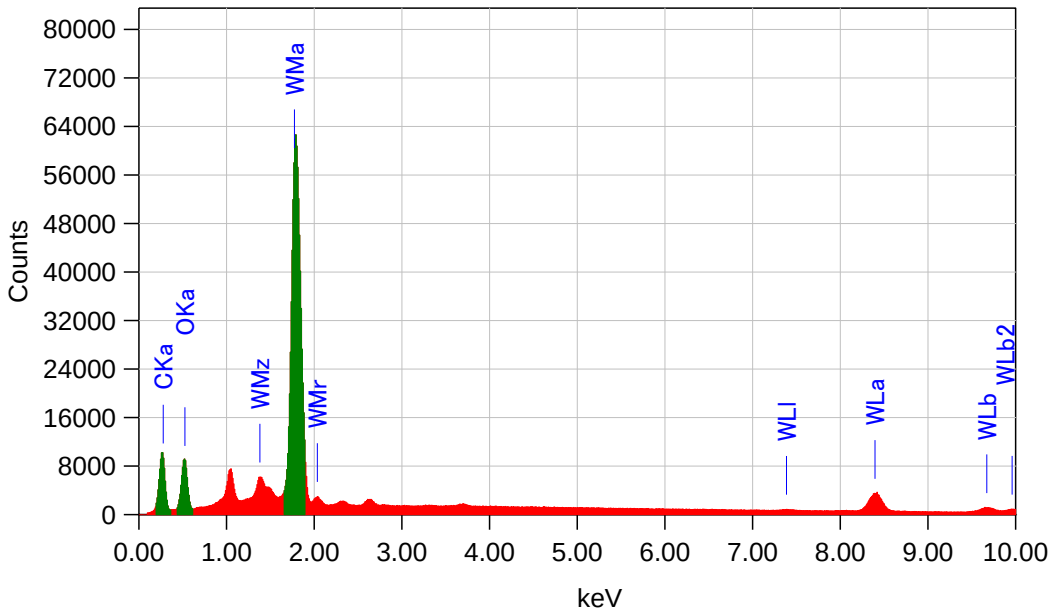

Fig. 6.7 EDX analysis results of the material on the micro-rod surface

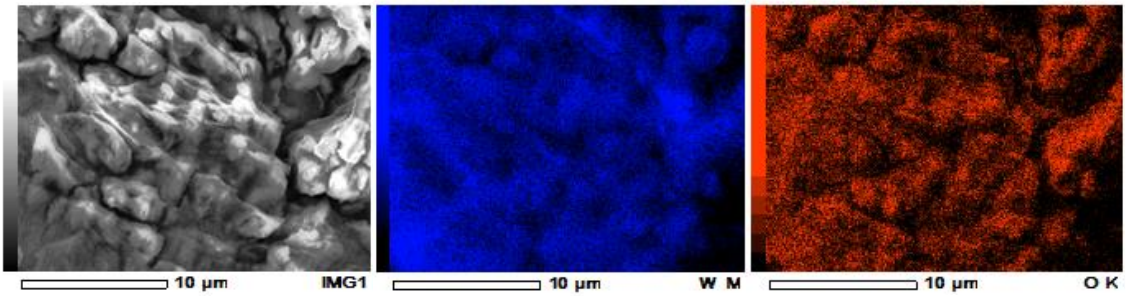

(a) Analyzed area (b) Tungsten element (c) Oxide element

Fig. 6.8 Distribution of tungsten element and oxide element

The experimental results show that the machining accuracy increased with increasing the frequency because the electrochemical dissolution was localized in a smaller working gap by a shorter pulse duration resulting in higher machining accuracy. To obtain a higher machining accuracy, the electrostatic induction feeding method was used to supply ultra-short pulse current because pulse current of several tens ns in pulse duration can be easily generated with this method. The influences of the feeding capacitance, concentration of electrolyte and electrolyte types on the machining characteristics were investigated in the following sections.

6.2.2 Influence of feeding capacitance

6.2.2.1 Experimental conditions

Influences of C_1 on machining characteristics were investigated using the electrostatic induction feeding method under the experimental conditions shown in Table 6.2. In the circuit shown in Fig. 4.2 used for machining metallic materials, a diode was used to obtain mono-polar current pulse. In the present experiment, however, the diode was not used to obtain bipolar current pulse. The pulse voltage with amplitude of 90 V, frequency of 500 kHz, duty factor of 50%, and rise/fall time of 40 ns, was used. The $NaNO_3$ aqueous solution with concentration of 2 wt% was used as electrolyte. The servo feed control system was not used in this experiment, and constant feeding method was used for the fundamental research. The feed speed was increased from 0.2 µm/s to 0.7 µm/s with an increment of 0.1. The workpiece was positioned over the top surface of tool electrode with an initial gap width of 5 µm. The cut depth in radial direction and feed distance in axial direction were set as 50 µm and 180 µm, respectively. In order to investigate the influence of feeding capacitance on the machining characteristics, the feeding capacitances of 250 pF and 350 pF were used in this experiment.

Table 6.2 Experimental conditions used to machine tungsten rods

Pulse voltage	Amplitude [V]	90
	Frequency [Hz]	500 k
	Duty factor [%]	50
	Rise/fall time [ns]	40
Feeding capacitance C_1 [pF]		250, 350
Electrolyte		$NaNO_3$ aq. 2 wt%
Tool electrode rotation [rpm]		3000
Feed speed [μm/s]		0.2, 0.3, 0.4, 0.5, 0.6, 0.7

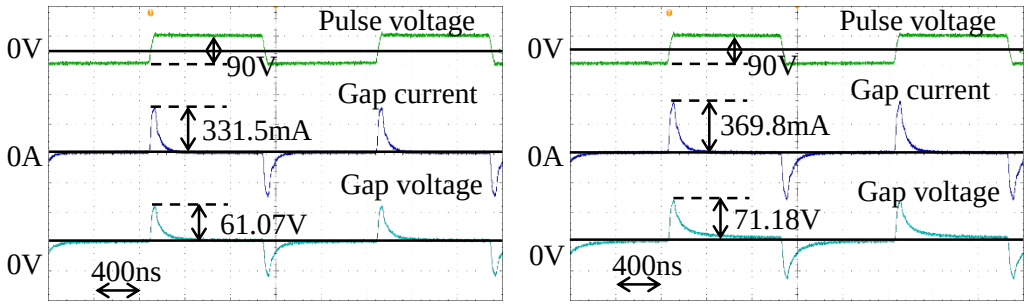

(a) 250 pF (b) 350 pF

Fig. 6.9 Waveforms with feed speed of 0.5 μm/s and different feeding capacitances

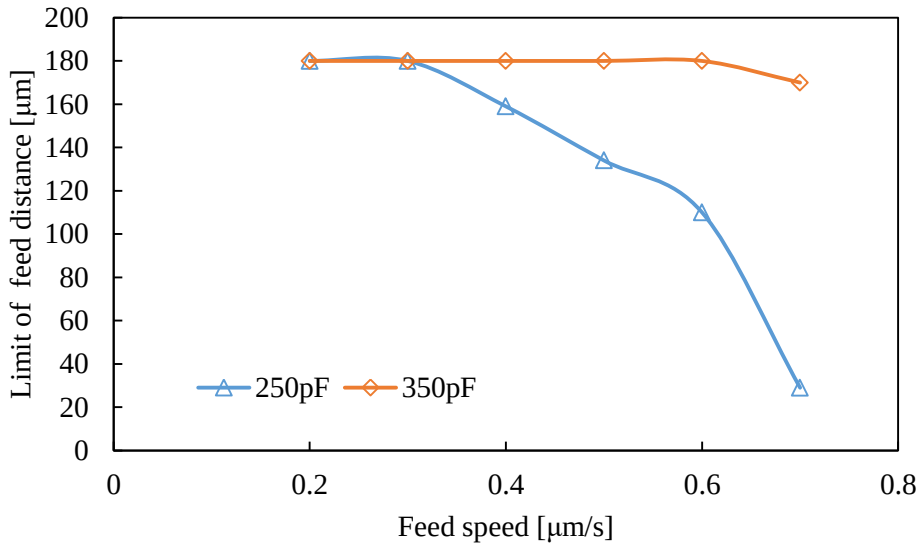

Fig. 6.10 Limit of feed distances with different feeding capacitances and feed speeds

6.2.2.2 Limit of feed distance with different feeding capacitances

Collison between electrodes occurs between electrodes with increasing the feed distance, because the stray current in the radial gap increases. Therefore, there is a limit

of feed distance for each machining process. Fig. 6.9 shows the gap current and voltage waveforms with the feed speed of 0.5 μm/s and different feeding capacitances. The gap current and voltage increased with increasing the feeding capacitance C_1 as described in Chapter 2. With C_1=250 pF, collision between electrodes occurred with high feed speeds resulting in the failure of the machining process as shown in Fig. 6.10. It is found that the limit of feed distance increased with C_1=350 pF, because the electrical charge $q=C_1E_0$ per pulse increased, resulting in higher material removal rate.

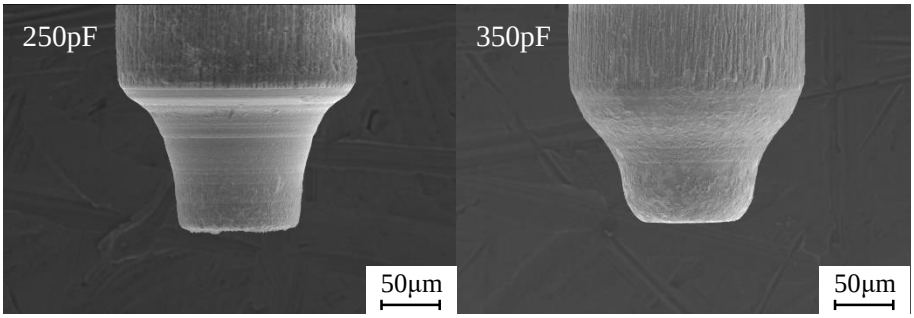

(a) Feed speed of 0.2 μm/s

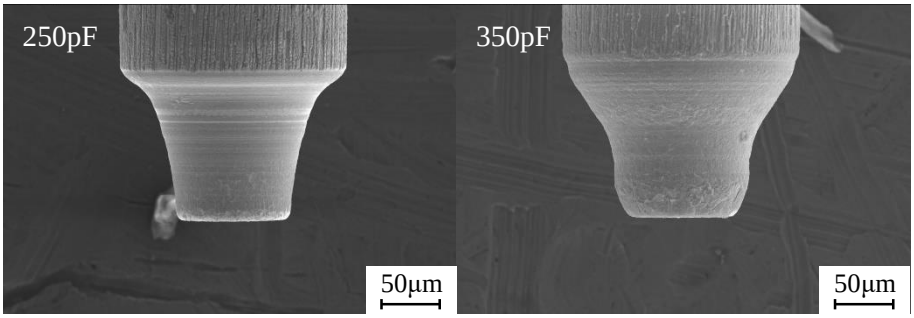

(b) Feed speed of 0.3 μm/s

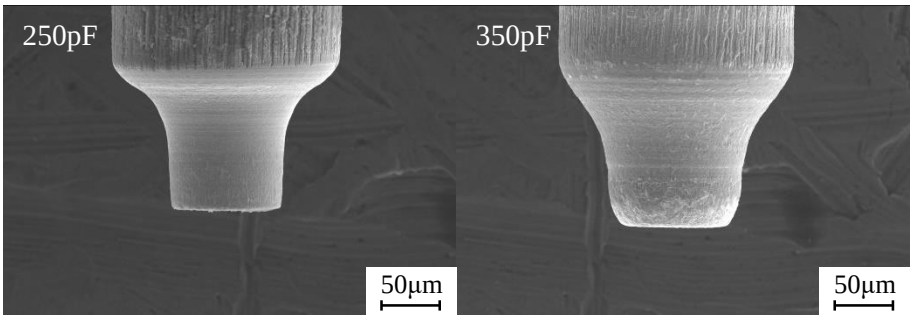

(c) Feed speed of 0.4 μm/s

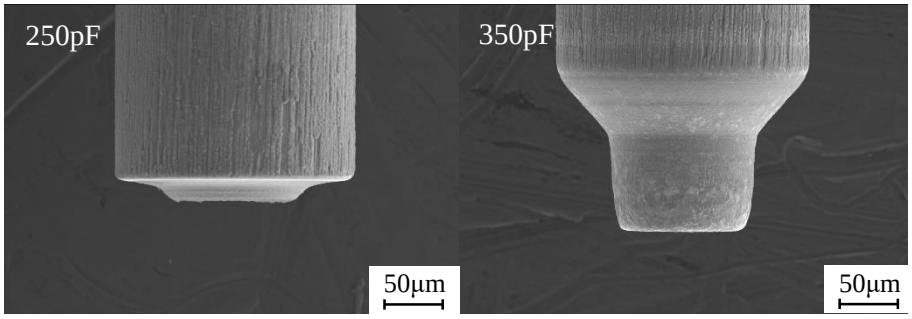

(d) Feed speed of 0.7 μm/s

Fig. 6.11 Micro-rods machined with different feed speeds

6.2.2.3 Material removal volume

Fig. 6.11 and Fig. 6.12 show the micro-rods machined and the material removal volume with different feeding capacitances. When the feeding capacitance C_1 was the same, the

material removal volume increased with increasing the feed speed. This is mainly because the current density increased with a smaller gap width and resistance, resulting in a higher current efficiency and material removal rate. With the feeding capacitance of 250 pF, the material removal volume decreased when the feed speed was 0.7 μm/s, because of collision between electrodes. However, the machining process was completed successfully under any feed speeds when the feeding capacitance was 350 pF. This is because the electric charge per pulse $q=C_1E_0$ increased with increasing the feeding capacitance.

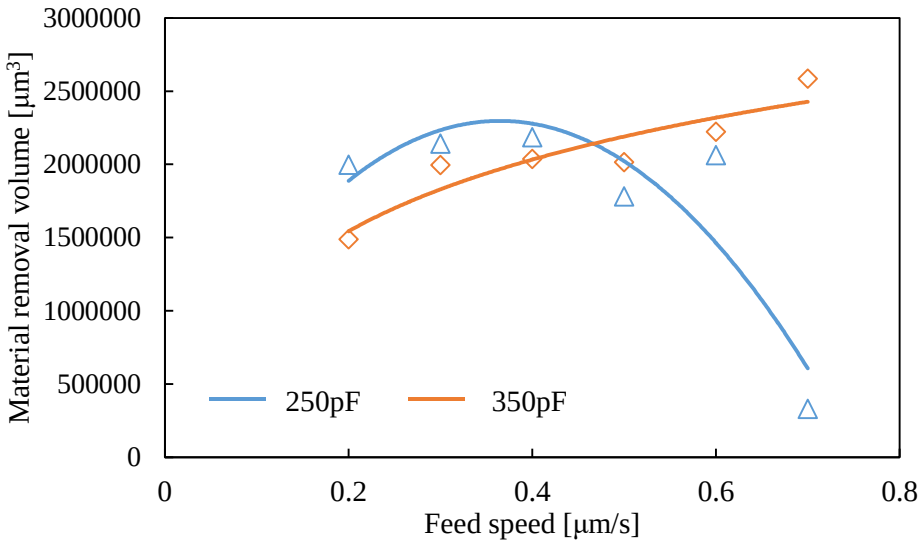

Fig. 6.12 Material removal volume with different feeding capacitances

6.2.2.4 Tool wear volume

Since the bipolar current was necessary, the tool electrode was worn as shown in Fig. 6.13. Fig. 6.14 show the tool wear volume with different feeding capacitances. With the same feeding capacitance, the tool wear volume decreased with increasing the feed speed. This is because the working gap decreased with increasing the feed speed, resulting in less material dissolution in the radial gap. In addition, it is found that the tool wear volume was increased with increasing the feeding capacitance when the feed speed was the same.

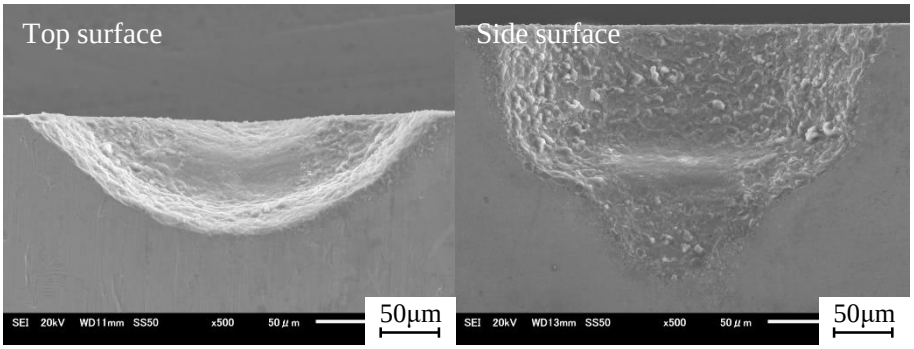

(Ⅰ) Feed speed of 0.2 μm/s

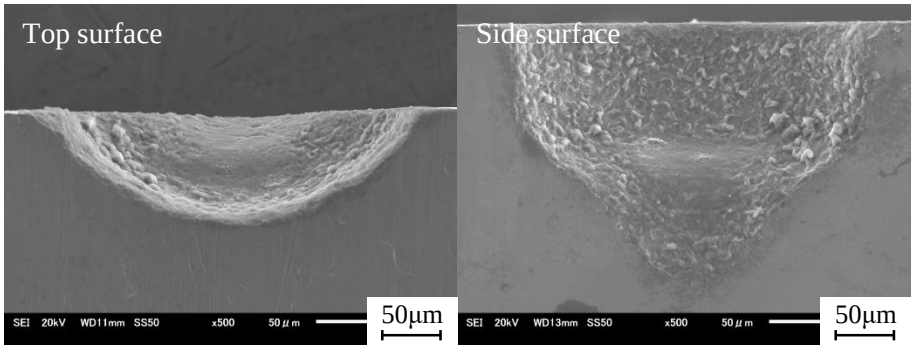

(Ⅱ) Feed speed of 0.3 μm/s

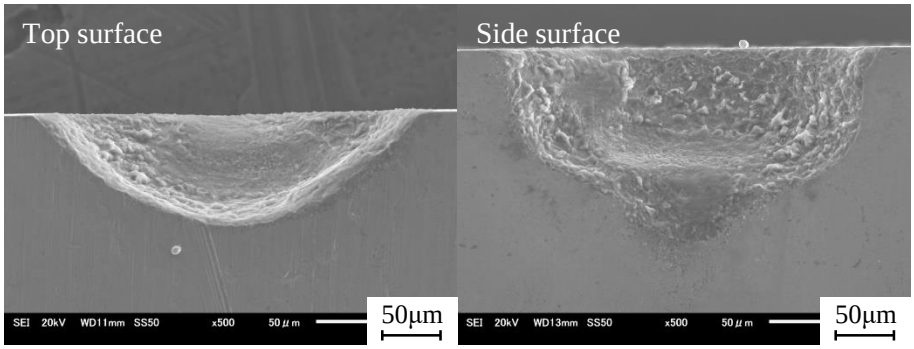

(Ⅲ) Feed speed of 0.4 μm/s

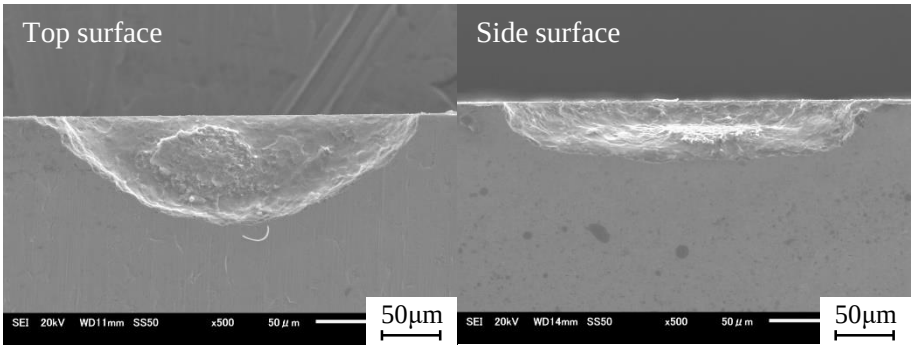

(Ⅳ) Feed speed of 0.7 μm/s

(a) Feeding capacitance of 250 pF

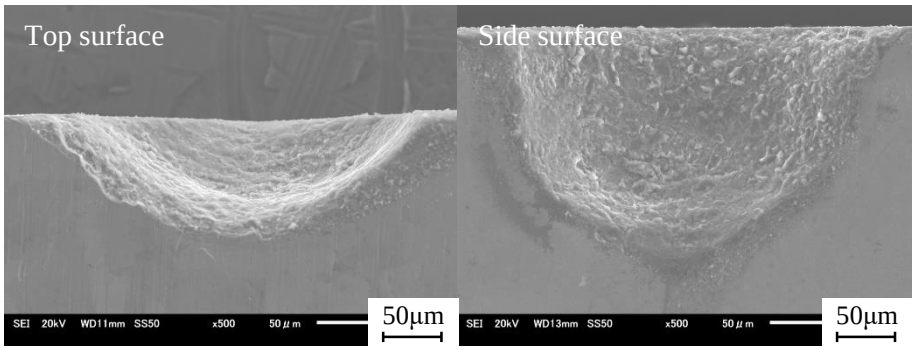

(Ⅰ) Feed speed of 0.2 μm/s

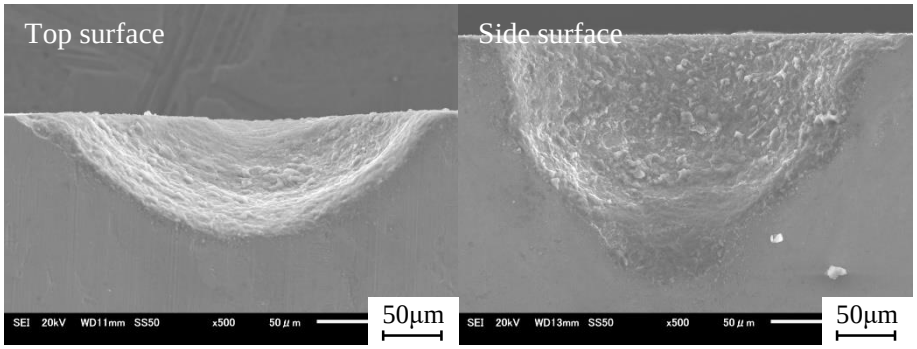

(Ⅱ) Feed speed of 0.3 μm/s

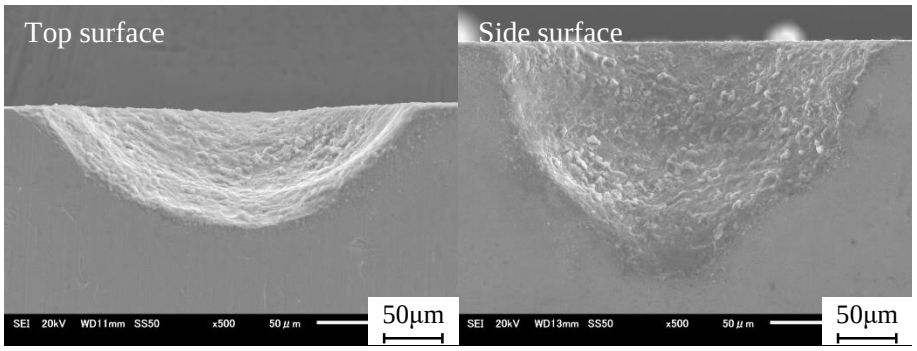

(Ⅲ) Feed speed of 0.4 μm/s

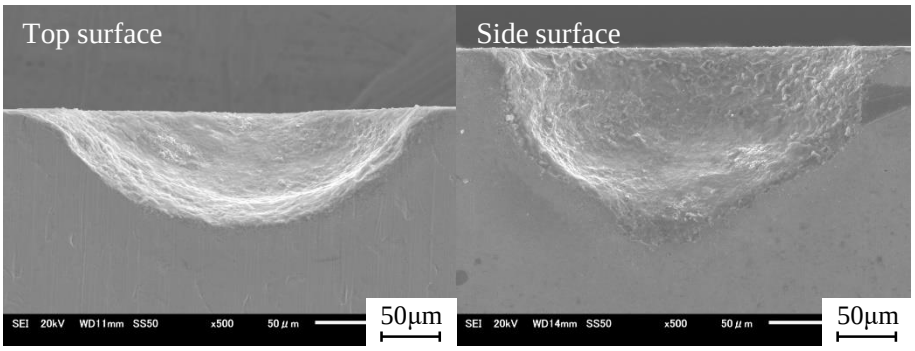

(Ⅳ) Feed speed of 0.7 μm/s

(b) Feeding capacitance of 350 pF

Fig. 6.13 Tool wear with different feeding capacitances

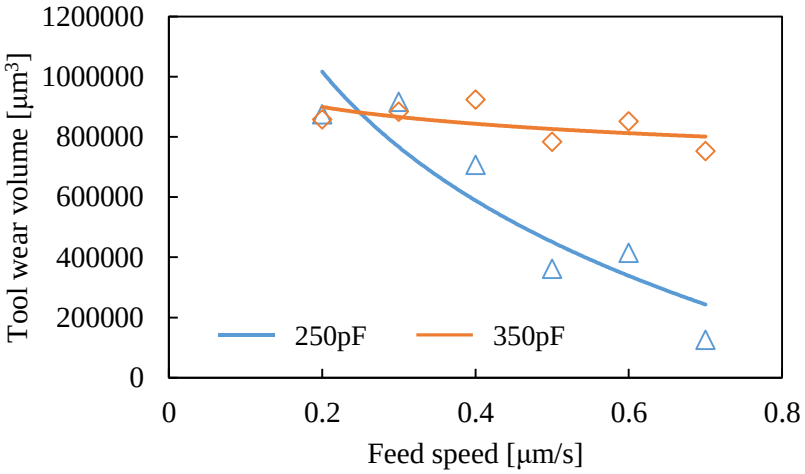

Fig. 6.14 Tool wear volume with different feeding capacitances

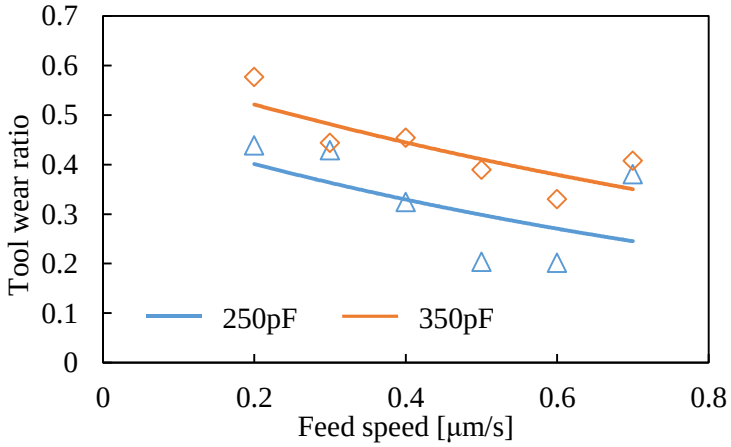

Fig. 6.15 Tool wear ratio with different feeding capacitances

6.2.2.5 Tool wear ratio

In this research, the tool wear ratio is defined as the ratio of the tool wear volume to the material removal volume. Fig. 6.15 shows the tool wear ratio with different feeding capacitances. It decreased with increasing the feed speed. In addition, the tool wear ratio decreased with decreasing the feeding capacitance when the feed speed was the same.

6.2.3 Influence of electrolyte concentration

6.2.3.1 Experimental conditions

The experimental conditions are shown in Table 6.3. The voltage was 90 V in amplitude with the frequency of 500 kHz, and the duty factor and rise/fall time were 50% and 40 ns, respectively. The feeding capacitance was 47 pF or 350 pF and the feed speed was increased from 0.4 μm/s to 1.2 μm/s with an increment of 0.1. The workpiece was

positioned over the top surface of tool electrode with an initial gap width of 5 μm. The cut depth in radial direction and feed distance in axial direction were set as 50 μm and 180 μm, respectively. The $NaNO_3$ aqueous solutions of 2 wt% and 6 wt% in concentration were used as electrolyte.

Table 6.3 Experimental conditions to machine tungsten rods with different electrolyte concentrations

Pulse voltage	Amplitude [V]	90
	Frequency [Hz]	500 k
	Duty factor [%]	50
	Rise/fall time [ns]	40
Feeding capacitance C_1 [pF]		47, 350
Electrolyte		$NaNO_3$ aq. 2 wt% & 6 wt%
Tool electrode rotation [rpm]		3000
Feed speed [μm/s]		0.4, 0.5, …, 1.1, 1.2

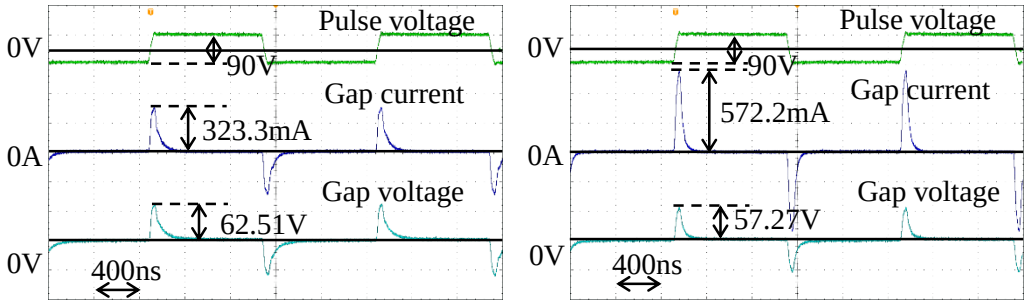

(a) $NaNO_3$ of 2 wt% (b) $NaNO_3$ of 6 wt%

Fig. 6.16 Waveforms with feed speed of 0.6 μm/s and different concentrations of electrolyte

6.2.3.2 Limit of feed distances with different concentrations

Fig. 6.16 shows the gap current and voltage waveforms with the feed speed of 0.6 μm/s and different concentrations of electrolyte. The gap current was increased with increasing the concentration of electrolyte. Fig. 6.17 shows the limit of feed distances with different concentrations of electrolyte in this experiment. Since the current density was increased with increasing the concentration of electrolyte resulting in higher current efficiency, the limit of feed distance increased with higher concentration of electrolyte.

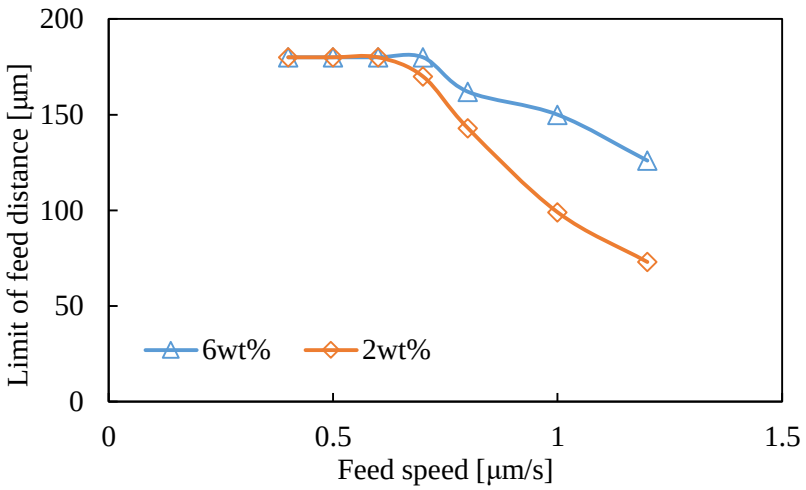

Fig. 6.17 Limit of feed distances with different concentrations of electrolyte

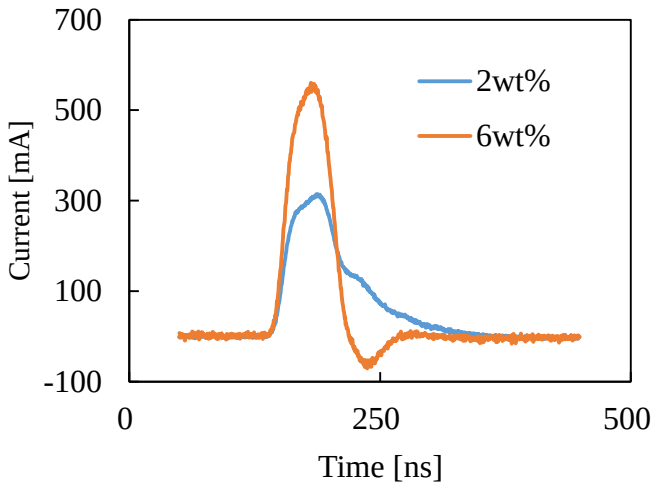

Fig. 6.18 Gap current waveforms with feed speed of 0.6 μm/s and different electrolyte concentrations

6.2.3.3 Material removal volume and machining accuracy

Gap currents with different concentrations at the feed speed of 0.6 μm/s and the feeding capacitance of 350 pF are shown in Fig. 6.18. It is found that the current duration decreased with increasing the concentration of electrolyte, because the electric charge per pulse $q=C_1E_0$ is constant. To keep the same electric charge per pulse, the higher gap current with the concentration of 6 wt% resulted in a shorter pulse duration. The measured electric charge per pulse q with the feeding capacitance of 47 pF and 350 pF is shown in Fig. 6.19. It is found that q is the same independent of the concentrations of 2 wt% and 6 wt%. The q increased with increasing the feeding capacitance because $q=C_1E_0$.

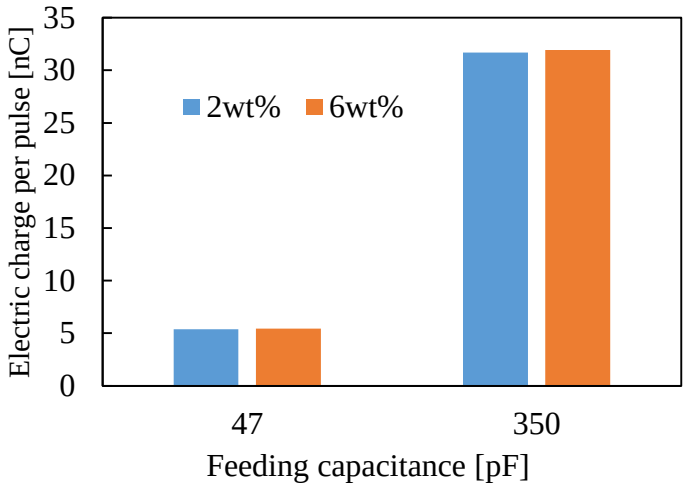

Fig. 6.19 Electrical charge per pulse with feeding capacitances of 47 pF and 350 pF

Fig. 6.20 shows the micro-rods machined with different concentrations of electrolyte. The machining accuracy increased with increasing the feed speed because of the smaller working gap width in the axial gap, resulting in the higher current density in the axial gap, thereby reducing the current density in the radial gap. In addition, the end edge of the micro-rod rounded with the lower concentration of 2 wt%. In contrast, the micro-rods machined with the higher concentration of 6 wt% have a better machining accuracy. Hence, it is considered that the machining accuracy increased with increasing the concentration of electrolyte with the electrostatic induction feeding method. In conventional pulse ECM, however, the machining accuracy increased with decreasing the concentration of electrolyte because the electrochemical dissolution can be localized in a smaller working gap[49]. This difference can be explained by the following reasons. The pulse duration time decreased and peak increased with increasing the concentration of electrolyte to keep the q constant when the electrostatic induction feeding method was used. On the other hand, the higher current density results in the higher current efficiency. However, since the bipolar current was needed for the tungsten machining with the neutral electrolyte, the tool electrode was worn after machining. Thereby, the corner at the root of the micro-rod machined was rounded with a large radius. Fig. 6.21 shows the material removal volume with different concentrations of electrolyte. The material removal volume was increased with higher concentration of electrolytes. The current increased with increasing the concentration of electrolytes, thereby, the duration time of pulse current was decreased. Hence, the machining accuracy was increased resulting in less tool wear due to the smaller working gap.

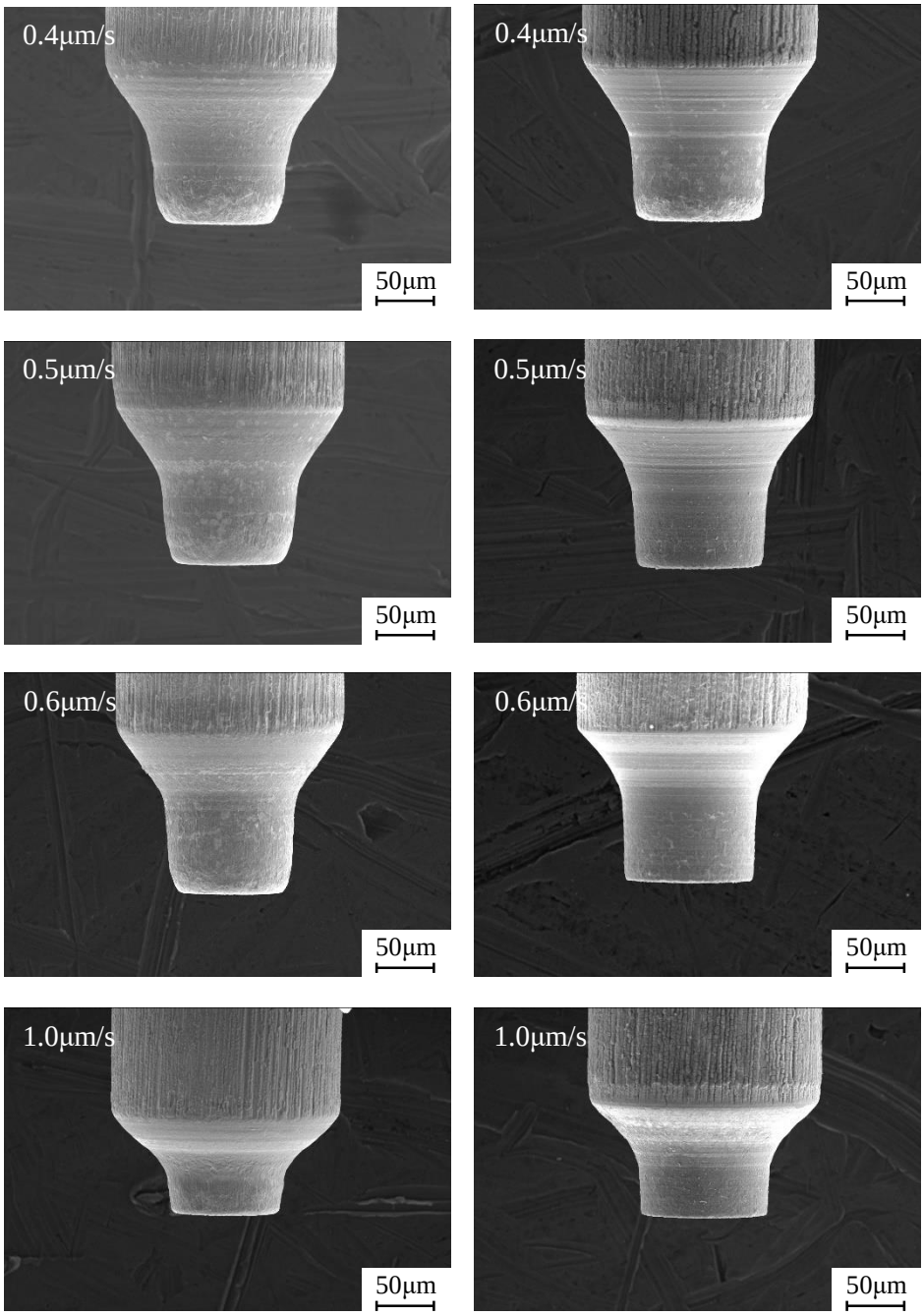

Fig. 6.20 Micro-rods machined with different feed speeds and concentrations of electrolyte

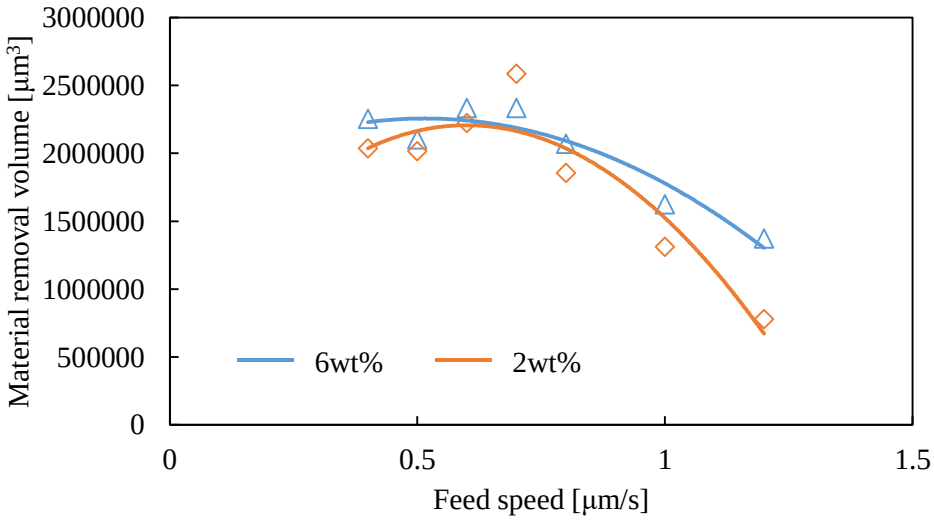

Fig. 6.21 Material removal volume with different concentrations of electrolyte

6.2.3.4 Tool wear volume

Fig. 6.22 and Fig. 6.23 shows the tool wear and tool wear volume with different concentrations of electrolyte, respectively. The difference of the tool wear volume with different concentrations of electrolyte was significantly small. Considering the machining processes were not completed with the higher feed speed than 0.7 μm/s, Fig. 6.24 shows the tool wear volumes with the feed speeds of 0.4 μm/s, 0.5 μm/s and 0.6 μm/s, with which the machining processes were completed using different concentrations of electrolyte. It is noted that the tool wear volume was smaller with high concentration of 6 wt%.

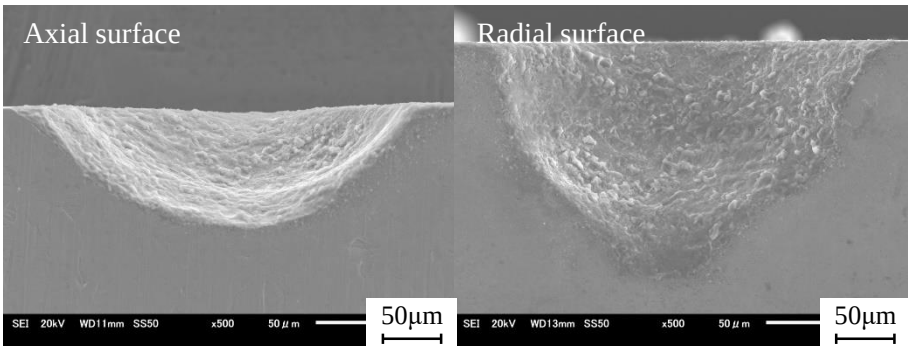

(Ⅰ) Feed speed of 0.4 μm/s

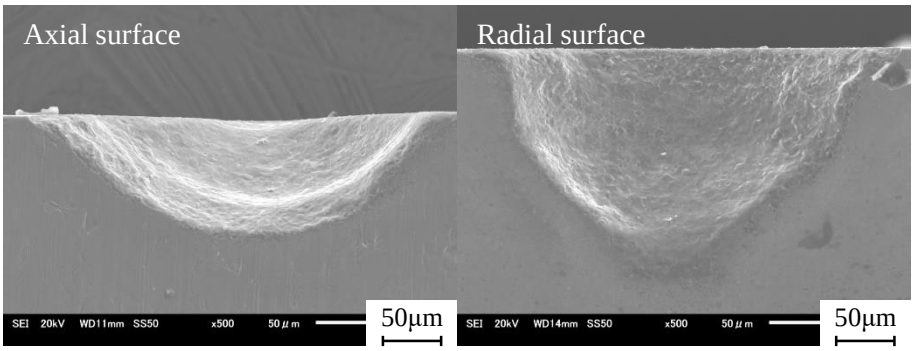

(Ⅱ) Feed speed of 0.5μm/s

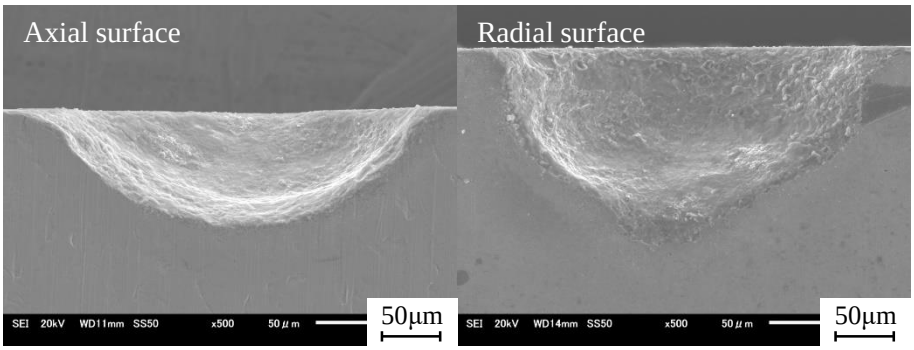

(Ⅲ) Feed speed of 0.6 μm/s

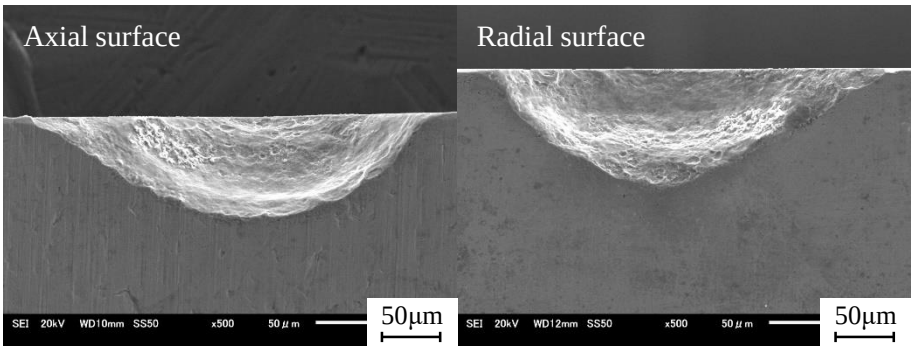

(Ⅳ) Feed speed of 1.0 μm/s

(a) $NaNO_3$ of 2 wt%

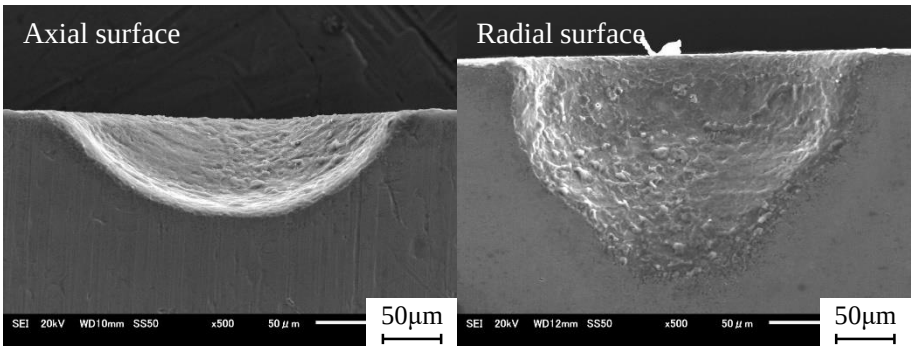

(Ⅰ) Feed speed of 0.4 μm/s

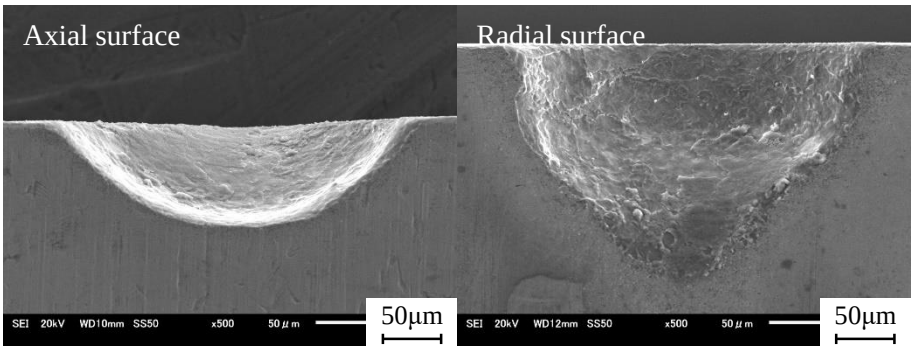

(Ⅱ) Feed speed of 0.5 μm/s

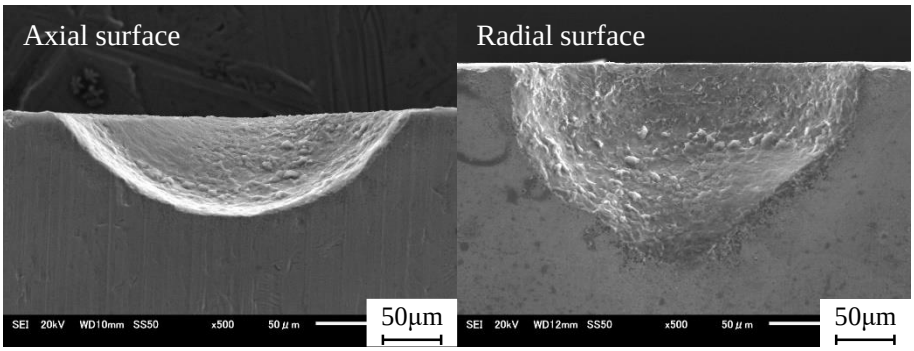

(Ⅲ) Feed speed of 0.6 μm/s

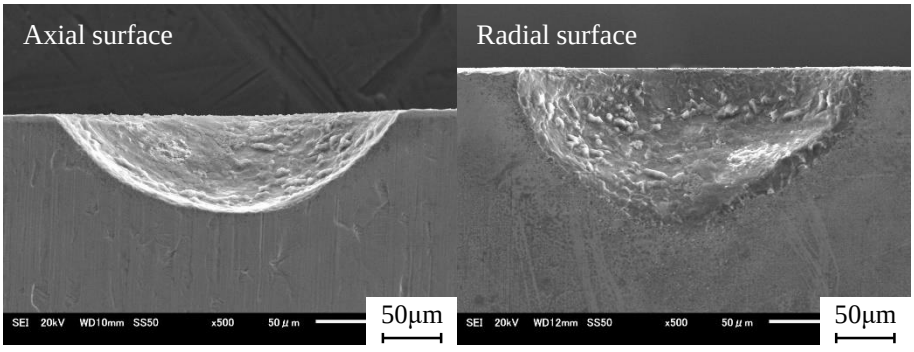

(Ⅳ) Feed speed of 1.0 μm/s

(b) $NaNO_3$ of 6 wt%

Fig. 6.22 Tool wear with different concentrations of electrolyte

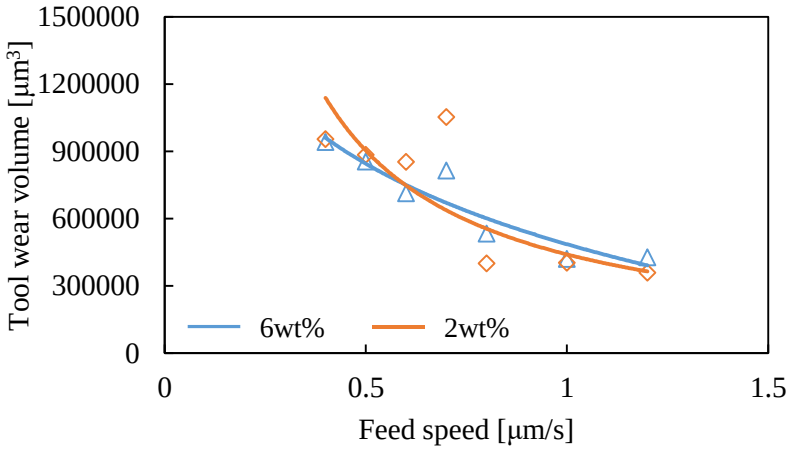

Fig. 6.23 Tool wear volume with different concentrations of electrolyte

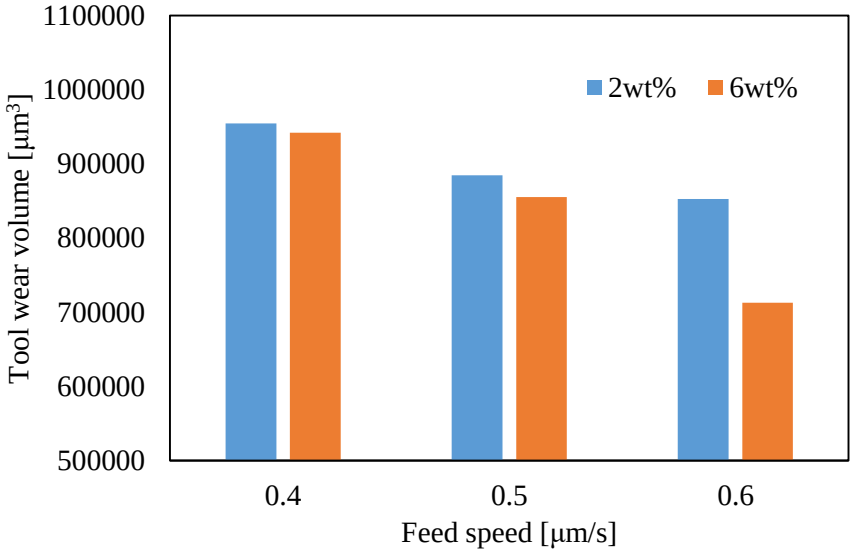

Fig. 6.24 Tool wear volume with feed speeds of 0.4 μm/s, 0.5 μm/s and 0.6 μm/s

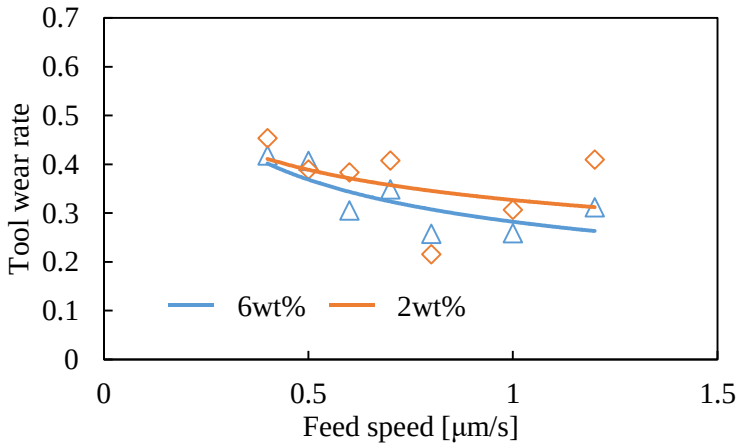

Fig. 6.25 Tool wear ratio with different concentrations of electrolyte

6.2.3.5 Tool wear ratio

Fig. 6.25 shows the tool wear ratio with different concentrations of electrolyte. It decreased with the concentration of 6 wt%. The current duration decreased with increasing the concentration of electrolyte as mentioned above.

6.2.4 Influence of different electrolytes

6.2.4.1 Experimental conditions

The experimental conditions are shown in Table 6.4. The feeding capacitance was 350 pF and the feed speed was increased from 0.4 μm/s to 1.2 μm/s with an increment of 0.1. The cut depth in radial direction and feed distance in axial direction were set as 50 μm and 180 μm, respectively. The $NaNO_3$ and NaCl aqueous solutions of 6 wt% in concentration were used as electrolyte in this experiment.

Table 6.4 experimental conditions used to investigate influence of different electrolytes

Pulse voltage	Amplitude [V]	90
	Frequency [Hz]	500 k
	Duty factor [%]	50
	Rise/fall time [ns]	40
Feeding capacitance C_1 [pF]		350
Electrolyte		NaCl & $NaNO_3$ aq. 6 wt%
Tool electrode rotation [rpm]		3000
Feed speed [μm/s]		0.4, 0.5, …, 1.1, 1.2

6.2.4.2 Feed distances with different electrolytes

Fig. 6.26 shows the gap current and voltage waveforms with the feed speed of 0.6 μm/s and different electrolytes. The gap currents were almost the same. Fig. 6.27 shows the feed distances with different electrolytes in this experiment. Because of the high current efficiency of NaCl aqueous solution, the machining process were completed even with the high feed speed of 1.2 μm/s. However, the machining process was interrupted by collision between electrodes with the feed speed higher than 0.7 μm/s using the electrolyte of $NaNO_3$ aqueous solution.

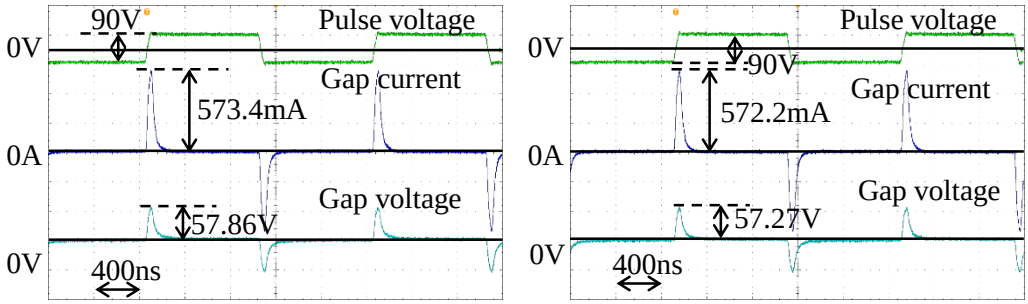

(a) NaCl aqueous solution (b) $NaNO_3$ aqueous solution

Fig. 6.26 Waveforms with feed speed of 0.6 μm/s and different electrolytes

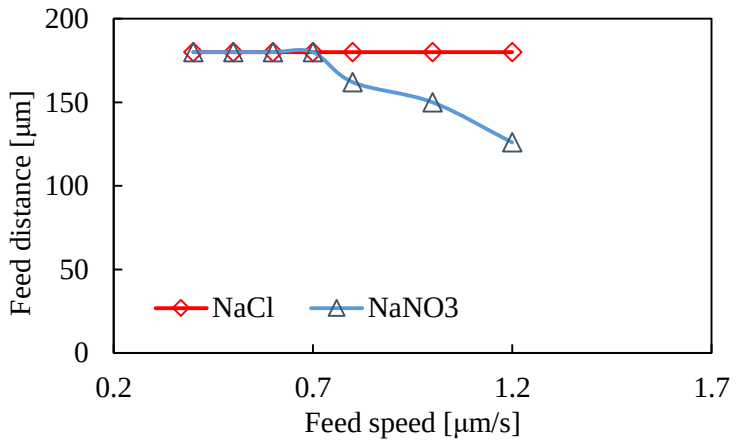

Fig. 6.27 Feed distances with different electrolytes

6.2.4.3 Material removal volume

Fig. 28 and Fig. 29 show the micro-rods machined and the material removal volumes with different electrolytes, respectively. The material removal volume decreased with the electrolyte of NaCl aqueous solution. This is because the tool wear volume was increased due to the influence of stray current in the radial gap and pitting corrosion, which will be shown in following section.

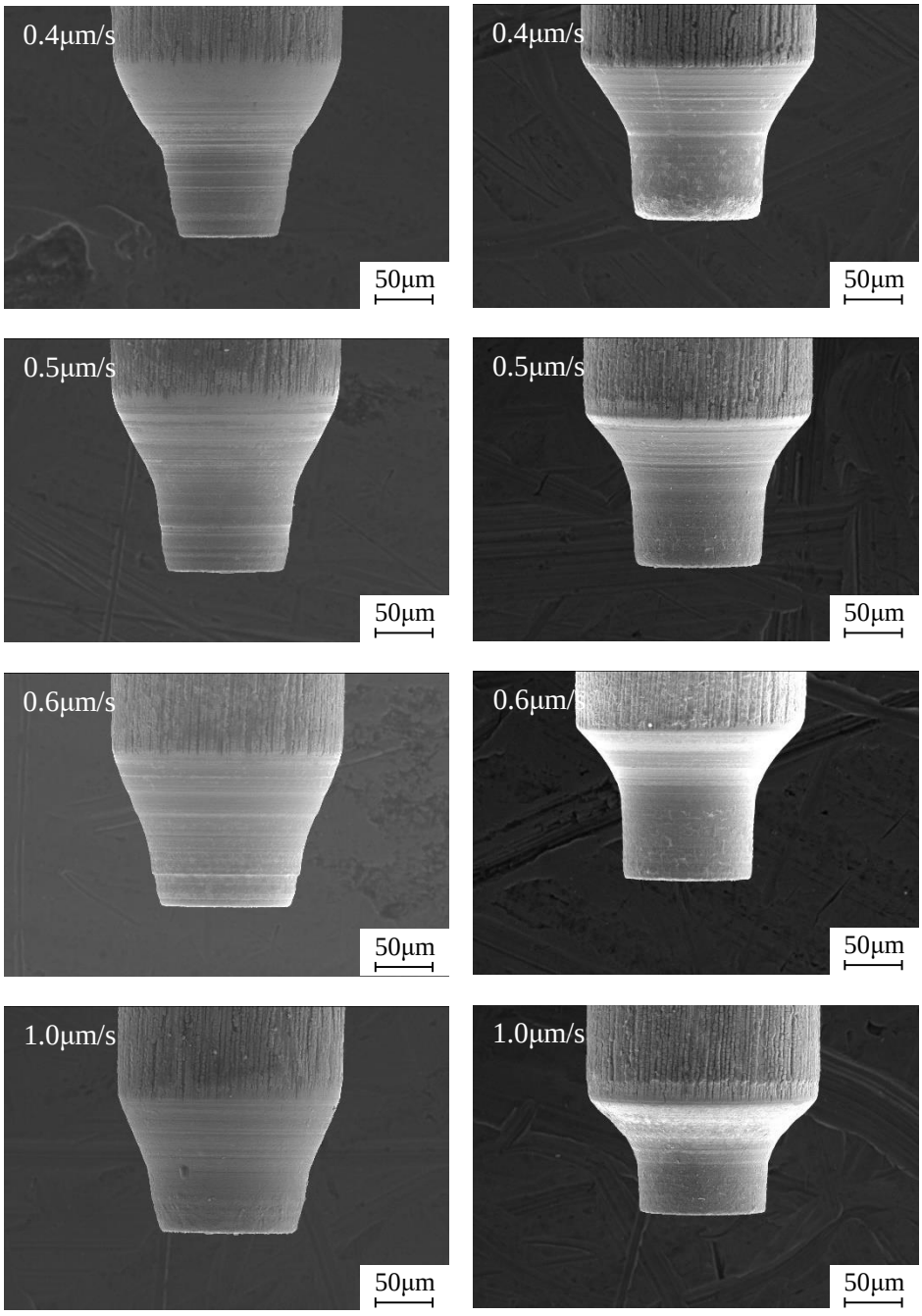

(a) NaCl aqueous solution (b) $NaNO_3$ aqueous solution

Fig. 6.28 Micro-rods machined with different electrolytes

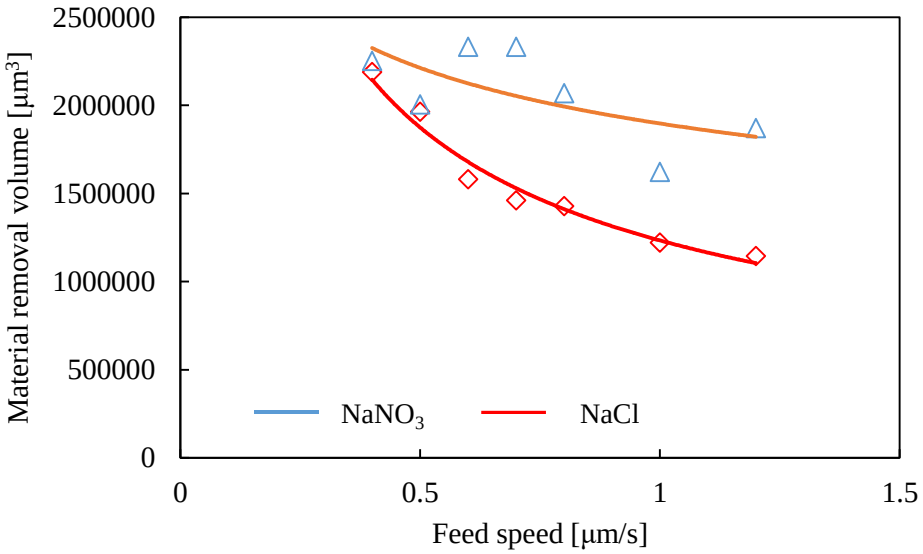

Fig. 6.29 Material removal volume with different electrolytes

6.2.4.4 Tool wear volume

Fig. 6.30 shows the tool wear with different electrolytes and Fig. 6.31 shows the corresponding tool wear volume. It is found that the influence of stray current was significantly serious with the electrolyte of NaCl aqueous solution. More material was dissolved on the radial surface of tool electrode with the electrolyte of NaCl aqueous solution as shown in Fig. 6.30(b).

The equilibrium gap width g_e can be expressed as,

$$g_e = \xi \frac{\sigma V}{v} \frac{k}{\rho} \tag{3}$$

where, σ is conductivity, V is voltage, v is feed rate, k is electrochemical equivalent, ρ is density, ξ is current efficiency. Because of the higher current efficiency with the NaCl aqueous solution, the electrochemical dissolution can occur at a larger gap width. Hence, more material on the radial surface of tool electrode was dissolved as shown in Fig. 6.30(b). In addition, the tool wear volume was also influenced by the pitting corrosion with the electrolyte of NaCl aqueous solution, because the low current density in the radial gap increased the probability of pitting corrosion. In the previous chapter, the experimental results showed that the influence of pitting corrosion was serious with the NaCl aqueous solution, however, it can be eliminated with the electrolyte of $NaNO_3$ aqueous solution. Hence, the tool wear volume was much higher with the NaCl aqueous solution than that with the $NaNO_3$ aqueous solution.

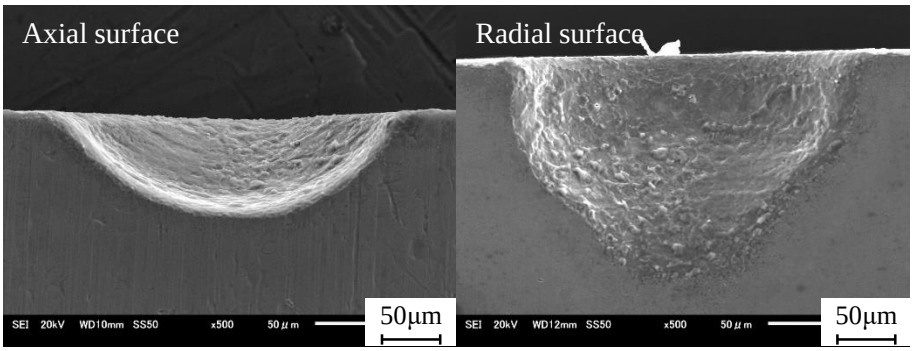

(Ⅰ) Feed speed of 0.4 μm/s

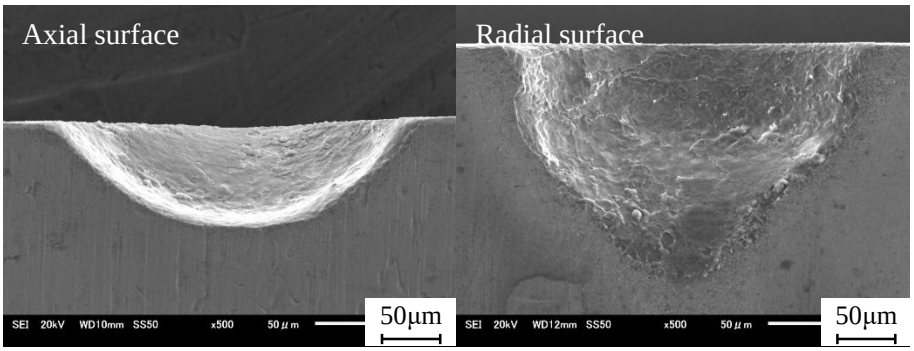

(Ⅱ) Feed speed of 0.5 μm/s

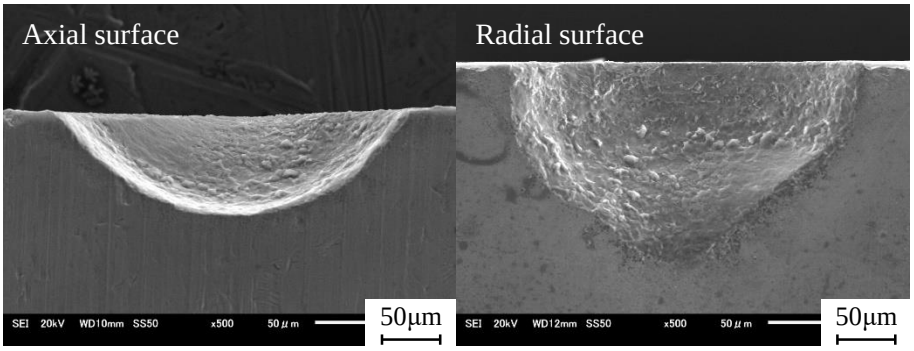

(Ⅲ) Feed speed of 0.6 μm/s

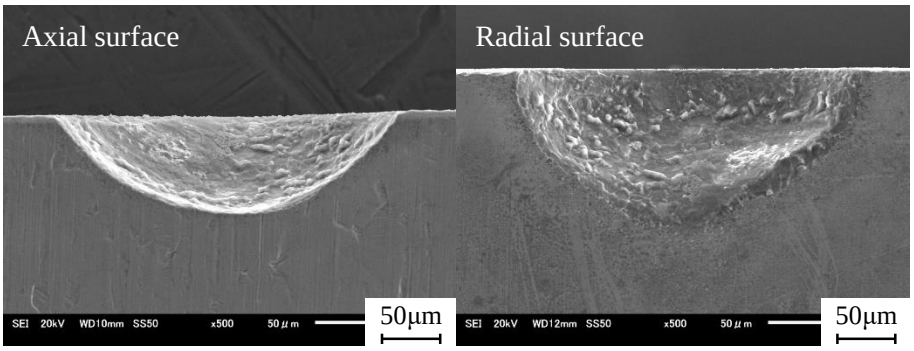

(Ⅳ) Feed speed of 1.0 μm/s

(a) $NaNO_3$ of 6 wt%

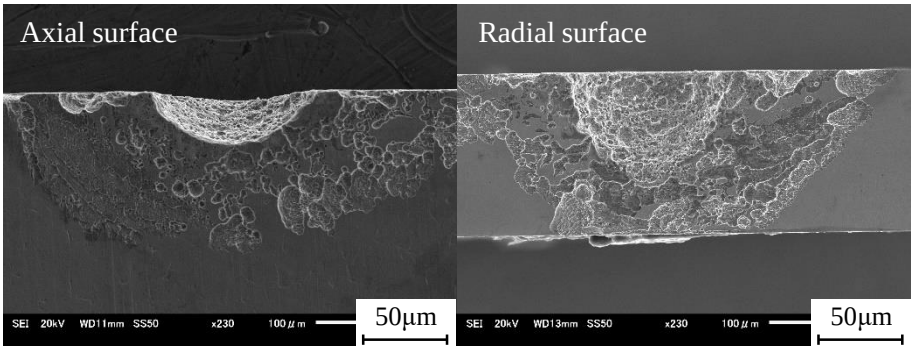

(Ⅰ) Feed speed of 0.4 μm/s

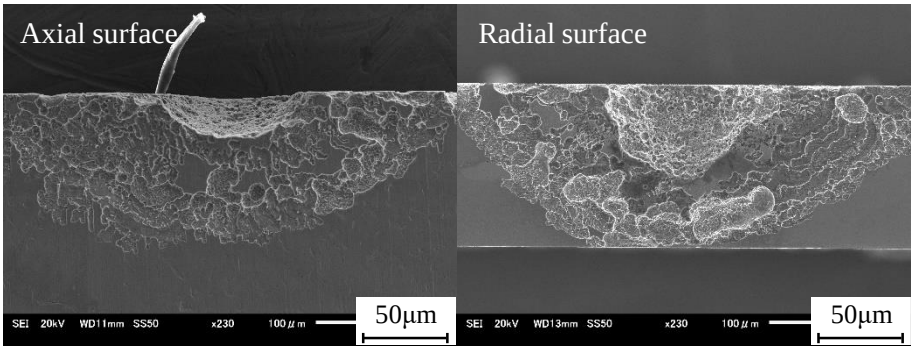

(Ⅱ) Feed speed of 0.5 μm/s

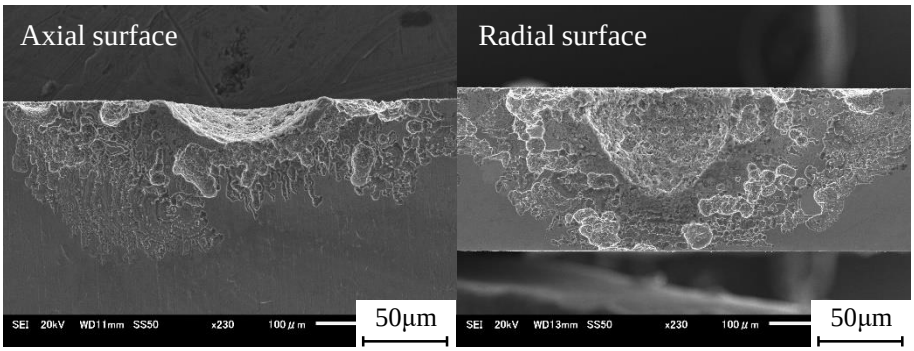

(Ⅲ) Feed speed of 0.6 μm/s

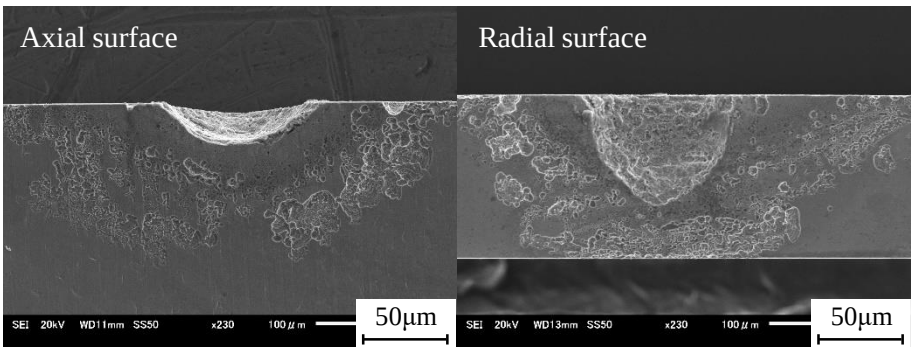

(Ⅳ) Feed speed of 1.0 μm/s

(b) NaCl of 6 wt%

Fig. 30 Tool wear with different electrolytes

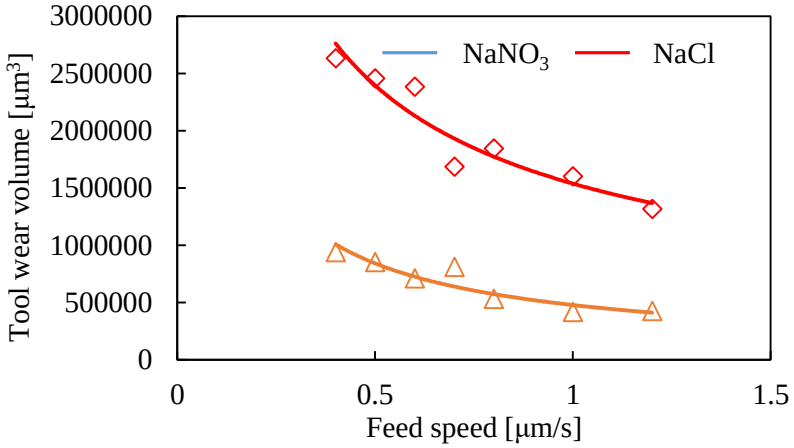

Fig. 6.31 Tool wear volume with different electrolytes

6.2.4.5 Tool wear ratio

Fig. 6.32 shows the tool wear ratio with different electrolytes. Because of the influences of high current efficient and pitting corrosion, the tool wear ratio was higher with the electrolyte of NaCl aqueous solution than the electrolyte of $NaNO_3$ aqueous solution.

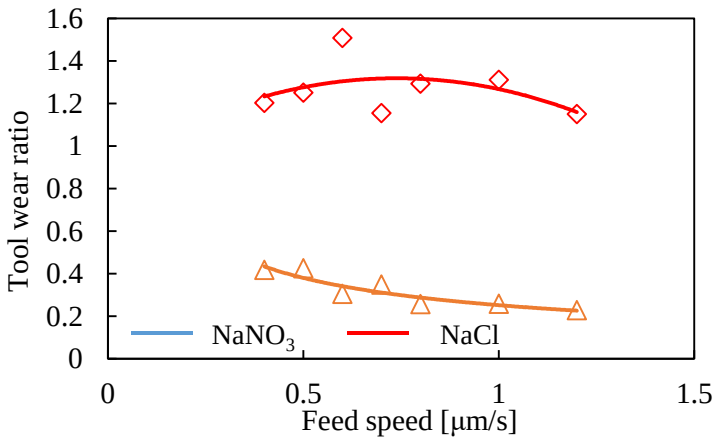

Fig. 6.32 Tool wear ratio with different electrolytes

6.2.5 High aspect ratio micro-rod machining

According to the above experimental results, the smaller feeding capacitance of 250 pF and higher concentration of $NaNO_3$ aqueous solution in 6 wt% are useful to machine an accuracy micro-rod with the speed range between 0.1 μm/s to 1.2 μm/s. Hence, long micro-rod was tried to be machined with the optimized machining conditions in this experiment.

6.2.5.1 Experimental conditions

The experimental conditions are shown in Table 6.5. The rise/fall time was 40 ns. The feed speeds of 0.2 μm/s and 0.6 μm/s were selected, which were considered as the

optimum feed speed corresponding to the feeding capacitances of 150 pF and 250 pF, respectively. $NaNO_3$ aqueous solutions in concentration of 6 wt% was used as electrolyte in this experiment. The cut depth in radial direction and feed distance in axial direction were set as 50 μm and 250 μm, respectively.

Table 6.5 Experimental conditions used to machine high aspect ratio tunsten rods

Pulse voltage	Amplitude [V]	90
	Frequency [Hz]	500 k
	Duty factor [%]	50
	Rise/fall time [ns]	40
Feeding capacitance C_1 [pF]		47
Electrolyte		$NaNO_3$ aq. 6 wt%
Tool electrode rotation [rpm]		3000
Feed speed [μm/s]		0.2, 0.6

6.2.5.2 High aspect ratio micro-rods machined

Fig. 6.33 and Fig. 6.34 show the micro-rods machined and tool wears with the feeding capacitances of 150 pF and 250 pF, respectively. The machining processes were interrupted by collision between electrodes and the feed distances were 150 μm and 246 μm for the feeding capacitances of 150 pF and 250 pF, respectively. It is noted that a micro-rod with the aspect ratio larger than 3 was difficult to be machined with this method. This is because the bipolar current was necessary with the neutral electrolyte, which causes the tool wear. Therefore, the current flowing through the radial gap would increase significantly with increasing the feed distance in axial direction, and the current flowing through the axial gap decreased due to the constant electrical charge per pulse with the electrostatic induction feeding method. Hence, collision between electrodes interrupted the machining process resulting in a limitation of the increase in the length of micro-rod.

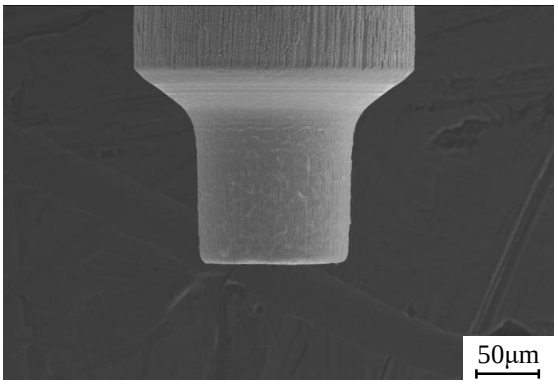

(a) Micro-rod machined

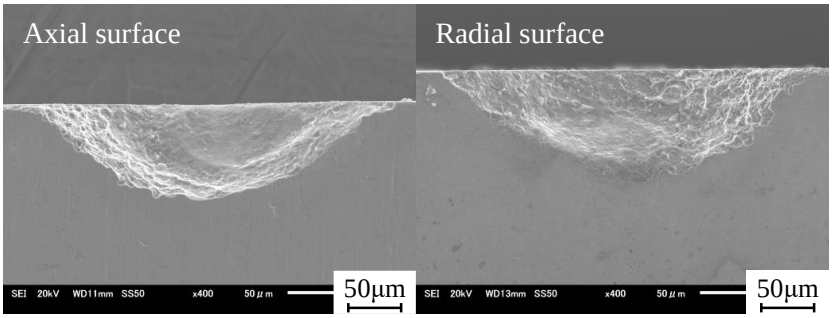

(b) Tool wear

Fig. 6.33 Micro-rod and tool wear with feeding capacitance of 150 pF

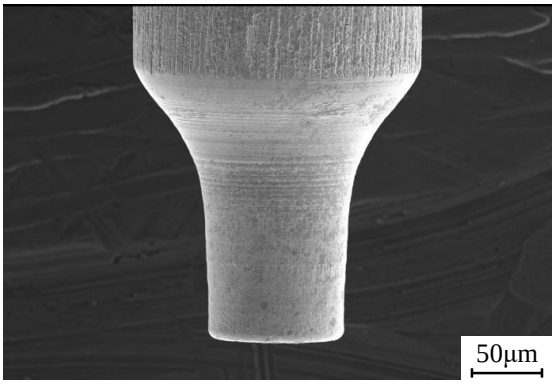

(a) Micro-rod machined

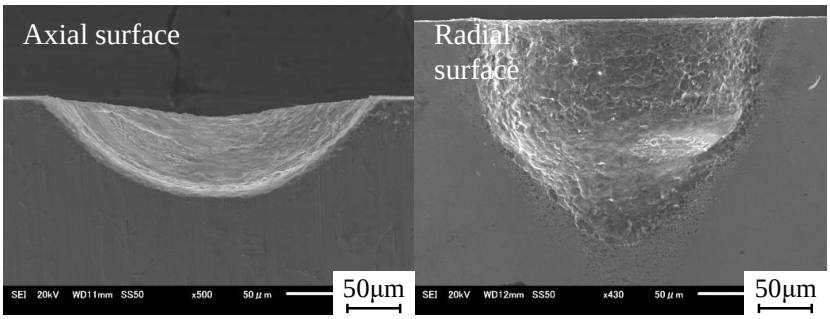

(b) Tool wear

Fig. 6.34 Micro-rod and tool wear with feeding capacitance of 250 pF

6.3 Fabrication of high-speed steel (SKH51) micro-rod

6.3.1 Experimental conditions

The experimental conditions are shown in Table 6.6. The amplitude of pulse power was 90 V. The frequency and rise/fall time of pulse power were 500 kHz and 40 ns, respectively. The electrolyte was sodium chloride (NaCl) and sodium nitrate ($NaNO_3$) of 2 wt% in concentration. The machining method is shown in Fig. 6.35, in which a diode was placed in parallel with the working gap to avoid tool wear with the bipolar current using the electrostatic induction feeding method. The tool electrode is shown in Fig. 6. 36. The feed speed was 0.7 μm/s. The diameter of workpiece was 200 μm. The feed distance in axial direction was 100 μm, and cut depth in radial direction was 50 μm. The workpiece rod was positioned on the top surface of the tool electrode with an initial gap width of 5 μm.

Table 6.6 Experimental conditions to machine high-speed steel

Pulse voltage	Amplitude [V]	90
	Frequency [Hz]	500 k
	Duty factor [%]	50
	Rise/fall time [ns]	40
Feeding capacitance C_1 [pF]		47
Electrolyte		NaCl & $NaNO_3$ aq. 2 wt%
Tool electrode rotation [rpm]		3000
Feed speed [μm/s]		0.7

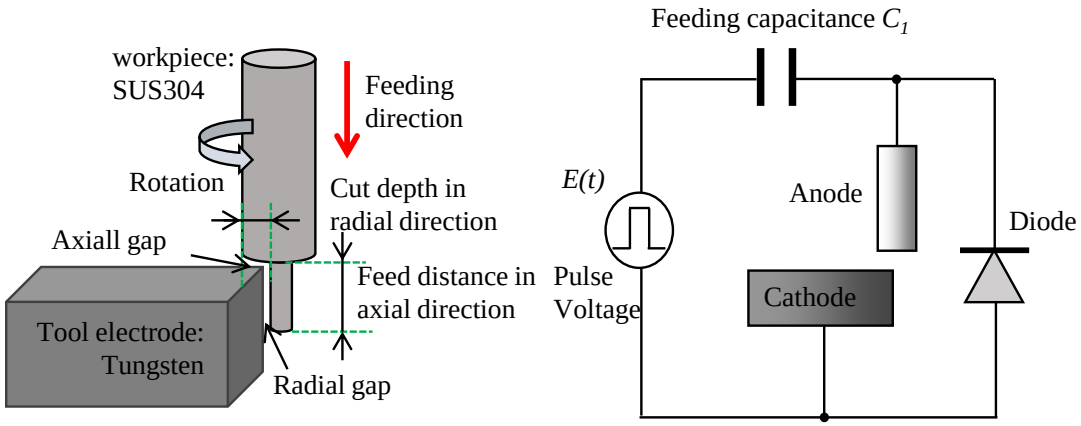

(a) Machining method of micro-rod (b) Diode was used to avoid tool wear

Fig. 6.35 Machining method of micro-rod and circuit

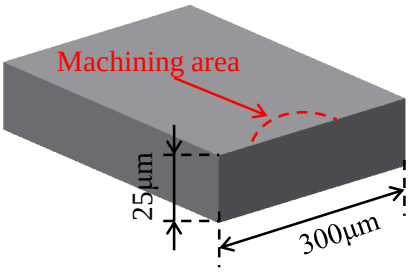

Fig. 6.36 Size of tungsten plate electrode

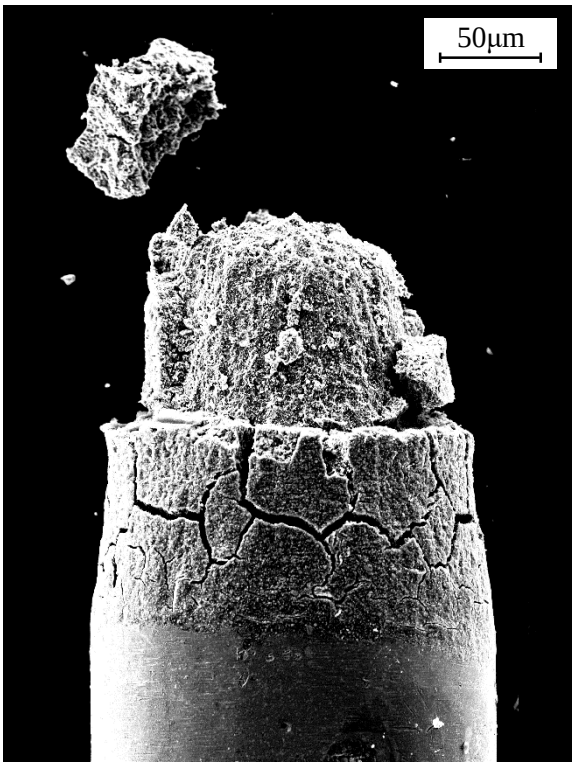

Fig. 6.37 Micro-rod machined with NaCl aqueous solution

6.3.2 Micro-rods machined with different electrolytes

The machining was completed with the electrolyte of NaCl aqueous solution. However, the machining surface was significantly rough as shown in Fig. 6.37. In addition, the machining area broke into pieces, and many cracks were generated on the side surface of the machined rod near the machining area. Fig. 6.38 shows the micro-rod machined with the electrolyte of $NaNO_3$ aqueous solution. A micro-rod was machined successfully. However, the tool electrode feed was interrupted by collision between electrodes with the electrolyte of $NaNO_3$ aqueous solution when the feed distance in axial direction was increased to 53 μm. Some scratches were observed on the axial surface as shown in Fig.

6.38(b), because of the collision. Hence, the electrolyte of $NaNO_3$ aqueous solution is better for SKH51 machining compared with NaCl aqueous solution.

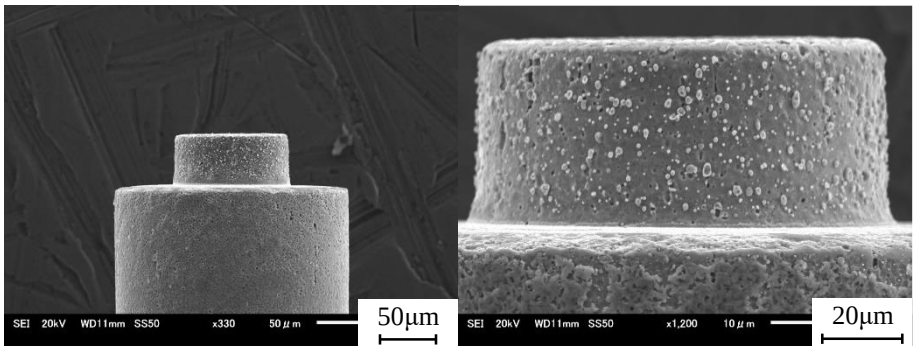

(a) Side surface of micro-rod

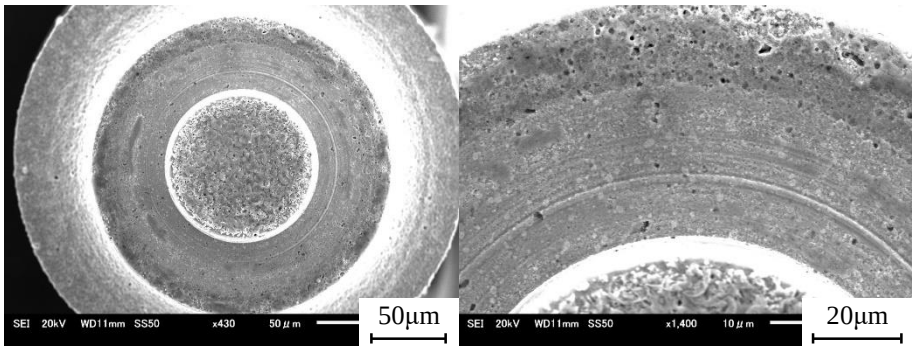

(b) Frontal surface of micro-rod

Fig. 6.38 Micro-rod machined with $NaNO_3$ aqueous solution

At last, Fig. 6.39 shows the tool electrode before and after machining, it is noted that there was almost no tool wear after machining, this is because the unipolar current was obtained with the help of the diode as shown in Fig. 6.35(b).

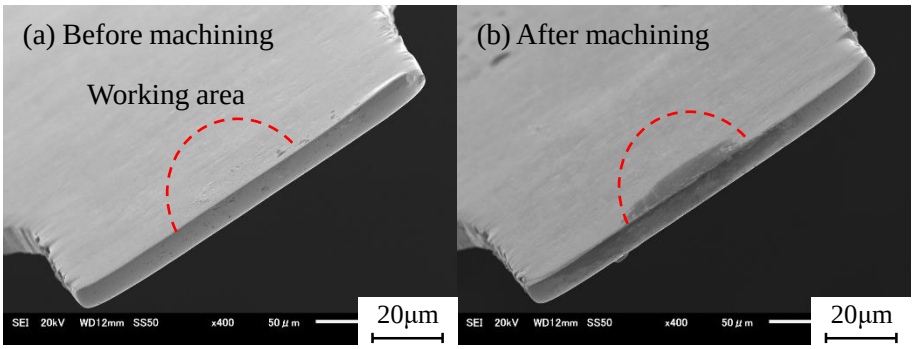

Fig. 6.39 Tool electrode before and after machining

6.4 Fabrication of cemented WC micro-rod

6.4.1 Experimental conditions

The experimental conditions are shown in Table 6.7. The amplitude of pulse power was 90 V. The frequency and rise/fall time of pulse power were 500 kHz and 40 ns, respectively. The electrolyte was sodium nitrate ($NaNO_3$) of 2 wt% in concentration. Bipolar current was supplied with the electrostatic induction feeding method due to the similar machining mechanism of tungsten micro-rod. The feed speed was 0.7 μm/s. The diameter of workpiece was 200 μm. The feed distance in axial direction was 100 μm, and cut depth in radial direction was 50μm. Since $NaNO_3$ aqueous solution gave better results than NaCl, only $NaNO_3$ aqueous solution was used in this experiment. Miyoshi and Kunieda[91] also used the same electrolyte and obtained a micro-rod shown in Fig. 6.40 using electrolyte jet machining (EJM).

Table 6.7 experimental conditions

Pulse voltage	Amplitude [V]	90
	Frequency [Hz]	500 k
	Duty factor [%]	50
	Rise/fall time [ns]	40
Feeding capacitance C_1 [pF]		47
Electrolyte		$NaNO_3$ aq. 2 wt%
Tool electrode rotation [rpm]		3000
Feed speed [μm/s]		0.7

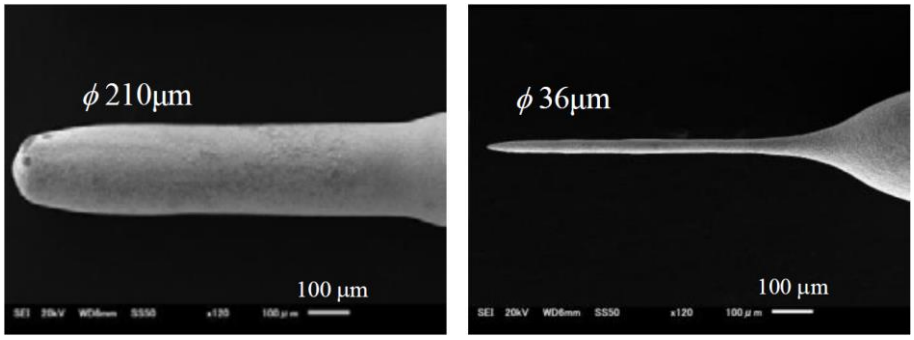

(a) Rough (b) Finish

Fig. 6.40 Machined WC micro rod using EJM

In addition, Miyoshi and Kunieda[91] has investigated the influence of grain size on the machining accuracy. The experimental results showed that the machining accuracy was improved with the smaller grain size, as shown in Fig. 6.41. The grain size used in this experiment was 2-4 μm.

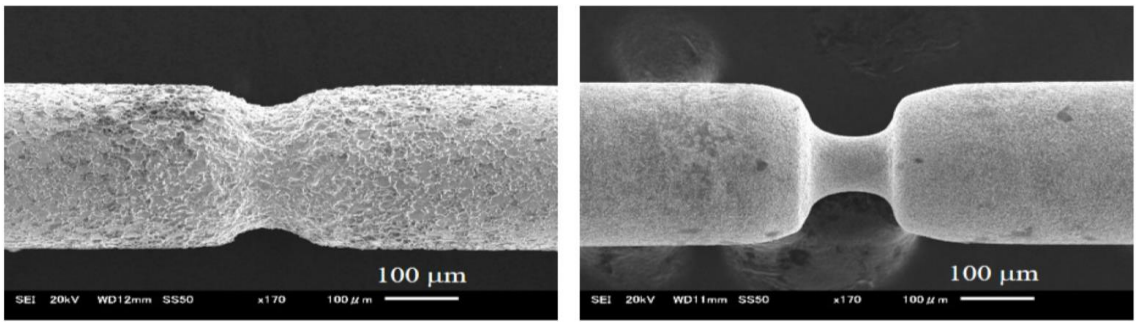

(a) Grain size of 10 μm (b) Grain size of 2-4 μm

Fig. 6.41 Influence of grain size on machining accuracy

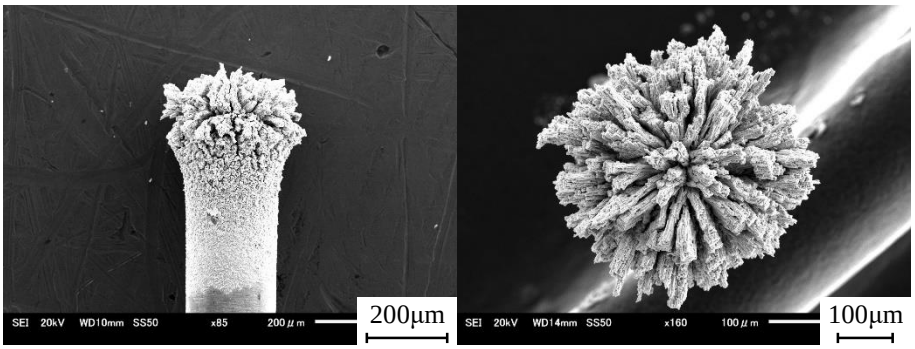

Fig. 6.42 Experimental result with material of cemented WC

6.4.2 Machining result with cemented WC

The experimental result is shown in Fig. 6.42. It was highly similar with the research result by Choi et al.[92], which is shown in Fig. 6.43. They reported that the formation of the tungsten oxide layer resulted in expansion of the volume of the raw material, as shown in Fig. 6.43, because the Pilling Bedworth ratio (the ratio of the volume of oxide formed to the volume of metal consumed) for W is 3.3[93]. From the analysis of sludge components using energy dispersive spectroscopy (EDS), it was shown that the ratio of Co is smaller in the sludge than in the raw material. Furthermore, the color of used electrolyte was converted to red, which is the color of Co ions. From these results, it was concluded that Co dissolved to form ions. Hence, it is considered that the sludge shown in Fig. 6.42 should be the tungsten oxide. In addition, compared with the results of Miyoushi and

Kunieda, it is considered that the much high current density used in EJM leaded to the significantly different machined results as shown in Fig. 6.40 and Fig. 6.42.

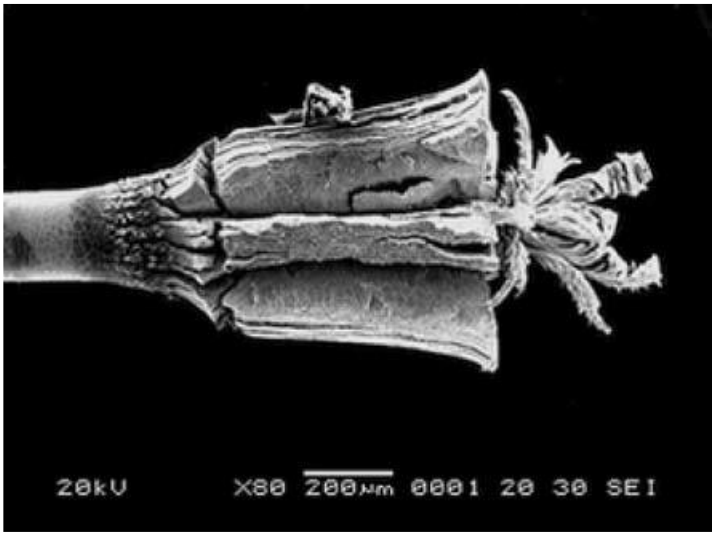

Fig. 6.43 Sludge growth on the specimen during WC etching[92)]

6.5 Conclusions

In this chapter, the machining characteristics of different materials were investigated, including tungsten, high-speed steel (SKH51) and tungsten carbide. The following conclusions were obtained.

With the material of tungsten, bipolar current was needed, which caused the tool wear. The machining accuracy increased with decreasing the pulse duration of pulse current because the electrochemical reaction was localized in a smaller working gap. The tool wear ratio increased with increasing the feeding capacitance when the feed speed was the same. In addition, the tool wear ratio decreased with $NaNO_3$ electrolyte of 6 wt% in concentration compared with that with 2 wt%. Compared with the electrolyte of NaCl aqueous solution, the tool wear ratio decreased with the electrolyte of $NaNO_3$ aqueous solution. The machinable length of tungsten micro-rod was limited by the collision between electrodes, because the influence of stray current in the radial gap increased with increasing the feed distance due to the increased gap area.

With the material of SKH51, the machined results showed a better machining characteristics with electrolyte of $NaNO_3$ aqueous solution, compared with the NaCl aqueous solution. The workpiece broke into pieces with the NaCl aqueous solution, and the surface machined was significantly rough. A micro-rod was successful machined with the electrolyte of $NaNO_3$ aqueous solution. With the material of tungsten carbide, the

volume of the material was swollen and a large amount of sludge was generated after machining, which was considered to result from the oxidation of tungsten.

It is wellknown that Electrical discharge machining (EDM) can be used with any difficult-to-machine materials regardless of its density, toughness, or hardness. However, because EDM is a thermal process, the machined surface is characterized by recast layers, including cracks and residual tensile stresses, which result in overall degeneration of the component's mechanical capabilities. In contrast, ECM relies on the mechanism of anode electrochemical dissolution to remove material, with the advantage that the machined surface has no recast layers and is free of residual stress and micro cracks. The main problem in ECM is to create conditions for the electrochemical dissolution localization, because during machining the area of dissolution is larger than the area of the electrode tool (machining delocalization). Furthermore, research results showed the ECM still has some limitation in the processing of difficult-to-machine materials, such as W, WC. In contrast, EDM is possible to machine these metal materials successfully. The comparison between EDM and ECM is listed in Table. 6.8. The differences between two machining technologies show that, to machine these difficult-to-machine materials, the EDM is more efficient than the ECM, however, the ECM has a significant advantage of good surface finish. Hence, a hybrid machining system combining the electrostatic induction feeding EDM and ECM using the same electrolyte method was proposed in the next chapter to compensate the disadvantages of the two different machining technologies.

Table 6.8 Comparison between EDM and ECM

Characteristics	Micro-EDM	Micro-ECM
Material removal rate	High	Low
Machining accuracy	High	Low
Recast layer	Exist	None
Cracks	Exist	None
Residual stress	Exist	None
Tool wear	Serious	None
Surface finish	Rough	Smooth
Difficult-to-machine metal	Any conductive materials	Easily passivated: W, WC, Pt, Nb, Ti; Semiconductor: Si, SiC; Novel metals: Au, Pt, Ag.

Chapter 7 Hybrid machining combining electrostatic induction feeding EDM and ECM

7.1 Introduction

Electrical discharge machining (EDM) is one of the most efficient machining processes for conductive materials. The process, based on the electro-thermal erosion of metallic materials, can be used with any difficult-to-machine material regardless of its density, toughness, or hardness. However, since EDM is a thermal process, the machined surface is characterized by recast layers, including cracks and residual tensile stresses. In contrast, electrochemical machining (ECM) relies on the mechanism of anode electrochemical dissolution to remove material, with the advantages that the machined surface has no recast layers and is free of residual stress and micro-cracks. The comparison between the two machining technologies in Chapter 3, 4, 5, 6 shows that the two machining technologies have different machining characteristics due to the different principles of material removal. Hence, it is considered to develop a hybrid machining system in Chapter 7 to take full advantages of the two machining technologies.

In this chapter, the hybrid machining system combining the electrostatic induction feeding EDM and ECM using the same electrolyte method was proposed. With this method, the conversion of EDM and ECM modes was realized by utilizing the oxide layer formed on the surface of tungsten electrode. Zeng et al. [94] conducted the micro-EDM shaping and micro-ECM finishing in sequence on the same machine tool. However, the different machining medium and power generator were needed for two different machining processes. In Kurita and Hattori[95]'s research, the EDM and ECM process were carried out in sequence on the same machine tool and tool electrode with deionized water used as the machining liquid. Nguyen et al. [96, 97] also realized the hybrid machining of micro-EDM and micro-ECM with deionized water using the same power generator. The conversion of the EDM and ECM processes was realized by decreasing and increasing the working gap for the EDM and ECM mode, respectively. However, the deionized water used as machining medium resulted in a significantly low material removal rate in the ECM process because of the low electrical conductivity. Compared with the previous researches, the hybrid machining method newly proposed in this chapter can realize the hybrid machining process with the same machining medium and power generator. The conversion of EDM and ECM modes can be easily realized by attaching and detaching a diode in parallel with the working gap.

This chapter describes the hybrid machining system combining the electrostatic induction feeding EDM and EDM in the same electrolyte. First, the principle of the hybrid method is explained. Then, the transition of the modes is verified through the observation of the discharge waveforms and machined surface. Finally, a micro-hole is machined using the hybrid system developed.

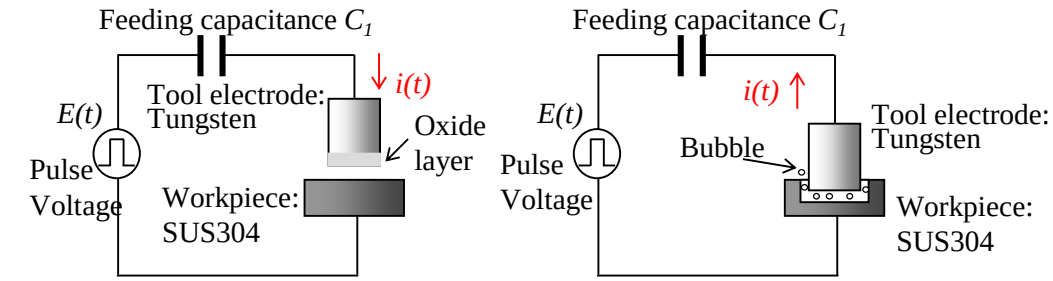

(a) Tungsten electrode is positive polarity (b) Tungsten electrode is negative polarity

Fig. 7.1 Principle of ECM mode

7.2 Principle of method to control EDM and ECM mode

The hybrid machining method utilizes the oxide layer formed on the surface of tungsten electrode to control the conversion of EDM and ECM modes. The ECM mode can be obtained as shown in Fig. 7.1. Bipolar current is generated with the electrostatic induction feeding method. When the polarity of tungsten electrode is negative with the bipolar current pulse, Maeda et al.[62] and Mazuzawa et al.[90] found that the electrochemical reaction in $NaNO_3$ aqueous solution is as follow:

$$2Na^+ + 2H_2O + 2e \rightarrow 2NaOH + H_2 \quad (7.1)$$

With the NaOH, the tungsten oxide layer generated on the tungsten electrode when the polarity of tungsten electrode is positive is dissolved by the following electrochemical reaction (7.2).

$$WO_3 + 2NaOH \rightarrow Na_2WO_4 + H_2O \quad (7.2)$$

Hence, the electrolysis current can flow through the gap, realizing the ECM mode as shown in Fig. 7.1. To convert the process from ECM to EDM, a diode is placed in parallel with the working gap as shown in Fig. 7.2. Current will flow in the diode instead of the working gap when the tungsten electrode is at negative polarity. Hence, NaOH cannot be generated by electrochemical reaction (1) resulting in the oxide layer un-dissolved on the surface of tungsten electrode. Thereby, the chemical reaction (7.1) and (7.2) cannot occur

to dissolve the oxide layer with the use of the diode. When the polarity of the tungsten electrode changes to positive, the current cannot easily flow through the working gap, because of the high resistivity of the passive oxide layer on the surface of tungsten electrode. Hence, the oxide layer plays the role of the dielectric fluid in electric discharge machining. Thereby, discharge occurs as shown in Fig. 7.2(b).

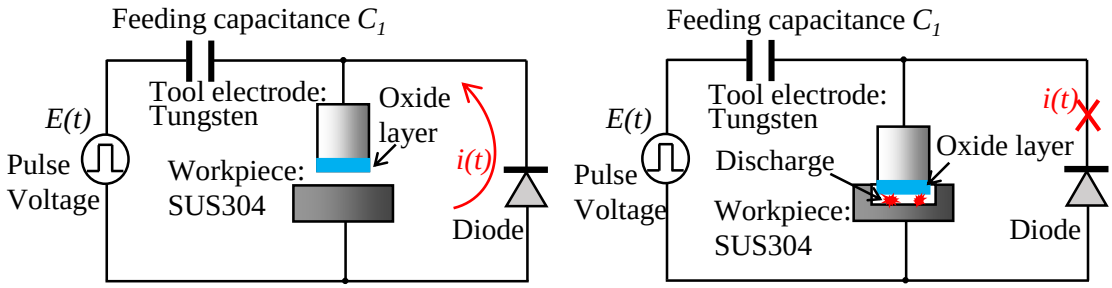

(a) Tool electrode is negative polarity (b) Tool electrode is positive polarity

Fig. 7.2 Principle of EDM process

The conversion of EDM and ECM mode depends on the oxide layer formed on the surface of the tungsten electrode, and the generation of the oxide layer is controlled by attaching and detaching a diode in parallel with the working gap. Hence, the tungsten electrode, diode and bipolar current are the key factors in the hybrid micro-EDM and micro-ECM machining using the same electrolyte method. In this research, the electrostatic induction feeding method was used to generate the necessary bipolar current.

7.3 Operation in EDM mode

The discharge waveforms were measured to verify the discharge process in EDM mode. Then, the influences of the feeding capacitance C_1 and rise/fall time of pulse voltage on the machining characteristics of the EDM mode were investigated.

7.3.1 Discharge waveforms measurement

In order to verify the occurrence of discharge machining in the EDM mode, the discharge waveforms were measured and compared with the waveforms of the ECM mode.

7.3.1.1 Experimental conditions

The experimental conditions are shown in Table 7.1. The materials of stainless steel (SUS304) and tungsten were used as workpiece and tool electrode, respectively, and micro-holes were machined on the SUS304 plate. The tool electrode was machined by the WEDG method to get a diameter of 100 μm, and positioned over the top surface of

workpiece plate with an initial gap width of 5 μm. The feed distance in axial direction was also set as 5 μm, and the feed speed was 0.1 μm/s. It is noted that $NaNO_3$ of 6 wt% in concentration was used as electrolyte. The waveforms of the ECM and EDM mode were measured using the oscilloscope during machining.

Table 7.1 Experimental conditions used in hybrid machining

Pulse voltage	Amplitude [V]	90
	Frequency [Hz]	500 k
	Duty factor [%]	50
	Rise/fall time [ns]	100
Feeding capacitance C_1 [pF]		220
Electrolyte		$NaNO_3$ aq. 6 wt%
Tool electrode rotation [rpm]		3000
Feed speed [μm/s]		0.1

7.3.1.2 Discharge waveforms

Fig. 7.3 shows the waveforms of ECM mode. Because of the reason described above, the passive oxide layer was dissolved with the bipolar current and the ECM process occurred stably.

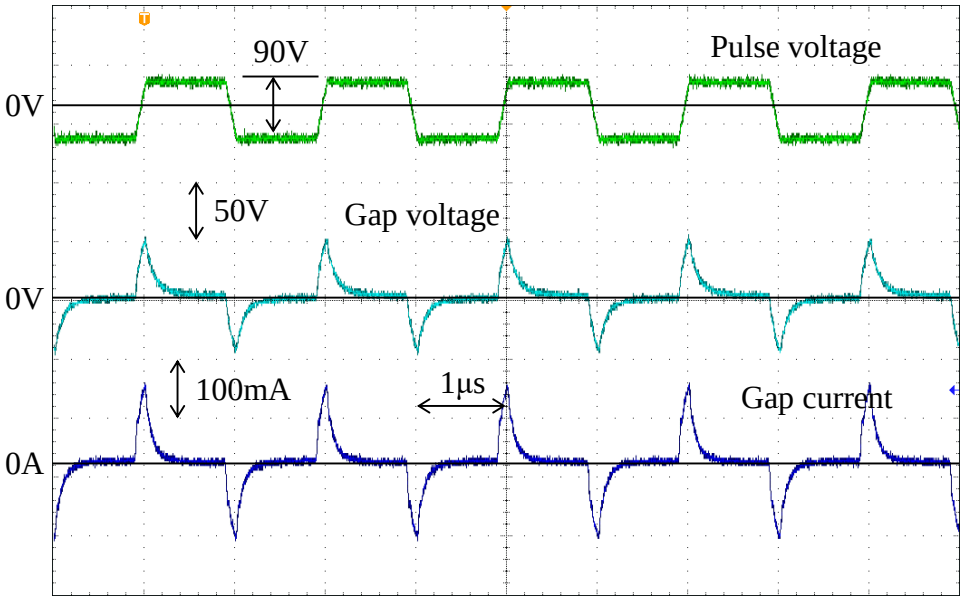

Fig. 7.3 Waveforms of ECM mode

Fig. 7.4 shows that discharge occurred 2 to 4 times within 10 μs in the EDM mode. It is noted that the gap current is not zero, when the polarity of the workpiece is changed to positive, although the current is lower than in ECM mode. This is because the working

gap was charged inversely, before the reversal of polarity. In addition, the polarity of tungsten tool electrode was always positive because the current flew through the diode when the tungsten electrode was with negative polarity as shown in Fig. 7.1(a). It is interesting to find that the decrease in the gap voltage is slow due to the thick oxide layer. This is the reason why discharge can occur during the pulse duration. In contrast, since the gap voltage is dropped within the pulse duration in the ECM mode, discharge cannot occur.

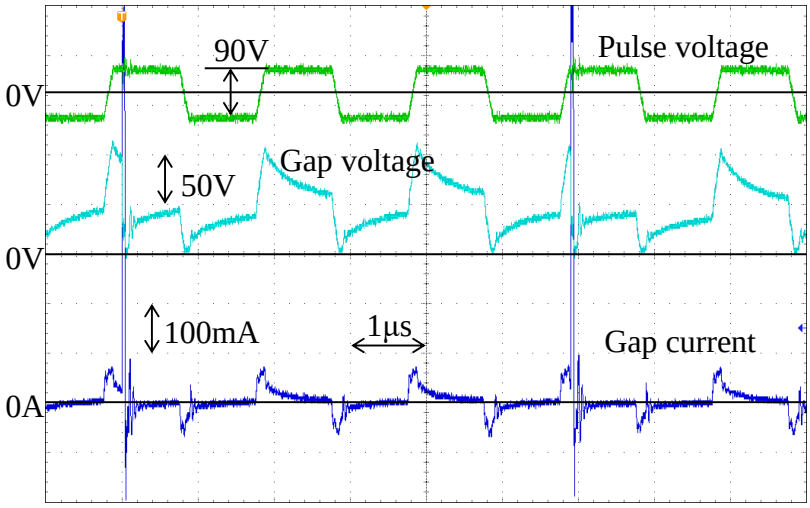

(a) Two discharges

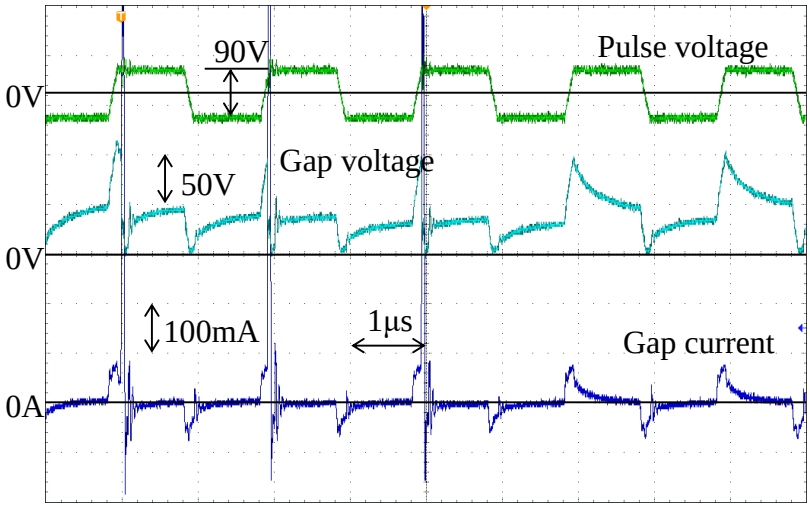

(b) Three discharges

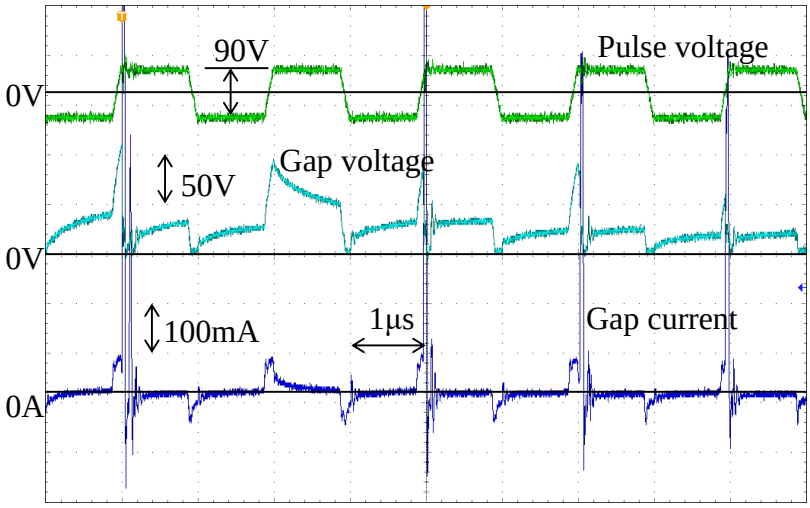

(c) Four discharges

Fig. 7.4 Different numbers of discharges

Fig. 7.5 shows waveforms of discharge current and voltage. The gap voltage was about 20V during discharge, which was the same as the normal EDM processes.

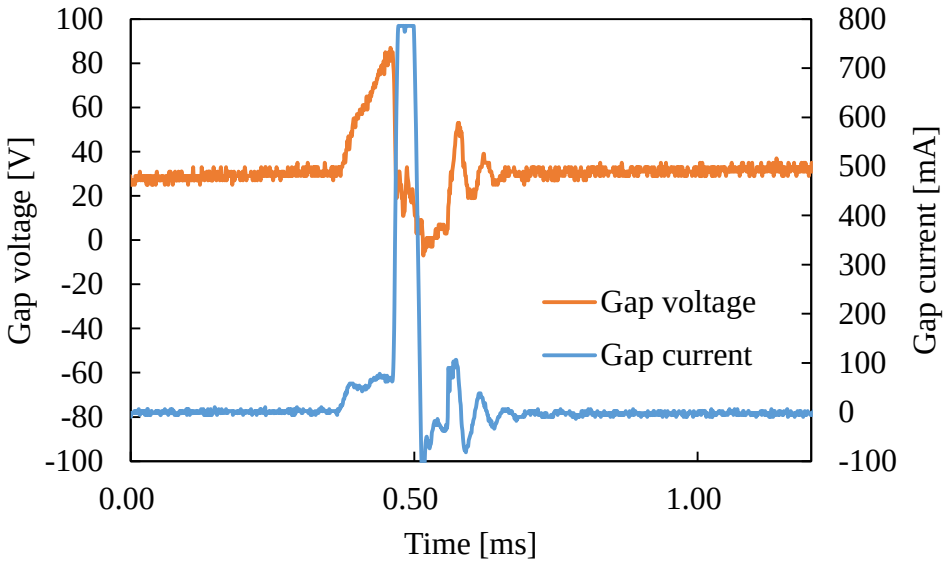

Fig. 7.5 Discharge waveforms

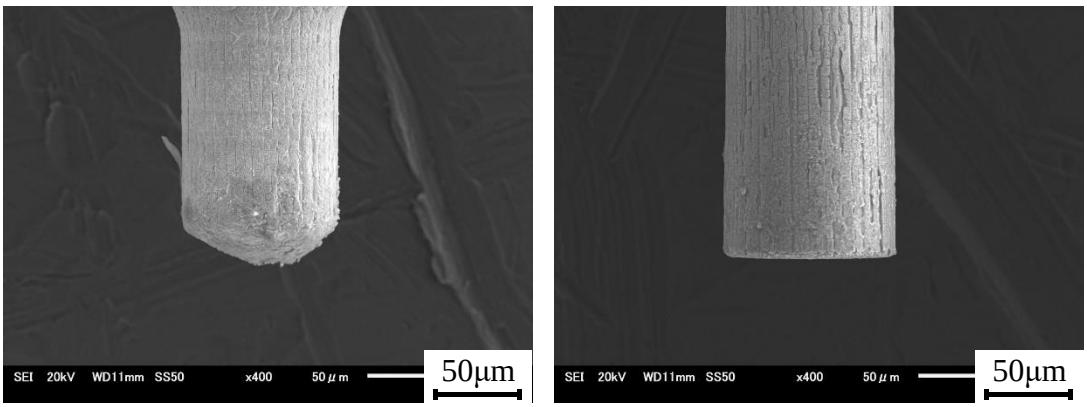

(a) ECM mode (b) EDM mode

Fig. 7.6 Tungsten electrodes after experiment

The tungsten electrodes were observed after experiment and shown in Fig. 7.6. Since the tungsten can be machined with bipolar current in a neutral electrolyte[62, 90], the tungsten electrode was significantly worn as shown in Fig. 7.6(a) after the ECM mode experiment. The EDM process should also cause tool wear due to thermal load, however, the tungsten electrode was not obviously worn after EDM mode experiment as shown in Fig. 7.6(b). It is considered that this is because the machining time was short.

Fig. 7.7 shows the SUS304 electrodes after experiment. Discharge craters were obviously observed in the EDM mode, while, there was no discharge crater in the ECM

mode. It is concluded that the conversion of the ECM and EDM modes with the hybrid machining method is effective.

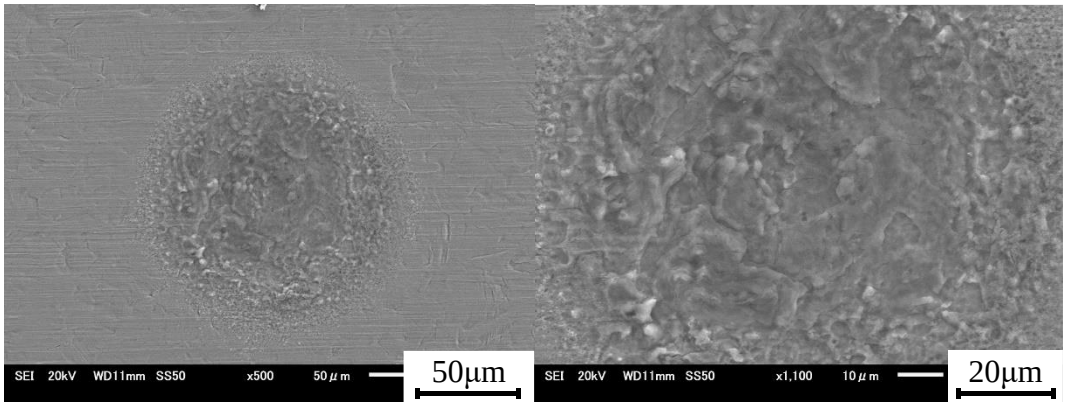

(a) ECM mode

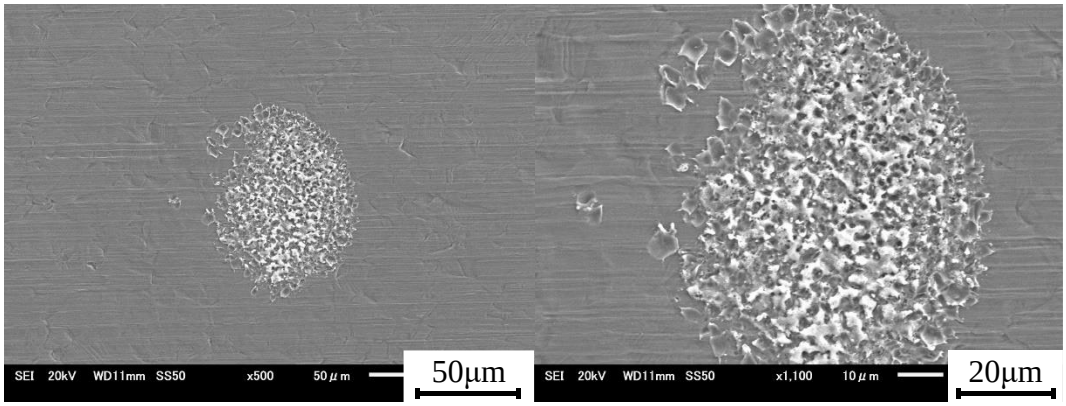

(b) EDM mode

Fig. 7.7 SUS304 electrodes after experiment

7.3.2 Influence of feeding capacitance

7.3.2.1 Experimental conditions

Table 7.2 shows the experimental conditions to investigate the influence of feeding capacitance on the EDM modes. The materials of stainless steel (SUS304) and tungsten were used as workpiece and tool electrode, respectively. The diameter of the tool electrode was 100 μm. In order to generate a few number of discharge craters, with which it was easy to observe the change in the discharge crater diameter with different feeding capacitances, the frequency of pulse voltage was set as low as 500 Hz and the feed distance of tool electrode was set as 4.2 μm. The feed speed of tool electrode was 0.3 μm/s. Since the jump flushing is necessary for the ECM mode to obtain a smoother surface finish, the tool electrode jumped during machining. Furthermore, in order to compare with the results of ECM mode, the EDM mode also used the jump flushing. In

this experiment, jump flushing was carried out for every feed distance of 0.3 μm by retracting the tool electrode, because the experimental results were compared with the ECM mode in which the jumping flushing is significantly important to flush away the bubbles and electrochemical products from the working gap. The jump speed and jump distance were 1mm/s and 500 μm, respectively. The feeding capacitance C_1 was 100 pF, 220 pF, 350 pF and 470 pF.

Table 7.2 Experimental conditions to investigate the influence of feeding capacitance

Pulse voltage	Amplitude [V]	90
	Frequency [Hz]	500
	Duty factor [%]	50
	Rise/fall time [ns]	40
Feeding capacitance C_1 [pF]		100, 220, 350, 470
Electrolyte		$NaNO_3$ aq. 6 wt%
Tool electrode rotation [rpm]		3000

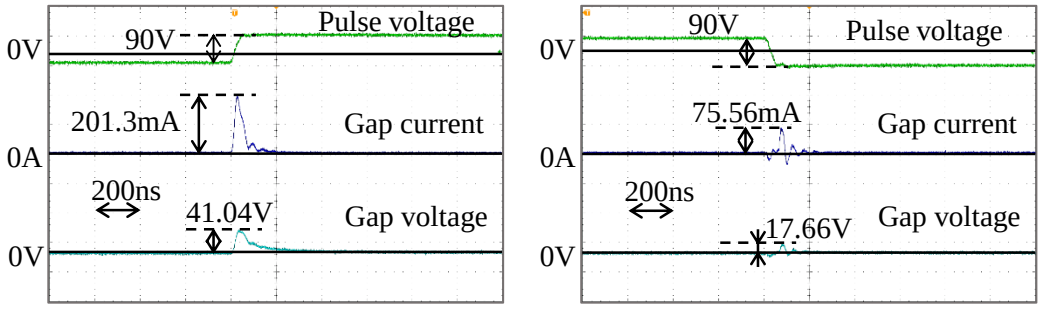

(a) Rise time (b) Fall time

Fig. 7.8 Gap current and voltage waveforms with feeding capacitance of 100 pF

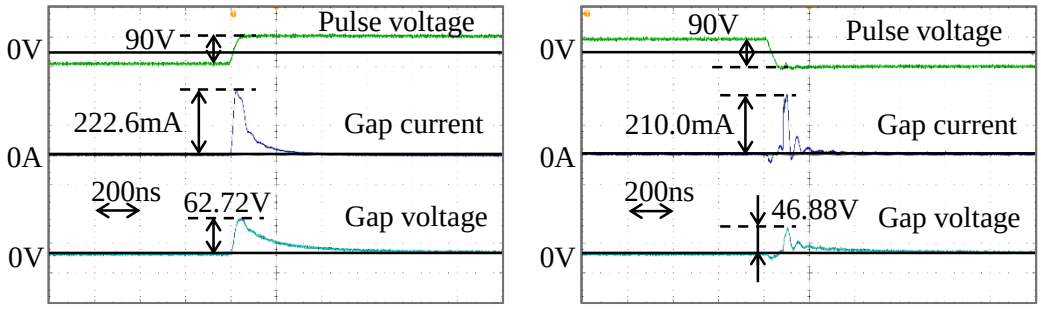

(a) Rise time (b) Fall time

Fig. 7.9 Gap current and voltage waveforms with feeding capacitance of 220 pF

7.3.2.2 Discharge crater

Fig. 7.8 and Fig. 7.9 show the gap current and voltage waveforms at the rise and fall time (not at the discharge moment) in the EDM mode with the feeding capacitances of 100 pF and 200 pF. Because of the low frequency of 500 Hz, it is difficult to show the waveforms at both rise and fall time in one figure clearly. Hence, the gap current and voltage waveforms at the rise and fall time of pulse voltage were shown separately. The gap current and voltage were increased with increasing the feeding capacitance as shown in Fig. 7.8 and Fig. 7.9. This is because the electrical charge per pulse $q= E_0C_1$ increased with increasing the feeding capacitance C_1 with the electrostatic induction feeding ECM. Thereby, the current increased with increasing the feeding capacitance due to the same pulse duration time which was determined by the rise/fall time of the pulse voltage. In addition, the gap voltage was always positive because the current flew through the diode when the tungsten electrode was negative polarity as shown in Fig. 7.1(a). Fig. 7.10 shows SEM images of the discharge craters with different feeding capacitances. Fig. 7.11 shows the change in the diameter of discharge craters with different feeding capacitances. The diameter of discharge craters was between 1 μm to 4 μm, and increased with increasing the feeding capacitance. This is because the discharge energy per pulse increased with increasing the feeding capacitance C_1 with the electrostatic induction feeding EDM. In addition, it can be found that the number of discharge craters was increased with increasing the feeding capacitance as shown in Fig. 7.10. This is because the discharge ignition was easy with the higher discharge energy due to the increased amount of debris particles generated by discharge with increasing the feeding capacitance C_1.

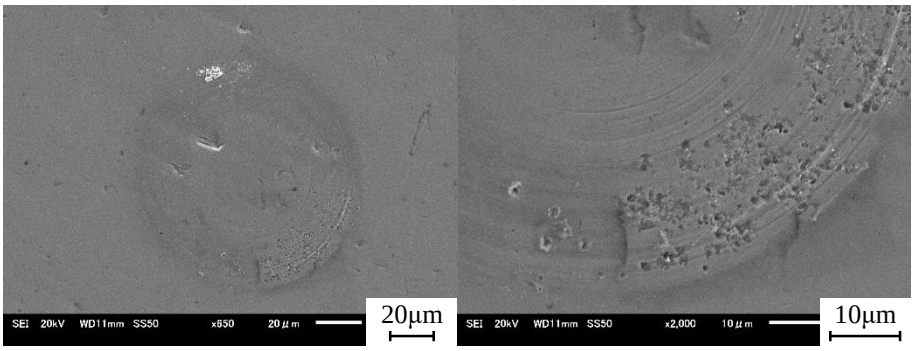

(a) 100 pF

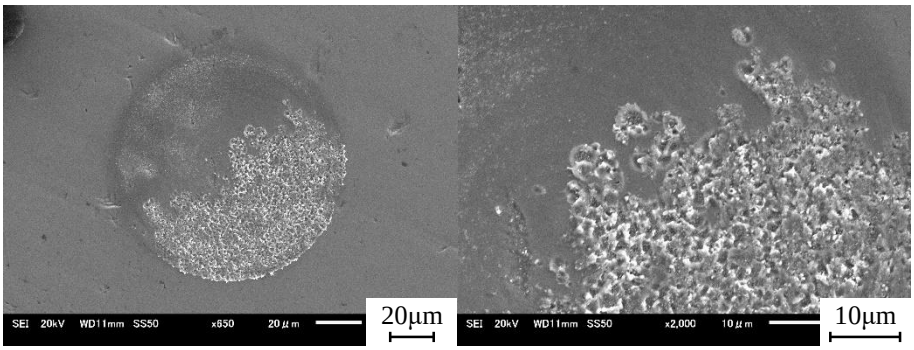

(b) 220 pF

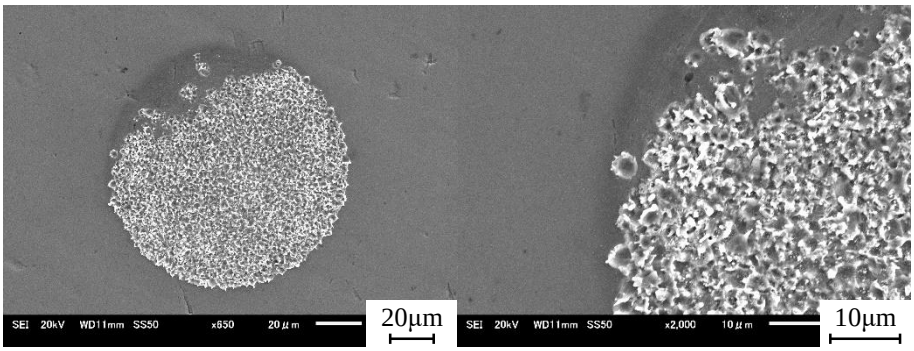

(c) 350 pF

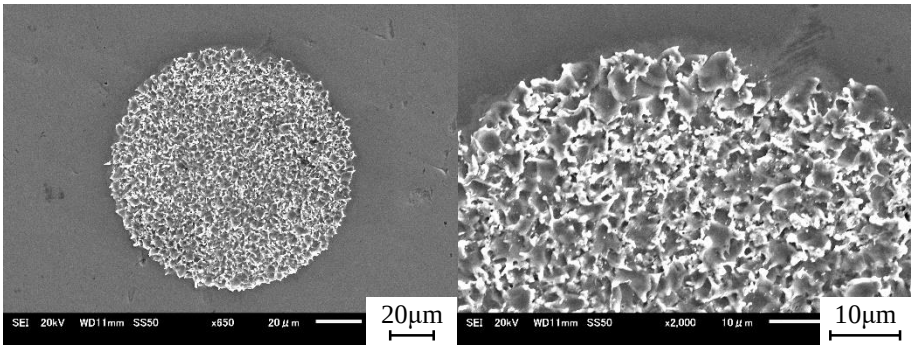

(d) 470 pF

Fig. 7.10 Discharge craters with different feeding capacitances

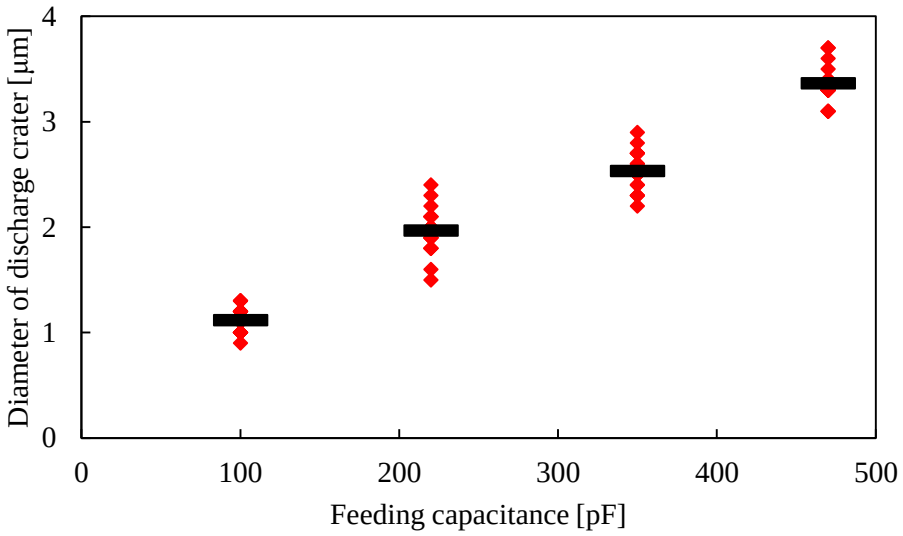

Fig. 7.11 Diameters of discharge craters with different feeding capacitances

7.3.3 Influence of rise/fall time of pulse voltage

7.3.3.1 Experimental conditions

Table 7.3 shows the experimental conditions to investigate the influence of rise/fall time pulse voltages in the EDM mode. The frequency of pulse voltage was 500 Hz and the feed distance of tool electrode was set as 4.2 μm. The feed speed of tool electrode was 0.3 μm/s. In this experiment, jump flushing was also carried out for every feed distance of 0.3 μm by retracting the tool electrode for the same reason described in Section 7.3.2.1. The rise/fall times of pulse voltages was 40 ns, 100 ns, 150 ns and 200 ns.

Table 7.3 Experimental conditions used to investigate the influence of rise/fall time of pulse voltage

Pulse voltage	Amplitude [V]	90
	Frequency [Hz]	500
	Duty factor [%]	50
	Rise/fall time [ns]	40, 100, 150, 200
Feeding capacitance C_1 [pF]		220
Electrolyte		$NaNO_3$ aq. 6 wt%
Tool electrode rotation [rpm]		3000

7.3.3.2 Discharge crater

Fig. 7.12 and Fig. 7.13 show the gap current and voltage waveforms at the rise and fall time (not at the discharge moment) in the EDM mode with the rise/fall times of 100 ns

and 200 ns, respectively. The current duration increased with increasing the rise/fall time, because the current duration equals to the rise/fall time of pulse voltage with the electrostatic induction feeding method. In addition, the gap current and voltage decreased with increasing the rise/fall time because the electric charge q per pulse is determined by the amplitude of pulse voltage E_0 and feeding capacitance C_1 as $q=C_1E_0$ with the electrostatic induction feeding ECM. Thereby, the current and voltage peaks decreased with increasing the pulse duration to keep the same electrical charge per pulse as shown in Fig. 7.12 and Fig. 7.13.

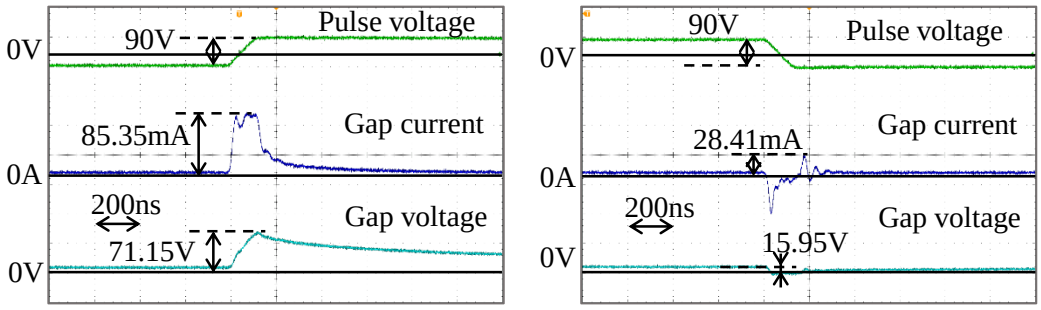

Fig. 7.12 Gap current and voltage waveforms with rise/fall time of 100 ns

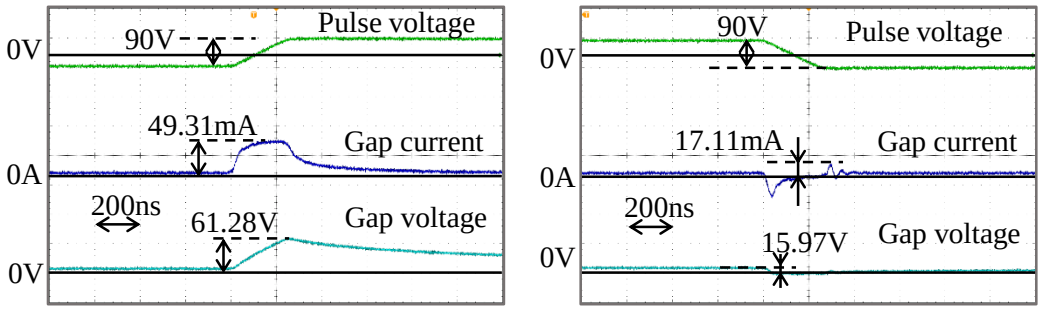

Fig. 7.13 Gap current and voltage waveforms with rise/fall time of 200 ns

Fig. 7.14 shows the discharge craters with different rise/fall times of pulse voltage. Fig. 7.15 shows the diameters of discharge craters with different rise/fall times of pulse voltage. The diameter of discharge craters decreased with increasing the rise/fall time of pulse voltage. In addition, the number of discharge craters were decreased with increasing the rise/fall time as shown in Fig. 7.14.

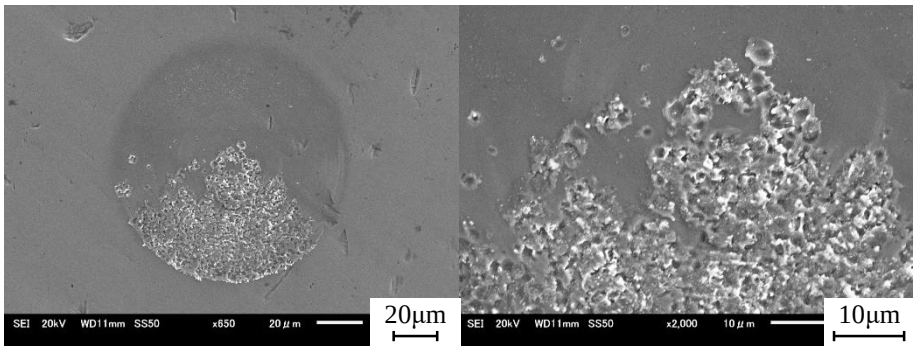

(a) 40 ns

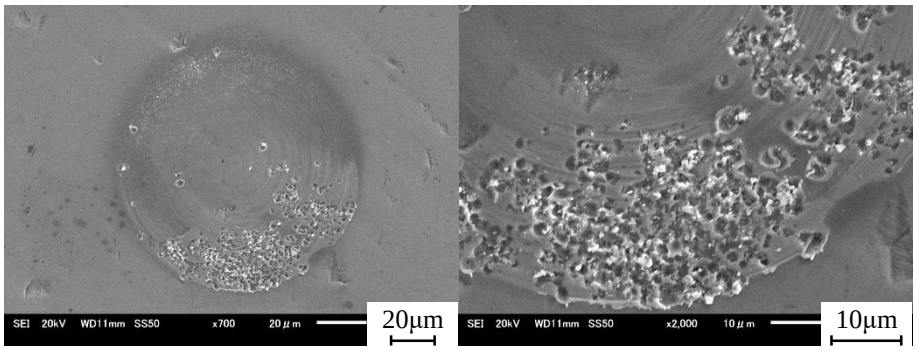

(b) 100 ns

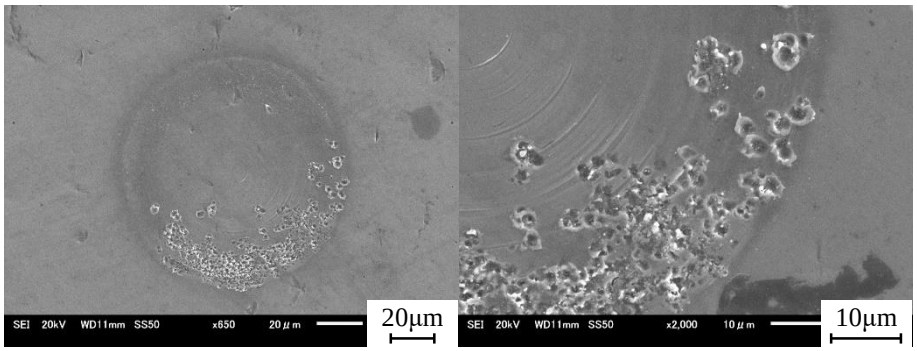

(c) 150 ns

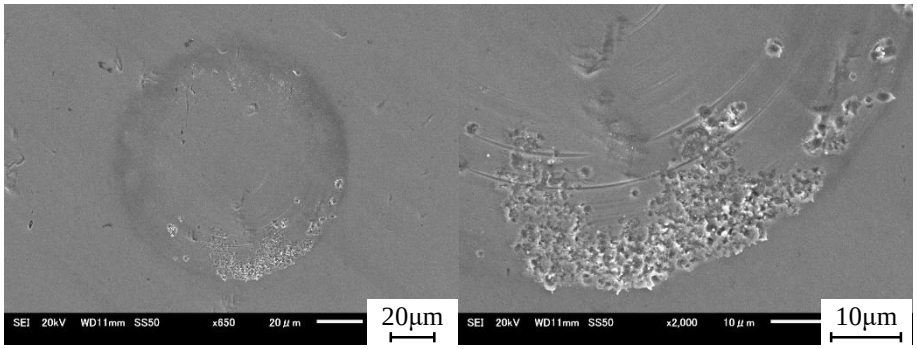

(d) 200 ns

Fig. 7.14 Discharge craters with different rise/fall times of pulse voltage

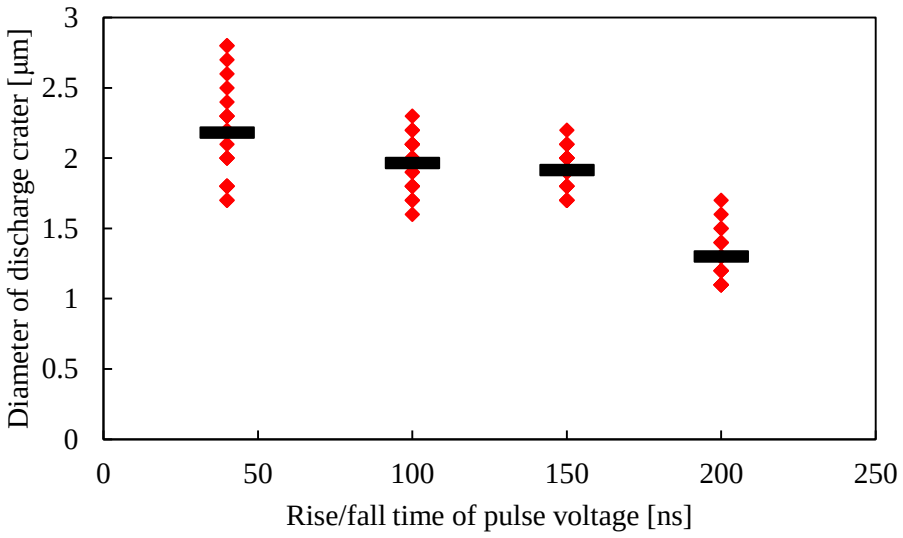

Fig. 15 Diameters of discharge craters with different rise/fall times of pulse voltage

7.4 Operation in ECM mode

The ECM mode of the hybrid machining system combining the electrostatic induction feeding EDM and ECM using same electrolyte method was investigated from the influence of frequency and rise/fall time of pulse voltage on the machining characteristics in this section.

Fig. 7.1 shows the principle of ECM mode, and the diode was removed to dissolve the oxide layer on the surface of tungsten electrode. Table 7.4 shows the experimental conditions. The feed distance of tool electrode was set as 7 μm. The feed speed of tool electrode was 0.1 μm/s. In this experiment, jump flushing was carried out for every feed distance of 0.1 μm by retracting the tool electrode. The frequencies of pulse voltage was 0.5 kHz, 1 kHz, 1.5 kHz, 3 kHz and 5 kHz.

Table 7.4 Experimental conditions to investigate the ECM mode

Pulse voltage	Amplitude [V]	90
	Frequency [kHz]	0.5, 1, 1.5, 3, 5
	Duty factor [%]	50
	Rise/fall time [ns]	100
Feeding capacitance C_1 [pF]		220
Electrolyte		$NaNO_3$ aq. 6 wt%
Tool electrode rotation [rpm]		3000

Fig. 7.16 shows the gap voltage and current waveforms with frequency of 1 kHz. It is noted that the gap current was bipolar without the diode. Since the oxide layer was dissolved due to the electrochemical reactions (7.1) and (7.2), the ECM mode occurred stably. Since the gap voltage drops to zero, discharge is difficult to occur.

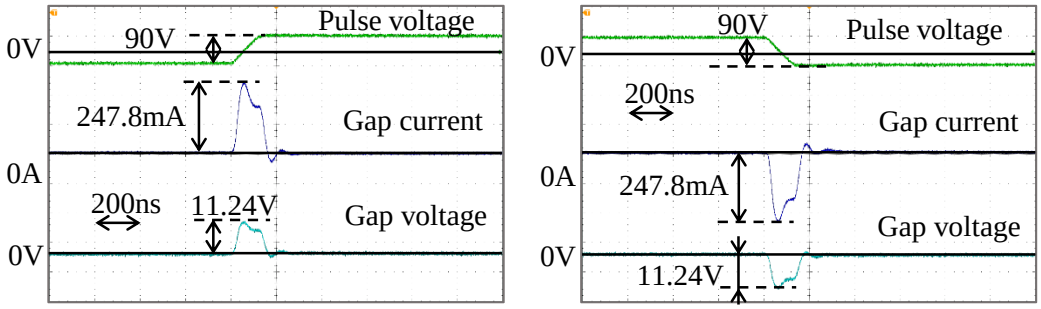

(a) Rise time (b) Fall time

Fig. 7.16 Gap current and voltage waveforms with pulse frequency of 1 kHz

7.5 Hybrid of EDM and ECM machining

The surface machined by EDM is covered by numbers of discharge craters. In contrast, the surface machined by ECM is significantly smooth because the material is removed by anodic electrochemical dissolution. Since the EDM and ECM can occur with the same electrolyte and tool electrode with the hybrid micro-EDM and micro-ECM machining using same electrolyte method, the improvement of the EDMed surface with the ECM process was conducted in this section.

7.5.1 Experimental conditions

An EDM surface was generated first, then the tool electrode was continuously fed after converting to ECM mode to polish the rough EDM surface. Table 7.6 and Table 7.7 show the experimental conditions of the EDM and ECM mode, respectively. The materials of stainless steel (SUS304) and tungsten were used as workpiece and tool electrode, respectively. The diameter of the tool electrode was 100 μm. The $NaNO_3$ aqueous solution of 6 wt% in concentration was used as electrolyte. The tool electrode was positioned on the top surface of workpiece with an initial gap width of 5 μm. In the EDM process, the feed distance was set as 6 μm with the feed speed of 0.3 μm/s, and jump flushing was carried out for every feed distance of 0.3 μm by retracting the tool electrode. The jump speed and jump distance were 1 mm/s and 500 μm, respectively. The gap width after EDM process was about 5.1 μm measured with the contact sensing function of the micro EDM machine (Panasonic, MG-ED72W). In the ECM process, the feed distance was set as 6 μm, based on the working gap width measured after the EDM process, with the feed

speed of 0.1 μm/s, and jump flushing was carried out for every feed distance of 0.1 μm by retracting the tool electrode. The jump speed and jump distance were 1mm/s and 4 μm, respectively. It is noted that the conversion of EDM to ECM mode did not need to change the electrolyte and tool electrode, and was realized by only removing the diode. The oxide layer was dissolved with removing the diode, resulting in the conversion of EDM to ECM mode. Based on the previous experimental results, the parameters of pulse voltage were changed to obtain a better machining accuracy of the ECM mode as shown in Table 7.7.

Table 7.6 Experimental conditions for EDM mode

Pulse voltage	Amplitude [V]	90
	Frequency [kHz]	500
	Duty factor [%]	50
	Rise/fall time [ns]	40
Feeding capacitance C_1 [pF]		220
Electrolyte		$NaNO_3$ aq. 6 wt%
Tool electrode rotation [rpm]		3000
Feed distance [μm]		0.3
Feed speed [μm/s]		0.3

Table 7.7 Experimental conditions for ECM mode

Pulse voltage	Amplitude [V]	90
	Frequency [kHz]	1
	Duty factor [%]	50
	Rise/fall time [ns]	100, 200
Feeding capacitance C_1 [pF]		220
Electrolyte		$NaNO_3$ aq. 6 wt%
Tool electrode rotation [rpm]		3000
Feed distance [μm]		6
Feed speed [μm/s]		0.1

7.5.2 Machining characteristics

Fig. 7.17 and Fig. 7.18 shows the gap voltage and current waveforms of the EDM and ECM process. Due to the influence of the passive oxide layer on the gap resistance, the gap current of the EDM mode at rise/fall times was smaller than the ECM mode. It is noted that the decrease in the gap voltage was slow in the EDM mode than the ECM

because of the thick oxide layer. This is the reason why discharge occurred during the pulse duration. If the gap voltage dropped, discharge cannot occur.

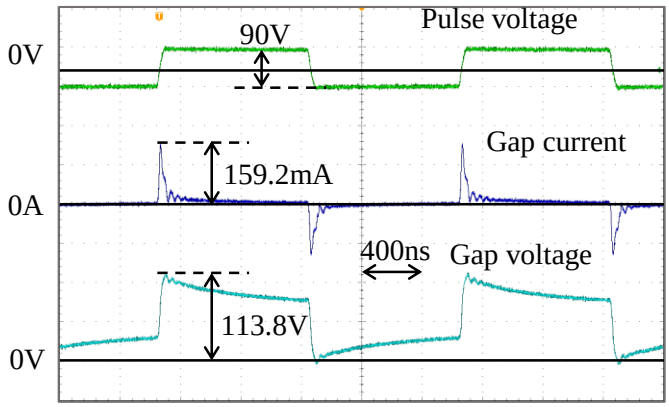

Fig. 7.17 Gap current and voltage of EDM process

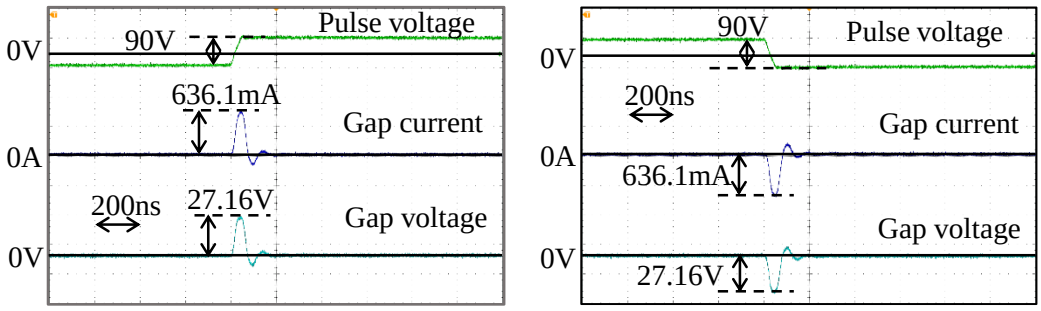

(a) Rise time (b) Fall time

Fig. 7.18 Gap current and voltage of ECM process

Fig. 7.19 shows the EDM surface and improved surfaces with the ECM mode using the rise/fall times of 100 ns and 200 ns. The experimental results showed that the EDM mode was realized using the same electrolyte and was converted to ECM mode with the hybrid micro-EDM and micro-ECM using same electrolyte method. The surfaces after ECM process became much smoother than the EDMed surface. However, the bottom was not flat, it is considered electrolyte flushing in the working gap was not sufficient due to the generation of sludge and bubbles from the electrochemical reaction. Fig. 7.20 shows the inlet side diameters of different surfaces. The diameter of inlet side increased after ECM process because more material volume was removed in the ECM process. In addition, the inlet side diameter was larger with longer rise/fall time of pulse voltage due to the electrochemical reaction occurred in a larger gap width.

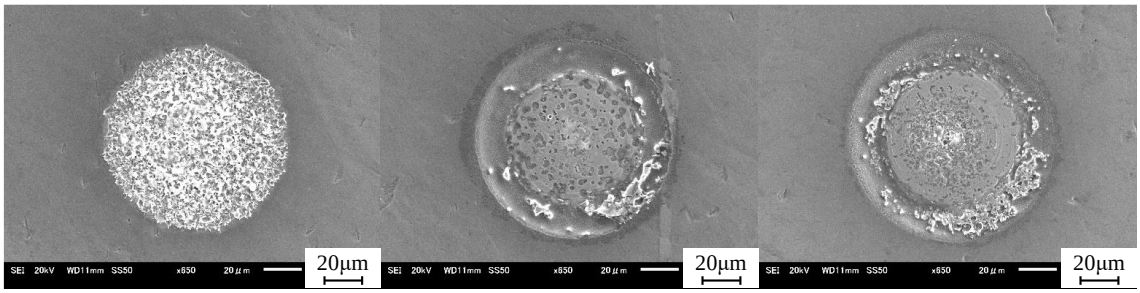

(a) EDM surface

(b) Improvement surface with rise/fall time of 100ns

(c) Improvement surface with rise/fall time of 200ns

Fig. 7.19 EDM surface and improved surfaces by ECM with rise/fall time of 100 ns and 200 ns

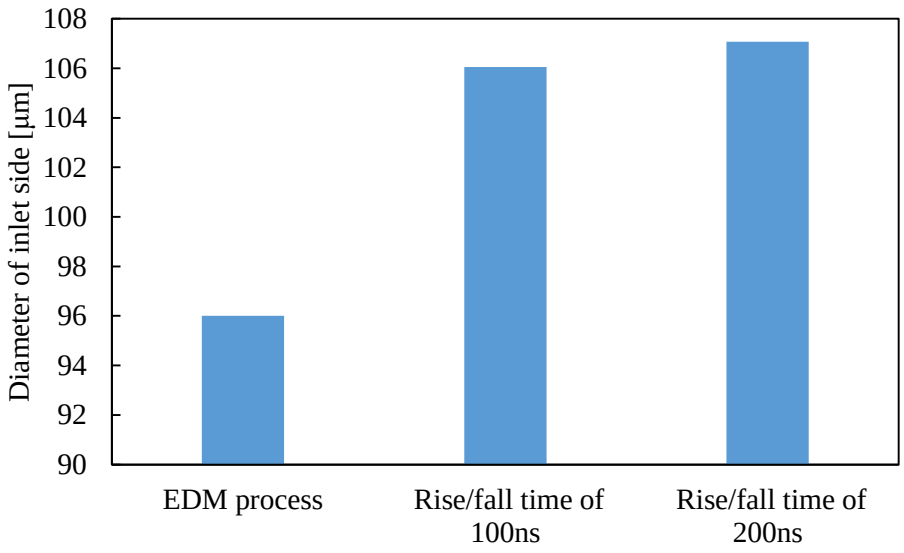

Fig. 7.20 Diameters of different surfaces

7.6 Conclusions

Since the EDM and ECM have different advantages and disadvantages as listed in Table 6.8, the hybrid machining system combining the electrostatic induction feeding EDM and ECM using the same electrolyte was proposed. The EDM mode can be used to rough-machine the materials or to machine the materials which are difficult to be machined by ECM, while, the ECM mode can be used when there is a high requirement of surface finish.

The conversion of EDM and ECM mode depends on the oxide layer formed on the surface of the tungsten electrode, and the generation of the oxide layer is controlled by attaching and detaching a diode in parallel with the working gap. When the oxide layer is formed on the surface of tungsten electrode, discharge occurs because the current cannot

flow through the working gap with the low conductivity of tungsten oxide layer. When the oxide layer is removed, the machining process is converted to ECM mode.

The waveforms of discharge current and voltage measured in the EDM mode showed that the EDM process was realized successfully. In addition, there was no discharge generated in the ECM mode. Hence, the conversion of the ECM and EDM modes was realized successfully with the hybrid machining system combining the electrostatic induction feeding EDM and ECM using the same electrolyte. In the EDM mode, the diameter of discharge crater increased with increasing the feeding capacitance, and the diameter of discharge crater decreased with increasing the rise/fall time of pulse voltage. The experimental results showed that the EDM mode was successfully converted to ECM mode and the surface finish of EDM process was improved by the ECM process.

Chapter 8 Conclusions

The electrostatic induction feeding ECM was investigated in this research. At first, the theory of this method used in micro-ECM was analyzed. According to the characteristics of this method, different gap control methods were proposed to design the servo feed control system. Micro-holes were drilled with the developed servo feed control system, and significantly smooth surfaces were obtained. Then, micro-rods were machined by applying the electrostatic induction feeding method. When $NaNO_3$ aqueous solution was used as electrolyte, micro-rod with the high aspect ratio of 20 was machined successfully with the stainless steel (SUS304) and tungsten used as workpiece and tool electrode materials, respectively. Furthermore, the influences of different materials of workpiece on the machining characteristics were investigated. As a result, advantages and disadvantages of the electrostatic induction feeding ECM method were clarified and compared with those of micro EDM processes. Hence, a hybrid system combining the electrostatic induction feeding EDM and ECM methods was proposed to compensate for the weakness of the present method. The main points of each chapter are concluded as following.

Chapter 1 introduced the principle and gap phenomena of electrochemical machining. In addition, the electrostatic induction feeding method developed for electrical machining processes: EDM and ECM, was introduced, and the principles of the electrostatic induction feeding EDM and ECM were explained. The problems to be solved in micromachining technologies using EDM and ECM were summarized, and purpose of the present study was described.

Chapter 2 analyzed the theory of the electrostatic induction feeding ECM and introduced the experimental equipments. According to the equivalent circuit, the calculation results verified that the current pulse width was determined by the rise/fall time of the pulse voltage regardless of the pulse on time. In addition, the gap current increased with increasing the feeding capacitance because the electrical charge per pulse $q=C_1E_0$ is constant with the electrostatic induction feeding method. Then, the experimental equipments of electrostatic induction feeding micro-ECM are introduced. With this method, the pulse signal of a function generator was amplified by a bipolar voltage amplifier to supply the pulse voltage for the electrostatic induction feeding method.

Chapter 3 investigated the machining characteristics of the servo feed control with the electrostatic induction feeding method. First, machining characteristics were investigated using the conventional servo feed control system which monitors the average gap voltage.

Experimental results showed that the material removal rate does not change obviously with different reference voltages. This is because the average gap voltage was 200 mV or less due to the pulse duration of several tens of ns with significantly low duty ratio. Hence, the gap control accuracy was not sufficiently high with the average gap voltage method because of the low signal to noise ratio (S/N ratio). In order to solve the problem of low S/N ratio and improve the gap control accuracy, a new method with monitoring the peak gap voltage was put forward. Compared with the average gap voltage method, the gap control sensitivity was improved due to the higher S/N ratio. In micro-hole drilling with the peak average method, lower reference voltage resulted in higher material removal rate, because of the higher current efficiency with the higher current density due to the smaller working gap. Since the electrochemical dissolution was mainly confined to the small working gap, the inlet radial gap width was smaller with low reference voltage. In addition, the material removal rate was higher with the larger feeding capacitance C_1. This is because the electric charge per pulse is proportional to C_1. The inlet gap width was nearly the same independent of C_1. With the peak gap voltage method, through-holes of 50 μm in diameter were machined on a stainless steel (SUS304) plate of 50 μm in thickness with different reference voltages. There was no difference in the taper angle, but the gap width was smaller and the finished surface was smoother with the lower reference voltage.

Comparison of the straightness and side gap width of the holes drilled by the present ECM method with those of micro EDM shows that the machining accuracy of the present method can compete with that of micro EDM. Furthermore, the material removal rate of electrostatic induction feeding EDM was much higher than the ECM. In EDM, the discharge occurs only at a single discharge location per each pulse, hence, volumetric removal rate is constant. On the other hand in ECM, electrolytic current flows simultaneously over the whole working surface with almost uniform current density. Hence, the feed rate of the tool electrode is constant and determined by the current density, independent of the working surface area. As a result, the volumetric removal rate of ECM is significantly high compared with EDM, when the machining area is large. In micro ECM, however, the advantage of the high removal rate is lost, because the machining area is small. Nonetheless ECM has advantages of no heat affected zone, no crack, and good surface equality. Therefore, it is considered that the electrostatic induction feeding ECM is more useful than micro EDM in finishing processes.

Chapter 4 introduced the micro-rod machining with the electrostatic induction feeding ECM using the electrolyte of NaCl aqueous solution. Two machining methods of micro-rod were investigated in this chapter: the feeding of workpiece in axial and radial direction

methods. With the feeding of workpiece in axial direction method, the machinable length limitation peaks at an optimum feed speed, because lower feed speed results in higher stray current density in the radial gap, and higher-than-necessary feed speed causes collision between the tool electrode and workpiece. At the optimum feed speed, the number density of the corrosion pits was lowest, and the taper angle was smallest. The maximum length of micro-rod was increased with increasing the pulse voltage amplitude. The maximum length of the micro-rod increased and the corrosion pits per unit area decreased with decreasing the thickness of tool electrode because the stray current flowing through the radial surface decreased. The influences of top surface area of tool electrode on the machining accuracy were insignificant because the difference in the total current on the shoulder surface of micro-rods was small, resulting in small difference in MRR. The influences of axial gap width, tool electrode thickness, and top surface area of tool electrode on the current density distribution on the workpiece surfaces were calculated with COMSOL Multiphysics. The results explained the machining results successfully. At last, a micro-rod with the average diameter of 9 μm and length of 78 μm was machined successfully by optimizing the cut depth in radial direction and feed speed. Since the target diameter of micro-rod was significantly small, the feed speed should be high enough so that the axial gap is decreased as small as possible to reduce the stray current in the radial gap.

With the feeding of workpiece in radial direction method, the number of corrosion pits per unit area increased with increasing the feeding distance in radial direction, because of the stray current around the end surface. The taper angle was increased with increasing the feeding distance due to same reason. It is noted the micro-rod started to be shortened by the stray current flowing through the end surface, when the feeding distance in radial direction was increased. A 3D model was built to simulate the material removal process with the COMSOL Multiphysics, and the simulation results of the material removal process was qualitatively in agreement with the experiment results.

Compared with the axial feeding method, the influence of pitting corrosion was smaller with the radial feeding method, because the current flowing through the radial gap was used for machining. Longer length of micro-rod was more easily obtained with the axial feeding method. This is because the end surface of the micro-rod is continuously exposed to the stray current with increasing the feed distance in radial direction when the feeding of workpiece in radial direction method was used.

Chapter 5 investigated the influences of the annealing process of the workpiece and different kinds of electrolytes on the machining characteristics. The experimental results showed that the machinable length limitation was decreased with the annealed workpiece.

It is considered that the annealing process conducted in air resulted in the damage due to oxidation of the material. In addition, the experimental results showed that the influence of pitting corrosion was eliminated with the electrolyte of $NaNO_3$ aqueous solution. This is because the chloride ion is a tiny and aggressive ion compared with nitrate ion, and thereby easily permeates the oxide film and triggers the occurrence of pitting corrosion. The gap width and taper angle were decreased with the electrolyte of $NaNO_3$ aqueous solution compared with those of the electrolyte of NaCl aqueous solution, because the electrochemical reaction can occur in a larger working gap with the NaCl aqueous solution due to the higher current efficiency. The machinable length of micro-rod was increased with the electrolyte of $NaNO_3$ aqueous solution compared with that of the NaCl aqueous solution due to elimination of pitting corrosion. A long micro-rod with 100 μm in diameter and aspect ratio of 20 was machined using the electrolyte of sodium nitrate aqueous solution. Furthermore, through optimizing the cut depth in radial direction and feed speed, micro-rod with the average diameter of 9 μm and length of 78 μm was machined successfully. Compared with the EDM, the machining accuracy and miniaturization limit were still lower with the electrostatic induction feeding ECM. However, since there are no residual stresses and cracks generated in ECM and the surface roughness is better, there is a possibility that the accuracy and miniaturization limit of ECM may become equivalent to those of EDM with the future development.

Chapter 6 investigated the machining characteristics with different materials of workpiece. With the material of tungsten, bipolar current was needed for the principle of material dissolution, which caused the tool wear. The tool wear rate was increased with increasing the feeding capacitance when the feed speed was the same. The tool wear rate was decreased with the electrolyte concentration of 6 wt% compared with 2 wt%, resulting in a better machining accuracy. Compared with the electrolyte of NaCl aqueous solution, the tool wear rate was decreased with the electrolyte of $NaNO_3$ aqueous solution.

With the material of high speed steel (SKH51), the machined results showed a better machining characteristics with the electrolyte of $NaNO_3$ aqueous solution, compared with the NaCl aqueous solution. The workpiece broke into pieces with the NaCl aqueous solution, and the surface machined was significantly rough. A micro-rod was successfully machined with the electrolyte of $NaNO_3$ aqueous solution. With the material of tungsten carbide, the volume of the material was swollen and a large amount of sludge was generated after machining, which was considered to result from the oxidation of tungsten.

Based on the obtained experimental results, the electrostatic induction feeding method was effectively used for micro-ECM of various kinds of materials. However, there are following several problems to be solved. At first, the machinable length of micro-rod with

the material of tungsten was limited by the collision between electrodes, because the machining area increased due to the tool wear resulting in the low current density. In the machining process, the material of the tool electrode was stainless steel (SUS304) and the tool wear rate was high. It is considered that the tool wear rate with different kinds of tool materials should be researched to decrease the tool wear rate and increase the machinable length limitation. Next, the experimental results with the material of tungsten carbide showed that it was difficult to fabricate a micro-rod with the electrolyte of $NaNO_3$ aqueous. The reason should be further researched to improve the machining characteristics, and the influence of different kinds of neutral electrolytes also need to be investigated.

In contrast, EDM is possible to machine these metal materials successfully. The differences between two machining technologies show that, to machine these difficult-to-machine materials, the EDM is more efficient than the ECM. Nevertheless, ECM has significant advantages such as good surface finish, no tool wear, and no residual stress or crack. Hence, a method to compensate for the disadvantage of the electrostatic induction feeding ECM is necessary.

Chapter 7 investigated the hybrid system between the electrostatic induction feeding EDM and ECM using the same electrolyte. Since the EDM and ECM have different advantages and disadvantages listed in Table 8.1, a hybrid machining system combining the electrostatic induction feeding EDM and ECM was proposed, by which it is possible to take full advantages of both machining technologies. The EDM mode can be used to rough-machine any conductive materials with high efficiencies or to machine the difficult-to-machine materials which are difficult to be machined by ECM, while, the ECM mode can be used when there is a high requirement of surface finish.

The conversion of EDM and ECM mode depends on the oxide layer formed on the surface of the tungsten electrode, and the generation of the oxide layer is controlled by attaching and detaching a diode in parallel with the working gap. When the oxide layer is formed on the surface of tungsten electrode, discharge occurs because the current cannot flow through the working gap with the low conductivity of tungsten oxide layer. When the oxide layer is removed, the machining process is converted to ECM mode.

The waveforms of discharge current and voltage measured in the EDM mode showed that discharge were ignited in the EDM mode. In addition, there was no discharge generated in the ECM mode. Hence, the conversion of the ECM and EDM modes was realized successfully with the hybrid machining method. In the EDM mode, the diameter of discharge crater increased with increasing the feeding capacitance, and decreasing the

rise/fall time of pulse voltage. The EDM mode was successfully converted to ECM mode and the surface finish of EDM mode was improved by the ECM mode.

Table 8.1 Comparison between EDM and ECM

Characteristics	Micro-EDM	Micro-ECM
Material removal rate	High	Low
Machining accuracy	High	Low
Recast layer	Exist	None
Cracks	Exist	None
Residual stress	Exist	None
Tool wear	Exist	None
Surface finish	Rough	Smooth
Difficult-to-machine materials	Any conductive materials	Easily passivated: W, WC, Ti, Nb; semiconductors: Si, SiC; novel metals: Au, Pt, Ag

At last, there are two main machining circuits used in the thesis as shown in Fig. 8.1. Fig. 8.1(a) used a diode which was attached in parallel with the working gap to obtain monopolar current and avoid tool wear. Fig. 8.1(b) did not use the diode and bipolar current was generated with the electrostatic induction feeding method. Table 8.2 lists the guideline of the electrostatic induction feeding method when it is used for different machining conditions.

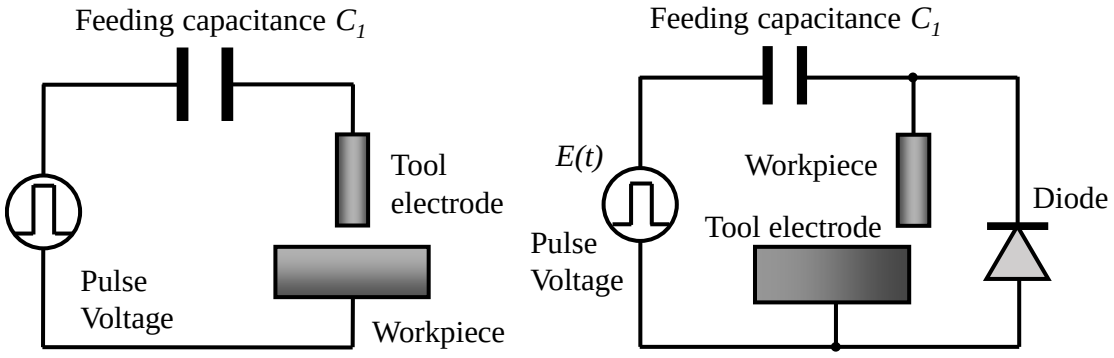

(a) Machining without diode (b) Machining with diode

Fig. 8.1 Machining circuit used in this thesis

With regard to the future works following the research in this thesis, the following research topics can be continuously investigated:

- To machine different materials
- Drilling holes with high aspect ratio
- ECM milling of 3D shapes with simple shape electrode
- Application of hybrid machining
- Non-contact electric feeding to high rotation speed electrode

Table 8.2 Machining circuit used in different experiments

Experiment	Workpiece material	Machining circuit
Micro-hole drilling	Stainless steel	With diode
Micro-rod machining	Stainless steel	With diode
Micro-rod machining	Tungsten	Without diode
Micro-rod machining	High speed steel	With diode
Micro-rod machining	Tungsten carbide	Without diode
EDM mode in hybrid machining experiment	Stainless steel (Tool: Tungsten)	With diode
ECM mode in hybrid machining experiment	Stainless steel (Tool: Tungsten)	Without diode

Reference

1) B. Bhattacharyya, Electrochemical Micromachining for Nanofabrication, MEMS and Nanotechnology, William Andrew, 2015.

2) J.P. Davim, Traditional Machining Processes, Springer, 2015.

3) K.P. Rajurkar, D. Zhu, J.A. McGeough, et al. New developments in electro-chemical machining. CIRP Annals-Manufacturing Technology, 1999, 48(2): 567-579.

4) 佐藤敏一, 電解加工と化学加工, 朝倉書店, 1970.

5) 木本康雄, 電気・電子応用精密加工, オーム社, 1982.

6) J. McGeough, Principles of Electrochemical Machining, 1974.

7) M. Datta. Microfabrication by Electrochemical Metal Removal. IBM Journal of Research and Development, 1998, 425: 655-669.

8) S.K. Sorkhel, B. Bhattacharyya. Parametric control for optimal quality of the work piece surface in ECM. International Journal of Material Processing Technology, 1994, 40: 271–286.

9) A.E. Debarr and D.A, Oliver. Elelctrochemical machining, Macdonald, 1968.

10) G.W. Akimov. Electrode potential. Crrosion, 1955, 11: 477-486.

11) A. J. de Bethune. ibid, 1953, 9.

12) B. Bhattacharyya, S. Mitra, A.K. Boro. Electrochemical machining: new possibilities for micromachining. Robotics and Computer-Integrated Manufacturing, 2002, 18(3): 283-289.

13) B. Bhattacharyya, S.K. Sorkhel. Investigation for controlled electrochemical machining through response surface methodology-based approach. International Journal of Materials Processing Technology, 1999, 86: 200–207.

14) 川船和儀, 能戸幸一, 日立評論, 1967.

15) B. Bhattacharyya, B. Doloi, P.S. Sridhar. Electrochemical Micro-Machining: New Possibilities for Micro-Manufacturing. Journal of Materials Processing Technology, 2001, 113(1): 301–305.

16) B. Bhattacharyya. Experimental investigation on the influence of electrochemical machining parameters on machining rate and accuracy in micromachining domain. International Journal of Machine Tools and Manufacture, 2003, 43(13): 1301-1310.

17) B.H. Kim, C.W. Na, Y.S. Lee, D.K. Choi, C.N. Chi. Micro Electrochemical Machining of 3D Micro Structure Using Dilute Sulfuric Acid. CIRP Annals-Manufacturing Technology, 2003, 54(1): 191-194.

18) M. Kock, V. Kirchner, R. Schuster. Electrochemical micromachining with ultrashort voltage pulses - a versatile method with lithographical precision. Electrochimica Acta, 2003, 48(20): 3213-3219.

19) K.P. Rajurkar, J. Kozak, B. Wei, J.A. McGeough. Study of Pulse Electrochemical Machining Characteristics. CIRP Annals-Manufacturing Technology, 1993, Vol. 42(1): 231-234.
20) M. Datta, D. Landolf. Electrochemical Machining under Pulse Current Conditions. Electrochemical Acta, 1981, 26(7): 899-907.
21) J. Kozak, K. Lubkowski, J. Peronczyk. Accuracy Problems of the Pulse Electrochemical Machining. Proceedings of the 22nd MTDR, 1981, 353-360.
22) J. Kozak, K.P. Rajurkar, B. Wei. Modeling and Analysis of Pulse Electrochemical Machining. ASME J. of Eng. for Ind., 1994, 116: 316-323.
23) B. Wei, J. Kozak, K.P. Rajurkar. Pulse Electrochemical Machining of Ti-6AI-4V Alloy. Trans. of NAMRVSME, 1994, XXII: 141-147.
24) K.P. Rajurkar, G. Levy, A. Malshe, M.M. Sundaram, J. McGeough, X. Hu, R. Resnick, A. DeSilva. Micro and nano machining by electro-physical and chemical processes. CIRP Annals-Manufacturing Technology, 2006, 55(2): 643-666.
25) B. Bhattacharyya, J. Munda, M. Malapati. Advancement in Electrochemical Micro-Machining. International Journal of Machine Tools and Manufacture, 2004, 44(15): 1577-1589.
26) C. Van Osenbrugger, C. de Regt. Electrochemical micromachining. Philips Technical Review, 1985, 42: 22–32.
27) M. Datta, L.T. Romankiw. Applications of chemical and electrochemical micromachining in the electronic industry. Journal of the Electrochemical Society, 1989, 136(6): 285-292.
28) Y. Zhou, J.J. Derby. The cathode design problem in electrochemical machining. Chemical Engineering Science, 1995, 50(17): 2679-2689.
29) M. Datta. Anodic dissolution of metals at high rates. IBM Journal of Research and Development, 1993, 37(2): 207-226.
30) O.H. Narayanan, S. Hinduja, C.F. Noble. The prediction of workpiece shape during electrochemical machining by the boundary element method, Int J Mach Tool Des Res, 1986, 26:323–338.
31) V.K. Jain, K.P. Rajurkar. An integrated approach for tool design in ECM. Precision engineering, 1991, 13(2): 111-124.
32) J. Deconinck, G. Maggetto, J. Vereecken. Calculation of current distribution and electrode shape change by the boundary element method, J. Electrochem. Soc. 1984, 132: 2960–2965.
33) S.K. Sorkhel, B. Bhattacharyya. Computer aided design of tools in ECM for accurate job machining. Proceedings of the ISEM-9, Japan, 1989, 240–243.
34) J.F. Thorpe. A mathematical model of electrochemical machining process. 3rd Int. Sem. on Optimisation of Manufacturing Systems, CIRP, Pisa, Italy, 1971.

35) F. Klocke, M. Zeis, S. Harst, A. Klink, D. Veselovac, M. Baumgartner. Modeling and simulation of the electrochemical machining (ECM) material removal process for the manufacture of aero engine components. Procedia CIRP, 2013, 8: 265-270.
36) M.S. Reddy, V.K. Jain, G.K. Lal. Tool design for ECM: correction factor method. Transactions of the ASME, 1998, 10: 111–118.
37) Y. Zhoo, J.J. Derby. The cathode design problem in ECM. Chemical Engineering Science, 1995, 50 (17): 2679–2689.
38) D. Zhu, C.Y. Yu. Investigation on the design of tool shape in ECM. ASME PED 1992, 58: 181–190.
39) K.P. Rajurkar, Z. Yu. 3D Micro-EDM Using CAD/CAM. CIRP Annals-Manufacturing Technology, 2000, 49(1): 127-130.
40) L. Yong, Z. Yunfei, Y. Guang, P. Liangqiang. Localized electrochemical micromachining with gap control. Sensors and Actuators A: Physical, 2003, 108(1): 144-148.
41) T. Masuzawa. A Combined Electrical Machining Process for Micronozzle Fabrication. CIRP Annals - Manufacturing Technology, 1994, 43(1): 189-192.
42) H. Ohmori, K. Katahira, Y. Vehara, Y. Watanabe, W. Liu. Improvement of mechanical strength of microtools by controlling surface characteristics. CIRP Annals-Manufacturing Technology, 2003, 52 (1): 467–470.
43) R. Snoeys, F. Staelens, W. Dekeyser. Current trends in non-conventional material removal processes. CIRP Annals-Manufacturing Technology, 1986, 35(2): 467-480.
44) A.D. Davydov, V.M. Volgin, V.V.L. Lyubimov. Electrochemical Machining of Metals: Fundamentals of Electrochemical Shaping. Russian Journal of Electrochemistry, 2004, 40(12): 1438-1480.
45) D. Clifton, A.R. Mount, D.J. Jardine, R. Roth. Electrochemical machining of gamma titanium aluminide intermetallics. Journal of Materials Processing Technology, 2001, 108(3): 338-348.
46) D. Landolt, P.F. Chauvy, O. Zinger. Electrochemical micromachining, polishing and surface structuring of metals: fundamental aspects and new developments. Electrochimica Acta, 2003, 48: 3185–3201.
47) M. Datta, D. Harris. Electrochemical micromachining: an environmentally friendly, high speed processing technology. Electrochimica Acta, 1997, 42: 3007–3013.
48) J. Kozak, K.P. Rajurkar, and Y. Makkar. Study of Pulse Electrochemical Micromachining. Journal of Manufacturing Processes, 2004. 6(1): 7-14.
49) R. Schuster, V. Kirchner, P. Allongue, et al. Electrochemical micromachining. Science, 2000, 289(5476): 98-101.
50) 斎藤長男，高鷲民生，毛利尚武，古谷政典，放電加工技術 - 基礎から将来展望まで - ，日刊工業新聞社 (1997).

51) 国枝正典，放電加工の原理と極間現象，精密工学会第 363 回講習会，東京大学 (2013).
52) T. Masuzawa. State of the Art of Micromachining. CIRP Annals-Manufacturing Technology, 2000, 49(2): 473-488.
53) T. Kawakami, M. Kunieda, Study on Factors Determining Limits of Minimum Machinable Size in Micro EDM. CIRP Annals-Manufacturing Technology, 2005, 54(1): 167-170.
54) 花田倫宏，国枝正典，新家一朗，静電誘導給電を用いた微細放電加工法の開発，精密工学会誌，2006, 72(5): 636-640.
55) M. Kunieda, A. Hayasaka, X.D. Yang, S. Sano, I. Araie. Study on nano EDM using capacity coupled pulse generator. CIRP Annals-Manufacturing Technology, 2007, 56(1): 213-216.
56) X.D. Yang, M. Kunieda, S. Sano. Study on Influence of Stray Capacitance on Micro EDM using Electrostatic Induction Feeding. International Journal of Electrical Machining, 2008, 13: 35-40.
57) 木森将仁，国枝正典. 静電誘導給電法を用いた放電加工の微細化. 精密工学会誌，2010, 76(10): 1151-1155.
58) T. Masuzawa, M. Fujino, K. Kobayashi, et al. Wire Electro-Discharge Grinding for Micro Machining. CIRP Annals-Manufacturing Technology, 1985, 34(1): 431-434.
59) X.D. Yang, C. Xu, M. Kunieda. Miniaturization of WEDM using electrostatic induction feeding method. Precision Engineering, 2010, 34(2): 279-285.
60) X. D. Yang, Z. Wu, G. Chi. Study on Micro WEDM Using Electrostatic Induction Feeding Method. Proc. of the 16th International Symposium on Electromachining, 2010, 675-679.
61) T. Koyano, M. Kunieda. Micro electrochemical machining using electrostatic induction feeding method. CIRP Annals-Manufacturing Technology, 2013, 62(1): 175-178.
62) S. Maeda, N. Saito, Y. Haishi. Principle and Characteristics of Electro-Chemical Machining. Mitsubishi Denki Giho, 1967, 41(10): 1267-1279 (in Japanese).
63) S. Skoczypiec, R. Adam. A sequential electrochemical–electrodischarge process for micropart manufacturing. Precision Engineering, 2014, 38(3): 680-690.
64) Z. Zeng, Y. Wang, Z. Wang, D. Shan, X. He. A study of micro-EDM and micro-ECM combined milling for 3D metallic micro-structures. Precision Engineering, 2012, 36(3): 500-509.
65) 原田慎治，夏 恒. 電流波形によるパルス電解加工状態検出の可能性. 2014 年度精密工学会春季大会学術講演会講演論文集, 1193-1194.
66) 門倉宏充, 夏 恒. パルス微細電解加工における極間距離の検出と制御に関する研究. 2015 年度精密工学会春季大会学術講演会講演論文集, 85-86.
67) A.K.M. De Silva, H.S.J. Altena, J.A. McGeough. Precision ECM by Process Characteristic Modelling. CIRP Annals-Manufacturing Technology, 2000, 49(1): 151–155.

68) C. Diver, J. Atkinson, H.J. Helml, L. Li. Micro-EDM drilling of tapered holes for industrial applications. Journal of Materials Processing Technology, 2004, 149: 296-303.
69) W. Wang, D. Zhu, N. Qu, S. Huang, X. Fang. Electrochemical drilling inclined holes using wedged electrodes. Int J Adv Manuf Technol, 2010, 47(9-12):1129–36.
70) T. Shimasaki, M. Kunieda. Study on influences of bubbles on ECM gap phenomena using transparent electrode. CIRP Annals-Manufacturing Technology, 2016, 65(1): 225-228.
71) The Chemical Society of Japan, Kagaku Binran, Basic Science Edition, Fifth Edition, Maruzen Publishing (in Japanese), 2004.
72) 小谷野智広：静電誘導給電法を用いた微細電気加工の研究,東京大学博士学位論文,2013.
73) A. Manabe, M. Kunieda. Research on Tool Wear in Electrochemical Machining by Electrochemical Induction Feeding Method. Journal of the Japan Society of Electrical Machining Engineers, 2014, 48(119): 186-193. (in Japanese).
74) 木森将仁, 国枝正典. 静電誘導給電法を用いた微細放電加工の微細化限界. 2009 年度精密工学会春季大会学術講演会講演論文集, 851-852.
75) L. Alting, F. Kimura, H.N. Hansen, G. Bissacco. Micro Engineering. CIRP Annals-Manufacturing Technology, 2003, 52(2): 635-657.
76) G. Spur, E. Uhlmann, U. Doll, N. Daus. WEDM of Microstructured Component Parts–Heat Conduction Model. IJEM 1999, 4: 41-46.
77) M.M. Sundaram, K.P. Rajurkar. Study on the surface integrity of machined tool in micro EDM. Proceedings of the 16th International Symposium on Electromachining, 2010, Shanghai, China, pp: 685–689.
78) K.P. Rajurkar, D. Zhu, J.A. McGeough, J. Kozak, A. De Silva. New Developments in Eletro-Chemical Machining. CIRP Annals-Manufacturing Technology, 1999, 48(2): 567–579.
79) R. Mathew, M.M.Sundaram. Modeling and fabrication of micro tools by pulsed electrochemical machining. Journal of Materials Processing Technology, 2012, 212(7): 1567-1572.
80) S.H. Ahn, S. H. Ryu, D. K. Choi, C.N. Chu. Electro-chemical micro drilling using ultra short pulses. Precision Engineering, 2004, 28(2): 129-134.
81) G.S. Frankle, L. Stockert, F. Hunkleer, H. Boehni. Metastable pitting of stainless steel. Corrosion, 1987, 43(7): 429-436.
82) T. Masaki, K. Kawata, T. Sato, T. Mizutani, T. Yonemoto, A. Shibuya, T. Masuzawa. Micro Electro-Discharge Machining, Proc. of ISEM 9, 1989, 26-29.
83) T. Masuzawa, M. Fujino, K. Kobayashi, T. Sutuki. Wire Electro-Discharge Grinding for Micro-Machining. CIRP Anneal-Manufacturing Technology, 34(1): 431-434.
84) B.H. Kim, Ryu, D.K. Choi, C.N. Chu. Micro electrochemical milling. Journal of Micromechanics and Microengineering, 2005, 15(1): 124-129.

85) B. Bhattacharyya, J. Munda. Experimental investigation on the influent of electrochemical machining parameters on machining rate and accuracy in micromachining domain. International Journal of Machine Tools and Manufacture, 2003, 43(13): 1301-1310.
86) Y.M. Lim, S.H. Kim. An electrochemical fabrication method for extremely thin cylindrical micropin. International Journal of Machine Tools and Manufacturing, 2001, 41(15): 2287-96.
87) Z.W. Fan, L.W. Hourng, C.Y. Wang. Fabrication of tungsten microelectrodes using pulsed electrochemical machining. Precision Engineering, 2010, 34(3): 489-496.
88) Y.M. Lim, S.H. Kim. An electrochemical fabrication method for extremely thin cylindrical micropin. International Journal of Machine Tools and Manufacture, 2001, 41(15): 2287-2296.
89) Z. Wang, B. Zhu, G. Cao. Fabricating microelectrode by electrochemical micromachining. Proc SPIE, 2006, 6041:1-5.
90) T. Masuzawa, M. Kimura. Electrochemical surface finishing of tungsten carbide alloy. CIRP Annals-Manufacturing Technology, 1991, 40(1): 199-202.
91) K. Miyoshi, M. Kunieda. Fabrication of Micro Rods of Cemented Carbide by Electrolyte Jet Turning. Procedia CIRP, 2016, 42: 373-378.
92) S.H. Choi, S.H. Ryo, D.K. Choi, C.N. Chu. Fabrication of WC micro-shaft by using electrochemical etching. The International Journal of Advanced Manufacturing Technology, 2007, 31(7-8): 682-687.
93) S.N. Basu, V.K. Sarin. Oxidation behavior of WC-Co. Materials Science and Engineering, 1996, 209(1): 206-212.
94) Z. Zeng, Y. Wang, Z. Wang, D. Shan, X. He. A study of micro-EDM and micro-ECM combined milling for 3D metallic micro-structures. Precision Engineering, 2012, 36(3): 500-509.
95) T. Kurita, H. Mitsuro. A study of EDM and ECM/ECM-lapping complex machining technology. International Journal of Machine Tools and Manufacture, 2006, 46(14): 1804-1810.
96) M.D. Nguyen, R. Mustafizur, S.W. Yoke. Simultaneous micro-EDM and micro-ECM in low-resistivity deionized water. International Journal of Machine Tools and Manufacture, 2012, 54: 55-65.
97) M.D. Nguyen, R. Mustafizur, S.W. Yoke. Modeling of radial gap formed by material dissolution in simultaneous micro-EDM and micro-ECM drilling using deionized water. International Journal of Machine Tools and Manufacture, 2013, 66: 95-101.

Acknowledgements

This thesis is a summary of the research results accomplished in Kunieda-Mimura laboratory in the University of Tokyo from 2013 to 2016.

Foremost, I would like to express my sincere gratitude to my supervisor, Prof. Masanori Kunieda, for the continuous support of my Ph.D study and research, for his greatest supervision, motivation, and encouragement. I greatly appreciate his immense knowledge and serous attitude to research and his assistance in writing papers and this thesis. His attitude to the research work will be the example in my whole life, and prompt me to try my best to do any research mission well in the future.

Besides my advisor, I would like to thank the other members of my thesis committee: Prof. Toshiyuki Obikawa, Prof. Kiyoshi Takamasu, Prof. Beom Joon Kim and Prof. Akio Yamamoto from the University of Tokyo for their kindness of taking time out from their busy schedule and their insightful comments and valuable questions to the thesis.

I would like to thank Associate Prof. Hidekazu Mimura in our laboratory for his kind advices to my research at the research meeting and his kind help to my life in Japan. I also need to thank Prof. Takahisa Masuzawa and Prof. Wataru Natsu for their suggestions to my research in the conferences.

I would also like to thank Dr. Ken Masaki, Dr. Tomohiro Koyano (currently in the Kanazawa University), Dr. Tomoo Kitamura (currently in the Nikon Corporation) and Dr. Yonghua Zhao for their kind guidance, help and advices to my research when I first came to Japan and that after.

Great thanks to Ms. Sumiko Tanabe and Ms. Satoko Kanari, the secretaries of Kunieda laboratory, for their dedication to the office work and their kind supports to my research work. Great thanks to Mr. Haruo Sai for his kind help in making the experimental setup

etc.

I must acknowledge Dr. Norliana Mohd Abbas, Mr. Takuma Kawanaka, Ms. Azumi Mori, Mr. Fuchen Chu and all the other members of Kunieda-Mimura laboratory for their kind help, support and encouragement to me in accomplishing the research and the thesis. Thanks for all the good times we have made.

I must also acknowledge Prof. Yinbiao Guo, Prof. Yunfeng Peng, Prof. Guo Bi and other professors from the Laboratory of MicroNano Manufacturing and Measuring in the Xiamen University, China, for their kind recommendation and great help supporting me to study abroad. Then I should thank our government for the scholarship to let me finish study.

At last, I would like to thank my parents: Yongzhong Han and Xiaorong Xiang, and my elder sister, Wei Han, and my young brother, Sheng Han, for their great love and support throughout my life.

Published papers related to this dissertation

Peer-reviewed Journal Paper

1) W. Han, M. Kunieda. Research on servo feed control of electrostatic induction feeding micro-ECM, Precision Engineering, 2016, 45: 195-202. (Chapter 3)

2) W. Han, M. Kunieda. Fabrication of micro-rods with electrostatic induction feeding ECM, Journal of Materials Processing Technology, 2016, 235: 92-104. (Chapter 4)

International Conference Paper

1) W. Han, M. Kunieda. Servo Feeding Control System used in Micro Electrochemical Machining with Electrostatic Induction Feeding Method, 10th International Symposium on Electrochemical Machining Technology, November 13-14, 2014, Saarbrücken, Germany.

2) W. Han, M. Kunieda. Research on micro-rods machining by ECM using electrostatic induction feeding method, 6th International Conference of Asian Society for Precision Engineering and Nanotechnology, August, 15-19, 2015, Harbin, P.R China.

3) W. Han, M. Kunieda. Influence of machining conditions on machining characteristics of Micro-rods by Micro-ECM with electrostatic induction feeding method, 18th CIRP Conference on Electro Physical and Chemical Machining (ISEM XVIII), April, 18-22, 2016, Tokyo, Japan.

Domestic Conference Paper

1) W. Han, M. Kunieda. Development of Servo Feeding System for Micro ECM using Electrostatic Induction Feeding Method, 精密工学会秋季学術講演会, 精密工学会学術講演会講演論文集 (2014), pp. 253-254.

2) W. Han, M. Kunieda. Research about machining characteristics for different working gap widths in electrochemical machining using electrostatic induction feeding method, 電気加工学会全国大会 (2014), 電気加工学会全国大会講演論文集, pp. 75-78.

3) W. Han, M. Kunieda. Fabrication of micro-rods by micro-electrochemical machining with the electrostatic induction feeding method, 精密工学会春季学術講演会, 精密工学会学術講演会講演論文集 (2015), pp. 75-76.

4) W. Han, M. Kunieda. Research on improvement of machining accuracy of micro-rods with electrostatic induction feeding ECM, 電気加工学会全国大会(2015), 電気加工学会全国大会講演論文集, pp. 56-59.

5) W. Han, M. Kunieda. Optimization of ECM conditions of micro-rods using electrochemical machining, 精密工学会秋季学術講演会, 精密工学会学術講演会講演論文集 (2015), pp. 253-254.

6) W. Han, M. Kunieda. Research on influence of electrolyte on micro-rod fabrication with the electrostatic induction feeding ECM, 精密工学会春季学術講演会, 精密工学会学術講演会講演論文集 (2016), pp. 65-66.
7) W. Han, M. Kunieda. Fabrication of tungsten micro-rod using electrochemical machining method with neutral electrolyte, 2016 精密工学会秋季学術講演会（2016/09/06 発表予定）.